

The Role of Wnt and BMP Signaling in Vertebrate Ocular Development and Disease

by

Sonya Angeline Widen

A thesis submitted in partial fulfillment of the requirements for the degree of

Doctor of Philosophy

in

Molecular Biology and Genetics

Department of Biological Sciences
University of Alberta

© Sonya Angeline Widen, 2019

Abstract

Axial patterning of the developing vertebrate eye is crucial for proper axon pathfinding, as well as critically important morphogenetic events such as closure of the ocular fissure. Perturbations in eye morphogenesis can lead to ocular coloboma (failed ocular fissure closure) and microphthalmia (small eyes), together a leading cause of pediatric blindness. An exquisitely regulated balance of morphogen gradients, imparting positional information to retinal cells in order to regulate regionally restricted gene expression, performs patterning of the dorsal-ventral axis of the eye. This is achieved in large part through the complex and incompletely understood interactions between the bone morphogenetic protein (BMP), Wnt, and Sonic hedgehog (Shh) signaling pathways and the downstream factors they regulate.

In this thesis, I have investigated the function of genes regulating both the BMP and Wnt signaling pathways in maintaining dorsal-ventral retinal identity, morphogenesis of the optic cup, and tissue fusion at the ocular fissure. I demonstrate that two members of a family of secreted Wnt inhibitors, *sfrp1a* and *sfrp5*, unexpectedly function to independently promote both Wnt and BMP signaling in the dorsal eye. Embryos with depleted *Sfrp1a/5* display coloboma, likely due to aberrant gene expression observed across the dorsal-ventral axis of the eye.

I assist in additionally characterizing a novel, conserved, highly transient fissure in the vertebrate dorsal eye and describe patients with a rare superior coloboma that results from incomplete dorsal fissure closure. Loss of dorsal BMP signaling, or increased Shh, alters the shape of the dorsal fissure and delays its closure. These data, combined with analyses of a BMP receptor mutation identified in a patient with superior coloboma,

demonstrate that dorsal fissure formation and closure is also dependent upon proper dorsal-ventral retinal patterning.

Finally, I identify and describe novel mutations that implicate two genes in causality of ocular coloboma and microphthalmia, the Wnt receptor *FZD5* and BMP family member *BMP3*. *In vitro* assays suggest that the identified FZD5 mutation encodes a secreted dominant negative receptor and, combined with data from Fzd5-depleted zebrafish embryos, preliminarily indicate Fzd5 can mediate both canonical and non-canonical Wnt signaling in the eye. Initial characterization of *bmp3* mutant zebrafish suggests a BMP- and patterning-independent role for Bmp3 and instead suggests it may directly regulate tissue fusion in the ocular fissure.

Preface

This thesis is an original work by Sonya A. Widen. The studies, of which this thesis is a part, have received research ethics approval from the University of Alberta Animal Policy and Welfare Committee. The protocols were approved by the University of Alberta's Animal Care and Use Committee (Protocol #427).

A version of Chapter 3 was published:

Holly*, V.S., Widen*, S.A., Famulski*, J.K., Waskiewicz, A.J. 2014. *Sfrp1a* and *Sfrp5* function as positive regulators of Wnt and BMP signaling during early retinal development. *Developmental Biology* 388: 192-204 *joint first authors

In this manuscript, I performed experiments, analyzed data, edited the figures and manuscript for revisions and wrote portions of the results and discussion. Figures 3.13, 3.14, 3.15 and 3.16 are the direct result of my thesis research.

A version of Chapter 4 was published:

Liu*, C., Widen*, S.A., Williamson*, K.A., Ratnapriya, R., Gerth-Kahlert, C., Rainger, J., Alur, R.P., Strachan, E., Manjunath, S.H., Balakrishnan, A., Floyd, J.A., UK10K Consortium, Li, T., Waskiewicz, A.J., Brooks, B.P., Lehmann, O.J., FitzPatrick, D.R., Swaroop, A. 2016. A secreted WNT-ligand-binding domain of FZD5 generated by a frameshift mutation causes autosomal dominant coloboma. *Human Molecular Genetics* 25(7): 1382-1391 *joint first authors

I performed all zebrafish work in this manuscript, analyzed data, wrote portions of the original manuscript draft, and edited the figures and manuscript for revisions. Figures 4.6 and 4.7 are the direct result of my thesis work.

A version of Chapter 5 was published:

Hocking*, J.C., Famulski*, J.K., Yoon, K.H., Widen, S.A., Bernstein, C., Koch, S.M., Weiss, O., FORGE Canada Consortium, Agarwala, S., Inbal, A., Lehmann, O.J., Waskiewicz, A.J. Morphogenetic defects underlie Superior Coloboma, a newly identified closure disorder of the dorsal eye. *PLoS Genetics*

In this work, I performed all of the *BMPRIA* injection experiments, subsequent imaging and analysis, and edited the figures and manuscript. My thesis work resulted in Figure 5.8C, Figure 5.9 and I assisted with data acquisition, analysis and creation of Figure 5.11.

Work with patients in Chapter 6 was performed by the Lehmann Lab (Figure 6.1), as was the analysis of exome and Sanger sequencing data (Table 6.1). The ANOLEA data was generated with assistance from Dr. Matthew Benson and Dr. Tim Footz (Figure 6.2). Dr. Lisa Prichard performed all cell culture work (Figure 6.4). I am responsible for all other figures and tables. A generous portion of the foundation of this project is owed to Dr. Mika Asai-Coakwell and Prajakta Desai and their work in the Lehmann lab.

This thesis is dedicated to the two people who most guide me, despite never having the privilege of knowing them.

Angeline Rose Lockwood, 1935 – 1980

Dr. Fred Oscar Schreiber, 1938 – 2015

Acknowledgements

First and foremost, I would like to express my deep gratitude to Andrew and my supervisory committee members, Drs. Dave Pilgrim and Ordan Lehmann for the support, encouragement, patience and advice. I count you among my colleagues, but also among my friends. You have all influenced the scientist and person I will be forever. Not any less important, thanks also for the coffee and beer, and for at least laughing while you shake your head in disapproval.

It takes a village to raise a PhD student. To my lab, Cats & Wine, and my fellow graduate students, thank you for helping me grow up here. Without the laughs, the happy hours, the board games, the Wednesday genetics beers on Thursday, the late night food deliveries, and the cat pictures, I'm not sure the bad days would have been worth it.

Thanks to my family and friends for sticking with me through years of being largely neglected while I stared at fish. A special thanks to my life partner, Spencer Balay, for teaching me that one small step at a time, I can climb the tallest mountains.

Table of Contents

Chapter 1: Introduction	1
1.1. Introduction to Early Vertebrate Ocular Development.....	2
1.2. Introduction to morphogen signaling pathways in eye development.....	6
1.3. Introduction to bone morphogenetic protein (BMP) signaling.....	7
1.4. BMP signaling in early development.....	10
1.5. Early eye patterning and BMP signaling.....	11
1.6. Introduction to Wnt signaling.....	15
1.7. Early eye development and Wnt signaling.....	16
1.8. Introduction to microphthalmia, anophthalmia and coloboma (MAC).....	18
1.9. Morphogens and MAC.....	20
1.10. Purpose of study and summary of research.....	22
1.11. Figures.....	25
Chapter 2: Materials and Methods	28
2.1. Ethics, animal care and general procedures.....	29
2.2. Morpholinos.....	30
2.3. Heat shock experiments.....	30
2.4. Live imaging.....	30
2.5. TALEN mutagenesis.....	31
2.6. CRISPR-Cas9 mutagenesis.....	31
2.7. Zebrafish genotyping.....	32
2.8. Whole mount in situ hybridization.....	33
2.9. Immunohistochemistry.....	35
2.10. FZD5 immunoblots and immunofluorescence.....	36
2.11. BMP3 Western blots.....	36
2.12. Phalloidin staining.....	38
2.13. Quantitative real-time PCR (qRT-PCR).....	38
2.14. Pharmacological treatments.....	40

2.15.	Manual and paraffin-embedded tissue sectioning.....	41
2.16.	mRNA expression constructs, synthesis and injections	42
2.17.	Site-directed mutagenesis.....	43
2.18.	Patients and DNA sequencing.....	44
2.19.	FZD5 mutagenesis and Wnt/beta-catenin pathway activation assay	45
2.20.	Active RhoA assay for Wnt5a stimulation	46
2.21.	Co-immunoprecipitation.....	46
2.22.	Retinal electroporation and explants culture	47
2.23.	Chick and mouse embryos, immunohistochemistry and imaging.....	47
2.24.	Atomic non-local environment assessment (ANOLEA).....	48
2.25.	Scanning electron microscopy (SEM).....	48
2.26.	Statistical analyses of eye size, prevalence, intensities, and gene expression 48	
2.27.	Members of FORGE Consortium Canada.....	49
2.28.	Tables	50

Chapter 3: Sfrp1 and Sfrp5 function as positive regulators of Wnt and BMP signaling during early retinal development.....

		59
3.1.	Introduction	60
3.1.1.	Summary	63
3.2.	Results	64
3.2.1.	Dorsal retina identity is initiated by BMP signaling and independent of Wnt signaling	64
3.2.2.	sfrp1a and sfrp5 are expressed in the zebrafish optic vesicle and retina during stages of dorsal-ventral axis initiation and maintenance.....	64
3.2.3.	Sfrp1a and Sfrp5 act synergistically during retinal morphogenesis.....	65
3.2.4.	Sfrp1a and Sfrp5 are required for canonical Wnt signaling in the retina.	67
3.2.5.	Depletion of Sfrp1a and Sfrp5 causes alterations to dorsal-ventral retina axis patterning.....	68
3.2.6.	Sfrp-depleted embryos have reduced BMP signaling.....	69
3.2.7.	Sfrps act as inhibitors at high concentrations	70

3.2.8. Sfrps act as facilitators of dorsal retina identity at low concentrations....	71
3.3. Discussion	72
3.4. Figures	77
Chapter 4: A secreted WNT-ligand-binding domain of FZD5 generated by a frameshift mutation causes autosomal dominant coloboma	95
4.1. Introduction	96
4.1.1. Summary	97
4.2. Results	99
4.2.1. A frameshift mutation in FZD5 causes autosomal dominant coloboma....	99
4.2.2. Expression of FZD5 A219Xfs*49 in zebrafish results in microphthalmia and coloboma.....	100
4.2.3. FZD5 A219X*fs49 is a secreted protein that binds to Wnt ligands, but is incapable of mediating WNT signaling	101
4.2.4. FZD5 A219X*fs49 antagonizes both canonical and non-canonical Wnt signaling	102
4.2.5. Forced expression of A219Xfs*49 FZD5 in mouse retina leads to apical junction defects similar to those observed in Fzd5/Fzd8 compound mutants...	103
4.3. Discussion	103
4.4. Figures	106
4.5. Tables.....	125
Chapter 5: Morphogenetic defects underlie Superior Coloboma, a newly identified closure disorder of the dorsal eye.....	126
5.1. Introduction	127
5.1.1. Summary	128
5.2. Results	129
5.2.1. Identification of patients with superior coloboma.....	129
5.2.2. Exome sequencing of superior coloboma patients.....	129
5.2.3. Vertebrate studies of dorsal ocular morphogenesis.....	130
5.2.4. CYP1B1 and the superior ocular sulcus.....	132
5.2.5. Bmp signaling regulates closure of the superior ocular sulcus.....	132

5.2.6.	Analysis of a second superior coloboma patient.....	134
5.2.7.	Superior ocular sulcus functions as a conduit for superficial vasculature 135	
5.3.	Discussion	137
5.4.	Figures	141
5.5.	Tables.....	163
Chapter 6: Bmp3 is a novel regulator of ocular fissure closure		178
6.1.	Introduction	179
6.2.	Results and discussion.....	181
6.2.1.	Patients with coloboma and/or microphthalmia have mutations in BMP3 181	
6.2.2.	BMP3 variant proteins have altered secretion in vitro	182
6.2.3.	Creation of bmp3 mutant zebrafish	184
6.2.4.	bmp3 ^{ua1020} homozygous larvae have optic fissure closure defects.....	185
6.2.5.	bmp3 is expressed in head mesenchyme during eye morphogenesis in zebrafish.....	187
6.2.6.	Bmp3 may be a novel ligand in retinal TGF β signaling	188
6.2.7.	Summary and future directions	190
6.3.	Figures	193
6.4.	Tables.....	206
Chapter 7: General discussion and future directions.....		208
7.1.	Summary of findings.....	209
7.2.	The complex nature of MAC disorders	210
7.3.	The importance of redundancy in development.....	212
7.4.	The importance of identifying factors downstream of morphogens.....	215
7.5.	Future analysis of combined effects in specific mutation cocktails.....	218
Literature Cited.....		219
Appendix A: Somite-derived retinoic acid regulates zebrafish hematopoietic stem cell formation		246

List of Tables

Table 2.1: Morpholino oligonucleotide sequences.....	50
Table 2.2: guide RNA target sequences for CRISPR-Cas9 mutagenesis.....	51
Table 2.3: Mutant zebrafish genotyping primer sequences.....	52
Table 2.4: Primer sequences for antisense plasmid-based RNA probes	53
Table 2.5: Primer sequences for antisense PCR-based RNA probes	54
Table 2.6: Primer sequences for quantitative real-time PCR	55
Table 2.7: Primer sequences for mRNA overexpression constructs	56
Table 2.8: Primer sequences for site-directed mutagenesis.....	57
Table 2.9: FZD5 Sanger sequencing primers in patients.....	58
Table 4.1: Rare <i>FZD5</i> variant identified in coloboma patients.....	125
Table 5.1: Superior coloboma patient information.....	163
Table 5.2: Genetic variants in superior coloboma patients.	164
Table 5.3: Select genetic variants identified in superior coloboma patient #2. Candidates were prioritized by expression within the developing eye or previously identified connections to coloboma.	177
Table 6.1: Candidate genes identified in a pedigree with coloboma.....	206
Table 6.2: BMP3 variants identified in a pedigree with coloboma and microphthalmia, and an unrelated cohort of patients with variable MAC.	207

List of Figures

Fig. 1.1 Overview of ocular fissure development and closure.	25
Fig. 1.2 Bone morphogenetic protein (BMP) signaling.	26
Fig. 1.3 Canonical Wnt/ β -catenin and non-canonical Wnt/PCP signaling.....	27
Fig. 3.1: BMP signaling regulates initiation of dorsal-ventral retina patterning.....	77
Fig. 3.2: <i>sfrp1a</i> and <i>sfrp5</i> mRNAs are expressed in the eye during retinal development....	78
Fig. 3.3: <i>sfrp2</i> is expressed at low levels in the retina and primarily in the RPE during retinal development.	79
Fig. 3.4: Sfrp1a and Sfrp5 depletion leads to small eyes and coloboma.....	80
Fig. 3.5: Non-overlapping <i>sfrp1a</i> and <i>sfrp5</i> morpholinos display similar ocular phenotypes.	81
Fig. 3.6: Live embryo analysis of <i>sfrp1a/sfrp5</i> depletion during retinal morphogenesis.....	82
Fig. 3.7: Sfrp1a/Sfrp5 positively regulate Wnt signaling.	83
Fig. 3.8: <i>sfrp1a/5</i> knockdown reduces Wnt signaling in <i>Tg(TOP:dGFP)</i> embryos.....	84
Fig. 3.9: Sfrp1a/Sfrp5 regulate retinal dorsal-ventral patterning.....	85
Fig. 3.10: Sfrp1a/5 loss of function does not affect nasal-temporal retinal patterning.	86
Fig. 3.11: Sfrp1a/Sfrp5 positively regulate BMP signaling during retinal development.	87
Fig. 3.12: Dorsomorphin treatment enhances BMP ligand expression.	89
Fig. 3.13: Overexpressing a high dose of <i>sfrp5</i> mRNA results in reduction of dorsal and expansion in ventral retina identity.	90
Fig. 3.14: Morphological assessment of zebrafish embryos injected with 100 pg of <i>sfrp5</i> mRNA.	91
Fig. 3.15: Injection of low dose (1 pg) of <i>sfrp5</i> mRNA causes an increase in dorsal marker gene expression and BMP signaling.....	92
Fig. 3.16: Morphological assessment of zebrafish embryos injected with 1 pg of <i>sfrp5</i> mRNA.	93
Fig. 3.17: Sfrp functions to regulate dorsal-ventral retina patterning.	94
Fig. 4.1: Compound <i>Fzd5</i> conditional knockout (<i>Fzd5</i> ^{-/-}) and <i>Fzd8</i> heterozygous mice have microphthalmia and coloboma.	106
Fig. 4.2: A <i>FZD5</i> frameshift mutation identified in a family with autosomal dominant coloboma.	107

Fig. 4.3: Microsatellite markers and haplotype analysis of Families 3484 and 111.	109
Fig. 4.4: Conservation of FZD5 WNT-binding cysteine rich domain (CRD) across species.	110
Fig. 4.5: Identification of a novel missense mutation in FZD5 (D97V).	111
Fig. 4.6: Morpholino knockdown and expression of <i>FZD5</i> causes microphthalmia and coloboma in zebrafish.....	113
Fig. 4.7: Eye size analysis of zebrafish embryos injected with <i>FZD5</i> mRNA.	115
Fig. 4.8: A219Xfs*49 FZD5 is incapable of mediating Wnt signaling.....	116
Fig. 4.9: Cellular localization of wild type and mutant FZD5 protein.	118
Fig. 4.10: FZD5 A219Xfs*49 binds to tagged Wnt3a and Wnt7a.	119
Fig. 4.11: Non-cell-autonomous dominant negative effect of A219Xfs*49 FZD5 on Wnt signaling.....	120
Fig. 4.12: Expression of <i>FZD5</i> A219Xfs*49 in retinas led to similar apical junction defects that were reported in mouse <i>Fzd5/Fzd8</i> compound mutants.	123
Fig. 4.13: A model of coloboma disease mechanism caused by <i>FZD5</i> A219Xfs*49.	124
Fig. 5.1: Superior Coloboma montage from patients with superior coloboma (numbers correspond to patients described in Table 5.1).	141
Fig. 5.2: Genetic variants identified in bilateral superior coloboma patient.	142
Fig. 5.3: The superior ocular sulcus in zebrafish, chick and mouse.	143
Fig. 5.4: Superior ocular sulcus in chick.	145
Fig. 5.5: Superior ocular sulcus in newt.	146
Fig. 5.6: Dynamics of the zebrafish superior ocular sulcus.....	147
Fig. 5.7: Reduced RA signaling does not impair closure of the superior ocular sulcus.	148
Fig. 5.8: The role of BMPR1 signaling in closure of the superior ocular sulcus.	149
Fig. 5.9: Patient variant in BMPR1A reduces protein function.....	150
Fig. 5.10: The role of Gdf6a signaling in superior ocular sulcus morphogenesis.	151
Fig. 5.11: Inhibition of Hedgehog signaling rescues closure of the superior ocular sulcus in Gdf6a-deficient embryos.	153
Fig. 5.12: <i>tbx2b</i> mutant zebrafish have delayed closure of the superior ocular sulcus.	154
Fig. 5.13: Developmental functions of the superior ocular sulcus.	155

Fig. 5.14: Abnormal ocular vasculature in <i>gdf6a</i> homozygous mutants.	156
Fig. 5.15: Aberrant SOS closure leads to abnormal vasculature.	158
Fig. 5.16: Interaction between Hedgehog and Bone Morphogenetic Protein signaling in formation of the dorsal radial vessel.	160
Fig. 5.17: Retinoic acid signaling and the superior ocular sulcus.	161
Fig. 5.18: Model of superior ocular sulcus morphogenesis and function.	162
Fig. 6.1: A <i>BMP3</i> missense mutation identified in a family with autosomal dominant coloboma and/or microphthalmia.	193
Fig. 6.2: <i>BMP3</i> amino acid substitutions are predicted to destabilize protein structure at multiple points within the peptide.	194
Fig. 6.3: Expression of wild type <i>BMP3</i> mRNA in zebrafish embryos does not cause detectable morphological phenotypes at 28-30 hpf.	195
Fig. 6.4: Two of three identified <i>BMP3</i> variant proteins show reduced or lost secretion from cells <i>in vitro</i>	196
Fig. 6.5: Zebrafish <i>bmp3</i> ^{ua1020} coding sequence alignment with wild type.	197
Fig. 6.6: The <i>bmp3</i> ^{ua1020} mutation encodes a prematurely truncated peptide that lacks the entire TGFβ ligand domain.	198
Fig. 6.7: <i>bmp3</i> ^{ua1020} mutant transcript does not undergo nonsense-mediated decay.	199
Fig. 6.8: Adult <i>bmp3</i> ^{ua1020} mutant zebrafish display aberrant craniofacial shape.	200
Fig. 6.9: <i>bmp3</i> is not maternally expressed in zebrafish.	201
Fig. 6.10: <i>bmp3</i> ^{ua1020} mutants show incompletely penetrant fissure closure defects.	202
Fig. 6.11: Zebrafish <i>bmp3</i> is expressed in head mesenchyme during optic fissure formation.	203
Fig. 6.12: pSmad3 signaling is active in the proximal ventral retina and partial pSmad3 inhibition synergizes with <i>bmp3</i> ^{ua1020} mutant fissure closure phenotypes.	204
Fig. 6.13: <i>bmp3</i> ^{ua1020} mutants do not have altered expression of dorsal or ventral marker genes.	205

List of Common Abbreviations

°C	Degrees celsius
1000G	1000 Genomes
aa	Amino acid
Acvr	Activin receptor
aldh	Aldehyde dehydrogenase
ANOLEA	Atomic non-local environment assessment
ANOVA	Analysis of variance
AP	Anterior-posterior
APC	Adenomatous polyposis coli
aPKC	Atypical protein kinase C
bambia	BMP and activin membrane bound inhibitor a
BCIP	5-bromo-4-chloro-3-indolyl-phosphate
BMP	Bone morphogenetic protein
bp	Base pairs
BRE	BMP response element
BSA	Bovine serum albumin
caBMPRI1A	Constitutively active BMP receptor 1A
Carb	Carbenicillin
cDNA	Complimentary DNA
CDS	Coding sequence
CHARGE	Coloboma, heart anomaly, choanal atresia, growth or mental retardation, genital and ear anomalies
CK1	Casein kinase 1
CM	Conditioned medium
CNV	Copy number variation
co-IP	Co-immunoprecipitation
CRD	Cysteine-rich domain
CRISPR	Clustered regularly interspaced palindromic repeats
CYP1B1	Cytochrome p450 1B1

Daam	Dishevelled associated activator of morphogenesis
DAN	Differential screening-selected gene aberrative in neuroblastoma
DAPI	4',6-diamidino-2-phenylindole
dbSNP	The Single Nucleotide Polymorphism Database
DEAB	Diethylaminobenzaldehyde
DEPC	Diethylpyrocarbonate
DIC	Differential interference contrast
DIG	Digoxigenin
dkk	Dickkopf
DMEM	Dulbecco's modified Eagle's medium
DMH1	Dorsomorphin homolog 1
DMSO	Dimethylsulfoxide
DNA	Deoxyribonucleic acid
dNTP	Deoxyribonucleotide triphosphate
dpf	Days post fertilization
DRV	Dorsal radial vessel
Dsh	Dishevelled
DV	Dorsal-ventral
ECM	Extracellular matrix
EDTA	Ethylenediaminetetraacetic acid
EM	Embryo media
ExAC	The Exome Aggregation Consortium
FGF	Fibroblast growth factor
FORGE	Finding Of Rare disease Genes
Fzd	Frizzled
GDF	Growth differentiation factor
GFP	Green fluorescent protein
Grem	Gremlin
GSK3	Glycogen synthase kinase 3
GTP	Guanosine triphosphate
HCl	Hydrogen chloride

HEK	Human embryonic kidney
HH	Hamilton and Hamburger
hpf	Hours post fertilization
HRM	High resolution melt
HRP	Horseradish peroxidase
hrs	Hours
hsp	Heat shock protein
kDa	Kilodaltons
LEF	lymphoid enhancer-binding factor
LOD	Logarithm of the odds
LRP	Low-density lipoprotein receptor-regulated protein
MAC	Microphthalmia, anophthalmia and coloboma
MeOH	Methanol
mg	Milligrams
MgCl₂	Magnesium chloride
mins	Minutes
ml	Millilitres
mM	Millimolar
mm	Millimeters
MO	Morpholino
mRNA	Messenger RNA
n.s.	Not significant
NaCl	Sodium chloride
NAD	Nicotinamide adenine dinucleotide
NaOAc	Sodium oxaloacetate
NaOH	Sodium hydroxide
NBT	Nitro-blue-tetrazolium
NHLBI	National heart, lung and blood institute
nL	Nanolitre
NT	Nasal-temporal
OC	Ocular coloboma

ORF	Open reading frame
PAM	Protospacer adjacent motif
Pax	Paired homeobox
PBS	Phosphate buffered saline
PBST	Phosphate buffered saline + 0.1% Tween-20
PBTr	Phosphate buffered saline + 0.15% TritonX-100
PCP	Planar cell polarity
PCR	Polymerase chain reaction
pg	Picograms
Pol	Polymerase
POM	Periocular mesenchyme
Pr-Di	Proximal-distal
ProK	Proteinase K
PTU	1-phenyl 2-thiourea
qPCR	Quantitative polymerase chain reaction
RA	Retinoic acid
rar	Retinoic acid receptor
RGC	Retinal ganglion cell
RhoA	Ras homolog gene family, member A
RNA	Ribonucleic acid
RNase	Ribonuclease
RPE	Retinal pigmented epithelium
rpm	Revolutions per minute
RT	Room temperature
Rx	Retinal homeobox gene
s	Seconds
SB	Splice-blocking
sCRD	Secreted cysteine-rich domain
SDS	Sodium dodecyl sulfate
SEM	Scanning electron microscopy
Sfrp	Secreted frizzled-related protein

sgRNA	Single guide RNA
Shh	Sonic hedgehog
SIS3	Specific inhibitor of Smad3
Smad	Sma and mad
SNP	Single nucleotide polymorphism
SOS	Superior ocular sulcus
Sox	SRY-box 2
ss	Somite stage
SSC	Sodium saline citrate
STF	Super top flash
T(m)	Melting temperature
TALENs	Transcription activator-like endonucleases
TB	Translation-blocking
TBST	Tris-buffered saline + 0.1% Tween-20
Tbx	T-box transcription factor
TCF	T cell-specific transcription factor
Tg	Transgene
TGFB	Transforming growth factor beta
TSC	Tuberous sclerosis complex
Twsg	Twisted gastrulation
μL	Microlitre
μm	Micrometer
μM	Micromolar
Vax	Ventral anterior homeobox
WES	Whole exome sequencing
Wnt	Wingless/integrated
WT	Wild type
xg	Times gravity
ZFNs	Zinc finger nucleases

Chapter 1

Introduction

1.1. Introduction to Early Vertebrate Ocular Development

Ocular development is a highly conserved process throughout vertebrates, as are the molecular pathways that govern it (Heavner and Pevny, 2012). Across vertebrate species, including humans, eye morphogenesis is tightly controlled through the precise spatial and temporal regulation of gene expression by the coordinated work of multiple developmental signaling pathways. When cellular communication goes awry during development, it can result in congenital (present at birth) eye disease and blindness. As such, the intricate interplay among signaling pathways, the upstream inputs they respond to, and the downstream effects they impart, have been and continue to be the focus of significant research efforts. While our knowledge of eye development has undoubtedly been expanded, how exactly these processes are coordinated is incompletely understood. Therefore, continued study is essential not only to fully understand the etiology of congenital eye disease, but also to appreciate at a molecular level how vertebrates are able to undergo precise regulation of tissue morphogenesis to build such a complex organ.

Since eye development is morphologically and genetically highly conserved in vertebrates, essentially all main vertebrate model organisms have played key roles in informing our basis of understanding. These include, but are not limited to, chick, mouse, rat, frog, medaka and zebrafish. Zebrafish have long been central to developmental biology but have also been recognized for their usefulness in modeling human disease (Ablain and Zon, 2013; Santoriello and Zon, 2012), including ocular disease. Along with their advantages such as large clutch sizes, relatively rapid development and small size, of particular importance to ocular studies are their external development and transparent embryos, allowing easy observation of early-occurring developmental processes like eye formation.

Advances in the field have provided zebrafish researchers with a wide selection of transgenic lines, genetic tools such as antisense morpholinos to inhibit splicing or translation of target mRNAs, and targeted mutagenesis techniques to disrupt gene function. In zebrafish, zinc-finger nucleases (ZFNs) and transcription activator-like effector nucleases (TALENs) have allowed the generation of a large number of targeted mutations. More recently, the field has seen rapid optimization of the Clustered Regularly Interspaced

Short Palindromic Repeats (CRISPR)-Cas9 system, which uses engineered guide RNA molecules that bind specific 20-nucleotide recognition sequences, directing a Cas9 enzyme to perform targeted double-strand breaks. Repair of double strand breaks is notoriously error-prone, frequently causing insertions or deletions, and this has revolutionized our ability to edit the genome in a targeted manner. Also pertinent to the study of disease, recent advances in the zebrafish CRISPR-Cas9 tool kit allow a piece of DNA to be “knocked in”, from small sequences to whole gene replacement, to precisely recapitulate and study the effect of DNA sequence variants identified in patients with disease. For these reasons, zebrafish is one of the most useful models in which to study eye development and associated human diseases.

In zebrafish, eye development begins with the specification of the eye field within the anterior neuroepithelium, transcriptionally distinct from presumptive forebrain tissue before any morphological difference can be detected (Li et al., 1997; Loosli et al., 2003; Wilson and Houart, 2004; Zaghoul et al., 2005). This is achieved through a transcription factor cascade initiated by Orthodenticle homeobox 2 (*Otx2*) and SRY-box 2 (*Sox2*) in the anterior neural ectoderm (Andreazzoli et al., 1999; Danno et al., 2008; Zuber et al., 2003), which activates the expression of the aptly-named transcription factor *retinal homeobox gene 3 (rx3)* in the presumptive eye field, thereby activating expression of additional eye field transcription factors such as *six3a*, *six3b*, *pax6a* and *pax6b* (Carl et al., 2002; Sinn and Wittbrodt, 2013). This specific cocktail of overlapping transcription factors will transcriptionally delineate eye field cells from surrounding neural tissue to maintain eye field fate, regulate proliferation within the eye field and will further assist in physically segregating cells fated to become eye field versus forebrain (Carl et al., 2002; Cavodeassi et al., 2013; Chuang and Raymond, 2001; Stigloher et al., 2006). The single eye field is separated along the midline into bilateral optic primordia by the anterior movement of diencephalic cells (Varga et al., 1999; Wilson and Houart, 2004) marking the start of ocular morphogenetic movements.

The optic primordia, once specified, will begin to evaginate laterally from the forebrain as early as 12 hours post fertilization (hpf) in zebrafish to form the optic vesicle (Schmitt and Dowling, 1994). Simultaneous with evagination, retinal progenitor cells

intercalate into the optic vesicle, in part facilitated by the expression of *rx3* that prevents retention of forebrain epithelium characteristics (England et al., 2006; Ivanovitch et al., 2013; Rembold et al., 2006; Sinn and Wittbrodt, 2013). Continued growth and lateral evagination achieves two things. Starting at 11 hpf, elongation and subsequent constriction of the tissue connecting the optic vesicle and forebrain will form the optic stalk, which later will give rise to the optic nerve (Schmitt and Dowling, 1994). This brings the optic vesicles in contact with a region of overlying surface ectoderm competent to be induced to form the lens vesicle, which thickens and begins to invaginate towards the optic vesicle at 15 hpf. The lens vesicle will bud off, forming the lens, and the optic vesicle will subsequently bend around the forming lens (Chow and Lang, 2001; Fuhrmann, 2010), giving rise to a bi-layered optic cup (Fig. 1.1A). It is somewhat contentious whether induction by the optic vesicle is strictly necessary for lens formation; while *eyeless* medaka mutants entirely lack a lens without the formation of the optic vesicles (Winkler et al., 2000), *rx3* mutant zebrafish that entirely lack optic vesicle evagination still form a small lens (Loosli et al., 2003).

Previous models of optic cup development suggest that surface ectoderm-derived signals induce the inner-most (distal) layer of the optic cup to become the neural retina, while the proximal layer gives rise to the retinal pigmented epithelium (RPE). This model was refined by Heermann et al. (2015) who showed that while bending of the presumptive neural retina was primarily driven by basal constriction of the retinal progenitor cells (Bogdanović et al., 2012; Martinez-Morales et al., 2009), the total basal surface area dramatically increases in size. Their time-lapse imaging and cell tracking assay in zebrafish showed that there is significant flow of cells from the proximal layer around the rim of the optic cup into the neural retina (Heermann et al., 2015). Preventing this epithelial flow from the outer to inner optic cup layers resulted in ectopic neural retina tissue positioned within the normal RPE domain, suggesting that cells originating from both layers of the optic cup will contribute to the eventual neural retina.

While the distal optic vesicle/cup navigates lens formation, the presumptive ventral (bottom) side of the optic cup undergoes important morphological changes that start at 18 hpf to form a deep groove, termed the choroid fissure. The choroid fissure, also referred to

as the optic or ocular fissure, transiently exists along the full length of the optic cup and down the optic stalk. It functions as an important entryway for early vasculature to invade and nourish the eye, as well as an eventual exit point for retinal ganglion cell axons to innervate the optic tectum (Adler and Canto-Soler, 2007; Schmitt and Dowling, 1994) (Fig. 1.1). While the choroid fissure normally closes progressively between 48-60 hpf, a wide variety of perturbations can prevent its proper closure and therefore lead to retained, permanent openings in ventral eye tissues. In humans, this potentially blinding disease is termed ocular coloboma and will be discussed in detail later.

At 21-22 hpf, a much more transient groove appears in the presumptive dorsal eye. It is infrequently described in the literature (Nordquist and McLoon, 1991) and its function has not yet been investigated. Interestingly, rare reports of patients with “atypical” coloboma exist, where the presentation of the coloboma is not consistent with failure of the choroid fissure to fuse. At least two patients display gaps in the dorsal (superior, in humans) eye tissues (Abouzeid et al., 2009; Mann and Ross, 1929) that could be explained by a retained dorsal groove, much like the relationship between the choroid fissure and ventral (inferior) coloboma. Studies into the relationship between dorsal groove and atypical coloboma are discussed in Chapter 5.

In addition to interactions between the optic vesicle (neural ectoderm) and overlying surface (non-neural) ectoderm, a third population of cells is crucial to vertebrate eye development: periocular mesenchyme (POM). POM is predominantly of cranial neural crest origin, though a subset of the population is mesodermally-derived (Fuhrmann, 2010). During early optic cup morphogenesis, neural crest-derived POM cells migrate from the dorsal neural tube and travel anteriorly over the developing eye, including into the choroid fissure (Langenberg et al., 2008) (Fig. 1.1D-E). The role of POM in eye development is not particularly well understood but it is known that they give rise, or contribute to, a number of anterior segment and extraocular structures such as the cornea, sclera, trabecular meshwork, extraocular muscles, as well as the early hyaloid vessels that grow into the choroid fissure (Creuzet et al., 2005; Gage et al., 2005). Past and recent work suggests POM regulates signaling and gene expression within the developing eye, and has a direct and crucial role in ocular fissure closure (Dee et al., 2013; Evans and Gage, 2005;

Fuhrmann et al., 2000; Gestri et al., 2018; Gestri et al., 2009; Lupo et al., 2011; McMahon et al., 2009; Sedykh et al., 2017). POM-derived endothelial cells within the early choroidal vasculature may directly mediate tissue fusion between the two choroid fissure lobes (James et al., 2016) and both inflated (Weiss et al., 2012) and absent (James et al., 2016) choroidal vasculature cause defects in fissure closure.

The orientation of eye tissues changes significantly through development; during morphogenesis, the eye will undergo almost 90° counter clockwise rotational movement so that, for example, the posterior optic vesicle becomes dorsal optic cup in its final position (Schmitt and Dowling, 1994). The combined efforts of the above events will form a continuous globe of retina and RPE, complete with a lens nested at its distal end and an optic stalk connecting it to the forebrain from which it was originally formed. Correct early development of overall eye structure is essential for subsequent specification of different cell types, all with essential roles in successful light detection and visual processing in the brain, ultimately laying the foundation for a functional visual system.

1.2. Introduction to morphogen signaling pathways in eye development

Similar to other organs in the vertebrate body plan, eye development is controlled through the combined efforts of multiple morphogens. Though there are exceptions, morphogens are defined as secreted molecules that are able to impart distinct signaling messages to cells in a concentration-dependent manner. For example, a high concentration of morphogen signal may instruct cells to take on a certain fate, while specifying an entirely separate fate at lower concentration (Wolpert, 1969). When we consider that morphogens have multiple concentration thresholds that confer distinct messages, and that multiple morphogens can act in the same tissue, it becomes clear there are almost limitless combinations of signals with which to differentiate parts of an embryo, organ or tissue.

There are five main types of morphogens that are especially crucial during regionalization of the vertebrate embryo: fibroblast growth factors (Fgfs), retinoic acid (RA), hedgehog (most commonly Sonic hedgehog; Shh), transforming growth factor-beta and bone morphogenetic proteins (TGFβ and BMP), and wingless/int family (Wnt)

proteins. Each signaling pathway uses a system of cell surface receptors and intracellular effectors to alter the fate of target cells (reviewed in (Freeman and Gurdon, 2002)).

Given that the eye develops from eye field tissue specified within forebrain tissue, the developing neural tube must first undergo regionalization along its anterior-posterior (AP) axis to delineate forebrain, midbrain and hindbrain/spinal cord identities. Within the forebrain, tissue is further subdivided into the telencephalon (anterior) and diencephalon (posterior) through the action of a Wnt gradient. Briefly, high Wnt activity specifies diencephalic identity, while low Wnt activity is necessary to specify telencephalic and eye field fate; this is achieved in part by the secretion of Wnt antagonists from the anterior neural border (Houart et al., 2002). Separation of the eye field into bilateral optic vesicles requires the action of Shh emanating from the ventral forebrain and prechordal plate (Echelard et al., 1993) and when disrupted, embryos often display cyclopia due to the existence of a single medial eye field (Chiang et al., 1996). After the eye field is specified, morphogens perform crucial roles in separation of the eye field, initiation and maintenance of patterning across multiple axes in the developing optic cup, as well as regulation of eye size, and will be discussed in subsequent sections.

1.3. Introduction to bone morphogenetic protein (BMP) signaling

Originally identified for their role in bone and cartilage formation Urist (1965), bone morphogenetic proteins (BMPs) play crucial and diverse roles in cell growth, proliferation and survival in almost every organ. As morphogens, they function in a dose-dependent manner, often to establish patterned cell identity across tissues to initiate and/or maintain developmental axes. BMPs are part of the larger transforming growth factor-beta (TGF β) superfamily of signaling molecules, which includes TGF β s, activins, inhibins, growth differentiation factors (GDFs), glial derived neurotrophic factors (GDNFs), Nodal, Lefty and anti-Müllerian hormone.

TGF β /BMP/GDF ligands are first synthesized as large precursor peptides (Massague, 1990), which form dimers linked by C-terminal disulfide bridges. Simultaneously, the C-terminal mature ligands are proteolytically cleaved from the N-

terminal pro-domain in the golgi by pro-protein convertases such as Furin (Constam, 2014) and the resulting ligand dimer is secreted from the cell. The ligands are thought to remain mostly extracellular matrix (ECM)-localized (Miyazaki et al., 2008), restricting their activity largely to cells within relatively close proximity. However, this is certainly not without exception, the most extreme example of which is found in Gdf8 and Gdf11 proteins that are capable of entering circulation and acting as hormones (reviewed in (Bueno et al., 2016; Jamaiyar et al., 2017)). Ligand homo- or heteroduplexes (more commonly the latter) first bind BMP receptor type I dimers on the cell surface, which then recruit type II receptor dimers (de Caestecker, 2004). Constitutively active type II receptors phosphorylate type I receptors, activating the serine/threonine kinase type I receptors and allowing them to phosphorylate intracellular effector proteins called Smads. Named for a combination of the *C. elegans* and *Drosophila* homologs, Sma and Mad respectively, receptor-regulated Smads (rSmads) remain localized within the cytoplasm until phosphorylated by type I receptors. rSmad1/5/8 mediate canonical BMP signaling and upon activation will complex with co-Smad4 (nuclear Smad) and translocate into the nucleus (Lagna et al., 1996; Packard et al., 2003), where the complex acts as a transcription factor to regulate the expression of target gene (Fig. 1.2). TGF β , Activin, Nodal, and Lefty ligands instead signal through rSmad2/3, which similarly require co-Smad4 for their activity. It should be noted that although each family of signaling molecules within the TGF β superfamily have “typical” rSmads that they use for signaling, this is heavily context-dependent and many are able to activate both Smad1/5/8 and Smad2/3 in certain conditions.

Regulation of BMP signaling can occur extracellularly, at the receptor level and intracellularly by multiple different mechanisms. The different extracellular BMP inhibitors are not overly well conserved, except for one main feature: most BMP inhibitors structurally resemble BMP ligands themselves, in that they have at least six conserved cysteine residues that form disulfide bridges in a cysteine knot that is also seen in almost all TGF β superfamily ligands. The importance of a cysteine knot domain is thought to center around strict maintenance of structural conformation; the disulfide bridges provide backbone stability to ensure proper folding and exposure of key hydrophobic residues (Avsian-Kretchmer and Hsueh, 2004; Scheufler et al., 1999). Extracellular BMP inhibitors

include members of the differential screening-selected gene aberrative in neuroblastoma (DAN) family of proteins (DAN, Cerberus, Gremlin 1, Protein Related to Dan or Cerberus [PRDC; or, Gremlin 2], and Coco), Chordin, Noggin, Follistatin and related proteins Twisted Gastrulation (Twsg) and Crossviesless-2 (CV2) (reviewed in (Brazil et al., 2015)). While most are thought to bind and sequester ligands to prevent receptor binding, Follistatin instead forms a complex with both the receptor and ligand to inhibit the activation of a signaling cascade (Iemura et al., 1998); reviewed in (Bragdon et al., 2011). Interestingly, some TGF β family ligands function as inhibitors of signaling instead, such as Gdf3, which has been shown to bind and inhibit Bmp4 extracellularly (Levine and Brivanlou, 2006).

Extracellular BMP inhibitors often work in at least partial redundancy to ensure a more robust system. For example, Noggin and Gremlin 1 interact to cooperatively maintain a BMP signaling-free zone during mouse sclerotome induction by Shh (Stafford et al., 2011). Interactions between inhibitors are not always amicable; BMP endothelial cell precursor-derived regulator (BMPER; the human ortholog of CV2) inhibits BMP4 to promote angiogenesis in mouse endothelial cells (Kelley et al. 2009), but addition of BMPER inhibits the pro-angiogenic effect of Twsg1 on endothelial cell sprouting (Heinke et al., 2013). Instead of cooperation, a complex balance between antagonism and synergy appears to exist between two BMP inhibitors.

Ligands at the cell surface can also be bound and sequestered by the pseudoreceptor BMP and activin membrane-bound inhibitor (Bambi), which has a ligand-binding domain similar to a type I BMP receptor, but lacks the intracellular domain and therefore the ability to transduce a signal (Sieber et al., 2009). Since different families within the TGF β superfamily use some common intracellular effectors, pathways can also antagonize one another by competing for these proteins. For example, BMP and TGF β signaling both require their activated rSmads to complex with co-Smad4 to translocate into the nucleus. Additionally, signaling can be inhibited at the transcript level by a growing list of micro-RNAs (for example, (Ahmed et al., 2011; Kang et al., 2012); reviewed in (Brazil et al., 2015)).

1.4. BMP signaling in early development

The varied roles of BMP signaling in vertebrate development have been the focus of significant research efforts, as BMP regulation is crucial to some of the most important developmental processes. Spemann and Mangold originally described the existence and properties of the dorsal organizer ((Spemann and Mangold, 2001); originally published in 1924) based on the ability of a transplanted organizer to induce ectopic dorsal identity and the formation of a secondary axis (De Robertis, 2006). While it was unknown at the time, the organizer secretes multiple BMP inhibitors in order to antagonize BMP ligands emanating from the presumptive ventral region. Also referred to as the Spemann-Mangold organizer, this powerful structure will organize the events of gastrulation in the embryo. Lewis Wolpert, one of developmental biology's forefathers, once said, "It is not birth, marriage, or death, but gastrulation, which is truly the most important time in your life." Hilde Mangold's dissertation on the embryonic organizer and its roles in gastrulation would provide much of the foundation for Hans Spemann's 1935 Nobel Prize.

Some of the most well studied roles for BMPs are rooted in gastrulation. For example, a number of zebrafish mutants identified in the early 1990s Tubingen screen in Christiane Nusslein-Volhard's lab displayed profound expansion of dorsal structures at the expense of ventral structures indicating a loss of ventral identity, including those later identified as carrying mutations in *bmp2b*, *bmp7* and *smad5* (Hammerschmidt et al., 1996; Hild et al., 1999; Kishimoto et al., 1997; Mullins et al., 1996). The combined activity of Bmp2b, Bmp4 and Bmp7 in promoting ventral identity during gastrulation is opposed by Chordin, Noggin and Follistatin produced in the shield (the zebrafish dorsal organizer). Perturbing this carefully regulated morphogen gradient through loss of BMP inhibitors or overexpression of ventral BMPs both produce similarly ventralized phenotypes (Hammerschmidt et al., 1996; Khokha et al., 2005; Schmid et al., 2000), predictably opposite of those seen in *bmp2b*, *bmp7* and *smad5* zebrafish mutants.

Interestingly, extracellular BMP inhibitors such as Chordin and Twisted Gastrulation are able to instead facilitate signaling in certain contexts (reviewed in (Umulis et al., 2009)); for example, they may enable BMP gradient formation by binding and shuttling ligands through extracellular space by actively preventing receptor-mediated

endocytosis, or passively by extending ligand half-life, providing more time for diffusion away from the source (Lander et al., 2002; Mizutani et al., 2005). While it was widely thought that a similar mechanism acted to refine the BMP gradient across the embryonic dorsal-ventral axis, recent work suggests it may instead be a source-sink dynamic wherein Chordin predominantly binds BMP ligands in the dorsal regions, allowing the formation of a diffusive gradient throughout ventral regions (Zinski et al., 2017).

BMPs also function in later stages of development to regulate processes such as specification neural versus non-neural ectoderm (Tanabe and Jessell, 1996; Wilson and Hemmati-Brivanlou, 1995), patterning of the neural tube by opposing notochord-derived Shh (Tanabe and Jessell, 1996), and many others (reviewed in (Wang et al., 2014)).

1.5. Early eye patterning and BMP signaling

Cells within the developing eye require information about their relative position within the tissue. Early retinal cells are provided this information through the expression of spatially restricted genes, whose activation is dependent upon morphogen patterning signals across both the nasal-temporal (NT) and dorsal-ventral (DV) axes of the eye. This will determine the boundaries for expression of axon guidance molecules, Eph ligands and Ephrin receptors, that allow the spatial organization of retinal ganglion cells (RGCs) in the retina to be preserved in that of their axons innervating the primary visual processing center of the brain (optic tectum in zebrafish, visual cortex in humans). By separating the eye into four quadrants, nasal, temporal, dorsal and ventral, patterning across both the NT and DV axes is necessary for correct topographical projections from the retina to the brain and therefore successful visual processing (reviewed in (Lemke and Reber, 2005)).

Patterning of the NT axis is initiated as the optic vesicle is beginning to evaginate at 11.5-12 hpf. Fgf ligands (Fgf3, Fgf8) emanating from the dorsal forebrain will signal to the presumptive nasal retina, as does Fgf24 from the olfactory placode (Picker and Brand, 2005; Picker et al., 2009). Together they activate expression of *forkhead-box transcription factor gl (foxgl)* in the nasal retina, while repressing *foxdl* expression in the temporal retina (Picker et al., 2009). Foxd1 and Foxg1 antagonize one another to maintain NT

identity, thereby preserving proper retinotectal mapping (Picker et al., 2009; Takahashi et al., 2009).

In zebrafish, DV patterning of the optic vesicles is initiated immediately after their formation by *growth differentiation factor 6a* (*gdf6a*) expressed in, and secreted from, extraocular ectoderm next to the presumptive dorsal eye starting at 11 hpf (French et al., 2009; Kruse-Bend et al., 2012). Previously shown to be required for the expression of multiple dorsal retina genes, we now know that Gdf6a is necessary to induce the first expression of the dorsal retinal transcription factor *t-box5a* (*tbx5a*) (Adler and Belecky-Adams, 2002; Asai-Coakwell et al., 2007; Chang and Hemmati-Brivanlou, 1999; French et al., 2009; Hanel and Hensey, 2006). Similarly, *bmp2b* is expressed in extraocular ectoderm between 11-15 hpf, and dorsal gene expression is never initiated correctly in *bmp2b* mutant embryos, suggesting it also is necessary to induce dorsal retinal fate. Importantly, loss of *gdf6a* does not alter *bmp2b* expression, implying that Gdf6a does not act upstream of *bmp2b*. Instead, Bmp2b likely acts up stream of *gdf6a*, as *bmp2b* mutants lack the non-neural ectoderm from which Gdf6a is normally secreted (Nguyen et al., 1998); as such, *gdf6a* expression adjacent to the presumptive dorsal retina is lost (Kruse-Bend et al., 2012).

The requirement of Gdf6a to suppress ventral identity is clear, as both *gdf6a* mutants and morphants display profound dorsal expansion of ventral marker genes (ex. *vax2*, *ephb2*, *aldh1a3*; (French et al., 2009; Gosse and Baier, 2009)). However, ventral gene repression by Gdf6a is accomplished independently of Tbx5a, as morpholino knockdown of Tbx5a activity does not alter ventral marker gene expression (French et al., 2009). *bmp4* is also expressed downstream of Gdf6a in the dorsal retina and, similar to in chick, mouse and *Xenopus* (Behesti et al., 2006; Koshiba-Takeuchi et al., 2000; Sasagawa et al., 2002), overexpression of *bmp4* in zebrafish causes expansion of dorsal markers at the expense of ventral markers, thereby also implicating it in promotion of dorsal fate (Gosse and Baier, 2009). Similar to Bmp2b, this effect is dependent upon Gdf6a, as the effect of *bmp4* overexpression is abolished in *gdf6a* mutant embryos (Gosse and Baier, 2009). Importantly, loss of *bmp4* in zebrafish does not alter expression of *tbx5a*, *gdf6a*,

ephB2a or *vax2*, suggesting it does not participate in dorsal retinal identity initiation (French et al., 2009; Kruse-Bend et al., 2012).

Dorsal retinal identity and subsequent expression of dorsal marker genes is an integral component of DV axis patterning in the eye, but equally important is their absence from the ventral eye. Dorsal and ventral retina identities mutually inhibit one another to ensure neither fully encompasses the retina. Ventral identity is induced by Shh emanating from the ventral midline and optic stalk and similarly induces the expression of ventral marker genes such as *ventral anterior homeobox 1* (*vax1*) and *vax2*. As such, overexpression of Shh expands ventral retinal identity and gene expression (Ekker et al., 1995; Sasagawa et al., 2002; Take-uchi et al., 2003; Zhang and Yang, 2001). Retinoic acid (RA) is thought to play a role in promoting ventral identity, based on the expression patterns of retinoic acid synthesis and degradation enzymes at the dorsal and ventral poles of the retina. Additionally, restriction of RA precursor molecules in quail causes ventral expansion of *Bmp4* as would be expected with reduced ventral identity, possibly through modulating dorsal Wnt signaling. The relationship between RA and ventral retinal identity appears to be more complicated, though; instead of simply ventral expansion, *Tbx5* and *Bmp4* are ectopically expressed in the presumptive RPE (Halilagic et al., 2007). Additionally, treatment of zebrafish with the pharmacological RA inhibitor AGN causes a significant reduction in *vax1* expression in the optic stalk and ventral retina, but not *vax2* (Lupo et al., 2005). Additional conflicting studies in mouse (Molotkov et al., 2006) and chick (Golz et al., 2004) further reinforce this uncertain connection between RA and ventral retinal identity and gene expression.

Similar to the requirement for a balance between *foxg1* and *foxd1* transcription factors in the NT retina, restriction of *tbx5a* and *vax2* to the dorsal and ventral retina, respectively, is necessary for correct retinal gene expression and retinotectal mapping (Barbieri et al., 2002; French et al., 2009; Koshiba-Takeuchi et al., 2000). The mechanism responsible for maintaining nasal versus temporal retinal identity, where *Foxd1* and *Foxg1* reciprocally inhibit expression of one another, is similarly seen in preservation of optic cup versus optic stalk identity; *Pax2* and *Pax6*, respectively found in optic stalk and cup, mutually inhibit promoter/enhancer activity of the other to precisely maintain tissue

boundaries. When the activity of Pax2 is lost, the *Pax6* expression domain expands and vice versa, as do the tissue identities and characteristics that each transcription factor imparts (Schwarz et al., 2000). However, a direct reciprocal inhibition mechanism does not appear to exist between Tbx5a and Vax2. This is initially suggested by their relative expression domains, as there is a significant space between the ventral-most edge of *tbx5a* and dorsal-most edge of *vax2* expression domains, unlike the immediately adjacent expression of *foxd1/g1* or *pax2/6*. Additionally, loss of *tbx5a* does not result in expansion of *vax2* expression, nor does loss of *vax2* necessarily cause expansion of *tbx5a* (Mui et al., 2005). It is therefore not well understood what factors directly antagonize dorsal versus ventral fate in the developing retina.

The absence of reciprocal repression between *tbx5a* and *vax2* suggests that there may be factors upstream of each that are responsible for repressing dorsal or ventral identity. This is supported by morphant, mutant and overexpression data for *gdf6a*; when Gdf6a activity is lost, the retina becomes effectively ventralized and *vax2* expression expands throughout (French et al., 2009; Gosse and Baier, 2009; Kruse-Bend et al., 2012). The opposite is seen when *gdf6a* is overexpressed, where *tbx5a* expression and dorsal identity is expanded but does not fully encompass the retina, as is seen in *vax2* expansion in ventralized eyes (French et al., 2009). A corresponding ventrally localized inhibitor of dorsal identity has not yet been characterized. Since BMP ligands act in the dorsal eye, a natural hypothesis was that members of the Chordin, Noggin and Follistatin group of BMP inhibitors may restrict BMP signaling from the ventral eye. Indeed, Ventroptin, a novel BMP inhibitor related to Chordin, antagonizes dorsal BMP ligands and specifies ventral fate in development of the chick retina (Sakuta et al., 2001). However, *ventroptin* appears to be a chick-specific gene and its expression has not yet been identified in any other organism, and therefore direct ventral antagonism of BMP signaling has yet to be fully understood.

1.6. Introduction to Wnt signaling

Wnt signaling encompasses a group of morphogen signaling pathways with wide and diverse functions in development. The name “Wnt” comes from a combination of two names given to the same gene, discovered independently; *integration 1*, named in a mouse model of breast cancer, and *wingless*, discovered in the *Drosophila* mutant screen by Christiane Nüsslein-Volhard and Eric Wieschaus. Since its discovery, the Wnt signaling pathway has been the focus of immense research efforts in embryonic development, adult tissue homeostasis, disease and disease treatments.

There are two main Wnt signaling pathways, canonical/ β -catenin and non-canonical/planar cell polarity (PCP) signaling (Fig. 1.3). Wnt/ β -catenin signaling results in alterations to target gene transcription in cells receiving the signal, while PCP signaling instead results in alterations to the actin cytoskeleton to control cell shape and polarity. While a third Wnt pathway, Wnt/calcium signaling, may have a role in photoreceptor cell type specification (Yu et al., 2004), it does not appear to regulate steps in early eye morphogenesis.

In general, Wnt/ β -catenin signaling is activated when extracellular Wnt ligands bind cell surface proteins called Frizzled (Fzd) receptors and low-density lipoprotein receptor-regulated protein (LRP) co-receptors. These receptor complexes transduce signals that alter a group of proteins termed the β -catenin destruction complex, whose core members include glycogen synthase kinase 3 β (GSK-3 β), adenomatous polyposis coli (APC), Axin and casein kinase 1 (CK1). When Wnt ligands are not present, cytoplasmic β -catenin is bound by the β -catenin destruction complex and targeted for proteasomal degradation. Upon activation of Fzd receptors, the β -catenin destruction complex is translocated to the receptor at the plasma membrane, as is another protein called Dishevelled (Dsh). Axin in the destruction complex is bound by the intracellular portion of LRP and becomes de-phosphorylated, while Dsh inhibits the GSK3 activity of the complex (Bhanot et al., 1996; Noordermeer et al., 2011). Ultimately, this results in increased cytoplasmic accumulation of β -catenin, allowing it to translocate into the nucleus where it binds T cell-specific transcription factor/lymphoid enhancer-binding factor 1 (TCF/LEF) to regulate the expression of downstream genes (Billin et al., 2000) (Fig. 1.3). The various

roles of this signaling pathway in development, disease and emerging therapeutics are reviewed in Nusse and Clevers (2017), and its roles in development and adult homeostasis are reviewed in (Steinhart and Angers, 2018).

The Wnt/PCP pathway uses many of the same proteins as canonical Wnt signaling, though its downstream effectors and biological functions vary. Though potentially all Wnt ligands may be able to activate either pathway in certain contexts, Wnt11 and Wnt5 most commonly activate the non-canonical Wnt pathway. This is usually accomplished through LRP-independent binding of Fzd5/6, though co-receptors such as Van Gogh-like (Vangl) are involved in some contexts. Similar to canonical Wnt signaling, PCP activation recruits Dsh to the plasma membrane, but activated Dsh instead complexes with dishevelled associated activator of morphogenesis 1 (Daam1) to signal through three main intracellular pathways that regulate cell movements and polarity in development (Fig. 1.3) (reviewed in (Butler and Wallingford, 2017)).

1.7. Early eye development and Wnt signaling

Both canonical Wnt and PCP signaling have roles in eye development, though the actions of canonical Wnt signaling are perhaps better understood. As previously mentioned, Rx genes are expressed specifically in the eye field and restricted from presumptive forebrain tissue. Rx will inhibit canonical Wnt signaling to prevent posteriorization of the anterior forebrain and to promote eye field fate (Martinez-Morales and Wittbrodt, 2009; Wilson and Houart, 2004). In zebrafish, mid-gastrula transplantation experiments show that cells overexpressing Wnt8b locally suppresses early eye field marker expression in nearby cells by signaling through Fzd8a, but overexpression of a dominant negative Wnt8 (Hoppler et al., 1996) results in expansion of the eye field at the expense of posterior diencephalic fates (Cavodeassi et al., 2005), suggesting canonical Wnt signaling antagonizes eye field specification. In contrast, loss of the non-canonical ligand activity (Wnt5 and Wnt11) results in reduced eye field specification and failure of segregation (Cavodeassi et al., 2005).

Canonical Wnt signaling is additionally required for lens development, choroid fissure closure (Lieven and R  ther, 2011; Veien et al., 2008), and RPE development ((Fujimura et al., 2009; Westenskow et al., 2009); reviewed in (Fujimura, 2016)). Zebrafish *fzd5* is specifically expressed in early eye field progenitors and mediates non-canonical signaling (Cavodeassi et al., 2005), but in *Xenopus* Fzd5 acts in the canonical Wnt pathway to regulate Sox2 in order to control the neural potential of retinal progenitors (Van Raay et al., 2005). Additionally, *Fzd5* appears to have a role in morphogenesis of the optic cup itself, as mice carrying homozygous *Fzd5* mutations have defects in choroid fissure closure and although they have changes to dorsal and ventral marker gene expression, both dorsal *Tbx5* and ventral *Vax2* are reduced, suggesting it is not simply a loss of canonical Wnt activity and therefore a reduction in dorsal identity that leads to fissure closure defects (Liu and Nathans, 2008).

While there are close to 20 or more identified Wnt ligands in zebrafish, only three have characterized expression within the developing eye: *wnt11r* has lens-specific expression and both *wnt2* and *wnt8b* are expressed in the RPE beginning at approximately 14-16 hpf. Morpholino knockdown of *wnt2* and *wnt8b* produces no overt phenotype, but modulating the Wnt pathway through expression of a heat shock-inducible Wnt inhibitor (*dickkopf 1*, *dkk1*) or repression of Wnt target genes using a heat shock-inducible dominant-repressive form of Tcf3 reveals robust changes to DV patterning (Veien et al., 2008). This likely reflects, in part, functional redundancy in Wnt ligands and/or the presence of additional Wnt ligands acting in the eye.

While BMP signaling is responsible for initiation of dorsal identity in the eye, canonical Wnt signaling is subsequently required to maintain expression of dorsal gene expression. Veien et al. (2008) showed that *tbx5a* expression in zebrafish is turned on in the dorsal eye immediately after optic vesicle evagination and while disruption of canonical Wnt signaling results in reduced maintenance of dorsal marker gene expression, it has no effect on the initiation of these genes. As such, we discuss retinal patterning in two distinct phases of initiation and maintenance, where there are different signaling requirements in each. In zebrafish, the requirement of Wnt signaling in eye patterning begins between 14 and 16 hpf (Veien et al., 2008), approximately 2-4 hours after optic

vesicle evagination begins. While initiation of dorsal identity depends upon extraocular morphogens, maintenance is instead performed by expression of morphogens within the eye itself (Kruse-Bend et al., 2012; Veien et al., 2008). Wnt ligands *wnt2* and *wnt8b* are expressed in the retinal pigmented epithelium (RPE) and signal to dorsal retinal cells where they are not only required for dorsal marker genes such as *aldh1a2*, *tbx5a* and *bamb1a*, but also to maintain expression of BMP ligands *gdf6a*, *bmp2b* and *bmp4* in the dorsal retina (Veien et al., 2008). These data are also supported by work in mouse where mutations in the Frizzled co-receptor *Lrp6* cause a similar loss of dorsal *Tbx5* and *Bmp4* expression and expansion of ventral *Vax2* expression (Zhou et al., 2008; Zhou et al., 2010).

1.8. Introduction to microphthalmia, anophthalmia and coloboma (MAC)

As previously discussed, an evolutionarily conserved hallmark of vertebrate eye development is the formation of the choroid or optic fissure within the ventral eye, allowing vasculature to enter and nourish the eye and retinal ganglion cell axons to exit to innervate the brain. The choroid fissure progressively fuses before 60 hpf in zebrafish, or between the 5th and 7th week of human fetal development. Failure of choroid fissure fusion can lead to ocular coloboma, a disease typically characterized by absent tissue or a gap in any ocular layer that is consistent with aberrant closure of the choroid fissure (Onwochei et al., 2000). Coloboma is estimated to occur at 1/4000 live births, and together with the etiologically related disorders microphthalmia (small eyes; 1/7000 est. prevalence) and anophthalmia (no eyes; 1/30,000 est. prevalence), represents the second leading cause of pediatric blindness at 3-11% of cases world wide (Morrison et al., 2002; Onwochei et al., 2000; Shah et al., 2011; Verma and FitzPatrick, 2007).

Collectively referred to as MAC, these disorders can present in one or both eyes (unilateral or bilateral, respectively). In cases of anophthalmia, some eye tissue may remain, but true anophthalmia is classified by the complete absence of the eye globe and associated structures such as the optic nerve (Gerth-Kahlert et al., 2013). The underlying mechanisms that cause MAC spectrum defects are far from fully understood, though presentation is almost certainly affected by which step during eye development has been

perturbed. For example, aberrant eye field specification or optic vesicle evagination typically result in severe microphthalmia or anophthalmia, while problems arising in later steps during eye development, such as tissue fusion between choroid fissure lobes, may result in isolated coloboma with very few additional ocular defects.

Coloboma may affect any ocular tissue layer, including but not limited to the iris, ciliary body, retina, choroid and optic nerve. The degree to which ocular coloboma affects vision depends upon not only the severity of the coloboma, but also where within the eye it occurs. For example, patients with iris coloboma may experience little to no effect in vision, as the eye is still able to function properly. However, colobomata that affect the retina or optic nerve can lead to severe or complete blindness. Interestingly, coloboma of other eye tissues may present simultaneously with lens coloboma, even though the lens never displays a ventral fissure during development (Li et al., 2011).

There is a strong genetic component to the disease, and as such it is found at a higher prevalence in populations with high degrees of consanguinity (Hornby et al., 2000; Shah et al., 2011). Coloboma occurrence is also thought to be sensitive to environmental risk factors such as vitamin A deficiency (Hornby et al., 2002; Rahi et al., 1995). Importantly, as many as 39 genes have been implicated in causality of MAC spectrum disorders (reviewed in (Patel and Sowden, 2017; Williamson and FitzPatrick, 2014)). However, this is estimated to represent only a fraction of cases, highlighting the need for continued study not only of underlying genetic lesions in humans, but of genes involved in regulating eye development. The incidence of MAC spectrum disorders can also occur as part of a number of different multisystem syndromes. For example, diseases such as Waardenburg anophthalmia, renal-coloboma syndrome, and CHARGE syndrome (coloboma, heart anomaly, choanal atresia, growth or mental retardation, genital and ear anomalies) can all present with MAC spectrum phenotypes (Williamson and FitzPatrick, 2014).

1.9. Morphogens and MAC

Though Fgf signaling is relatively well characterized in nasal-temporal (NT) patterning of the retina (discussed in section 1.5) and proximal-distal patterning of the optic cup (Adler and Canto-Soler, 2007; Hyer et al., 2003; Martinez-Morales and Wittbrodt, 2009), it has only briefly been discussed in the context of choroid fissure closure, possibly due to a lack of viable models of Fgf deficiency. To get around this, a study in mouse examined optic vesicle-specific deletions of two Fgf receptors, *Fgfr1* and *Fgfr2*, and found that they caused optic disc (retina and optic stalk interface) and nerve dysgenesis resulting in ocular coloboma. This likely represents an additional function for Fgfs in eye development, as *Fgfr1/2* deficiency caused fissure closure defects without affecting axial patterning of the optic cup (Cai et al., 2013).

Sonic hedgehog is not only important for development of the eye itself but proper patterning of the brain tissue from which the eye is derived. As such, mutations affecting the core pathway components of Shh signaling often lead to holoprosencephaly (failed separation of cerebral hemispheres) and other severe birth defects, which either preclude or complicate the study of the requirement of Shh in human eye development. Null or hypomorphic alleles in the *SHH* gene itself are likely incompatible with life in most cases but one such instance exists where a novel mutation in *SHH* was found in a family with non-syndromic colobomatous microphthalmia (Schimmenti et al., 2003). Additionally, mutations in direct targets of Shh (*PAX2* and *PAX6*) and a transmembrane inhibitor bound by Shh protein (*PTCH1*) can cause variable MAC spectrum disorders (Azuma et al., 2003; Ribeiro et al., 2006), reviewed in (Williamson and FitzPatrick, 2014).

One of the most common genes mutated in patients with MAC is *aldehyde dehydrogenase 1a3* (*ALDH1A3*), which codes for an RA synthesis enzyme. Patients with *ALDH1A3* mutations display highly variable phenotypes, both in type and severity of MAC and are thought to represent up to 10% of MAC cases (Abouzeid et al., 2014; Aldahmesh et al., 2013; Fares-Taie et al., 2013; Mory et al., 2014; Roos et al., 2014); reviewed in (Williamson and FitzPatrick, 2014)). Unlike *ALDH1A3* mutations, which cause non-syndromic MAC, mutations in an RA pathway transporter protein, *STRA6*, and a nuclear RA receptor, *RAR β* , can cause syndromic cases of MAC (Slavotinek et al., 2012;

Williamson and FitzPatrick, 2014). The role of RA in eye development has yet to be fully understood, but studies in model organisms have shown that RA regulates choroid fissure closure and ventral eye development (Hyatt et al., 1996; Lupo et al., 2011). The expression of RA synthesis enzymes is exquisitely regulated in the vertebrate eye and is only found in narrow domains surrounding both the choroid and dorsal fissures (Duester, 2009; Rhinn and Dollé, 2012). It is yet unclear what cells are the target of ocular RA; one possibility is that it is signaling to incoming periocular mesenchyme and therefore indirectly regulates eye development and fissure closure (Lupo et al., 2011; Matt et al., 2005).

The roles for canonical Wnt and Wnt/PCP signaling in eye development have been previously discussed in section 1.7, including requirements at multiple steps in eye development such as eye field specification, optic vesicle evagination, RPE development and dorsal-ventral patterning of the retina. Many of these studies circumvent complications in functional redundancy of Wnt ligands by using alternative methods to genetic mutations that more broadly affect the pathway (ex. inducible overexpression of inhibitors, dominant negative ligands, dominant repressive transcription factors). There are, however, genetic models for other Wnt pathway components. Mice carrying heterozygous mutations in the Wnt inhibitor *Dkk* have both ocular coloboma and anterior segment defects (Lieven and Rütther, 2011). Consistent with roles for canonical Wnt signaling in DV patterning, *Lrp6* mutant mice display defects in DV marker genes and obvious microphthalmia and fissure closure defects (Zhou et al., 2008). Though this study and others definitively link changes in DV axis patterning and failure of the optic fissure to close, the exact mechanism by which patterning regulates closure is still unclear. Additionally, no component of the Wnt pathway has been implicated in causality of MAC in humans (Williamson and FitzPatrick, 2014).

Similar to Wnt signaling, TGF β /BMP signaling is heavily involved in patterning of the developing eye and events controlling optic cup morphogenesis (discussed in section 1.5). Two different BMP ligands that are expressed in the dorsal eye in zebrafish and other vertebrate model organisms, *gdf6a* and *bmp4*, have multiple alleles identified in patients with varying presentation and severity of MAC, usually in combination with skeletal or other extraocular phenotypes (Asai-Coakwell et al., 2009; Bakrania et al., 2008; den

Hollander et al., 2010; Reis et al., 2011; Ye et al., 2010; Zhang et al., 2009). *Bmp7* is also known to regulate multiple aspects of eye morphogenesis, as mice carrying homozygous *Bmp7* mutations show defects in choroid fissure invagination, optic disc, nerve and vasculature, and reduced expression of *Pax2* in the ventral eye (Zhang et al., 2013). Correspondingly, mutations in *BMP7* can cause various types of coloboma, microphthalmia, anophthalmia and multiple extraocular systemic abnormalities (Dudley et al., 1995; Wyatt et al., 2010). Lastly, multiple different mutations in *GDF3* were found in patients with ocular anomalies, including microphthalmia and coloboma, with and without additional extraocular phenotypes (Ye et al., 2010). More recently, an additional patient carrying an already identified missense mutation was reported to have unilateral anophthalmia (Bardakjian et al., 2017), further highlighting how variable and apparently stochastic the presentation of MAC phenotypes can be.

1.10. Purpose of study and summary of research

Overall, in this thesis I will focus on two main developmental signaling pathways, Wnt and TGF β /BMP signaling, and their roles in early retinal development, choroid fissure closure and ocular coloboma. We hope to expand not only our understanding of vertebrate eye development, but also that of the genetic lesions that can cause ocular coloboma in humans.

Wnt and BMP signaling are known to work together to pattern the DV axis in the developing retina; their activities in the dorsal eye are essential, as is their absence from the ventral eye, though it is unclear exactly how the DV boundary is maintained. Chapter 3 will assess the roles of a group of extracellular Wnt modifiers, secreted frizzled-related proteins (Sfrps), in retinal patterning and fissure closure. We show that Sfrp proteins function to inhibit Wnt signaling in the ventral eye to assist in maintaining the balance between dorsal and ventral retinal identity. Unexpectedly, we also characterize a role for Sfrps in modulating the BMP signaling pathway in a dose-dependent manner, not only to inhibit BMPs ventrally where Sfrp protein is present in high concentrations, but possibly to

facilitate their diffusion and promote BMP signaling in the dorsal eye where Sfrp concentrations are much lower.

Chapter 4 will also address Wnt signaling in eye development. Fzd5 expression is precisely restricted to the eye field and is thought to be involved in Wnt/PCP signaling during specification of eye field versus forebrain cell fates and subsequent organization of cells during optic vesicle evagination. Studies in other organisms, though, have shown that Fzd5 is also able to transduce canonical Wnt signals. Given that canonical Wnt is also critical to forebrain and eye development, we used mouse and zebrafish studies to investigate the role of Fzd5 in optic cup morphogenesis and fissure closure, and we attempt to determine the pathway on which it functions. Additionally, through extensive analysis of a large coloboma pedigree, we characterize a frameshift allele in *FZD5* and its effect on eye development, representing the first report of mutations in a Wnt pathway member implicated in a structural ocular disorder in humans.

Rare reports in the literature describe incidences of “atypical coloboma” where the presentation is not consistent with failure of the choroid fissure to fuse. A subset of these reports, combined with patients with ocular coloboma but oriented dorsally instead of ventrally, hinted at the existence of another possible developmental fissure in the eye. In chapter 5, we use a combination of patient sequencing and experiments in model organisms to characterize a novel structure in the vertebrate eye, the superior fissure, and describe the existence of a rare form of coloboma resulting from failed superior fissure closure. Additionally, we show that the superior fissure is likely a conduit for early vasculature in the dorsal eye and that a balance of BMP and Shh signaling across the dorsal-ventral axis is integral to timely closing of the superior fissure.

The signaling pathways regulating early eye development leading up to choroid fissure fusion are not yet fully understood. However, even more poorly understood are the molecular events that accomplish tissue fusion between the fissure lobes. Chapter 6 will investigate a novel player in the process of choroid fissure fusion, the TGF β ligand, Bmp3. Sequencing of patients with coloboma and microphthalmia in both a pedigree and an unrelated MAC panel identified deleterious missense mutations in *BMP3*. Through *in vivo* and *in silico* modeling of the BMP3 variants identified, as well as analysis of *bmp3* mutant

zebrafish, we test the hypothesis that Bmp3 is a novel ligand that controls ocular fissure closure.

Taken together, this thesis will add to our understanding of the complex roles of morphogen signaling pathways in vertebrate eye development and MAC spectrum disorders.

1.11. Figures

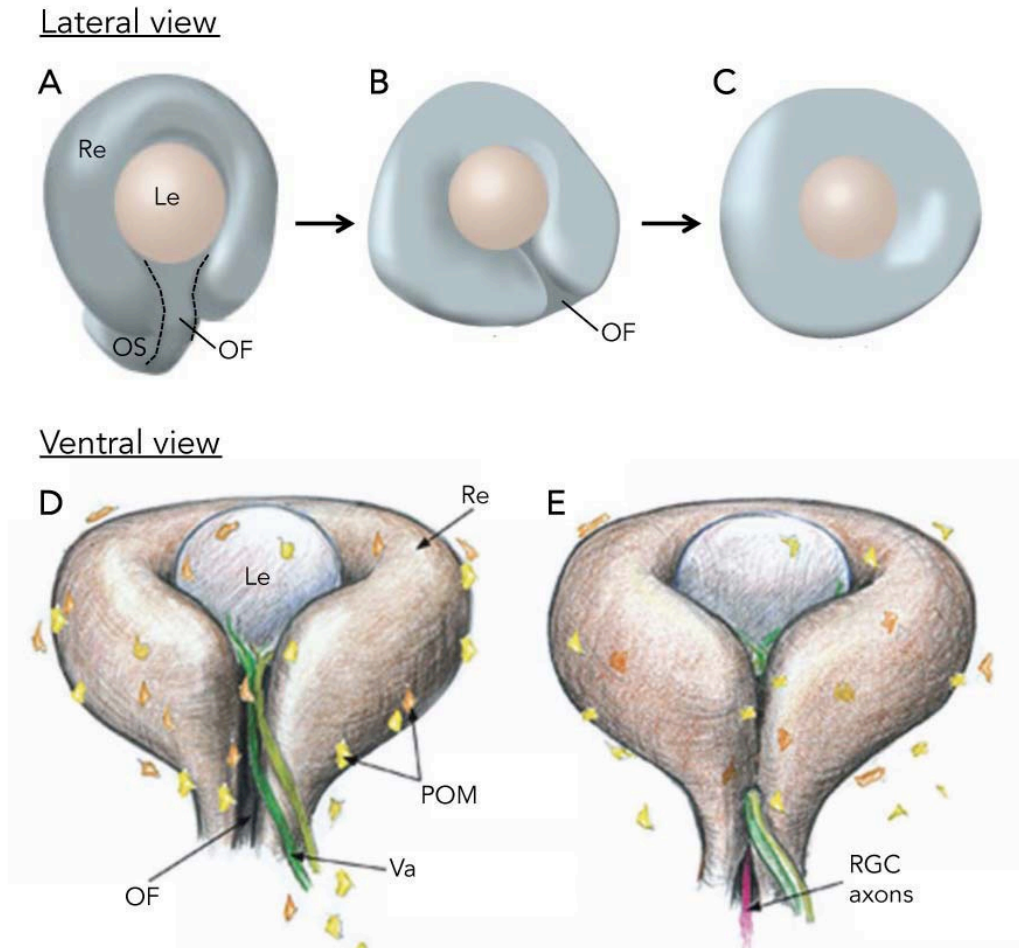


Fig. 1.1 Overview of ocular fissure development and closure. The ocular fissure (OF; dashed outline) forms in the ventral retina (re) and extends down the optic stalk (OS), beginning soon after lens (le) formation (A). Morphogenetic events cause the fissure lobes to come in close proximity (B), permitting tissue breakdown at the fissure site and fusion of the lobes to complete the globe of the eye (C). Ventral views of the developing ocular fissure pre-fusion (D), highlighting the neural crest- and mesoderm-derived perocular mesenchyme (POM) surrounding the eye and the invading vasculature (Va). Fusion of the ocular fissure (E) begins centrally and progresses both proximally toward the brain and distally toward the lens, surrounding the retinal ganglion cell (RGC) axons projecting to the brain to form the optic stalk. A-C modified from original by Dr. Caroline Cheng; D-E adapted with permission from Gestri et al. (2012).

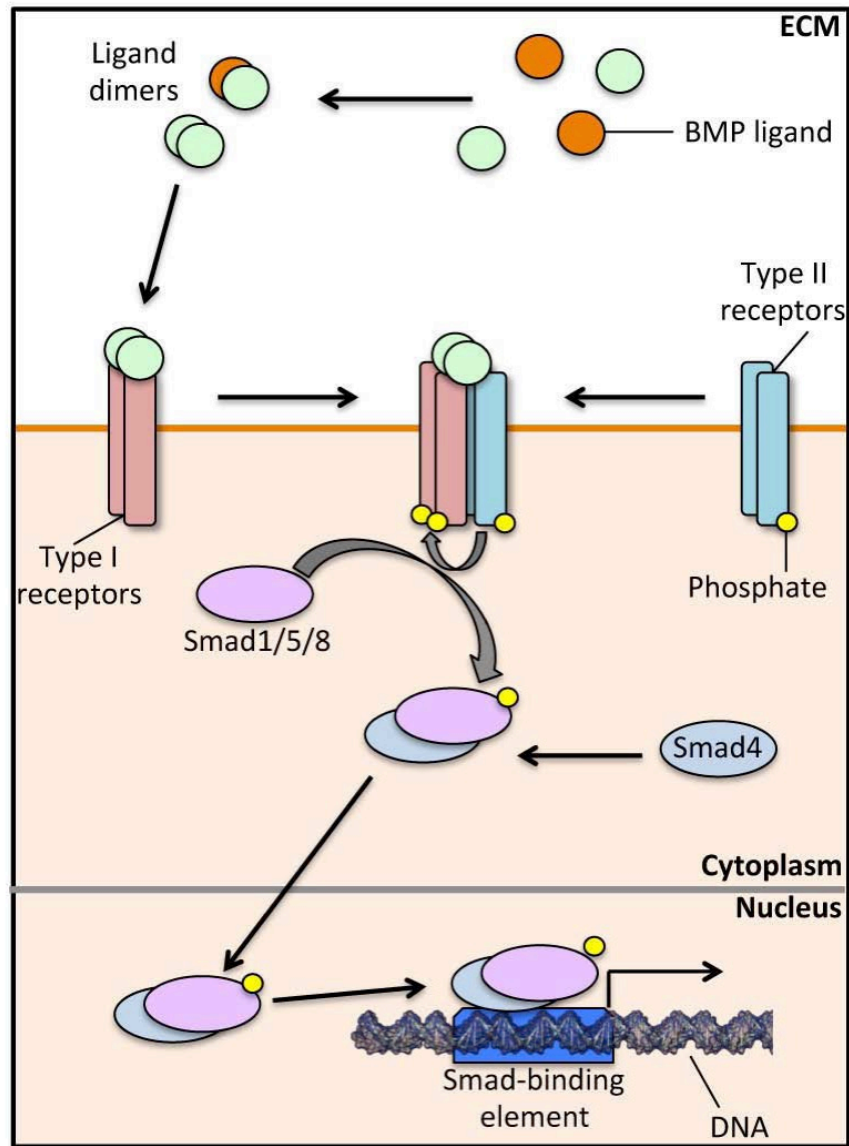


Fig. 1.2 Bone morphogenetic protein (BMP) signaling. BMP ligand homo- or heterodimers bind Type I BMP receptors (red) on the cell surface, recruiting constitutively active Type II receptors (blue) to form a heterohexameric complex. Type II receptors cross-phosphorylate Type I receptors to activate them, enabling them to activate receptor-regulated Smad1/5/8 proteins. pSmad1/5/8 proteins complex with a required co-Smad4, translocate into the nucleus where they bind Smad-binding elements to regulate the expression of target genes.

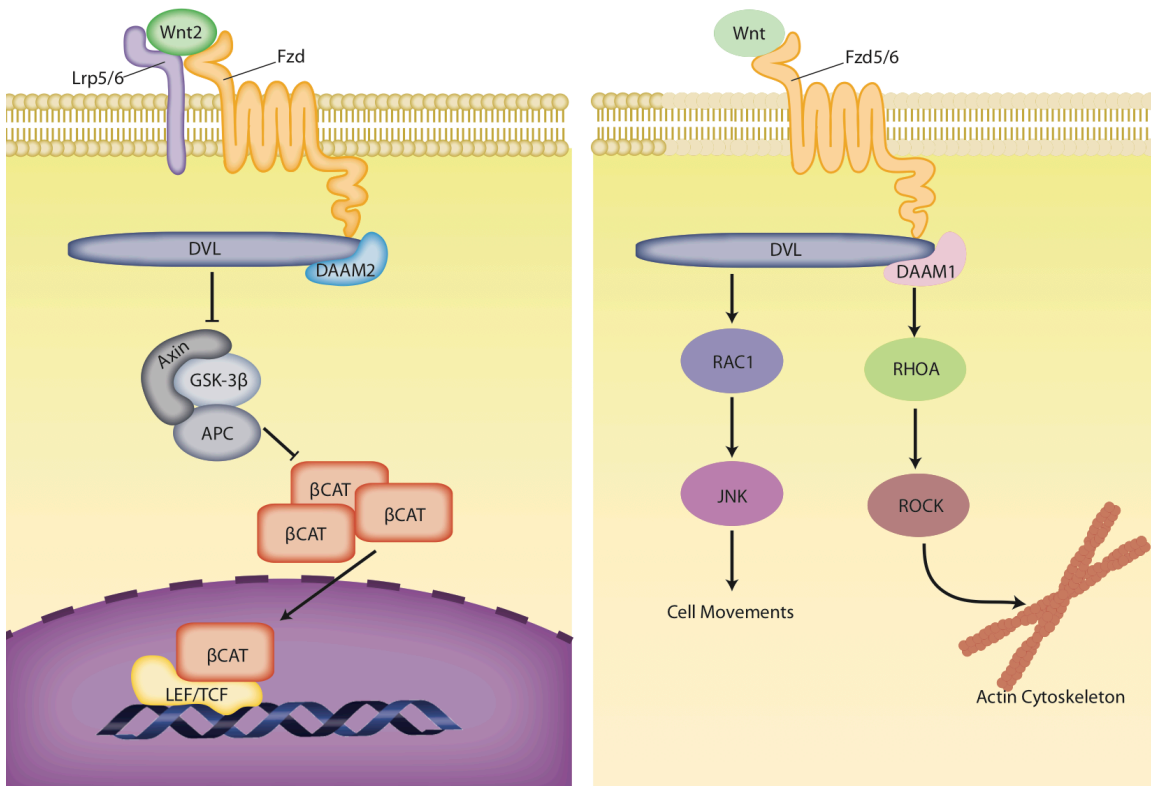


Fig. 1.3 Canonical Wnt/ β -catenin and non-canonical Wnt/PCP signaling. In canonical Wnt signaling (**Left**), extracellular Wnt ligands bind the cysteine-rich ligand binding domain of Frizzled receptors and the required co-receptor LRP5/6. Ligand binding stimulates the intracellular domain of the Frizzled receptor to recruit both DVL and DAAM2 to the plasma membrane, resulting in sequestration and DVL-mediated inhibition of a complex of proteins termed the β -catenin destruction complex (primarily comprising Axin, GSK-3 β , and APC). This relieves inhibition on β -catenin, allowing it to accumulate in the cytoplasm and translocate into the nucleus, where it binds with transcription factors LEF/TCF to mediate the expression of downstream genes. Non-canonical Wnt/PCP signaling (**Right**) is also stimulated by extracellular ligands binding Frizzled receptors, but is independent of LRP5/6 co-receptors. This similarly results in DVL recruitment to the membrane with DAAM1, but instead this triggers a cascade of kinase activity to modify the actin cytoskeleton, controlling cell shape and polarity. Original figure acknowledgement: Dr. Caroline Cheng.

Chapter 2

Materials and Methods

2.1. Ethics, animal care and general procedures

Embryonic, larval and adult zebrafish were cared for according to guidelines set by the Canadian Council of Animal Care and protocols were approved by the University of Alberta's Animal Care and Use Committee (Protocol #427).

Embryos were raised at 25.5°C, 28.5°C or 33°C in embryo media (EM) and staged according to developmental hallmarks (Kimmel et al., 1995). For all injections, 1000 units penicillin/0.1mg/mL streptomycin (Sigma) was added to EM. Zebrafish embryos grown past 24 hours post fertilization (hpf) were treated with 0.004% 1-phenyl 2-thiourea (PTU; Sigma-Aldrich) before 22 hpf to prevent pigmentation. Anesthesia of larvae or adults was performed with a 4% dilution of 0.4% tricaine stock solution prior to fixation or imaging, or for termination as needed. Zebrafish were fixed at appropriate developmental stages in 4% paraformaldehyde (PFA) in PBS (Phosphate Buffered Saline; 137mM NaCl, 2.7mM KCl, 10mM NaH₂PO₄, 1.75 mM KH₂PO₄, pH 7.4) at room temperature for 5 hrs or overnight at 4°C on a rotating platform, unless otherwise stated.

Experiments on wild type embryos used the AB wild type strain, unless otherwise stated. Transgenic zebrafish lines used include *Tg(hsp701:dkk1b-GFP)^{w32}*, *Tg(rx3:GFP)*, *Tg(kdrl:eGFP)^{la116}*, *Tg(BMPRE-AAV.Mlp:eGFP)*, *Tg(kdrl:mCherry)^{ci5}*, and *Tg(TOP:dGFP)^{w25}* (Choi et al., 2007; Collery and Link, 2011; Dorsky et al., 2002; Proulx et al., 2010; Rembold et al., 2006; Stoick-Cooper et al., 2007). Mutant lines used include *gdf6as³²⁷* (Gosse and Baier, 2009), *tbx2b^{by}* (Snelson et al., 2008), *cyp1b1* (see section 2.5), and *bmp3^{ua1020}* (see section 2.6). The *gdf6as³²⁷* mutation encodes a S55X truncation producing a 54 amino acid peptide lacking the mature domain. The *tbx2b^{by}* mutation is a point mutation resulting in a T>A substitution, resulting in a premature stop codon within the T-box sequence. The *bmp3^{ua1020}* mutation is described in Chapter 6.

The experiments in Chapter 5 on chick and mouse was performed at the University of Texas and approved by their institutional animal care committee (#2015–00089).

Animal Care and Use Committee of the National Eye Institute approved all procedures involving the use of mice in Chapter 4. *Fzd5* and *Fzd8* compound mutants were created and maintained as described previously (Liu et al., 2012).

2.2. Morpholinos

All morpholino experiments were performed using morpholino oligonucleotides (MOs) from GeneTools that were resuspended and diluted in nuclease-free water or Danieau solution. They were first heated at 65°C for 10 mins and allowed to cool before injecting into 1–2 cell stage zebrafish embryos. The sequences of MOs used and additional information about them can be found in Table 2.1.

2.3. Heat shock experiments

Heat shock experiments using *Tg(hsp701:dkk1b-GFP)^{w32}* were performed on transgenic heterozygous outcrosses to wild type by incubating embryos in a microfuge tube at 39°C from 12-14 hpf. They were then screened for GFP fluorescence prior to fixation at 15 hpf and used for subsequent in situ hybridization. The effectiveness of the heat shock treatment was assessed by recapitulation of effects on BMP ligand expression reported in (Veien et al., 2008).

2.4. Live imaging

Prior to imaging, embryos in Chapter 3 were injected with indicated morpholino doses, then dechorionated at 18 hpf, laterally mounted in low melting point agarose (1.5%) and submerged in embryo media. Images were taken using a Zeiss Axio Imager Z1, Zeiss LSM700 laser confocal scanner, and a 20x water-emersion objective lens. The Zeiss Zen software was programmed to image every 10 mins over a span of 24 hrs, with ambient temperature maintained at 28°C.

Live zebrafish larvae in Chapter 4 were first anesthetized and then photographed in EM using an Olympus stereoscope with a Qimaging micropublisher camera.

Anesthetized live transgenic embryos shown in Chapter 5 were mounted laterally in a 35mm dish in 1% low-melting temperature agarose and imaged using a Zeiss W Plan-Apochromat 20x/1.0 water immersion objective and a Zeiss LSM700 laser scanning unit

mounted on a Zeiss Axioimager Z1 compound microscope. Z-stacks were made by taking optical slices at intervals of 2–3 μm for a total of $\sim 60 \mu\text{m}$, and maximum projections or surface projections were created from the resulting stacks using either ZEN (Carl Zeiss) or Imaris (Bitplane) software. All DIC images were taken on an Axiocam HR digital camera mounted on a Zeiss Axioimager Z1 compound microscope. Photos and videos were annotated, assembled and processed for brightness and contrast in Adobe Photoshop software.

2.5. TALEN mutagenesis

TALEN mutagenesis constructs targeting the Cyp1b1 cytochrome P450 domain (nts 924–977) were created by Golden Gate cloning (Cermak et al., 2011). The target region was TTCGGGGCCAGTCAAGACACtctgtctacagctCTCCAGTGGATCATCCTGCTA, with the spacer region shown in lowercase. 100 pg of RNA for each TAL construct was injected into one-cell stage zebrafish embryos and the offspring were screened for mutations by HRM. The 13 bp deletion causes a frameshift at aa317 (p.Cys317SerfsX23), followed by a stop codon at aa340.

2.6. CRISPR-Cas9 mutagenesis

Mutations in zebrafish *bmp3* were generated using CRISPR-Cas9. Target sites were designed using ChopChop and gene-specific oligos used are listed in Table 2.2. sgRNAs were generated according to (Gagnon et al., 2014) with the following changes: equal volumes of the gene-specific oligo and constant oligo were mixed (100 μM ; rehydrated in 1x tris-EDTA) with NEB buffer 3 and sterile water, to a total reaction volume of 20 μL . Microfuge tubes were then parafilmmed and submerged in a beaker of boiling water and allowed to cool passively to room temperature. Cas9 protein (PNA Bio, CP01) was reconstituted in sterile water to a concentration of 50 $\mu\text{g}/\text{mL}$ and 2 μL was mixed with 1 μL of each sgRNA for injections. One- or two-cell stage embryos were injected with 1 nL of Cas9/sgRNA mixture and allowed to grow to sexual maturity. Carriers of frameshift alleles

were identified using high resolution melt (HRM; described below) curve analysis and initially confirmed by Sanger sequencing.

2.7. Zebrafish genotyping

Primers used for all zebrafish genotyping assays can be found in Table 2.3. The offspring of *gdf6a* heterozygous incrosses were genotyped by high resolution melt (HRM) temperature analysis performed on genomic DNA extracted in 10 μ L of 50 mM NaOH (95°C, 10 minutes) and neutralized with 2 μ L Tris-HCl, pH 8.0. PCR was performed using primers optimized for HRM and Qiagen Master Mix on a Qiagen Rotor Gene Q qPCR machine (Qiagen). Conditions for amplification were 1 cycle at 95°C for 5 mins, 40 cycles of 95°C for 10 s, 55°C for 30 s, followed by HRM ramp from 70–90°C, 0.1°C per step.

Fish carrying the *cyp11b1* mutation were HRM genotyped as above using a 52°C annealing temperature for amplification. Results were analyzed via Qiagen software v2.02 (Qiagen) and variants initially confirmed by Sanger sequencing.

tbx2b^{by} mutants were genotyped by PCR followed by MseI restriction digest. Genomic DNA was extracted as above and diluted 1/10 in water for use as template. PCR was performed with ExTaq DNA Polymerase (TaKaRa Bio Inc.). Conditions for amplification were 1 cycle at 94°C for 2 min, 40 cycles of 94°C for 15 s, 58°C for 15 s, and 72°C for 20 s, followed by 1 cycle at 72°C for 3 mins. The PCR products were then digested with MseI (NEB) for 2 hrs and analyzed via gel electrophoresis using a 3% agarose gel.

bmp3^{ua1020} mutants were genotyped using PCR followed by gel electrophoresis. Genomic DNA was extracted in 20 μ L 50 mM NaOH (95°C for 15 mins) and neutralized with 2 μ L Tris-HCl, pH 8.0, then diluted 1/2 in sterile water to use for PCR template. PCR was performed with recombinant Taq DNA polymerase (Thermo Scientific, EP0405). Conditions for PCR amplification were 1 cycle at 94°C for 2 min, 40 cycles of 94°C for 15 s, 58°C for 15 s, and 72°C for 12 s, followed by 1 cycle at 72°C for 3 mins. Wild type and deletion PCR product sizes can then be resolved on a 3% agarose gel. Alternatively, the 5 bp deletion (c.887_891delCATGG) introduces a novel EcoNI restriction site that can be used for a restriction fragment length polymorphism assay.

2.8. Whole mount in situ hybridization

Antisense riboprobes labeled with digoxigenin (DIG) were transcribed either from purified, linearized plasmid DNA containing a gene-specific insert or from a gene-specific PCR product with an integrated T7 RNA polymerase site (Thisse and Thisse, 2008). Primers used to generate probe template PCR products are listed Table 2.4, and probe plasmids are listed in Table 2.5. 200-400 ng of linearized, purified plasmid DNA or PCR product was incubated with 2 μ l of 10X transcription buffer, 1 μ l T7 RNA polymerase (Roche), 2 μ l of DIG labeling mix (Roche), 1 μ l RNaseOUT (Life Technologies), and DEPC-treated water (20 μ l total volume) for 1 hr at 37°C. Following the addition of 1 μ l RNA polymerase, the reaction was incubated for another 1 hr at 37°C. 1 μ l of TURBO DNase (Life Technologies) was added, and the reaction was incubated for 30 min at 37°C. 2 μ l of 0.2M EDTA, pH 8.0 in DEPC-treated water was then added to stop the reaction. Probe was purified using SigmaSpin post-reaction clean-up columns (Sigma-Aldrich) according to manufacturer's specifications: the column was placed in a collection tube and centrifuged at 2,500 rpm for 2 mins. The base of the column and lid were removed and the column was centrifuged for another 2 mins at 2,500 rpm. The probe synthesis reaction was placed in the column in a new collection tube. This was centrifuged for four minutes at 2,500 rpm. 0.5 μ l of RNaseOUT (Life Technologies) was added to the purified probe to inhibit degradation by RNases, and the undiluted probe was stored at -80°C. Additionally, a working stock of probe diluted in pre-hybridization solution (described below) was stored at -20°C.

Analysis of mRNA expression by whole mount in situ hybridization was performed essentially as previously described (Prince et al., 1998), except probes were not hydrolyzed. Proteinase K (ProK) permeabilization was performed for 1 min (2 somite to 10 somite stage), 3 mins (18 hpf), 5 mins (24-28 hpf), or 30 mins (48 hpf). All washes were performed with gentle shaking at room temperature (RT) unless otherwise specified.

Fixed embryos were washed 4x 5 mins in PBS + 0.1% Tween-20 (PBST), permeabilized with ProK in PBST for times indicated above, refixed in 4% PFA in PBS for 20 mins and rewashed 4x 5 mins in PBST. Embryos were then incubated in hybridization solution (50% formamide + 5X sodium saline citrate [SSC] + 50 μ g/ml heparin + 0.1%

Tween-20 + 0.092 M citric acid) with 500 µg/ml tRNA, for 1 hr at 65°C. They were then incubated in hybridization solution + tRNA containing DIG-labeled riboprobe overnight at 65°C. The following washes were then performed at 65°C: 5 mins in 66% hybridization solution, 33% 2X SSC. 5 mins in 33% hybridization solution, 66% 2X SSC. 5 mins in 2X SSC. 20 mins in 0.2X SSC + 0.1% Tween-20. 2x 20 mins in 0.1X SSC + 0.1% Tween-20. The following washes were then performed at RT: 5 mins in 66% 0.2X SSC, 33% PBST. 5 mins in 33% 0.2X SSC, 66% PBST. 5 mins in PBST. Embryos were then blocked in PBST containing 2% sheep serum and 2 mg/ml bovine serum albumin (BSA) for 1-4 hrs. Embryos were incubated in a 1:5000 dilution of anti-DIG alkaline phosphate-conjugated Fab fragments (Roche) in blocking solution 2 hrs at RT or overnight at 4°C. Embryos were then washed at least 5x 15 mins each in PBST. Colouration was performed by washing embryos 4x 5 mins each in colouration buffer (100 mM Tris-HCl, pH 9.5 + 50 mM MgCl₂ + 100 mM NaCl + 0.1% Tween-20). Embryos were incubated in 45 µl 4-nitro blue tetrazolium chloride solution (NBT; Roche) and 35 µl 5-bromo-4-chloro-3-indolyl-phosphate, toluidine-salt solution (BCIP; Roche) diluted in 10 ml of colouration buffer at RT or 4°C until formation of visible coloured precipitate. The colouration reaction was stopped by washing embryos 3x 5 mins in 100% methanol + 0.1% Tween-20, followed by 2 more washes at least 30 mins each, then an additional overnight wash at 4°C. Embryos were then washed through a methanol-PBST series (70% MeOH, 50% MeOH, 30% MeOH, PBST) and stored in PBST at 4°C until imaging.

Embryos used for in situ hybridization were imaged whole in 3% methyl-cellulose with an Olympus stereoscope with a Qimaging micropublisher camera, or manually deyolked and allowed to sink to the bottom of microfuge tubes in 30%, 50% and 70% glycerol (Sigma-Aldrich) in PBS before being slide mounted in 70% glycerol. When applicable, eyes were dissected off of embryos on the slide before mounting. In situs were imaged on a Zeiss AxioImager Z1 compound microscope with AxioCam HR digital camera (Carl Zeiss Microscopy, LLC). All in situ experiments were performed at least twice.

2.9. Immunohistochemistry

Immunofluorescence to label alpha-Laminin was performed as previously described (French et al., 2009) using a rabbit polyclonal (1/200) (Sigma L9393). In particular for this antibody, freshly diluted 4% PFA that was made from freshly made 8% was used for fixing, and larvae in Chapter 6 were fixed only for 2 hrs at room temperature (RT). Larvae were fixed at 48 hpf and permeabilized with 10 µg/ml Proteinase K for 5 mins, followed by a second permeabilization step with pre-chilled 100% acetone for 7 mins at -20°C (this step was not performed for anti-Laminin experiments in Chapter 6), washed in water for 5 mins, 4x 5 mins in PBST, then blocked for 1 hr at RT in 5% normal goat serum (ThermoFisher) and 2% bovine serum albumin (BSA; Sigma-Aldrich), and then incubated overnight at 4°C in anti-Laminin primary antibody diluted in block. After 5x 15 min washes in PBST, embryos were incubated at RT for 2 hrs in goat anti-rabbit Alexa Fluor 488 or 568 secondary antibody (1/1000, Molecular Probes). All embryos were washed at least 5x 15 mins in PBST after secondary antibody incubations. Samples were manually de-yolked, processed and slide mounted as described for in situ hybridization above, and imaged on a Zeiss Axio Imager Z1, Zeiss LSM700 laser confocal scanner.

Experiments instead labeling phosphorylated Smad3 (pSmad3) at 28 hpf was carried out according to Casari et al. (2014) with the same primary (Abcam, ab59203) and goat anti-rabbit IgG secondary antibody, AP-conjugated (Millipore Sigma, AP123A). pSmad3 immunohistochemistry was performed comparably to anti-Laminin staining described above, with the following changes: in all cases, 0.15% TritonX-100 in PBS (PBTr) was used instead of PBST, blocking solution used was instead 4% BSA in PBTr, and secondary antibody was diluted 1/800 in block. Before imaging, embryos were passed through a glycerol series as described in the in situ hybridization section, and dissected comparably except to preserve more periocular tissue, the heads were dissected off the yolk immediately anterior to the otic vesicle and split down the midline of the brain with a fine insect pin so that each half of the head is mounted on the slide midline-down, eye-up.

2.10. FZD5 immunoblots and immunofluorescence

For examining expression of *FZD5* wild type and mutant proteins, plasmid DNA of each construct was transfected into HEK293T cells cultured in six-well dishes. A total of 2 µg DNA was used for transfection for each well, and biological and technical triplicates were made for each transfection. Transfected cells were cultured for 36 hrs, supplemented with the serum-reduced medium (Opti-minimal essential medium, Life Technologies, 31985), continually cultured for another 24 hrs. The cell medium was collected and store at -80°C. Total cell extracts were prepared by adding two-time SDS Laemmli buffer (BioRad) onto cells rinsed with phosphate buffered saline (PBS). To prepare extracellular matrix (ECM) proteins, cultured cells were washed with PBS and incubated in PBS containing 10 mM Ethylenediaminetetraacetic acid (EDTA) at 37°C for 30–45 mins to remove the cells. ECM proteins are retained on the dish and then subsequently solubilized in Laemmli buffer.

Immunoblotting for FZD5 was performed as described previously (Liu et al., 2012) using custom-made rabbit antibody against the N-terminus 143 residues (27–169 amino acids) of the mouse *Fzd5* protein. The signal intensities were quantified using ImageJ from three representative western blots, and analyzed in Microsoft Excel. To detect wild type and mutant FZD5 cellular or extracellular localization, 2 µg DNA was used for transfection in each well (six-well plate) carrying coated coverslips. Transfected cells were cultured in Dulbecco's modified Eagle's medium (DMEM)-F12 for 48 hrs. Immunofluorescence staining was conducted using the same antibody for detection of mutated/variant FZD5 proteins. To avoid cytoplasmic staining, live cells were first incubated with anti-Fzd5 antibody in the cultured medium at 4°C for 2 hrs, washed with PBS and then post-fixed with PFA. After rinsing with PBS, secondary antibody was added to further proceed with immunohistochemistry.

2.11. BMP3 Western blots

Wild type *BMP3* ORF was ordered from ASU BioDesign Institute in pDNR-Dual and was moved into pcDNA3.2/V5. Site-directed mutagenesis (see section 2.17) was performed in

Dr. Ordan Lehmann's lab to generate constructs carrying c.C1178T (p.S393F), c.T1349A (p.F450Y), and c.G1408C (p.A470P) variants individually. DNA for the four constructs was isolated by maxi prep (Qiagen) and sequenced to confirm the mutation sites. Cos7 cells were transfected using Lipofectamine 2000 following the manufacturer's instructions.

Briefly, cells were plated to 6 well dishes and were transfected at 80% confluency. Approximately 3 ug of DNA was transfected per well. Transfected cells were grown in low serum (0.1%) conditions for 48 hrs and then harvested. Media was removed and saved for secreted protein analysis (see below). Cell monolayers were rinsed once in PBS, and 500 ul of cold lysis buffer was added. Cells sat on ice for approximately 10 mins and were then scraped and collected into Eppendorf tubes. Samples were boiled for 3 mins, transferred to QiaShredder tubes (Qiagen), centrifuged, and the flow-through was collected in new tubes. Protein concentration was determined using the standard colourimetric BioRad protein assay.

Proteins from media were concentrated by acetone precipitation (1:1.5 media to acetone volume). Samples were put at -80°C for 1 hr, centrifuged at 13,000x g for 10 mins, and pellets were air dried briefly. Lysis buffer was added to resuspend the pellets (minimal volume to get the pellet into solution). Cell lysates and concentrated media lysates were resolved on 4-12% Bis-Tris gradient gels following manufacturer's instructions: gels were run for 1 hr at 200 volts and were transferred to PVDF at 22 volts for 1 hr on the semi-dry blotter. Blots were blocked in 5% milk in TBST for 2 hrs and primary antibody was added for overnight incubation at 4°C. Primary V5 antibody (ThermoFisher, MA5-15253) was used at 1:5000 dilution (in 5% milk) and anti-tubulin was used at 1:10,000. Blots were rinsed 3x15 mins in TBST, goat anti-mouse HRP secondary was added at 1:5000 for 1 hr at room temperature, final rinses done 3x15 mins in TBST followed by water. ECL reagent was added for 3 mins and detection was performed using the ChemiDoc MP Imaging System.

2.12. Phalloidin staining

Embryos were grown to 48 hpf and fixed in 4% PFA. Fixed embryos were permeabilized in 4% Triton-X100 (Sigma-Aldrich) and incubated with Alexa-488 phalloidin (1/100, Invitrogen) over night at 4°C on a rotating platform. Embryos were washed in 1X TBS + 0.1% Tween-20 and incubated in TO-PRO3 nuclear stain (1/1000; Invitrogen) for 30 min. Samples were processed, mounted and imaged as described for immunohistochemistry (see section 2.9).

2.13. Quantitative real-time PCR (qRT-PCR)

Total RNA was extracted from at least 25 embryos at 15 hpf (*sfrp5* mRNA injection experiments) or 28 hpf (*sfrp1a/5* MO experiments) in Chapter 3, or from 256-cell stage embryos in *BMPRIA* injections in Chapter 5, each using RNeasy RNeasy-4PCR (Ambion) according to the manufacturer's specifications. All centrifugation steps described below were performed at full speed. Embryos were homogenized by vortex-based agitation in 350 µl of Lysis/Binding solution. 350 µl of 64% ethanol was added, and the solution was vortexed for 30 s. The solution was transferred to a filter column in a collection tube, centrifuged for 1 min, and flow-through was discarded. 700 µl of Wash Solution #1 was added to the column, which was then centrifuged for 1 min and flow-through was discarded. 500 µl of Wash Solution #2/3 was added to the column, centrifuged for 1 min and the flow-through was discarded. This last step was repeated and the column was transferred to a new collection tube, 40 µl of 70°C Elution Solution was added to the column, and centrifuged for 30 s, then repeated with an additional 30 µl. DNA removal was performed by adding 19 µl of diethylpyrocarbonate (DEPC)-treated water, 10 µl of 10X DNase I Buffer and 1 µl DNase I (Ambion) to the eluted RNA. This solution was incubated for 30 mins at 37°C.

Extracted RNA was purified using the RNeasy Mini Kit (Qiagen) according to the manufacturer's specifications: 350 µl of Buffer RLT + 1% beta-mercaptoethanol was added to the DNase I-treated RNA and vortexed, then 250 µl of 100% ethanol was added to the solution and mixed by pipetting. The solution was placed in a column in a collection tube,

centrifuged for 15 s at 10,000 rpm, flow-through was discarded, and the column was transferred to a new collection tube. 500 μ l of Buffer RPE was added to the column, centrifuged for 15 s at 10,000 rpm, and flow-through was discarded. 500 μ l of Buffer RPE was added to the column, centrifuged 2 mins at 10,000 rpm. The column was transferred to a new collection tube, centrifuged for 1 min at maximum speed, and transferred to a new collection tube. RNA was eluted with 10 μ l of DEPC-treated water centrifuged 1 min at 10,000 rpm and stored at -80°C. RNA quantity and quality was assessed by spectrophotometry.

First-strand cDNA synthesis for qPCR assays in Chapter 3 was performed using the High Capacity cDNA Reverse Transcription kit (Applied Biosystems), following the manufacturer's recommendations. Per 20 μ l reaction, 2 μ l 10X RT Buffer, 0.8 μ l 25X dNTP Mix, 2 μ l 10X RT Random Primers, 1 μ l Multiscribe Reverse Transcriptase, 3.2 μ l of nuclease-free water, 1 μ l RNaseOut (separate from cDNA synthesis kit; Invitrogen). Between 2.5-3 μ g of purified RNA was added to each reaction, and topped up to 20 μ l with more nuclease-free water. The cDNA synthesis PCR program was 25°C for 5 mins, 42°C for 30 mins and 95°C for 5 mins and cDNA was stored at -20°C.

For qPCR assays in Chapter 5, first-strand cDNA synthesis was performed using the AffinityScript QPCR cDNA Synthesis Kit (Agilent), with random primers, according to the manufacturer's specifications: 3 μ g of purified RNA was added to 10 μ l 2X cDNA Synthesis Master Mix, 3 μ l random primers, and 1 μ l RT/RNase Block Enzyme Mixture, to total volume 20 μ l with molecular biology-grade water. The PCR conditions were the same as described above.

qPCR analysis of cDNA was performed using Brilliant SYBR Green QPCR Master Mix (Stratagene) and the StepOnePlus Real-Time PCR System (Applied Biosystems). All cDNA samples were run in replicates of at least 6 and each experiment was performed at least twice. The PCR cycle conditions were 95°C for 10 mins, then 40 cycles of 95°C for 20 s, 55°C for 1 mins, and 72°C for 30 s. Fluorescence readings were taken after the 55°C annealing step. The Ct values were analyzed using the comparative Ct method ($2^{-\Delta\Delta Ct}$ method) (Livak and Schmittgen, 2001) using *elongation factor 1-alpha (ef1a)* as an endogenous control.

qPCR primers for *GFP* and *efla* were selected from the Universal Probe Library Assay Design Center for Zebrafish (Roche), while others were designed with Primer3Plus and only primers generating intron-spanning amplicons were used. qPCR primer sequences are listed in Table 2.6. Each primer set was validated before use by analyzing an amplification plot was produced from a standard cDNA two-fold dilution series. Primer sets were analyzed with StepOne Software version 2.0 for StepOne Real-Time PCR Systems (Applied Biosystems) to eliminate any outliers and analyze the resulting standard/melting curves. Chosen primers in Chapter 3 had a coefficient of determination (R²) values close to 0.98, percent efficiency close to 100%, and a standard curve slope within 0.01 of the control group (*efla*). Primer sets in Chapter 5 produced linear regression slopes of -3.3 ± 0.1 with an R² value of at least 0.98.

2.14. Pharmacological treatments

For all pharmacological treatments, embryos were dechorionated prior to being transferred into the treatment solution.

Dorsomorphin (Biomolecules) was dissolved in dimethyl sulfoxide (DMSO) and added to fish water to a final concentration of 100 μ M. Embryos were treated in Dorsomorphin solution or an equal volume of DMSO in fish water from tailbud stage (10 hpf) until fixation at 28 hpf.

To inhibit BMP, RA and Shh signaling respectively, DMH1 (Sigma-Aldrich), N,N-diethylaminobenzaldehyde (DEAB; Sigma-Aldrich), or cyclopamine (Sigma-Aldrich) treatments were performed on embryos from either 10 hpf or 18 hpf until fixation or imaging (in live imaging experiments), as indicated. DMH1 and DEAB were dissolved in DMSO and used at concentrations of 0.05-0.2 μ M and 1-5 μ M in fish water, respectively, and cyclopamine was dissolved in ethanol and used at 1-10 μ M. Equivalent volumes of DMSO or ethanol in fish water was used in controls. Treatments were carried out in 35 mm dishes with 5 mL of solution, with 15 embryos in each.

Pharmacological inhibition of Smad3 was accomplished with Specific Inhibitor of Smad 3 (SIS3; Calbiochem) dissolved in DMSO to a stock concentration of 3 mM and stored at -20°C. Stock was mixed with fish water to final concentrations of either 6 μ M or 9 μ M, keeping the amount of DMSO added consistent in each group and control solutions (0 μ M). The working solutions were mixed fresh, preheated to 28.5°C, added to each dish and appropriate embryos were added. Embryos were stage matched at 10 hpf, and transferred at 24 hpf to 35 mm petri dishes with 5 mL of the appropriate SIS3 solution (15 embryos/dish). Embryos were then incubated at 28.5°C for six hours until 30 hpf, rinsed thoroughly with fish water 3 times, and returned to 28.5°C. Fish water was changed at 48 hpf and larvae were fixed at 65 hpf for 2 hrs at RT, washed 5x with PBST, and scored on a stereoscope for open fissures. All larvae showed consistent phenotypes between left and right eyes.

2.15. Manual and paraffin-embedded tissue sectioning

To visualize *bmp3* expression in longitudinal and cross section, wild type embryos were grown to 22 hpf and fixed in 4% PFA for 5 hrs and the above in situ hybridization protocol was carried out. After the colouration reaction was stopped with methanol washes (100% methanol, 0.01% Tween-20), embryos were then left overnight in 50% methanol/50% PBST. The following day, embryos were wash into PBST, mounted and oriented in a block of 2% agar, which were then placed in labeled cassettes and put in formalin overnight. Cassettes were washed in 50% ethanol for 1 hr and put into a Leica tissue processor (TP1020) where cassettes were taken through the following washes: 70% ethanol (1 hr), 90% ethanol (1 hr), 100% ethanol (2x 1.5 hrs), 1:1 ratio of ethanol and toluene (1.25 hrs), toluene (2x 30 mins), and wax (2x 2 hrs). All tissue processor washes were under vacuum and with agitation, except 70% ethanol. The following day, the samples were embedded in paraffin wax blocks, allowed to harden and then sectioned at an 8 μ m thickness on a Leica microtome (RM2125). Sections were picked up on slides and dried in a 37°C oven, then de-waxed with toluene (2x5 mins), taken through an ethanol to distilled water series (2 mins wash each), and then DPX mounting media and a coverslip was applied. Sections were imaged as described for in situ hybridization above.

Embryos stained with Alexa-488 phalloidin and TO-PRO3 in Chapter 3 were instead sectioned using a tungsten wire, slide mounted, and imaged using the Zeiss Axio Imager Z1, Zeiss LSM700 laser confocal scanner with a 20X objective.

2.16. mRNA expression constructs, synthesis and injections

To generate expression constructs for zebrafish genes, full-length coding sequences were amplified from first-strand cDNA made as described in the qPCR section. Human *FZD5* cDNAs were amplified from pRK5 constructs supplied by Dr. Anand Swaroop. Human wild type and mutant *BMP3* cDNAs were amplified from constructs generated for cell culture experiments (described in below). PCR products were cloned into pCR4-TOPO (Invitrogen) for sequencing confirmation and sub-cloned into pCS2+ for mRNA synthesis. Primers used to amplify cDNAs for mRNA expression constructs and related information are listed in Table 2.7.

MGC Human *BMPRIA* Sequence-Verified cDNA was obtained (Dharmacon; MHS6278-202807127 glycerol stock) was used as a template for PCR. PCR products were cloned into pCR4-TOPO and sub-cloned into pCS2+. Using site-directed mutagenesis (see section 2.17), a constitutively activating mutation was introduced (caBMPR1a; (Zou et al., 1997)) and the patient's mutation was subsequently added (R471H-caBMPR1a). The constructs were sequenced to confirm they were identical except for the patient mutation.

To generate purified DNA template for mRNA synthesis, 10 µg of plasmid DNA was linearized (total volume of 50 µl) then incubated with 2.5 µl 10% SDS and 2 µl of 10 mg/mL ProK and 50°C for 1 hr to denature any RNases present. Plasmid DNA was then purified by phenol/chloroform extraction and ethanol precipitation: DEPC-treated water and 10 µl of NaOAc (pH 5.3) was added to the plasmid DNA (total volume 200 µl). 200 µl of chloroform-saturated phenol (ThermoFisher) was added, the solution was vortexed for 20 s, then centrifuged for 5 mins at maximum speed. The upper layer was transferred to a new tube, 200 µl of chloroform (ThermoFisher) was added, and the solution was vortexed for 20 s, then centrifuged for 5 mins at maximum speed. The upper layer was transferred to a new tube. 20 µl of 3 M NaOAc (pH 5.2) and 600 µl of 95% ethanol was added to the tube

to precipitate the plasmid DNA, then incubated at -20°C for at least 15 mins (maximum overnight). The solution was centrifuged for 20 mins at 4°C to pellet DNA. The DNA pellet was washed in RNase-free 70% ethanol and dried in the fume hood. DNA was resuspended in 10 µl of DEPC-treated water.

mRNA was generated from linearized templates using the SP6 mMessage mMachine kit (Ambion) according to manufacturer's instructions: 2 µg of template DNA was added to 10 µl of 2X NTP/CAP, 2 µl 10X Reaction Buffer, 2 µl of Enzyme Mix, and nuclease-free water (total volume 20 µl). The reaction was incubated 2 hrs at 37°C. 1 µl of TURBO DNase (Life Technologies) was added to degrade template DNA, and the solution was incubated 30 min at 37°C.

mRNA was purified using Amicon Ultra 50K centrifugal filters (Millipore) according to manufacturer's specifications, with the following changes: 480 µl DEPC-treated water was added to the mRNA. The solution was placed into a column in a collection tube and spun for 4 mins at 14,000x g and flow-through was discarded. Columns were inverted into a new collection tube and spun for 2 mins at 1000x g. Another 480 µl DEPC-treated water was added to the flow through, put into a fresh column and spun in a collection tube for 3 mins at 14,000x g. Columns were inverted into fresh collection tubes, spun for 2 mins at 1000x g. mRNA concentration was determined via spectrophotometry, mRNAs were diluted in molecular biology-grade water and stored at -80°C.

Embryos were injected with the indicated mRNAs and doses at the single-cell stage. The solutions were diluted to the appropriate concentrations in order to always ensuring 1 nl total volume was injected. All mRNA overexpression experiments were performed at least twice. The *BMPRIA* mRNA (Chapter 5) was newly synthesized for each round of injections and both the injections and analyses were performed in a blinded fashion.

2.17. Site-directed mutagenesis

Site directed mutagenesis primers are listed in Table 2.8. The PCR reaction contained: 500 ng of template plasmid DNA, 17 µl of master mix (100 µl 10x PFU buffer,

792 µl water, 2 µl each of 100 mM dNTPs), 1 µl (10 mM) NAD, 0.5 µl (200 ng) each primer, 0.5 µl DMSO, 0.3 µl Taq DNA Ligase (NEB), 1 µl PfuUltra DNA Polymerase (Agilent), and 1.5 µl water. The PCR cycle conditions were 95°C for 2 mins, then 30 cycles of 95°C for 1 min, 55°C for 1 min, and 65°C for 10 mins. PCR products were then digested with 1 µl of DpnI (NEB) for 30 mins at 37°C to digest the original plasmid. Constructs were verified by Sanger sequencing to ensure the mutation was introduced correctly.

In the case of *BMPRIA* constructs in Chapter 5, the above protocol was performed sequentially for each introduced mutation in order to generate the construct containing the constitutively active and patient mutations.

2.18. Patients and DNA sequencing

Individuals analyzed in Chapter 4 with microphthalmia, anophthalmia and/or coloboma were subjected to exome and Sanger sequencing. Genomic DNA samples from coloboma probands were analyzed by the National Eye Institute Clinical Eye Center, UK10K consortium, MRC Human Genetics Unit at the Institute of Genetic and Molecular Medicine, University of Edinburgh and the University of Alberta. Informed consent was obtained from each participant, and study approval provided by the relevant ethics boards [National Institutes of Health (NIH) Institutional Review Board (IRB); U of A Health Research Ethics Board (reference no. 01227), UK Multiregional Ethics Committee (reference no. 06/MRE00/76)]. Five affected individuals from family 3483 (UK10K) were subjected to whole exome sequencing (WES), and Sanger sequencing was used to test for the *FZD5* mutation in all other available members of this branch of the family. Four affected individuals from Family 111 were Sanger sequenced for the *FZD5* gene. Exome sequencing was performed as described (Olbrich et al., 2012) with burrows-wheeler alignment 0.5.9 used for alignment, Picard 1.43 for duplicate marking, genome analysis tool kit (GATK) 1.0.5506 for realignment around insertions/deletions and base quality scores recalibration, and GATK Unified Genotyper for variant calling. The LOD score was calculated using paramlink package in R (Egeland et al., 2014). The primers used to PCR amplify *FZD5* in patient samples are listed in Table 2.9.

For patients analyzed for superior coloboma (Chapter 5), whole exome sequencing was performed on genomic DNA from each proband (#1 - #5) as part of FORGE Canada Consortium at the McGill University and Genome Quebec Innovation Centre. Exome target enrichment was performed using the Agilent SureSelect 50Mb (V3) All Exon Kit and sequencing was performed on the Illumina HiSeq 2000, multiplexing three samples per lane. The mean coverage of coding sequence regions, after accounting for duplicate reads was greater than 70x. WES data was analyzed by performing alignment with BWA, duplicate read removal with Picard, local insertion/deletion realignment with GATK, variant calling with SAM-tools, and annotation with Annovar and custom scripts (Beaulieu et al., 2014). Subsequently, exome sequencing was repeated commercially (Beijing Genomics Institute). In parallel, array CGH was performed to identify any causative copy number variations (CNV) using an Affymetrix cytoscan HD array that comprises approximately 1,800,000 CNV and 700,000 genotyping probes. Within patients #1–5, we identified 783, 843, 942, 708, and 721 rare (<1%) non-synonymous and stop-gain/loss variants, respectively. By filtering such variants using MutationTaster (score >0.95), patients #1–5 contain 163, 155, 139, 112, and 148 higher probability variants, respectively. Subsequent prioritization included literature searches associating genes with ocular function and zfin.org examination of in situ hybridization expression patterns within the developing eye at 18–24 hpf, yielding a restricted subset of high priority variants in each proband.

2.19. FZD5 mutagenesis and Wnt/beta-catenin pathway activation assay

FZD5 cDNA was cloned into pRK5 expression vector with a Cytomegalovirus promoter and site-directed mutagenesis was performed to generate the *FZD5* A219Xfs*49 frameshift mutation. For testing canonical Wnt signaling activity, DNA constructs were transfected into Super Top Flast (STF) HEK293 cells with a seven-time *TCF* promoter-driven firefly luciferase reporter stably integrated in the genome (Liu and Nathans, 2008). Fixed amounts of Wnt9b and *FZD5* were co-transfected together with pCAG-Renilla luciferase plasmids (used for internal expression control) into STF cells. Different amounts of *FZD5* A219Xfs*49 and secreted cysteine-rich domain (sCRD) plasmids were transfected

into regular HEK293 cells, respectively. 12 hrs after transfection, both STF and HEK293 cells were lifted off by trypsin-EDTA, and mixed at a 1:1 ratio and seeded into new plate for another 36 hr culture. Biological and technical triplicates were prepared for each transfection. Cell extracts were then prepared for Firefly luciferase and Renilla luciferase assay using the Dual-luciferase assay system (Promega, E1960). Luminescence was measured sequentially by a Turner Biosystem Modulus microplate reader. Firefly luciferase activity was normalized against Renilla luciferase.

2.20. Active RhoA assay for Wnt5a stimulation

HEK293 cells were cultured to 80% confluence in DMEM in six-well dishes, transfected with appropriate plasmids, cultured for 24 hrs, then serum starved for 24 hrs. Wnt5a recombinant protein conditioned medium (Wnt5a CM; Roche, 645-WN-010/CF) was applied for 30 mins at 250 ng/ml. Cells were lysed and then subjected to active GTP-RhoA assays according to the manufacturer instructions (pull-down assay: RhoA/Rac1/Cdc42 assay kit, Cytoskeleton, Bk-030; G-lisa assay: RhoA G-lisa kit, Cytoskeleton, Bk-124). Signal intensity was acquired in ImageJ from three representative immunoblots. Light absorbance/optic density of horseradish peroxidase colorimetric reaction was measured (SpectraMax-M) and the data were analyzed in Excel.

2.21. Co-immunoprecipitation

HEK293T cells were transfected with 1.5 μ g DNA in each well of six-well dishes. Myc-tagged Wnt3a or HA-tagged WNT7A were co-expressed, respectively, with wild type FZD5 or FZD5 A219Xfs*49. Cell extracts and co-IP procedure were performed essentially as described (Carmon and Loose, 2008). Antibodies used were mouse anti-HA (TransGene Biotech, HT301), rabbit anti-myc (Sigma-Aldrich, C3956) and rabbit anti-FZD5 (custom made, approximate epitope location described in section 2.10).

2.22. Retinal electroporation and explants culture

Mouse embryonic retinas were dissected in the DMEM medium at E13.5 excluding lens and RPE. Retinas were subjected to electroporation with a BTX ECM830 electroporator in an embryo global positioning system (GPS) chamber (SunIVF, EGPS-010) supplied with 250 ng/ μ l of DNA solution in PBS. The following parameters were set for electroporation: 21 volts for electric field strength, five-time current pulses (50 ms duration), and 900 ms intervals between pulses. Retinas were then cultured in DMEM:F12 (Invitrogen, 12660-012) for 72 hrs, harvested in PBS, fixed in 4% PFA, and subjected to sectioning and immunohistochemistry as described above and in Liu et al. (2012).

2.23. Chick and mouse embryos, immunohistochemistry and imaging

For the chick studies, fertilized Leghorn eggs (Texas A&M, Bryan, TX) were incubated at 38°C in a humidified forced-draft incubator. Chick embryos were staged according to Hamburger and Hamilton (1951) and Swiss Webster mice were collected at E10.5. Immunohistochemistry was performed as previously described (Eom et al., 2011). Chick embryos were stained with antibodies against Laminin-1 (Developmental Hybridoma Studies Bank, 3HL1; 1:250), whereas for mouse Laminin alpha 1 stains, we utilized a different antibody (Sigma, L9393). Alexa-Fluor conjugated Goat anti-Rabbit IgG (Life Technologies, 411008; 1:250) was used for fluorescent detection (Amarnath and Agarwala, 2017). Antibodies used in the current study were validated for use in chicks in previous studies (Amarnath and Agarwala, 2017; Halfter and Von Boxberg, 1992). DAPI staining was used for detecting nuclei. Confocal images were obtained with an Olympus IX51 spinning disc microscope and data analyses carried out with Slidebook Pro (3I, CO). Images are presented as single 0.5–0.8 μ m thick optical sections. The position in the dorsal-ventral plane is based on the acquisition of multiple serial sections and respective alignment to those sections (just ventral) that contain lens tissue.

2.24. Atomic non-local environment assessment (ANOLEA)

The crystal structure for the BMP3 ligand has been solved and published (Allendorph et al., 2007). Using this structure, *in silico* modeling of BMP3 mutations were performed using Swiss-pdbViewer (Guex and Peitsch, 1997) and the results were analyzed using the ANOLEA server (melolab.org/anolea). The difference in energy requirements provided by ANOLEA at each amino acid location within the mature peptide was calculated in Excel (mutant - wild type values).

2.25. Scanning electron microscopy (SEM)

Embryos at 22 hpf from wild type and *gdf6a*^{+/-} incrosses were fixed overnight in 2.5% Glutaraldehyde; 2% PFA. After washing in 0.1 M phosphate buffer, embryos were gradually dehydrated in ethanol, transferred to Hexamethyldisilazane (HMDS; Electron Microscopy Sciences) and left to dry overnight. Embryos were then mounted on SEM stubs, sputter coated with Au/Pd using a Hummer 6.2 Sputter Coater (Anatech), and imaged on a XL30 scanning electron microscope (FEI) operating at 20 kV.

2.26. Statistical analyses of eye size, prevalence, intensities, and gene expression

For measurement of eye size, embryos were fixed at indicated ages and imaged using an Olympus stereoscope with a Qimaging micropublisher camera. Eye size was measured using ImageJ software and statistical analysis was performed using an unpaired student's t-test, or an ANOVA in experiments with greater than two treatment conditions. To analyze the prevalence of phenotypes (coloboma, microphthalmia, proportion of embryos with affected gene expression) experiments were repeated at least 2 times and n-values represent pooled data from all experiments. Data represent prevalence as a percentage of total, reported +/- standard deviation. This categorical data was analyzed using Fisher's Exact to test for statistical significance. When multiple comparisons were

made (prevalence of coloboma in single- or double-MO injected embryos), a Bonferroni correction was used to obtain a corrected p-value and is indicated in figure legends.

Mean fluorescence intensity was measured in *Tg(BMPRE-AAV.Mlp:eGFP)* (referred to as *BRE:GFP* in-text) embryos injected with *sfrp1a/5* MO at 28 hpf (Chapter 3). After fixation, eyes were dissected, mounted in glycerol and imaged with a Zeiss Axio Imager Z1, Zeiss LSM700 laser confocal scanner with a 20x lens using Zeiss Zen software. Mean fluorescence intensity was measured using ImageJ software and analyzed for statistical significance using an unpaired student's t-test.

Two-factor analysis in Chapter 5 was done using a student's t-test. Multivariable analysis was performed by two-tailed, one- or two-factor ANOVA with Tukey post-hoc test.

2.27. Members of FORGE Consortium Canada

FORGE Canada Consortium: Finding of Rare Disease Genes in Canada; Steering Committee: Kym Boycott (leader; University of Ottawa), Jan Friedman (co-lead; University of British Columbia), Jacques Michaud (co-lead; Universite de Montreal), Francois Bernier (University of Calgary), Michael Brudno (University of Toronto), Bridget Fernandez (Memorial University), Bartha Knoppers (McGill University), Mark Samuels (Universite de Montreal), Steve Scherer (University of Toronto).

2.28. Tables

Table 2.1: Morpholino oligonucleotide sequences

Name	Type	Sequence 5'-3'	Dosage
<i>sfrp1a</i> -MO1 ¹	SB	TAGTCATTTAGACTTACCGTTGGGT	3ng + sfrp5-MO1
<i>sfrp1a</i> -MO2 ¹	SB	TGTCCTGAAAGAGAGAAAATGCTGT	
<i>sfrp1a</i> -MO3 ¹	TB	GGACAAAGATGCAAGGGACTTCATT	
<i>sfrp5</i> -MO1 ¹	SB	TGAGTGCTGTAGATAGAACAAAAGA	3ng + sfrp1-MO1
<i>sfrp5</i> -MO2 ¹	TB	ACACCTGCCTCTTCAGCTCCGCCAT	
<i>gdf6a</i> -MO1 ²	SB	GCAATACAAACCTTTCCCTTGTC	5-10ng + 2ng p53
<i>p53</i> ²	TB	GCGCCATTGCTTTGCAAGAATTG	2ng
<i>fzd5</i> -MO1 ³	TB	GATGCTCGTCTGCAGGTTTCCTCAT	8ng
<i>fzd5</i> -MO2	TB	TGCAGG TTTCCCTCATACTGGAAAGC	

¹Holly et al. 2014

SB, splice blocking

²French et al. 2009

TB, translation blocking

³Cavodeassi et al. 2005

Table 2.2: guide RNA target sequences for CRISPR-Cas9 mutagenesis

sgRNA name	Target site with PAM (5'-3')	Exon	PAM site (CDS bp)
<i>bmp3-2</i>	GGGACTTCATATCATGGCAGTGG	2	547
<i>bmp3-4</i>	GGGAGCTCATTGTTCTGCAGTGG	2	835
<i>bmp3-8</i>	GGCTGGCCTCATCCCATGTAGGG	2	905

Table 2.3: Mutant zebrafish genotyping primer sequences

Gene	Allele	Primers (5'-3')	Method
<i>cyp1b1</i> ¹		F - CCATCTCAGATATTTTCGGGG R - GTTATT TACCTGACAAGTAGCAG	HRM
<i>tbx2b</i> ²	fbv	F - TGTGACGAGCACTAATGTCTTCCTC R - GCAAAAAGCATCGCAGAACG	RFLP
<i>gdf6a</i> ³	s327	F - GCGTTTGATGGACAAAGGTC R - CCGGGTCCTTAAAATCATCC	HRM
<i>bmp3</i> [*]	ua1020	F - AGCAGACGATCCACCAACATCC R - TAATGGTCTGCTCATCGAACTGCAG	PCR

¹Hocking et al. 2018²Snelson et al. 2008³Gosse and Baier 2009^{*}Designed by author

Table 2.4: Primer sequences for antisense plasmid-based RNA probes

Gene	Vector	Antibiotic	Linearize	RNA Pol.
<i>aldh1a2</i>	pSPORT	Carb	EcoRI	SP6
<i>aldh1a3</i>	pCR4-TOPO	Carb	NotI	T3
<i>bambia</i>	pCR4-TOPO	Carb	NotI	T3
<i>ephb3a</i>	pCR4-TOPO	Carb	PmeI	T7
<i>vax2</i>	pCR4-TOPO	Carb	NotI	T3
<i>sfrp1a</i>		Carb	NotI	T3
<i>sfrp5</i>		Carb	NotI	T3
<i>eGFP</i>			NotI	T3
<i>gdf6a</i>	pBSKII	Carb	NotI	T7

Table 2.5: Primer sequences for antisense PCR-based RNA probes

Gene	Primer sequence (5'-3')	RNA Pol	Size (bp)	T(m)
<i>bmp4</i>	F - GCCGCTAAACGGAGACTCTTACC		1278	52
	R - GGGTCGCTTGGCTATGTGTTTC	T7		
<i>foxd1</i>	F - AGGCAACTACTGGACGCTAGACCCTG			
	R - GAACAGACCGTGTAATAATATCACACTCC	T3		
<i>foxg1</i>	F - AAATGGCTTGAGTGTTGACAGACTCG		1164	55
	R - GAAAGAATGTGACCTGCATGGTGGTGAC	T3		
<i>sfrp2</i>	F - GGTGTGTTTGGATGACCTGGACG		583	58
	R - GACTGAAGTTTGCGAATGCTGCGAG	T3		
<i>wnt2</i>	F - AACCCGTAGACAAGTGCCTGAACG		759	58.1
	R - GAGTATTTTTTGCGAAGATAGTCACCCGTC	T3		
<i>wnt8b</i>	F - TGGTGACTTTGATAACTGTGGATGTG		708	55
	R - GATTCTTGACCCGTTTGCTTCTCTTC	T3		
<i>tbx5a</i>	F - GAGGGAAGTTCGCTATCAACCG		713	52
	R - TCCATTGTTTTTCATCCGCCTTG	T7		
<i>tbx5a**</i>	F - CACGTCTTACCAAACCACAAGATCAC		974	62
	R - GCACAATGTTTGCTGCTTCATTTTAATG	T7		
<i>bmp3*</i>	F - AGGACTGAATTCTGCTGCATGAACGTCG		1119	67
	R - CATAAGGGTACTCTGGACCTGGGAGCTC	T7		
<i>eve1*</i>	F - GAGACCACAATAAAGGTCTGGTTCC		800	61.3
	R - TACATGGGTTTGTATCAGTGTTTCAGG	T7		
<i>acvr2b*</i>	F - CTAGAGCGTCATCTACTGTTGAAAAC		857	60.1
	R - GGTAGATGACGCATTACATTCATGAG	T7		

*Designed by author

T7: TAATACGACTCACTATAGGG

**Designed by author, used only in Chapter 6

T3: CAATTAACCCTCACTAAAGG

Table 2.6: Primer sequences for quantitative real-time PCR

Gene	Forward Primer (5'-3')	Reverse Primer (5'-3')
<i>efla</i>	CTTTCGTCCCAATTCAGG	CCTTGAACCAGCCCATGT
<i>GFP</i>	GTGGTGCCCATCCTGGTTCG	AGCTTGCCGTAGGTGGCAT
<i>bmp2b</i>	TAGGAGACGACGGGAACG	GCGACCATGATCAGTCAGTTC
<i>bmp4</i>	CCCATGCTTTATTTTCTGTTCG	CTCCAGTAGGACTTGGCATA
<i>wnt2</i>	CATGAACCTGCACAACAACC	CACCATGACACTTACACTCCAGAT
<i>wnt8b</i>	TTTGGAGGTTTATTATTACGCTTTC	GGCCGGTCATCAGGAAAT
<i>tbx5a</i>	TGGACAAAGTTTCATGAAGTGG	GTTCAACCCGGTGACCTTC
<i>efla</i> *	CCTTCGTCCCAATTCAGG	CCTTGAACCAGCCCATGT
<i>BMPRIA</i> **	CGTGTTCAAGGACAGAATCTGG	AAAGGCAAGGTATCCTCTGGTG

*Designed by author, *efla* endogenous control primers used only with *BMPRIA* in Chapter 5

**Designed by author

Table 2.7: Primer sequences for mRNA overexpression constructs

Gene	Primer sequence (5'-3') (RE site)	RE site	Size (bp)	T(m)
<i>sfrp5</i> *				
<i>BMPRIA</i> **	CACAGGATCCACCATGCCTCAGCTATACATTT ACATCAGATTATTG	BamHI	1599	62
	CACAGAATTCCTCAGATTTTACATCTTGGGAT TCAACCATC	EcoRI		
<i>BMP3</i> **	CACAGGATCCATGGCTGGGGCGAGCAGGC	BamHI	1419	66
	RCACATCTAGATTATCTGCAAGGGCAAGACTC TACTGTCATG	XbaI		
<i>FZD5</i> **	CACAGGATCCACCATGGCTCGGCCTGACCCAT CCGC	BamHI	1758	70
	CACAGAATTCCTACACGTGCGACAGGGACAC CTGCTTG	EcoRI		

*Designed by J. Famulski

**Designed by author

Table 2.8: Primer sequences for site-directed mutagenesis

Gene	Mutation	Primer sequence (5'-3')
<i>BMPRIA</i>	Q233D	F - GCGAACTATTGCCAAA <u>G</u> <u>A</u> CATTTCAGATGGTCCGGCAAGTTG R - CAACTTGCCGGACCATCTGAAT <u>G</u> <u>T</u> CTTTGGCAATAGTTCGC
<i>BMPRIA</i>	R471H	F - GTGATCCGTCATACGAAGATATGC <u>A</u> TGAGGTTGTGTGTGTCAAAC R - GTTTGACACACACAACCTCA <u>T</u> GCATATCTTCGTATGACGGATCAC

Underlined letters indicate altered nucleotides

Table 2.9: FZD5 Sanger sequencing primers in patients

Name	Primer sequence (5'-3')
<i>FZD5</i> Primer1F	TGCCAGGCGCGCTCGCCCTCC
<i>FZD5</i> Primer2F	TAACCGTCTCTCCCCAGCCCTATC
<i>FZD5</i> Primer3F	CGCGACGCCGAGGTCCTCTGCATG
<i>FZD5</i> Primer4F	GCAGTACTTCCACCTGGCTGCGT
<i>FZD5</i> Primer5R	CACCCACTACCTCTCAGGCAC
<i>FZD5</i> Primer6R	AGAAACGCAAATAGAATACAC
<i>FZD5</i> Primer7R	CGTCTTGGTGCCGCCCTGCTTG
<i>FZD5</i> Primer8R	GGTAGCAGGGTACCGCGCAG
<i>FZD5</i> Primer9R	GATGGGTCAGGCCGAGCCATC
<i>FZD5_ex2_1</i> F	GTAGCGCGACGGCCAGTGAGATTTGGAGACAGCTCGC
<i>FZD5_ex2_2</i> F	GTAGCGCGACGGCCAGTCTGGAGGTGCACCAGTTCT
<i>FZD5_ex2_3</i> F	GTAGCGCGACGGCCAGTGTCTTCAGTGCCGACGAG
<i>FZD5_ex2_4</i> F	GTAGCGCGACGGCCAGTGCAACCAGAACCTGAACTCG
<i>FZD5_ex2_1</i> R	CAGGGCGCAGCGATGACGCAGACAGATGGGCGTGTA
<i>FZD5_ex2_2</i> R	CAGGGCGCAGCGATGACTCCATGTTCGATGAGGAAGGT
<i>FZD5_ex2_3</i> R	CAGGGCGCAGCGATGACGAAGAGCGACACGAAGCC
<i>FZD5_ex2_4</i> R	CAGGGCGCAGCGATGACTAAACGGAAGTGACCTTGGC

Chapter 3

Sfrp1 and Sfrp5 function as positive regulators of Wnt and BMP signaling during early retinal development

A version of this chapter has been published. Vanessa L. Holly, Sonya A. Widen, Jakub K. Famulski, Andrew J. Waskiewicz (2014). Sfrp1 and Sfrp5 function as positive regulators of Wnt and BMP signaling during early retinal development. *Developmental Biology* **388**: 192-204

3.1. Introduction

A functional visual system requires precise axonal connections between the retina and brain. Retinal ganglion cell (RGC) projections create a topographic (or retinotopic) map of the visual field in the brain's visual processing center. Patterning of the developing retina defines dorsal-ventral and nasal-temporal axes, thereby specifying expression domains of axon guidance molecules in RGCs. Axes are initiated by coordinated actions of extracellular signaling molecules, establishing the expression domains of transcription factors in the dorsal, ventral, nasal, and temporal quadrants (reviewed in (Lemke and Reber, 2005)). Retinal transcription factors subsequently activate expression of the guidance cue molecules, Eph and Ephrin, receptor–ligand pairs that mediate changes in the cytoskeleton of RGC growth cones during axon guidance (Scicolone et al., 2009).

Sonic Hedgehog (Shh) signaling from the midline and optic stalk establishes ventral retina identity (Ekker et al., 1995; Sasagawa et al., 2002; Zhang and Yang, 2001). Opposing this signal, extraocular Bone Morphogenetic Proteins (BMPs), which are located lateral to the evaginating optic vesicle, initiate presumptive dorsal identity (Adler and Belecky-Adams, 2002; French et al., 2009; Gosse and Baier, 2009). Initiation of dorsal retina gene expression is apparent just after evagination of the optic vesicle in zebrafish, with markers such as *t-box 5a* (*tbx5a*) and *BMP and activin membrane bound inhibitor a* (*bambia*) expressed at 12 hours post fertilization (hpf) in zebrafish. Embryos lacking either of two BMPs, *growth and differentiation factor 6a* (*gdf6a*) or *bmp2b*, display profound defects in dorsal retina patterning, including decreased expression of *tbx5a* and *bambia* (French et al., 2009; Kruse-Bend et al., 2012). Dorsal and ventral retina identities mutually inhibit each other to ensure neither tissue encompasses the entire retina. Ectopic expression of ventral genes expands ventral identity at the expense of dorsal retina; *ventral anterior homeobox 2* (*vax2*) mRNA overexpression in *Xenopus* causes a marked expansion of other ventral markers such as *pax2* and a reduction in the dorsal marker *vent2* (Barbieri et al., 1999). Ventralization of the retina is also associated with aberrant RGC projection, where nearly all dorsal RGCs incorrectly innervate the optic tectum (Sakuta et al., 2001; Schulte et al., 1999). Alterations of dorsal markers can also influence the ventral retina. Reduction in the dorsally expressed *gdf6a* causes ventralization, with a complete expansion of *vax2* into the

dorsal-most region of the retina (French et al., 2009; Gosse and Baier, 2009). Conversely, overexpression of the dorsal retina gene *bmp4* in mouse dorsalizes the retina and reduces the expression domain of *vax2* (Behesti et al., 2006). Overexpression of chick *Tbx5* mRNA also dorsalizes the retina, though with more subtle changes in retinotopic mapping than *vax2*-induced retina ventralization (Koshiba-Takeuchi et al., 2000).

Wnt signaling, likely emanating from the retinal pigmented epithelium (RPE), has been implicated in the maintenance of dorsal retina identity. Initiation of ocular Wnt signaling in zebrafish, as determined by the Wnt signaling transgenic, *Tg(TOP:dGFP)_{w25}* (Dorsky et al., 2002), occurs after optic vesicle formation and initiation of dorsal–ventral eye patterning (Veien et al., 2008). To date, only three *wnt* genes have documented expression in the eye during early ocular patterning in zebrafish. *wnt11r* has lens-specific expression and *wnt2* and *wnt8b* are expressed in the RPE between 14 and 16 hpf. Overexpression of the Wnt inhibitors *dickkopf 1b* (*dkk1b*) or dominant repressive *tcf7la* (the zebrafish ortholog of mouse *Tcf3*) inhibits canonical Wnt signaling. In congruence with canonical Wnt activity appearing subsequent to dorsal–ventral retina axis initiation, blockade of Wnt signaling does not affect expression of early dorsal or ventral retina markers (Veien et al., 2008). However, embryos at later stages display severe defects in dorsal retina gene maintenance including loss of *aldehyde dehydrogenase 1a2* (*aldh1a2*), *tbx5a*, and *bambia* and the ablation of the dorsally expressed BMP ligands, *bmp2b*, *bmp4*, and *gdf6a*. Dorsal eye phenotypes caused by loss of Wnt signaling are rescued by overexpressing *bmp4*. This leads to the model that Wnts act upstream of BMP signaling during the retinal maintenance phase to establish proper dorsal-ventral patterning in the retina (Veien et al., 2008). In support of this, mutation of the mouse Frizzled (Fzd) co-receptor, Lrp6, causes ocular defects including an expansion of ventral markers (*Vax2*) at the expense of dorsal ones (*Tbx5* and *Bmp4*) (Zhou et al., 2008; Zhou et al., 2010).

Robust specification of axial pattern typically requires both morphogens and opposing antagonists. We have previously shown that BMP signaling in the dorsal retina antagonizes and constrains the ventral domain (French et al., 2009). However, a ventral antagonist of the dorsal BMP and Wnt signaling has yet to be identified. As the dorsal retina is specified by BMP and Wnt signaling, researchers searched for ventral retina-

specific molecules known to inhibit the activities of these growth factors. BMP signaling is opposed by the *chordin*, *noggin*, and *follistatin* gene families (reviewed in (Brazil et al., 2015)). A *chordin*-related chick gene, *ventroptin*, specifies ventral retina identity by antagonizing dorsal BMP ligands (Sakuta et al., 2001). However, *ventroptin* expression has thus far only been identified in the chick, leaving the identity of a zebrafish ventral antagonist unclear. Our goal was therefore to identify molecules that modulate retinal BMP or Wnt signaling during retinal patterning.

Wnt signaling is modulated by Secreted frizzled-related proteins (Sfrps), a family of extracellular proteins that contain a cysteine-rich domain (CRD) that is homologous to the extracellular portion of the Wnt-binding receptor, Fzd. Based on their structural similarity to the CRD of the Fzd receptor, Sfrps were classically assumed to be Wnt inhibitors. In support of this model of Sfrp function, original experiments investigating the relationship between Sfrps and Wnts showed that *Xenopus sfrp3* (zebrafish *frzb*) mRNA rescues the ventralization phenotypes resulting from *wnt8* mRNA overexpression (Leyns et al., 1997; Wang et al., 1997). Similar conclusions were also obtained in zebrafish following rescue of *wnt8b* ventralization phenotypes with *sfrp1a* mRNA overexpression (Kim et al., 2007). Furthermore, overexpression of *wnt11* can rescue foregut defects caused by *sfrp5* overexpression in *Xenopus* (Li et al., 2008). Recent experiments, however, have led to an emerging model whereby Sfrp function is dependent on both dose and context (Esteve et al., 2011; Lopez-Rios et al., 2008). The simple model that Sfrp proteins target only Wnt signaling has also been questioned, with evidence that the Sfrp-related Sizzled functions to oppose embryonic BMP signaling (Muraoka et al., 2006).

To identify potential modulators of retinal BMP and Wnt signaling, we cloned *sfrp* genes that are expressed in the early zebrafish retina. The zebrafish genome contains seven known *sfrp* genes: *sfrp1a*, *sfrp1b*, *sfrp2*, *sfrp3* (*frzb*), *sfrp5*, *sizzled*, and *tlc*. On the basis of phylogenetic analysis, *sfrp1a*, *sfrp1b*, *sfrp2*, and *sfrp5* are more closely related (Tendeng and Houart, 2006). In this study, we focused on *sfrp1a* and *sfrp5*, which are both expressed in the developing retina at the time of retinal patterning. Using morpholinos knockdown, we unexpectedly determined that Sfrp1a and Sfrp5 function as Wnt and BMP signaling facilitators during retinal development. Morpholino knockdown of Sfrp1a and Sfrp5 leads

to reduction in the expression domain of dorsal patterning markers as well as BMP and Wnt signaling reporters. Furthermore, we show that *Sfrp1a* and *Sfrp5* are also involved in choroid fissure fusion, a morphological process known to require proper retinal patterning. On the basis of careful analysis of dorsal retina gene expression we propose a model whereby *Sfrp1a* and *Sfrp5* act to facilitate BMP signaling during initiation of dorsal retina identity, while during the maintenance phase *Sfrp1a* and *Sfrp5* enhance activation of Wnt signaling therefore maintaining dorsal-ventral axis patterning.

3.1.1. Summary

Axial patterning of the developing eye is critically important for proper axonal pathfinding as well as for key morphogenetic events, such as closure of the optic fissure. The dorsal retina is initially specified by the actions of Bone Morphogenetic Protein (BMP) signaling, with such identity subsequently maintained by the Wnt- β catenin way. Using zebrafish as a model system, we demonstrate that Secreted frizzled-related protein (*Sfrp*) 1a and *Sfrp5* work cooperatively to pattern the retina along the dorsal-ventral axis. *Sfrp1a/5*-depleted embryos display a reduction in dorsal marker gene expression that is consistent with defects in BMP- and Wnt-dependent dorsal retina identity. In accord with this finding, we observe a marked reduction in transgenic reporters of BMP and Wnt signaling within the dorsal retina of *Sfrp1a/5* depleted embryos. In contrast to studies in which canonical Wnt signaling is blocked, we note an increase in BMP ligand expression in *Sfrp1a/5*-depleted embryos, a phenotype similar to that seen in embryos with inhibited BMP signaling. Overexpression of a low dose of *sfrp5* mRNA causes an increase in dorsal retina marker gene expression. We propose a model in which *Sfrp* proteins function as facilitators of both BMP and Wnt signaling within the dorsal retina.

3.2. Results

3.2.1. *Dorsal retina identity is initiated by BMP signaling and independent of Wnt signaling*

Dorsal retina identity, as denoted by expression of the transcription factor *tbx5a*, initiates in the optic vesicle at 12 hpf (French et al., 2009; Veien et al., 2008). By 13 hpf, *vax2* and *bambina* are expressed in the optic vesicle's ventral and dorsal regions, respectively. The combined activities of BMP and Wnt signaling pathways are necessary to specify dorsal-ventral patterning within the presumptive retina (French et al., 2009; Gosse and Baier, 2009; Kruse-Bend et al., 2012). To evaluate their respective roles in initiating dorsal identity, we analyzed zebrafish embryos lacking either BMP (*gdf6a* knockdown) or Wnt signaling (via *Tg(hsp701:dkk1b-GFP)*). Embryos injected with *gdf6a* morpholino display a loss of both *bambina* and *tbx5a* expression at 15 hpf (Fig. 3.1A,C,G,I) and an expansion of ventral-specific *vax2* (Fig. 3.1D,F) (French et al., 2009). To inhibit canonical Wnt signaling, we employed a strain possessing a heat shock inducible *dickkopf1b* transgene, *Tg(hsp701:dkk1b-GFP)* (Veien et al., 2008). Heat shock treatment of such embryos at 9 hpf, causes no discernable alteration in the initiation phase of dorsal-ventral patterning as *tbx5a*, *bambina* and *vax2* expression is unaffected (Fig. 3.1A–B,D–E, G–H). On the basis of this experiment and previously published reports on BMP and Wnt signaling, we conclude that initiation of dorsal retina identity is regulated by BMP signaling with Wnt signaling required only for subsequent maintenance (French et al., 2009; Gosse and Baier, 2009; Veien et al., 2008).

3.2.2. *sfrp1a and sfrp5 are expressed in the zebrafish optic vesicle and retina during stages of dorsal-ventral axis initiation and maintenance*

Both BMP and Wnt signaling pathways are modulated by the activities of secreted proteins, including Noggin, Chordin, Follistatin, and Sfrps. We focused on the Sfrp family of secreted growth factor modulators, as *Sfrp1a* and *Tlc* have previously been shown to inhibit zebrafish Wnt signaling (Houart et al., 2002; Kim et al., 2007). The expression

patterns of zebrafish *sfrp1a*, *sfrp1b*, *sfrp2*, *sfrp3*, and *sfrp5* between 40% epiboly and 48 hpf have been published (Tendeng and Houart, 2006). Only *sfrp1a*, *sfrp2*, and *sfrp5* are expressed in the developing zebrafish eye. To investigate the precise spatio-temporal expression of *sfrp* genes during eye morphogenesis, we performed whole mount in situ hybridization for *sfrp1a*, *sfrp2*, and *sfrp5*. Retinal *sfrp1a* mRNA is readily detectable at 12 hpf, encompassing both ventral and dorsal regions (Fig. 3.2A). By 15 and 18 hpf, retinal expression of *sfrp1a* persists, with the exception of a small region of dorsal tissue, from which *sfrp1a* is excluded (Fig. 3.2B–C). By 25–36 hpf, *sfrp1a* expression is maintained in the ventral retina with slightly higher levels observed temporally (Fig. 3.2D–E). By 48 hpf, expression is restricted to the closing choroid fissure (Fig. 3.2F). At 12–18 hpf, the expression of *sfrp5*, although similar to *sfrp1a*, is more restricted to presumptive ventral retinal tissues (Fig. 3.2G–I). By 25–36 hpf, expression of *sfrp5* is noticeably weaker and by 48 hpf, signal is not detected (Fig. 3.2J–L). In contrast to the retina-specific expression patterns of *sfrp1a* and *sfrp5*, *sfrp2* is barely detectable and restricted to the RPE in later stages (Fig. 3.3). As such, we concentrated our efforts on the function of zebrafish Sfrp1a and Sfrp5 during dorsal-ventral retina patterning.

3.2.3. *Sfrp1a* and *Sfrp5* act synergistically during retinal morphogenesis

Mouse Sfrp1 and Sfrp2 have been previously shown to act cooperatively during patterning of the dorsal optic cup (Esteve et al., 2011). In zebrafish, *sfrp1a* and *sfrp5* share domains of overlapping expression in the ventral eye during morphogenesis (Fig. 3.2). To block the activity of zebrafish Sfrp1a and Sfrp5, we utilized gene-specific morpholino oligonucleotides (MOs) that inhibit translation or splicing of the mRNA. Separate injection of a 3 ng dose of either *sfrp1a* or *sfrp5* MO fails to elicit overt ocular phenotypes. Compared to wild type, eye size is unchanged in the embryos singly injected with *sfrp* MOs (Fig. 3.4A–C). However, co-injection of both morpholinos results in a statistically significant reduction of eye size (9% +/- 1.4% reduction in retinal area, n=53, p<0.05), when compared to embryos injected singly with *sfrp1a* or *sfrp5* MOs (Fig. 3.4A–D,I). We also note existence of a dorsal retina groove in embryos co-injected with *sfrp1a/5* MOs

(Fig. 3.4D). In addition to eye size, we also examined retinal architecture by analyzing phalloidin staining in retinal sections. At 48 hpf, *sfrp1a* or *sfrp5* MO injected embryos display no overt retinal phenotype (Fig. 3.4E–F).

To visualize and quantify the occurrence of coloboma, we immunostained embryos with antibodies directed against the basement membrane component Laminin. Laminin is degraded during optic fissure closure as the two lobes of the eye fuse. In wild type embryos at 48 hpf we observe the complete apposition of retinal lobes and initiation of Laminin dissolution (Fig. 3.4G). Both *sfrp1a* (prevalence: 2.6% +/- 3.6%, n=75) and *sfrp5* (prevalence: 2.9% +/- 4.0, n=64) MO-injected embryos display low frequencies of ocular coloboma at 48 hpf, as measured by retained Laminin immunoreactivity between nasal and temporal lobes. However, co-injection of both *sfrp1a* and *sfrp5* MOs (3 ng each) results in a significantly increased prevalence of ocular coloboma in comparison to singly injected embryos (prevalence: 46.3% +/- 4.5%, n=76, $p < 0.0036$) (Fig. 3.4G–H, J). Similar phenotypes were observed with non-overlapping MOs, indicating the specificity of observed results (Fig. 3.5). Such data is indicative of a role for Sfrp1a and Sfrp5 in regulating aspects of retinal patterning that are central to closure of the ventral optic fissure, a phenotype that is also seen in embryos with loss of BMP or Wnt signaling.

We further analyzed the consequence of *sfrp1a/5* MO knockdown on retinal morphogenesis by performing confocal microscopy on live *Tg(Olr3:GFP)* embryos, which express GFP in the developing retina. Time-lapse imaging reveals that embryos injected with both *sfrp1a/5* MOs display optic cup formation and apposition of the retinal lobes in a similar fashion to wild type controls (Fig. 3.6). We do, however, observe that 25.7% (+/- 0.71%, n=66, $p < 0.0001$) of *sfrp1a/5* MO co-injected embryos display thinning of the ventral retina tissue (Fig. 3.6). From our analyses of morphology, fissure closure, and morphogenesis, we conclude that Sfrp1a and Sfrp5 function cooperatively to regulate retinal development in zebrafish.

3.2.4. *Sfrp1a* and *Sfrp5* are required for canonical Wnt signaling in the retina

Sfrps are known modulators of Wnt signaling with context-dependent roles inhibiting or facilitating pathway activity (Esteve et al., 2011). Canonical Wnt signaling is essential for maintenance of dorsal retina genes in zebrafish (Veien et al., 2008; Zhou et al., 2008). Investigation of mouse *Sfrp1* and *Sfrp2* function during eye development revealed a novel role for facilitation of Wnt signaling and diffusion in the dorsal optic cup (Esteve et al., 2011). We detect changes in canonical Wnt signaling in the eyes of *sfrp1a/5* MO-injected embryos using the *Tg(TOP:dGFP)^{w25}* transgenic strain, which provides a readout of β -catenin-dependent *Lef1* transcriptional activity (Dorsky et al., 2002). We utilized in situ hybridization to detect *gfp* mRNA, as this is more temporally sensitive than directly visualizing GFP signal using confocal microscopy. In situ hybridization against *gfp* in the *Tg(TOP:dGFP)^{w25}* strain reveals that *Sfrp1a* and *Sfrp5* are required for normal Wnt signaling. Overall, 81.6% (+/- 19.1%, n=59, p<0.0001) of *sfrp1a/5* MO-injected embryos display reduced expression levels and domain area of *gfp* throughout the body at 28 hpf (Fig. 3.7A–B; Fig. 3.8). To confirm this finding, we utilized quantitative real-time PCR (qRT-PCR) on RNA isolated from whole embryos, with results showing a 0.73 fold change (p<0.001) in *gfp* transcript levels in *sfrp1a/5* MO-injected embryos as compared to uninjected control embryos (Fig. 3.7C). Consistent with reports on mouse *Sfrp1/2*, our data demonstrate that zebrafish *Sfrp1a* and *Sfrp5* act as facilitators of dorsal retina Wnt signaling (Esteve et al., 2011).

Changes to Wnt signaling could be accounted for by alterations in *wnt* gene expression. Two genes, *wnt2* and *wnt8b*, are expressed in the RPE during eye development and are candidate ligands in regulating dorsal retina identity (Veien et al., 2008). To analyze *wnt2* and *wnt8b* expression, we performed whole mount in situ hybridization on *sfrp1a/5* MO-injected embryos. Of such embryos, 81.6% (+/- 2.2%, n=59, p<0.0001) display expanded *wnt2* mRNA and 58.6% (+/- 16.7%, n=63, p<0.0001) express an expanded domain of *wnt8b* at 28 hpf in the RPE (Fig. 3.7D–G). We sought to confirm these results by performing qRT-PCR of *wnt2* and *wnt8b* mRNA in *sfrp1a/5* MO-injected embryos at 28 hpf. Such analyses indicate a statistically significant 1.38 fold change (p<0.0001) in *wnt2* mRNA levels, while *wnt8b* displays a 1.33 fold change (p<0.0054)

(Fig. 3.7H). Expanded *wnt* gene expression with concurrent decreases in Wnt signaling suggests a block in the pathway downstream of *wnt* gene transcription and is consistent with a model where Sfrp1a and Sfrp5 act as extracellular facilitators of retinal Wnt activity.

3.2.5. Depletion of *Sfrp1a* and *Sfrp5* causes alterations to dorsal-ventral retina axis patterning

Wnt signaling is required for the maintenance of dorsal retina identity during eye morphogenesis (Veien et al., 2008). In light of our findings that Sfrp1a and Sfrp5 function as Wnt facilitators in the dorsal retina, we analyzed dorsal-ventral patterning in *sfrp1a/5* MO-injected embryos. We analyzed the ventral markers *aldh1a3*, *ephb3a*, and *vax2* at 28 hpf and observe mild increases in the expression domain of *aldh1a3* and *vax2*, with no overt difference in expression of *ephb3a* when compared to wild type (Fig. 3.9A–F). The results are more striking at 48 hpf, a stage at which we observe significant expansion of ventral expression for *aldh1a3* (prevalence: 44.5% +/- 17.9%, n=36, p<0.0001) and *vax2* (prevalence: 26.7% +/- 22.9%, n=33, p<0.01) (Fig. 3.9M–P). In addition to ventral markers, we also analyzed dorsal retina marker expression of *aldh1a2*, *bambia* and *tbx5a*. Our data indicate a slight reduction in the expression domain of *aldh1a2* (prevalence: 52.1% +/- 28.8%, n=42, p<0.0001), *bambia* (prevalence: 58.1% +/- 20.7%, n=59, p<0.0001) and *tbx5a* (prevalence: 88.7% +/- 10.5%, n=47, p<0.0001) at 28 hpf (Fig. 3.9G–L). Similar to the results of ventral marker analysis, the effects are more obvious at 48 hpf, with embryos displaying a significant reduction in the expression domain of *bambia* (prevalence: 32.2%, n=31, p<0.01) and *tbx5a* (prevalence: 30.1%, n=23, p<0.0001) (Fig. 3.9Q–T). We therefore conclude that in the absence of Sfrp1a/Sfrp5 function, ventral retina marker expression domains expand at the expense of dorsal markers. This was most obvious at the later 48 hpf stage, when Wnt signaling is known to be required for the maintenance of patterning. These findings therefore further support the idea that Sfrp1a and Sfrp5 positively modulate Wnt signaling during retinal morphogenesis.

In addition to dorsal-ventral patterning, we also analyzed the consequence of *sfrp1a/5* knockdown on nasal-temporal patterning. Examination of temporal and nasal

markers *foxd1* (n=14) and *foxg1a* (n=17) indicates that *Sfrp1a* and *Sfrp5* do not regulate nasal-temporal patterning of the retina (Fig. 3.10).

3.2.6. *Sfrp*-depleted embryos have reduced BMP signaling

BMP signaling is important both for initiation and maintenance of dorsal retina markers, as well as the restriction of ventral retina markers. Our data suggest that the zebrafish retina is partially ventralized when *Sfrp1a* and *Sfrp5* are depleted, but such phenotypes are consistent with loss of either Wnt or BMP signaling. To investigate changes in BMP signaling we used a transgenic zebrafish strain, the *Tg(BMPRE-AAV.Mlp:eGFP)* line, which contains a binding site (84 bp BMP Response Element derived from mouse *Id1* promoter) for phosphorylated Smads (Collery and Link, 2011). In situ hybridization analysis of *gfp* mRNA in *Tg(BMPRE-AAV.Mlp:eGFP) sfrp1a/5* MO-injected embryos reveals a decrease in retinal intensity of BMP signaling (% affected embryos: 51.9% +/- 2.7%, n=81, p<0.0001) (Fig. 3.11A,B). Fluorescence confocal imaging was used to measure eGFP signal in *sfrp1a/5* MO-injected and control eyes (Fig. 3.11C,D). Mean fluorescence measurements indicate a 34.1% reduction in *sfrp1a/5* MO-injected eyes compared to wild type (+/- 11.4%, n=28, p<0.0001) (Fig. 3.11E). Previous studies have demonstrated that loss of BMP signaling results in a morphological groove in the dorsal retina (French et al., 2009). We note the appearance of this dorsal groove in 15.4% (n=52) of *sfrp1a/5* MO-injected embryos examined at 48 hpf (Fig. 3.4D). Taken together, such data are consistent with *Sfrp1/5* proteins playing a key role in facilitating BMP signaling in the dorsal retina.

One plausible explanation for reduced BMP signaling in *sfrp1a/5* MO-injected embryos is a reduction in Wnt activity. Blockade of canonical Wnt signaling, as seen in heat-shock inducible *dkk1b* zebrafish, causes a marked reduction in *bmp2b*, *bmp4* and *gdf6a* expression (Veien et al., 2008). Therefore, in addition to measuring BMP signaling we also analyzed the expression of these BMP ligands known to be involved in retinal BMP signaling. In situ hybridization of *bmp2b*, *bmp4* and *gdf6a* reveals that despite a

reduction in BMP signaling, the expression domain of these BMP ligands is expanded (prevalence: *bmp2b*: 90.9% +/- 8.4%, n=89, p<0.0001; *bmp4*: 70.3% +/- 17.1%, n=40, p<0.0001; *gdf6a*: 94.2% +/- 5.8%, n=66, p<0.0001) (Fig. 3.11F–G, I–J, L–M). qRT-PCR of *bmp2b* and *bmp4* confirmed the in situ hybridization results (*bmp2b*: 1.38 fold change, p<0.0001; *bmp4*: 1.47 fold change, p<0.0001) (Fig. 3.11O). This phenotype is in stark contrast to that seen in embryos induced to overexpress the Wnt inhibitor *dkk1b* (Fig. 3.11H,K,M and Veien et al. (2008)). This finding suggests that Sfrp1a and Sfrp5 may regulate BMP signaling independent of their facilitation of Wnt signaling. As a test of this model, we examined BMP ligand expression in embryos treated with Dorsomorphin, a pharmacological inhibitor of BMP signaling. Similar to what is seen in *sfrp1a/5* MO-injected embryos, we note an increase in BMP ligand expression in Dorsomorphin-treated embryos (Fig. 3.12). To confirm that Sfrp proteins are regulating BMP signaling, we analyzed the expression of dorsal-ventral patterning markers *tbx5a*, *bambina* and *vax2* during the Wnt-independent initiation phase (15 hpf) of retinal morphogenesis (see Fig. 3.1). At 15 hpf, *sfrp1a/5* MO-injected embryos show a reduction in the expression of *tbx5a* (prevalence: 58.7%, n=46, p<0.0001) and *bambina* (prevalence: 50%, n=48, p<0.0001) while the expression of ventral *vax2* (n=51) appears unaffected (Fig. 3.11P–U). Since the initiation of dorsal retina identity is BMP-dependent and Wnt-independent (see Fig. 3.1), these results are consistent with an early function for Sfrp1a/5 proteins in facilitating BMP signaling.

3.2.7. *Sfrps* act as inhibitors at high concentrations

Our results, although similar to Esteve et al. (2011), run against the original paradigm that Sfrp proteins function as inhibitors of growth factor signaling. In the dorsal retina, *sfrp1a/5* expression is at low levels and based on our morpholino experiments, we conclude that this low level of expression allows Sfrp1a/5 to function as facilitators of BMP and Wnt signaling. In the ventral retina, a region of high *sfrp* expression (see Fig. 3.2) is located in a domain that lacks BMP signaling. In order to examine the functions of this high level of Sfrp protein, we injected 100 pg *sfrp5* mRNA into embryos and analyzed for

dorsal-ventral retina markers and BMP signaling at 15 hpf. We used *sfrp5* as it has been previously shown that *sfrp5* mRNA causes a more severe phenotype than *sfrp1a* (Peng and Westerfield, 2006). In situ hybridization analysis for *gfp* mRNA in the *Tg(BMPRE-AAV.Mlp:eGFP)* BMP reporter line displayed a decrease in expression in *sfrp5* mRNA injected embryos (prevalence: 79.5% +/- 10.6%, n=30, p<0.0001) (Fig. 3.13G–H,J). Furthermore, in situ hybridization for *tbx5a* (prevalence: 78% +/- 2.8%, n=30, p<0.0001) and *bambina* (prevalence: 87 +/- 1.0%, n=55, p<0.0001) showed a decrease in expression levels (Fig. 3.13A–D,J). Conversely, the ventral marker *vax2* shows both an increase in expression levels and an expansion of domain (prevalence: 79% +/- 2.3%, n=75, p<0.0001) (Fig. 3.13E–F,J). qRT-PCR for *tbx5a* indicated a 0.5 fold decrease in expression (p<0.0001) (Fig. 3.13I). These data are consistent with the model that ventral retina Sfrp5 can act as a BMP inhibitor at high concentrations.

We assessed overall morphology of embryos injected with 100 pg *sfrp5* mRNA at 22 hpf to determine if changes in eye patterning could be due to morphological defects. We find that embryos have varying degrees of dorsalization suggesting dorsal-ventral axis defects, but that despite this, all embryos correctly form eye tissue (Fig. 3.14). This leads us to conclude that any changes in retinal patterning genes in 100 pg mRNA-injected embryos are not due to morphological defects.

3.2.8. *Sfrps act as facilitators of dorsal retina identity at low concentrations*

Given the known dose-dependent context of Sfrps in regulation of Wnts, we then wondered what the effect of low concentrations of Sfrp5 would be. Sfrps have been known to modulate Wnt signaling in a biphasic manner, where high concentrations inhibit and low concentrations facilitate signaling (Uren et al., 2000). We reasoned that Sfrps may act in a similar manner to modulate BMP signaling. We would therefore expect that injection of low concentrations of *sfrp5* mRNA would facilitate BMP signaling in the dorsal eye, causing the subsequent expansion of dorsal retina markers at the expense of ventral markers. To test this, we injected 1 pg *sfrp5* mRNA into embryos and analyzed dorsal retina markers and *gfp* expression in *Tg(BMPRE-AAV.Mlp:eGFP)* embryos at 15 hpf. We

find that indeed, dorsal retina marker expression domains are expanded while ventral marker domains are reduced, leading us to conclude that low concentrations of Sfrps facilitate BMP signaling in the dorsal eye. In situ hybridization analysis for *gfp* mRNA in the *Tg(BMPRE-AAV.Mlp:eGFP)* reporter line shows an expansion of the expression domain in *sfrp5* mRNA-injected embryos (prevalence: 21.2% +/- 1.47%, n=33, p<0.0006) (Fig. 3.15G–H,J). Additionally, in situ hybridization analysis of *tbx5a* (prevalence: 26.0% +/- 1.90%, n=50, p<0.0001) and *bambina* (prevalence: 30% +/- 1.86, n=50, p<0.0001) (Fig. 3.15A–D,J) shows an expanded dorsal domain, while analysis of *vax2* expression reveals a significant reduction ventral domain (prevalence: 30% +/- 1.8%, n=50, p<0.0001) (Fig. 3.15E–F,J). qRT-PCR for *tbx5a* indicates an average fold increase of 1.17 (p<0.0061) (Fig. 3.15I). These results support the model that low concentrations of endogenous Sfrp5 present in the dorsal retina can facilitate BMP signaling.

To assess the possibility that morphological defects are responsible for the changes in retinal patterning genes that we observe, we analyzed the overall morphology of embryos injected with 1 pg *sfrp5* mRNA at 22 hpf. We find that *sfrp5* mRNA-injected embryos show no change in phenotype compared to the uninjected controls (Fig. 3.16) and therefore conclude that any change in retinal patterning is not due to a change in morphology.

3.3. Discussion

Our examination of Sfrp1a and Sfrp5 function during zebrafish retinal morphogenesis and patterning reveals roles in regulation of both Wnt and BMP signaling pathways. Analysis of dorsal-ventral marker expression in *sfrp1a/5* morpholino oligonucleotide (MO) injected embryos is consistent with retinal ventralization (Fig. 3.9). With the use of transgenic reporter lines, we have also shown that BMP and Wnt signaling is diminished in the absence of Sfrp1a/5 activity (Fig. 3.7 and Fig. 3.11). BMP signaling initiates dorsal retina patterning, while Wnt signaling is required during the subsequent maintenance phase (Fig. 3.1) (Veien et al., 2008). In our MO-injected embryos, we observe a reduction of dorsal identity at 15 hpf, indicative of Sfrp1a/5 function during the BMP-dependent initiation phase (Fig. 3.11). Furthermore, the loss of proper dorsal-ventral

patterning also results in aberrant retina morphogenesis and the failure of choroid fissure fusion with a subsequent coloboma phenotype (Fig. 3.4). We therefore conclude that Sfrp1a/5 act cooperatively to activate and maintain BMP and Wnt signaling during initiation and maintenance of retinal morphogenesis and dorsal–ventral patterning.

MO knockdown of *sfrp1* or *sfrp5* in Medaka produces phenotypes including microphthalmia (small eyes) or anophthalmia (no eyes), consistent with functioning as Wnt antagonists during eye field specification (Lopez-Rios et al., 2008; Ruiz et al., 2009). In contrast, we observe only a minimal alteration in eye size in zebrafish injected with sfrp1a/5 MOs (Fig. 3.4). Although it is possible that such results reflect species-dependent effects, a more plausible explanation involves a key difference in our methodology. In our study, inhibition of Sfrp1a and Sfrp5 was achieved primarily through the use of splice-blocking morpholinos, thereby targeting only zygotically expressed genes and bypassing early requirements for Sfrp1a/5 proteins during gastrulation. As maternal zebrafish Sfrp1a functions as a Wnt antagonist in defining the embryonic dorsal–ventral axis (Lu et al., 2011), the use of translation blocking morpholinos in Medaka blocks both maternal and zygotic *sfrp1a/5*, and could plausibly result in very different effects than methods targeting only zygotic transcripts.

While originally identified as Wnt inhibitors, Sfrps have recently been shown to act as facilitators of Wnt signaling (Esteve et al., 2011; Lopez-Rios et al., 2008; Mii and Taira, 2009). Our findings indicate that in the absence of Sfrp1a/5 function, Wnt signaling, as observed using the *Tg(TOP:dGFP)* line, is clearly attenuated. Co-injection of fluorescently tagged Wnt8 and Sfrp (Frzb) proteins increased the spread of Wnt8 in the *Xenopus* gastrula, as compared to tagged Wnt8 injected alone (Mii and Taira, 2011). Furthermore, expression of murine Sfrp1 in *Drosophila* imaginal wing discs increased the extracellular diffusion of Wingless (Wg, a Wnt ortholog) (Esteve et al., 2011). Inhibition of Sfrp function, as seen in *Sfrp1^{-/-};Sfrp2^{-/-}* mouse mutants, prevented proper diffusion of tagged Wnt11 in retina explants (Esteve et al., 2011). These latest findings, along with research that showed a correlation between Sfrp and β -catenin levels in hematopoietic stem cells (Renström et al., 2009), suggest that Sfrp functions in certain tissues as facilitators of Wnt signaling. In support of this model, Sfrps contain both Wnt-binding and Fzd-binding domains

(Bovolenta et al., 2008; Lin et al., 1997; Lopez-Rios et al., 2008; Uren et al., 2000), which are hypothesized to aid Wnt–Fzd interaction by bringing the receptor and ligand in close proximity (Bovolenta et al., 2008).

Although almost exclusively linked with Wnt signaling, additional evidence is building that Sfrps influence other developmental signaling pathways. In particular, Sfrps have been linked to BMP signaling. The first Sfrp identified as a BMP antagonist was Sizzled, which was characterized as a dorsalizing factor in the *ogon* mutant zebrafish (Muraoka et al., 2006). Sizzled function as a BMP inhibitor was confirmed by dorsalization phenotypes resulting from *sizzled* misexpression, and rescue of *ogon* mutants by inhibiting BMP signaling (Lee et al., 2006). In contrast to the proposed functions of Sizzled, our study suggests that Sfrp1a and Sfrp5 positively regulate BMP signaling during retinal development. Their depletion causes a decrease in phosphorylated SMAD signaling, as observed in the *Tg(BMPRE-AAV.Mlp:eGFP)* line, as well as decreased expression of BMP target genes *tbx5a* and *bambiasia* during initiation of dorsal retina identity (Fig. 3.11). Furthermore, *sfrp1a/5* MO-injected embryos possess a morphological groove in the dorsal retina, a phenotype that is highly similar to the BMP mutant *gdf6a*^{-/-}, and not seen in embryos overexpressing *dkk1b*.

An outstanding question remains as to how Sfrp1a/5 regulate BMP signaling. Sizzled is an inhibitor of Tolloid, a chordinase that degrades the BMP inhibitor Chordin (Lee et al., 2006). Crescent, a *Xenopus* Sfrp for which no zebrafish ortholog has been identified, is able to inhibit Tolloid-mediated digestion of Chordin (Ploper et al., 2011). Mammalian Sfrp2 also binds Tolloid and potentially acts as an inhibitor (Ploper et al., 2011). In contrast to Sizzled and Crescent, our study shows that Sfrp1a and Sfrp5 function as BMP facilitators and as such likely do not inhibit Tolloid. We speculate that they may facilitate BMP ligand diffusion or modify ligand access to the extracellular matrix by regulating metalloproteinases, and therefore enhance BMP signaling activation. Previous studies have shown that Sfrps can facilitate the diffusion of Wnt ligands, suggesting that Sfrps may also modulate diffusion of BMP ligands (Mii and Taira, 2011).

Although BMP signaling is reduced in *sfrp1a/5* MO-injected embryos, we observe an increase in the expression of Wnt and BMP ligands (Fig. 3.7 and Fig. 3.11). This

suggests the existence of a feedback loop regulating Wnt and BMP ligand expression. Previous studies have predicted that BMP ligand expression is regulated in a feed-forward manner. For example, embryos lacking *gdf6a*, a BMP ligand, display a reduction in other ligands such as *bmp2b* and *bmp4* (French et al., 2009; Gosse and Baier, 2009). However, when BMP signaling is inhibited at the level of receptor activation (Dorsomorphin treatment, Fig. 3.10), BMP ligand expression is enhanced, thus indicating a feedback regulation of BMP ligand expression. We observe similar results in *Sfrp1a/5* depleted embryos (Fig. 3.11), indicating that Sfrps modulate BMP signaling at the receptor level and therefore likely regulate BMP ligand diffusion and or function. Although the mechanism of such regulation remains to be elucidated, it is clear that the roles we have described represent an additional method by which Sfrp proteins can influence growth factor signaling.

In our *sfrp* MO-injected embryos we observe significant alterations in dorsal retina identity as well as both Wnt and BMP signaling. Yet, *sfrp1a* and *sfrp5* are predominantly expressed in the ventral retina. Analysis of Sfrp function in *Drosophila* suggests that Sfrps can function as Wnt inhibitors at high levels, and facilitators at low levels (Uren et al., 2000). Sfrp proteins are known to be secreted, suggesting that *Sfrp1a/5* function is not constrained by its expression domain. As such, we suggest that diffusion of *Sfrp1a/5* proteins from the ventral retina supplies the dorsal retina with a low level of extracellular Sfrp protein, which facilitates both Wnt and BMP signaling (Fig. 3.17). Such a model is consistent with the results observed from overexpression of 1 pg of *sfrp5* mRNA, which causes a significant expansion of dorsal marker gene expression domains and an increase in BMP signaling during the initiation phase of retinal patterning (Fig. 3.15). On the other hand, the ventral retina expresses high levels of *sfrp1a/5* mRNA, allowing Sfrps to act in a concentration-dependent manner as inhibitors of signaling in the ventral retina. In accord with this, overexpression of high doses (100 pg) of *sfrp5* mRNA resulted in a reduction of BMP signaling in the dorsal retina and a decrease in dorsal marker gene expression levels as well as an expansion of ventral identity (Fig. 3.13). Overall, our data is consistent with a model in which low concentrations of *Sfrp1a/5* enhance BMP signaling in the dorsal retina and higher levels function to restrict BMP signaling in the ventral retina (Fig. 3.17). In conclusion, our analysis of *Sfrp1a* and *Sfrp5* function during retinal development has

revealed a novel and unexpected regulatory mechanisms for the initiation and maintenance of dorsal-ventral identity.

3.4. Figures

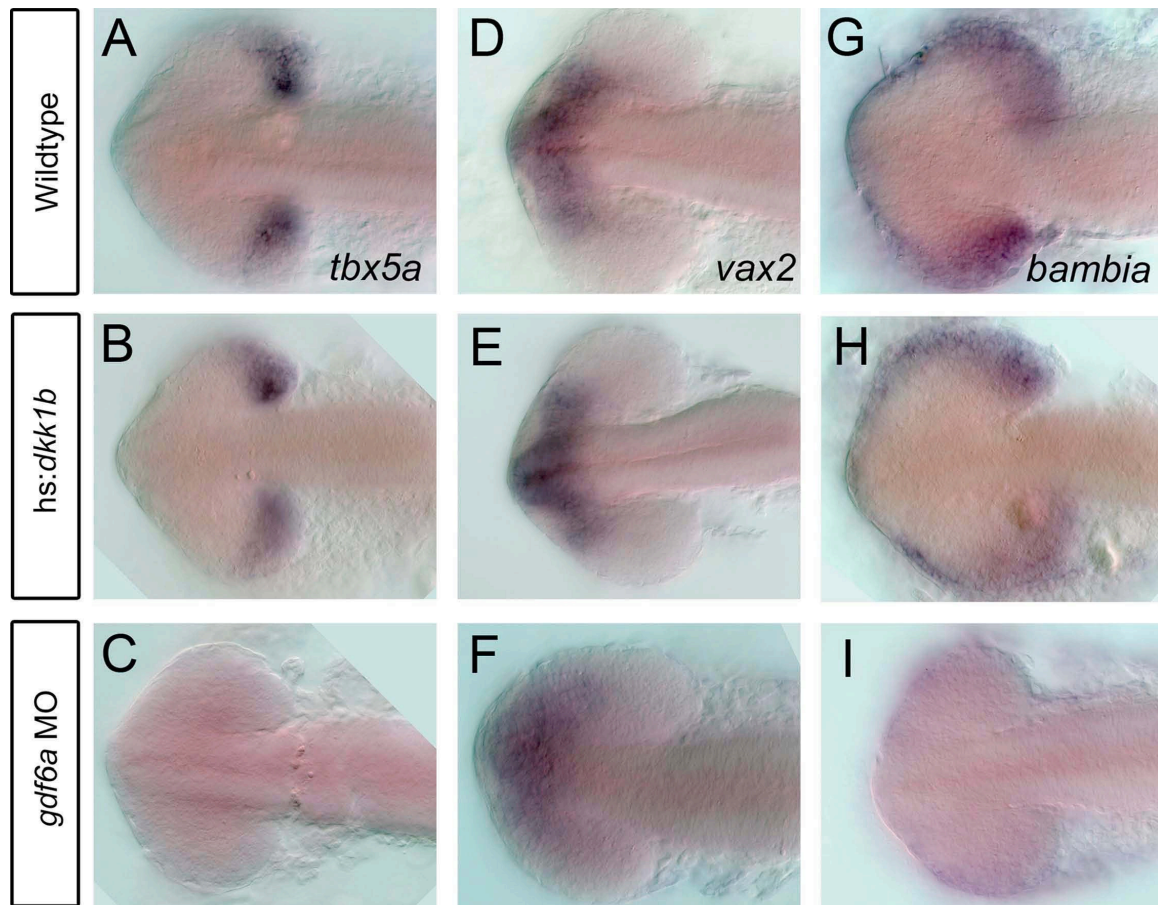


Fig. 3.1: BMP signaling regulates initiation of dorsal-ventral retina patterning. To examine the roles of extra cellular signaling pathways in initiating dorsal retina identity, we carried out in situ hybridization for dorsal (*tbx5a*, *bambia*) and ventral (*vax2*) retina markers in 15 hours post fertilization (hpf) embryos. To block Wnt signaling, we utilized a heat shock inducible Wnt inhibitor *dickkopf 1b* (*dkk1b*). In parallel, we blocked BMP signaling by injecting embryos with morpholinos targeting *growth differentiation factor 6a* (*gdf6a* MO). Dorsal retina genes *tbx5a* (A-C), and *bambia* (G-I) are significantly reduced in the absence of BMP but not Wnt signaling. The ventral retina gene *vax2* (D-F) is also unaffected by the absence of Wnt signaling, while slightly expanded in embryos lacking BMP signaling. All embryos are shown in dorsal mount with anterior aligned to the left.

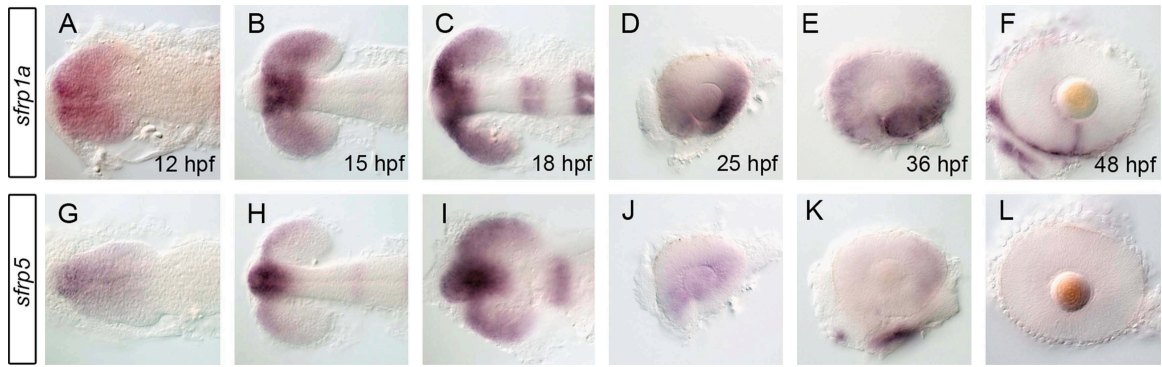


Fig. 3.2: *sfrp1a* and *sfrp5* mRNAs are expressed in the eye during retinal development.

The spatio-temporal pattern of *secreted frizzled related protein* (*sfrp*) mRNA expression was assessed using whole mount in situ during zebrafish eye development. Initial expression of *sfrp1a* demarcates the presumptive eye field (A,B) with later stages displaying patterns specific to the presumptive ventral retina (C–E). Expression of *sfrp1a* persists in the ventral retina up to 48 hpf where it becomes constrained to the choroid fissure (F). In contrast, *sfrp5* expression is more ventrally restricted early (G–I), then decreases significantly from 25 hpf and is absent from the retina by 48 hpf (J–L). Embryos shown are flat-mounted in dorsal (A–C,G–I) or lateral views of dissected eyes (D–F, J–L).

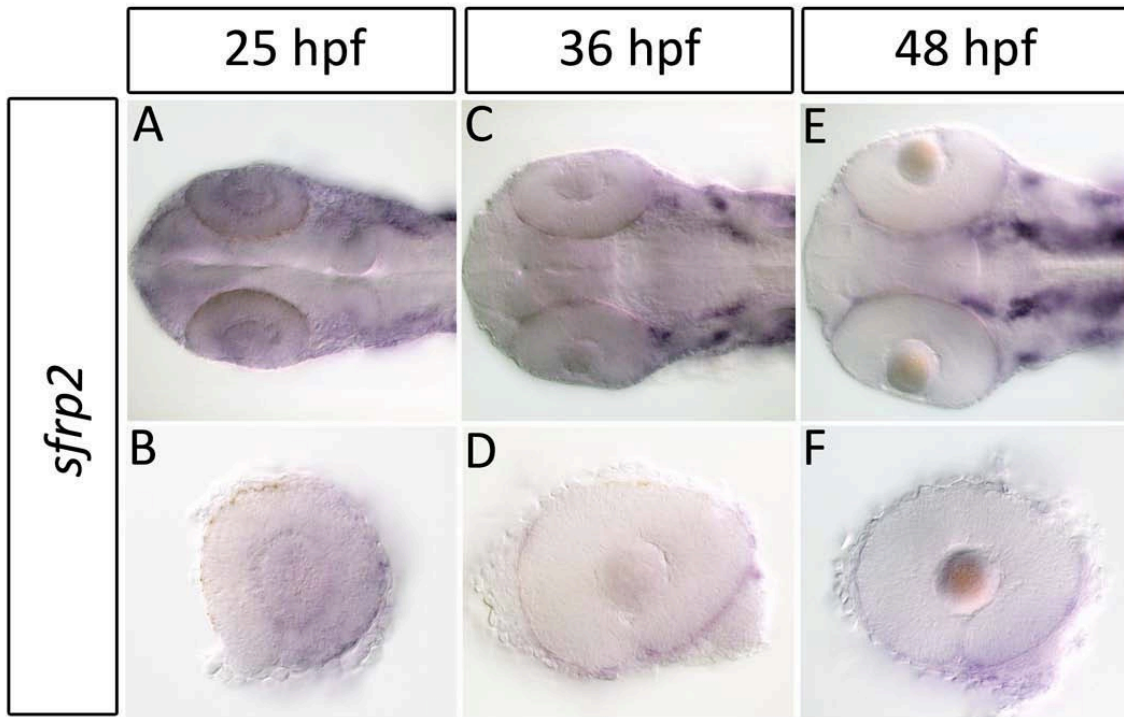


Fig. 3.3: *sfrp2* is expressed at low levels in the retina and primarily in the RPE during retinal development. Expression of *sfrp2* during retinal development was analyzed using in situ hybridization. *sfrp2* is expressed at low levels in the retina and lens at 25 hpf (A-B). By 36 hpf, *sfrp2* expression is confined to the RPE (C-F).

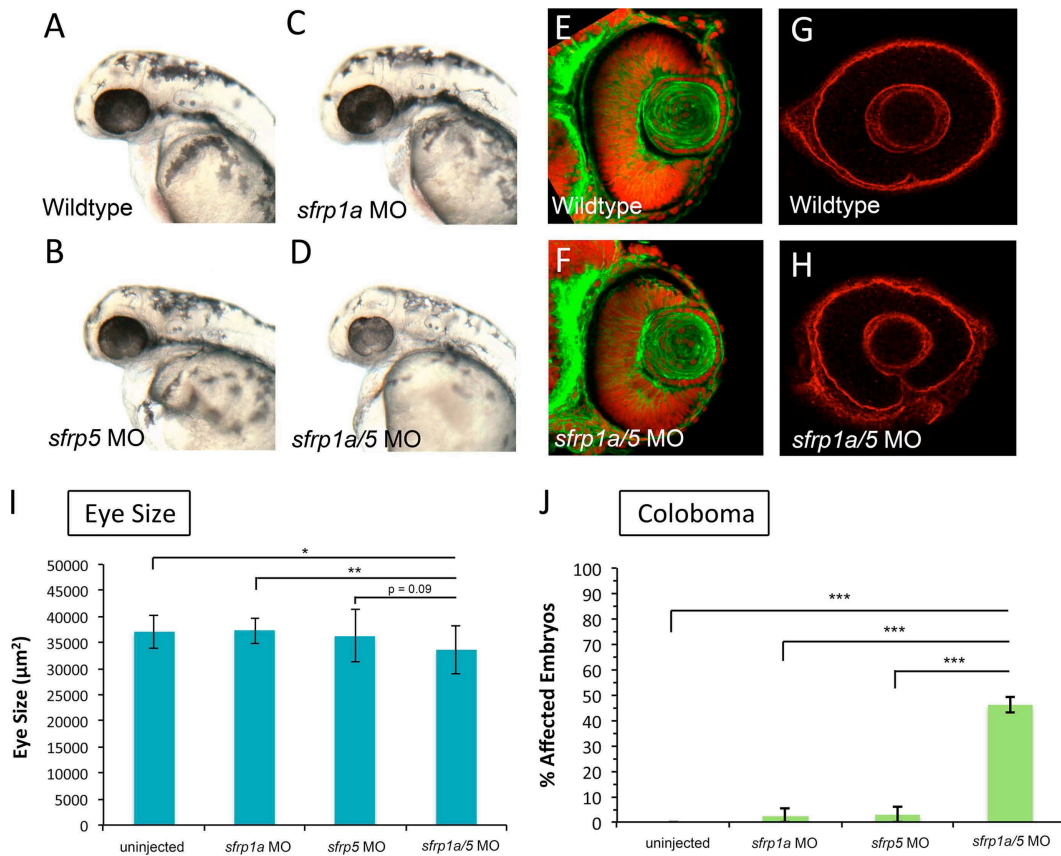


Fig. 3.4: Sfrp1a and Sfrp5 depletion leads to small eyes and coloboma. To ascertain the function of Sfrp proteins during retinal development, we injected one-cell stage zebrafish embryos with morpholinos (MO) targeting *sfrp1a* and/or *sfrp5*. Embryos injected singly with 3 ng of *sfrp1a* or *sfrp5* MO display overtly normal eye size at 25 hpf (A–C). In contrast, *sfrp1a/5* MO co-injected embryos (3 ng each MO) display smaller eyes (D, I) (*, $p < 0.05$; **, $p < 0.01$, ANOVA). 48 hpf retinas stained with phalloidin and TO-PRO3 display no overt difference between wildtype and *sfrp1a/5* MO co-injected embryos (E F). At 48 hpf WT embryos display a dissolution of Laminin staining at the choroid fissure (G). *sfrp1a/5* MO embryos display persistent Laminin staining at the choroid fissure, indicating a coloboma phenotype (G,H). The increase in observed coloboma frequency is statistically significant (***, $p < 0.0036$, Fisher’s Exact) when compared with wild type or embryos injected singly with *sfrp* MOs (J).

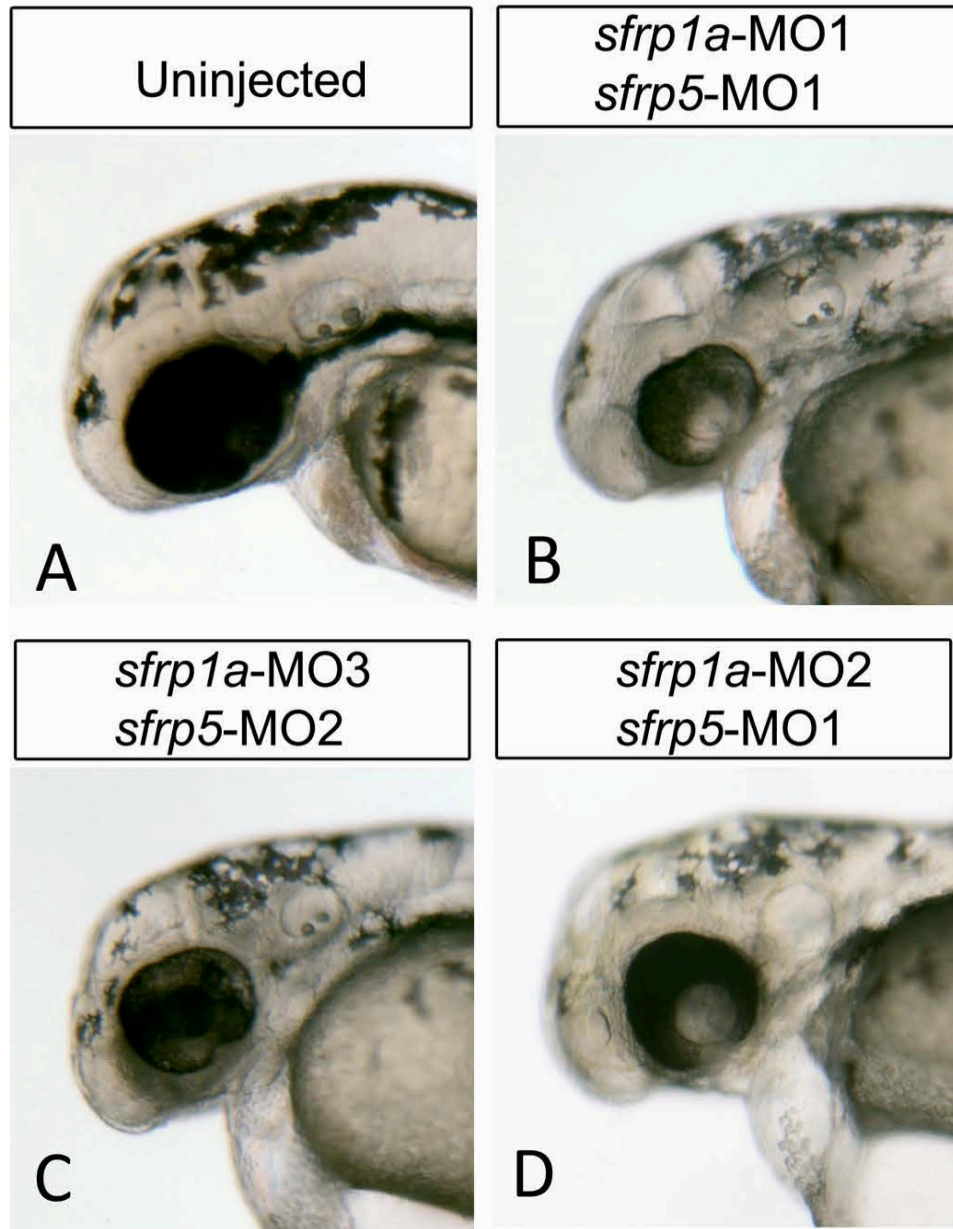


Fig. 3.5: Non-overlapping *sfrp1a* and *sfrp5* morpholinos display similar ocular phenotypes. Embryos injected with combinations of morpholino oligonucleotides (MO) (3 ng each) are analyzed for eye size and morphology at 48 hpf (A-D). The MOs were designed as either translation or splice blocking, with *sfrp1a* MO1 and MO2 splice blocking, and MO3 translation blocking. *sfrp5* MO1 is splice blocking while MO2 is translation blocking.

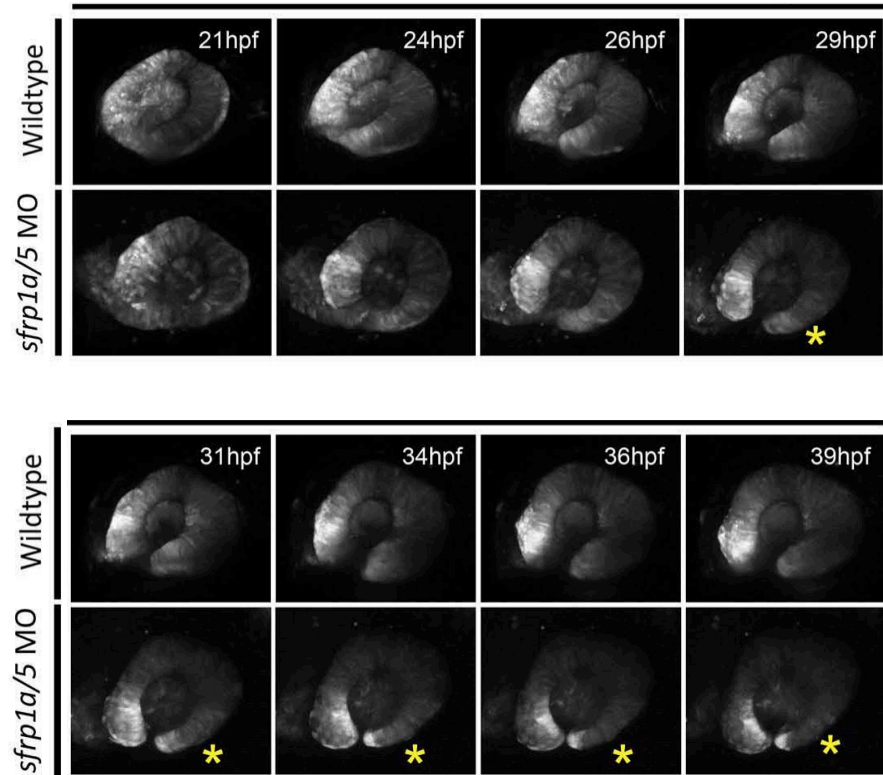


Fig. 3.6: Live embryo analysis of *sfrp1a/sfrp5* depletion during retinal morphogenesis. Time lapse live confocal imaging of the *Tg(Olr3:GFP)* line was employed to visualize retinal morphogenesis. Images are maximum projections of 30 slices collected every 3 μm at 10 minute intervals. Compared to WT, *sfrp1a/5* MO-injected embryos display thinning of the ventral retina as development proceeds from 24 hpf (frames 26 hpf to 39 hpf). Thinning retinal tissue is indicated with a yellow asterisk.

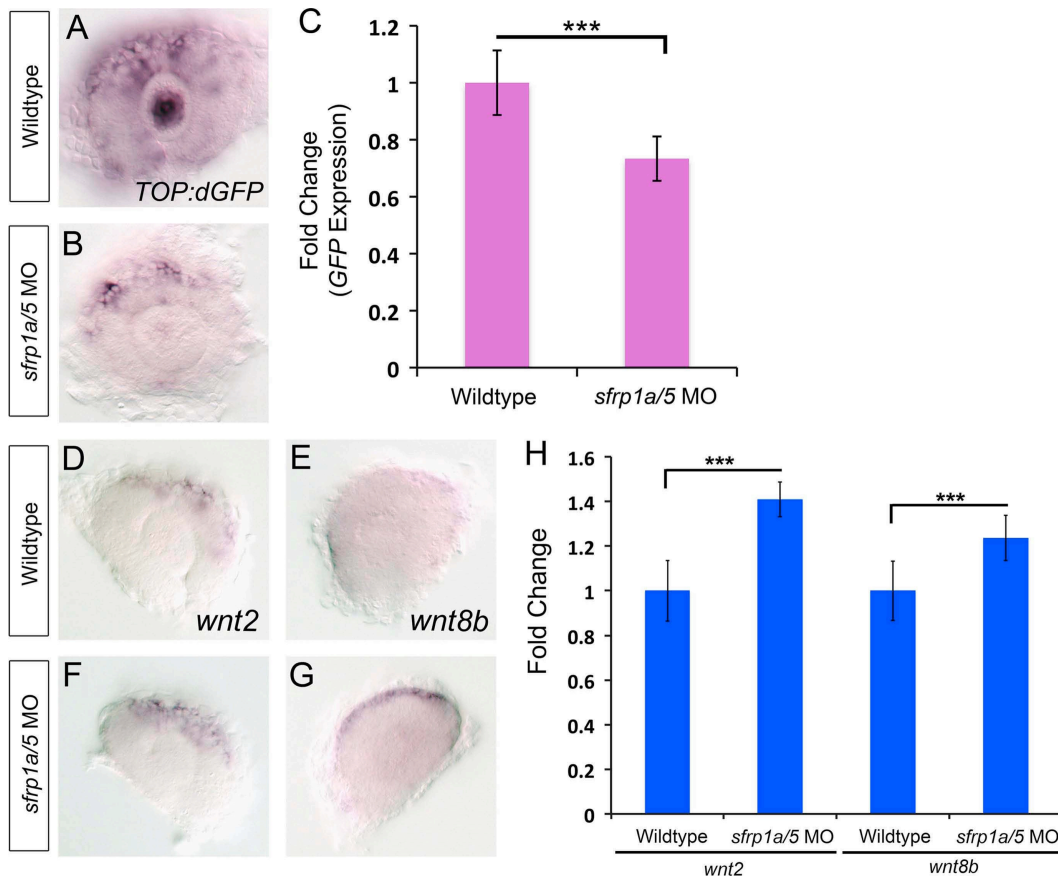


Fig. 3.7: Sfrp1a/Sfrp5 positively regulate Wnt signaling. To determine the function of Sfrp proteins in regulating Wnt signaling, we examined Wnt ligand mRNA expression and a transgene reporter of Wnt signaling using whole mount in situ hybridization and quantitative RT-PCR. In situ hybridization for *egfp* mRNA in the *Tg(TOP:dGFP)* line shows a decrease in *egfp* expression in *sfrp1a/5* MO co-injected embryos, indicating a decrease in Wnt signaling at 28 hpf (A,B). The effects of Sfrp depletion on *egfp* expression were significantly different (C, ***, $p < 0.001$). In situ hybridization of Wnt ligands *wnt2* and *wnt8b* at 28 hpf show an expansion in the expression domain of *wnt2* and *wnt8b* in the dorsal retina in *sfrp1a/5* MO injected embryos (D–G). qRT-PCR confirmed a 1.33 fold change in *wnt2* and 1.38 fold change in *wnt8b* expression (H, ***, $p < 0.005$).

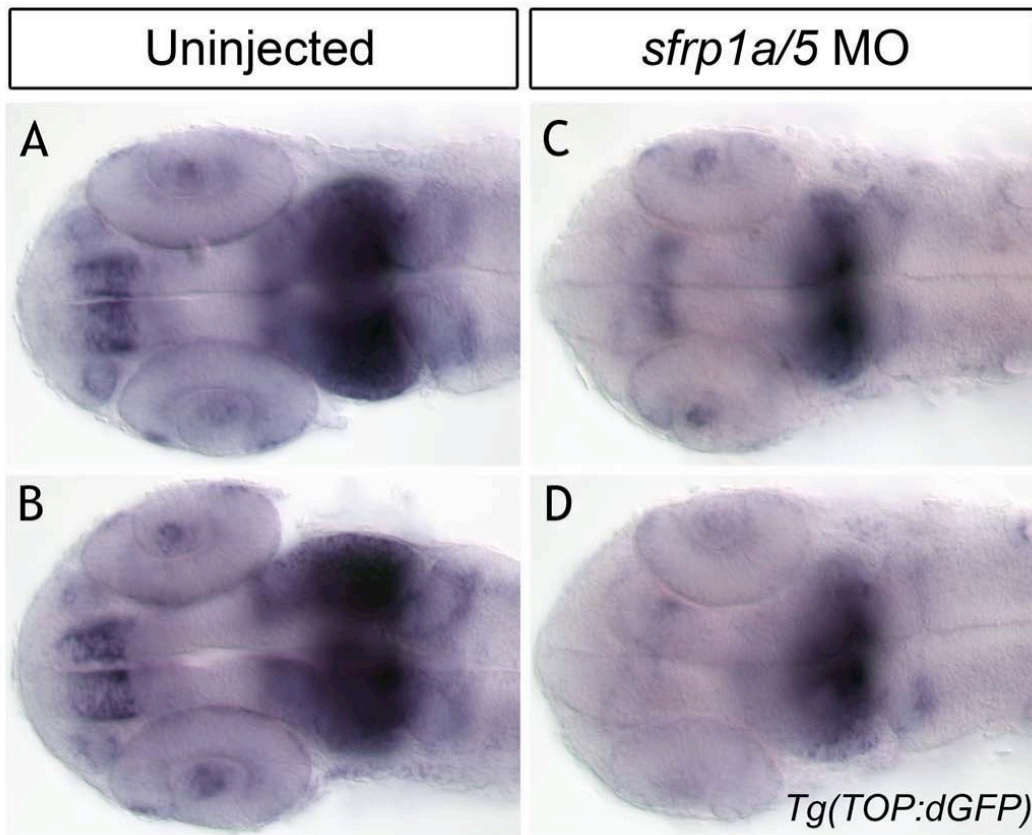


Fig. 3.8: *sfrp1a/5* knockdown reduces Wnt signaling in *Tg(TOP:dGFP)* embryos. In situ hybridization for *egfp* mRNA in the *Tg(TOP:dGFP)* line shows a pattern of Wnt signaling regionalized in the forebrain and midbrain at 24 hpf (A-B). We note a decrease in domain and intensity of *egfp* signal in *sfrp1a/5* MO injected embryos (C-D), indicating a decrease in Wnt signaling in these tissues.

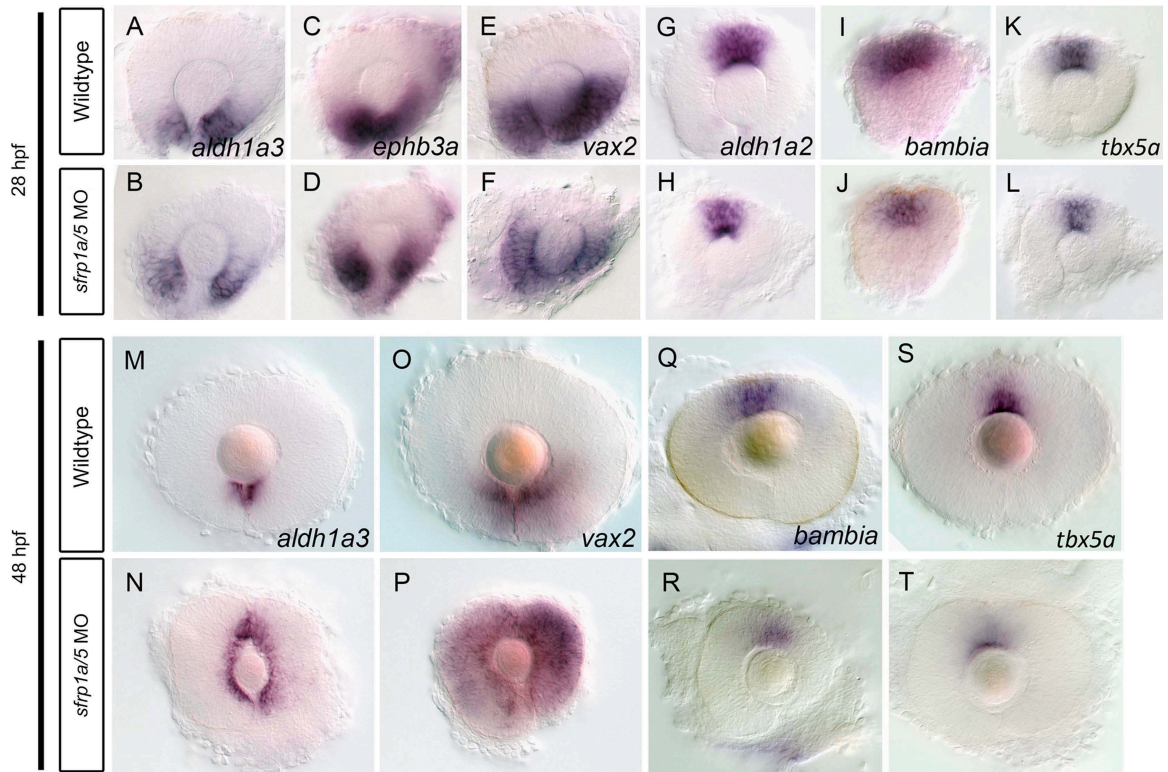


Fig. 3.9: Sfrp1a/Sfrp5 regulate retinal dorsal-ventral patterning. To examine dorsal-ventral retina patterning in *sfrp1a/5* MO co-injected embryos, we employed in situ hybridization of ventral marker genes *aldh1a3*, *ephb3a* and *vax2*, as well as dorsal markers *aldh1a2*, *bambia*, and *tbx5a* at 28 and 48 hpf. At 28 hpf, *sfrp1a/5* MO injected embryos display a normal domain of ventral markers compared to WT, though with slightly reduced levels (A–F). Analysis of 28 hpf dorsal retina patterning in *sfrp1a/5* MO embryos also demonstrates a decreased expression of markers (G–L). By 48 hpf, in comparison to controls, *sfrp1a/5* MO injected embryos display an expansion of both *aldh1a3* and *vax2* expression into the dorsal regions of the retina (M–P). Analysis at 48 hpf demonstrates a clear reduction of *tbx5a* and *bambia* expression domains and levels in *sfrp1a/5* MO injected embryos (Q–T).

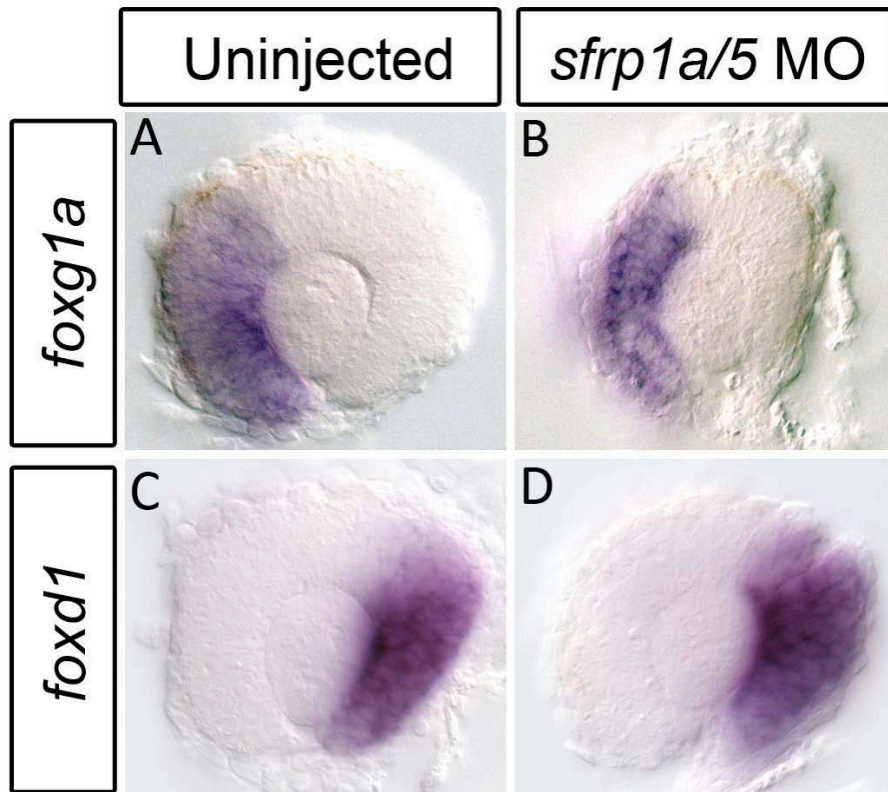


Fig. 3.10: *Sfrp1a/5* loss of function does not affect nasal-temporal retinal patterning. Having observed alterations in dorsal-ventral patterning in *sfrp1a/5* morpholino (MO) injected embryos, we sought to analyze nasal-temporal patterning by performing in situ hybridization for temporal (*foxd1*) and nasal (*foxg1a*) retina markers. Compared to WT, *sfrp1a/5* MO injected embryos display no change in the expression pattern of *foxg1a* (A-B) (n=17/17) or *foxd1* (C-D) (n=14/14) at 28 hpf.

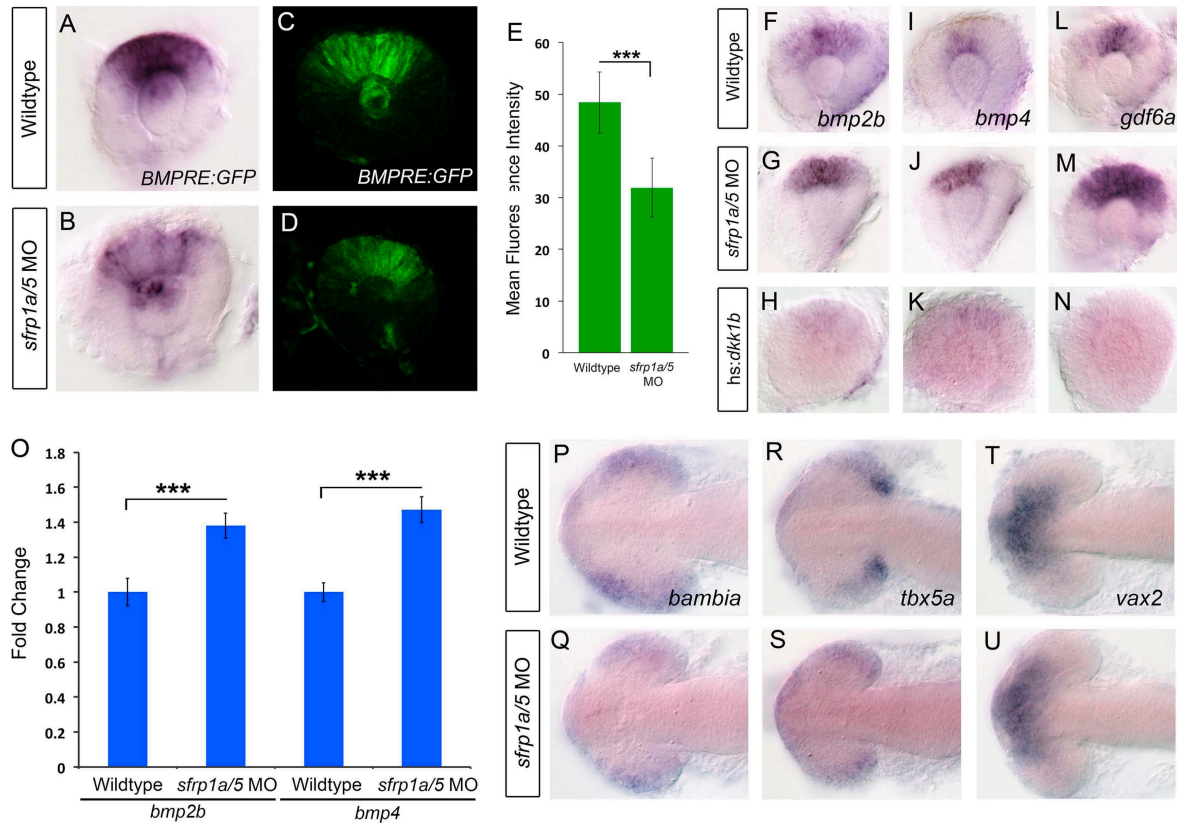


Fig. 3.11: Sfrp1a/Sfrp5 positively regulate BMP signaling during retinal development.

Given the observed alterations in dorsal retina marker gene expression, we sought to investigate the activity of BMP signaling in Sfrp depleted retinas. We measured BMP pathway activity by employing a BMP responsive transgene, *Tg(BMPRE-AAV.Mlp:eGFP)*, which is abbreviated *BMPRE:GFP*. In situ hybridization for *gfp* mRNA, or fluorescence microscopy results indicate that compared to WT, *sfrp1a/5* MO co-injected embryos display a marked decrease in GFP signal at 28 hpf (A–D). Measurements of mean retinal fluorescence intensity indicate a significant decrease in GFP signal in *sfrp1a/5* MO injected embryos (E, ***, $p < 0.0001$). To assess expression of BMP ligand mRNAs, we conducted in situ hybridization of BMP ligands *bmp2b*, *bmp4* and *gdf6a* at 28 hpf. Compared to WT, *sfrp1a/5* MO injected embryos display an increase in BMP ligand expression (F–G, I–J, L–M). Conversely, inhibition of Wnt signaling by heat shock activation of *dkk1b*, greatly reduces expression of *bmp2b*, *bmp4* and *gdf6a* at 28 hpf (H,K,N). qRT-PCR of *bmp2b* and *bmp4* confirmed a 1.38 and 1.47 fold increase in expression respectively (O, ***, $p < 0.0001$). To assess the functions of Sfrp proteins in the BMP-dependent initiation phase of retinal patterning, we conducted in situ hybridization for *bambia* and *tbx5a* and ventral

marker *vax2* during the initiation of dorsal eye patterning at 15 hpf. Compared to WT, *sfrp1a/5* MO injected embryos display a decrease in *tbx5a* and *bambias* expression levels and domain while *vax2* appears unaffected (P-U).

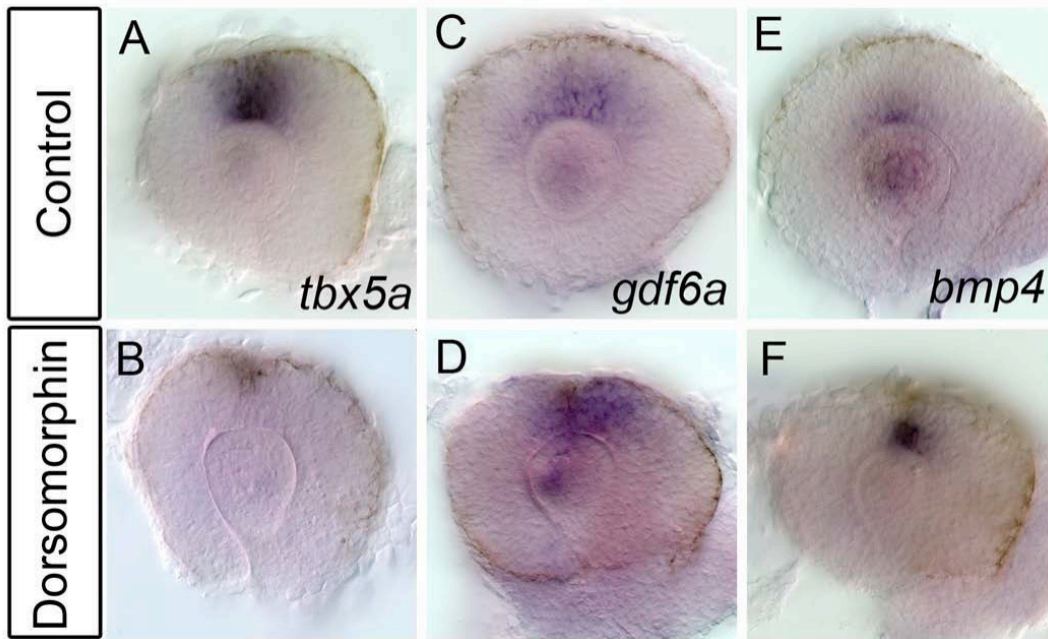


Fig. 3.12: Dorsomorphin treatment enhances BMP ligand expression. In order to analyze regulation of BMP ligand expression, BMP signaling was inhibited with 100 μ M dorsomorphin. To confirm BMP inhibition, *tbx5a* expression was analyzed using in situ hybridization. Loss of *tbx5a* expression at 28 hpf indicates loss of BMP signaling (A-B). Expression of BMP ligands, *gdf6a* and *bmp4* at 28 hpf, analyzed using in situ hybridization, is increased upon dorsomorphin treatment (C-F).

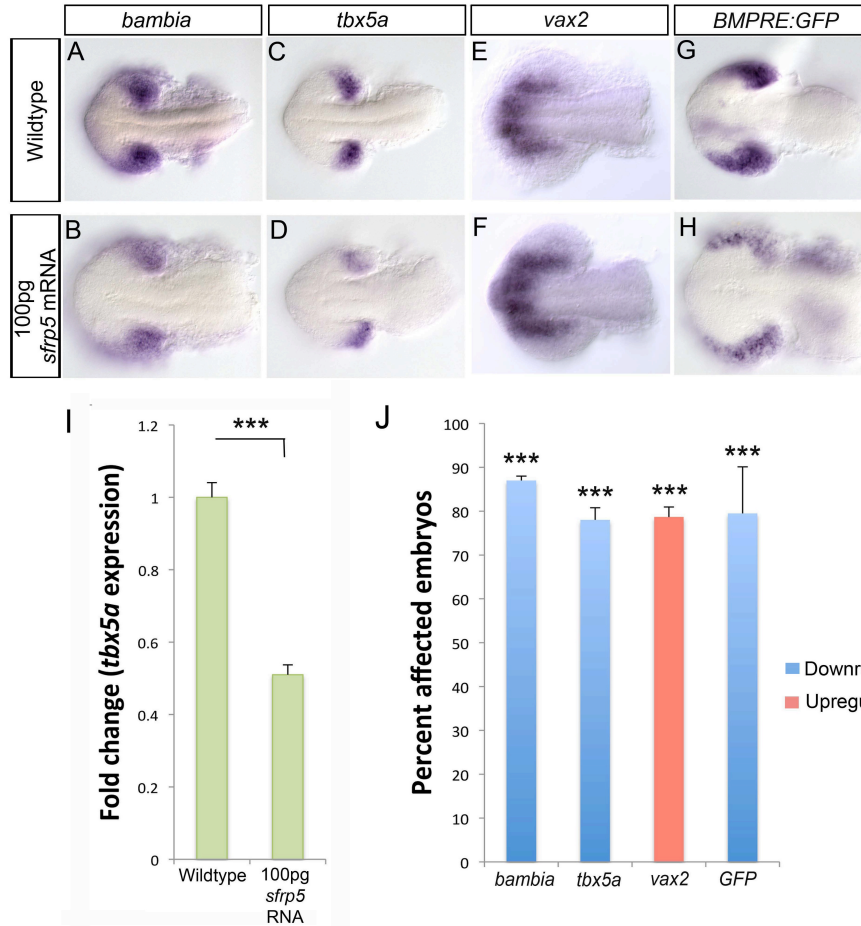


Fig. 3.13: Overexpressing a high dose of *sfrp5* mRNA results in reduction of dorsal and expansion in ventral retina identity. Using in situ hybridization, we analyzed dorsal markers *bambia* and *tbx5a* and the ventral marker *vax2* at 15 hpf in embryos injected with 100 pg *sfrp5* mRNA. Compared to WT, the levels of both *tbx5a* and *bambia* expression is significantly reduced in *sfrp5* mRNA injected embryos (A–D) while *vax2* shows both an increase in expression levels and an expansion of the domain (E–F). We measured BMP signaling using the *Tg(BMPRE-AAV.Mlp:eGFP)* transgenic strain, which is abbreviated *BMPRE:GFP*. In situ hybridization for *egfp* mRNA in 15 hpf embryos injected with 100 pg *sfrp5* mRNA indicates a decrease in BMP signaling compared to wildtype (G–H). Prevalence of change in expression for all probes was quantified and significance was assessed using Fisher’s Exact Test (J, ***, $p < 0.0001$). qRT-PCR results for *tbx5a* expression at 15 hpf in *sfrp5* mRNA injected embryos indicate a 0.5 fold decrease in expression (I, ***, $p < 0.0001$, Student’s t-test).

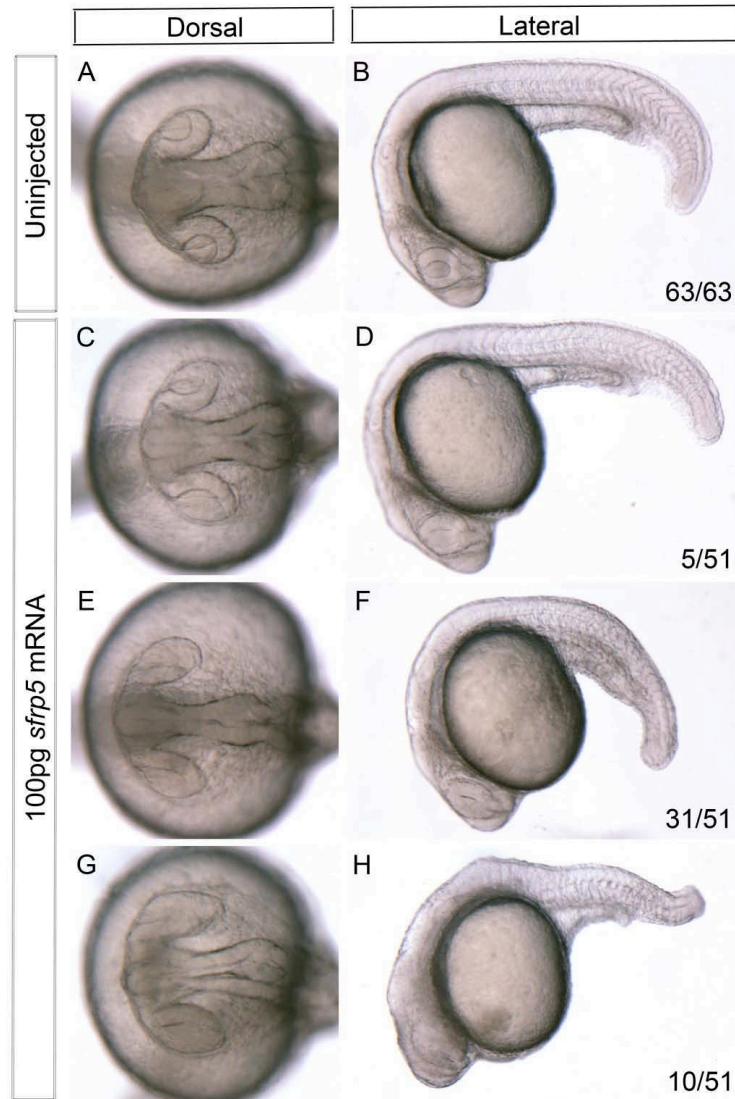


Fig. 3.14: Morphological assessment of zebrafish embryos injected with 100 pg of *sfrp5* mRNA. One-cell stage embryos were injected with a high dose (100 pg) of *sfrp5* mRNA. Embryos were grown to 22 hpf and analyzed for gross morphological defects. Uninjected controls display no aberrations in either eye or axis specification (A-B, n=63/63). Of the embryos injected with a high dose of *sfrp5* mRNA, 5/51 display no overt phenotype (C-D), 31/51 display subtly elongated eyes and very mild dorsalization (E-F), and 10/51 display extensive elongation of eyes as well as moderate dorsalization (G-H).

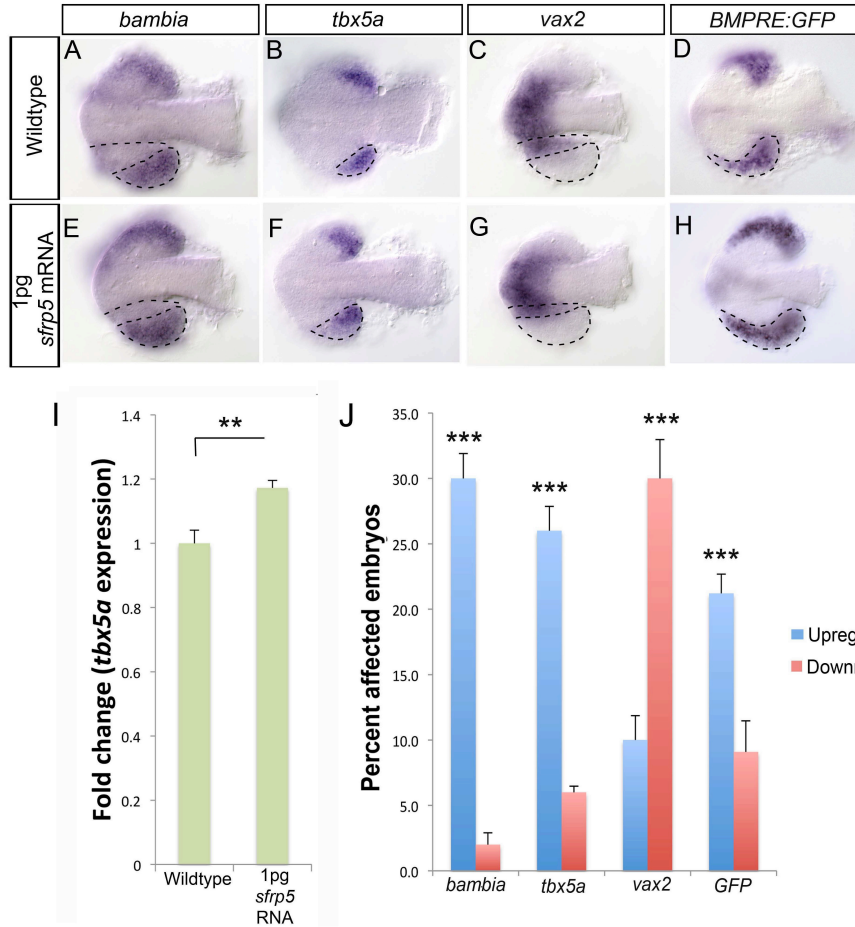


Fig. 3.15: Injection of low dose (1 pg) of *sfrp5* mRNA causes an increase in dorsal marker gene expression and BMP signaling. We used in situ hybridization to assess dorsal markers *bambia* and *tbx5a* and the ventral marker *vax2* at 15 hpf in embryos injected with 1 pg *sfrp5* mRNA. Both *tbx5a* and *bambia* expression domains are expanded in *sfrp5* mRNA injected embryos compared to wild type (A–D) while the *vax2* domain is significantly reduced (E–F). We measured BMP signaling using the *Tg(BMPRE-AAV.Mlp:eGFP)* transgenic strain, which is abbreviated to *BMPRE:GFP*. In situ hybridization for *egfp* mRNA in 15 hpf embryos injected with 1 pg *sfrp5* mRNA indicate an increase in BMP signaling compared to wild type (G–H). Prevalence of change in expression for all probes was quantified and significance was assessed using Fisher’s Exact Test (J, ***, $p < 0.0001$). qRT-PCR results for *tbx5a* expression at 15 hpf in *sfrp5* mRNA injected embryos indicate a 1.17 fold increase in expression (I, **, $p < 0.01$, Student’s t-test).

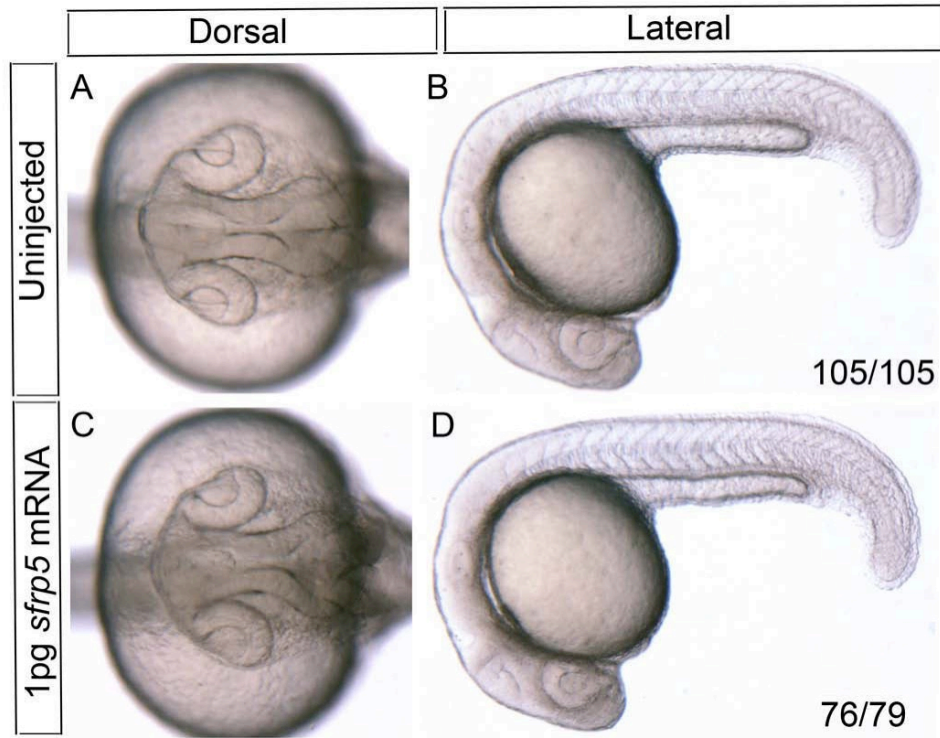


Fig. 3.16: Morphological assessment of zebrafish embryos injected with 1 pg of *sfrp5* mRNA. One-cell stage embryos were injected with a low dose (1 pg) of *sfrp5* mRNA. Embryos were grown to 22 hpf and analyzed for gross morphological defects. Uninjected controls display no aberrations in either eye or axis specification (A-B, n=105/105). Of the embryos injected with a low dose of *sfrp5* mRNA, 76/79 display no overt phenotype (C-D).

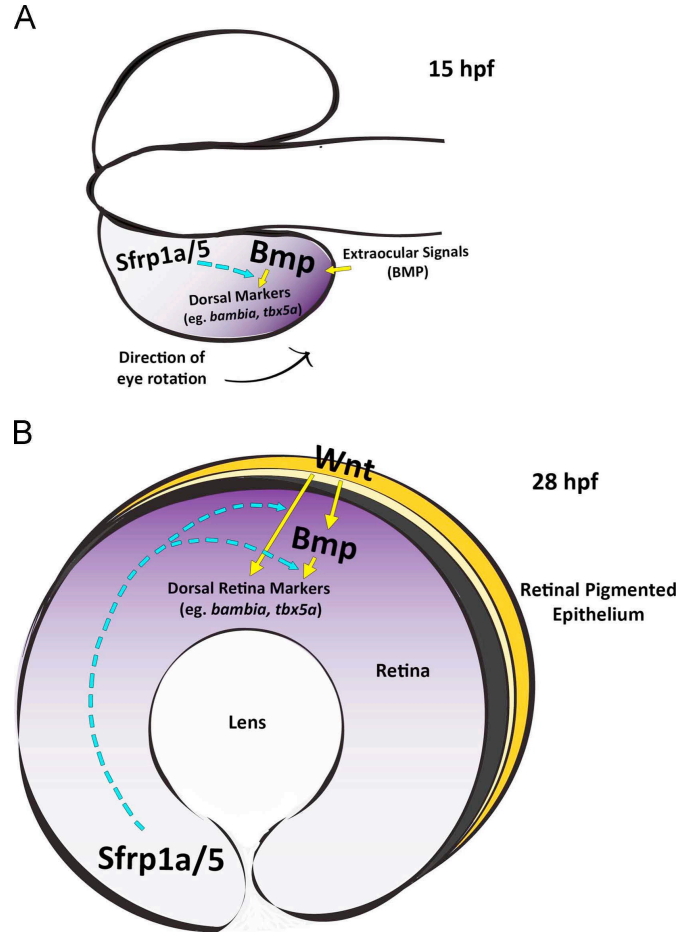


Fig. 3.17: Sfrp functions to regulate dorsal-ventral retina patterning. Dorsal retina identity requires BMP and Wnt signaling to drive expression of dorsal genes such as *tbx5a* and *bambio*. During the initiation phase of dorsal retina identity (A; 15 hpf), extraocular BMP ligands activate marker genes (*bambio* and *tbx5a*) in the adjacent optic cup. The presumptive dorsal domain of the retina is denoted with purple shading. The activity of BMP in this phase of retinal patterning is facilitated by the activity of Sfrp1a and Sfrp5 (dotted blue lines). At 28 hpf (B), dorsal retina identity is maintained by the combined activities of Wnt and BMP signaling. *sfrp1a/5* are expressed in the ventral retina and the proteins diffuse across the retina toward the dorsal BMP expression domain. At low concentrations found in the dorsal retina, Sfrp1a/Sfrp5 can enhance both Wnt and BMP activity and therefore facilitate levels and/or extend the boundaries of BMP signaling.

Chapter 4

A secreted WNT-ligand-binding domain of FZD5 generated by a frameshift mutation causes autosomal dominant coloboma

A version of this chapter has been published. Chunqiao Liu, Sonya A. Widen, Kathleen A. Williamson, Rinki Ratnapriya, Christina Gerth-Kahlert, Joe Rainger, Ramakrishna P. Alur, Erin Strachan, Souparnika H. Manjunath, Archana Balakrishnan, James A. Floyd, UK10K Consortium, Tiansen Li, Andrew Waskiewicz, Brian P. Brooks, Ordan J. Lehmann, David R. FitzPatrick, and Anand Swaroop (2016). A secreted WNT-ligand-binding domain of Fzd5 generated by a frameshift mutation causes autosomal dominant coloboma. *Human Molecular Genetics*, **25**(7): 1382-1391

4.1. Introduction

Ocular coloboma (OC) is a developmental structural defect caused by the abnormal persistence of the optic fissure in postembryonic life. In combination with microphthalmia (small eyes) and anophthalmia (absent eyes), OC represents a spectrum of malformations that account for an estimated 10–15% of pediatric blindness (Hornby et al., 2000). Transcription factors and signaling pathways play crucial roles in optic cup morphogenesis and fissure closure (Gregory-Evans et al., 2004; Williamson and FitzPatrick, 2014). Accordingly, human genetic studies together with vertebrate models have implicated bone morphogenetic protein (Asai-Coakwell et al., 2007; Bakrania et al., 2008; Rainger et al., 2011; Wyatt et al., 2010), hedgehog (Hh; (Schimmenti et al., 2003)), retinoic acid (Fares-Taie et al., 2013; Pasutto et al., 2007; Srour et al., 2013) and hippo (Williamson et al., 2014) pathways in the pathogenesis of these ocular malformations (Morcillo et al., 2006; Reis et al., 2011; Schimmenti et al., 2003; Ye et al., 2010). Defects in components of Wnt signaling have been attributed to syndromic and non-syndromic ocular diseases, including Norrie disease (Chen et al., 1993; Nikopoulos et al., 2010), osteoporosis-pseudoglioma syndrome (Gong et al., 2001) and familial exudative vitreoretinopathy (Chen et al., 1993; Nikopoulos et al., 2010; Poulter et al., 2012; Robitaille et al., 2002; Toomes et al., 2004), but not as a cause of abnormal ocular morphogenesis.

A growing body of evidence from several vertebrate models indicates that Wnt signaling is indispensable in eye field development and ocular morphogenesis. In the Wnt pathway, non-canonical (β -catenin-independent) signaling interacts with canonical (β -catenin-dependent) signaling to control presumptive retinal versus forebrain fates (Cavodeassi et al., 2005). Loss of non-canonical ligands, Wnt5 and Wnt11, causes failure of eye field segregation (Cavodeassi et al., 2005), whereas inactivation of β -catenin prior to optic vesicle differentiation causes anophthalmia (Hägglund et al., 2013). At later stages of development, the canonical pathway also contributes to optic cup morphogenesis, with overexpression of the Wnt inhibitor *dickkopf-related protein 1* (*dkk1*) leading to abnormal lens formation and coloboma (Lieven and Rütger, 2011; Veien et al., 2008). Furthermore, the loss of the Secreted Frizzled (Fzd)-Related Proteins (Sfrps; known modulators of Wnt signaling) causes defects in optic cup patterning (Holly et al., 2014). The Wnt receptor

Fzd5 mediates both canonical and non-canonical signaling in a context-dependent manner (Cavodeassi et al., 2005; Liu and Nathans, 2008). During eye field specification, Fzd5 is specifically expressed in evaginating eye precursors (Borello et al., 1999; Sumanas and Ekker, 2001). In zebrafish, Wnt11–Fzd5 signaling promotes eye field specification using the non-canonical pathway (Cavodeassi et al., 2005). In *Xenopus*, Fzd5 acting via the canonical pathway controls the neural potential of retinal progenitors through regulation of *Sox2* (Van Raay et al., 2005). Mouse *Fzd5*^{-/-} mutants display extreme optic cup invagination defects with failure to induce lens formation (Burns et al., 2008), whereas conditional *Fzd5* mutants (Fig. 4.1) exhibit both microphthalmia and coloboma with disrupted retinal epithelial apical junctions (Liu and Nathans, 2008; Zhou et al., 2008), implicating *Fzd5* in mammalian ocular morphogenesis and early neurogenesis. Additionally, mouse knockout mutants of *Lrp6*, encoding a Fzd co-receptor presumed to be in the canonical Wnt signaling pathway (Zhou et al., 2008), demonstrate ocular phenotypes similar to those observed in the conditional *Fzd5* mutants. We therefore hypothesized that mutations in *FZD5* may be involved in the development of human congenital ocular malformations.

In this study, we identified an autosomal dominant pedigree of colobomatous patients carrying a detrimental variant in *FZD5*. Functional analysis of the mutant protein using zebrafish, mouse retinal explants and co-culture assays, strongly suggests a dominant-negative effect on Wnt signaling, which is likely responsible for optic fissure closure defects. The present study, therefore, directly implicates WNT–FZD signaling in the pathogenesis of human coloboma.

4.1.1. Summary

Ocular coloboma is a common eye malformation resulting from incomplete fusion of the optic fissure during development. Coloboma is often associated with microphthalmia and/or contralateral anophthalmia. Coloboma shows extensive locus heterogeneity associated with causative mutations identified in genes encoding developmental transcription factors or components of signaling pathways. We report a rare, heterozygous

frameshift mutation in *FZD5* (p.Ala219Glufs*49) that was identified independently in two branches of a large family with autosomal dominant non-syndromic coloboma. *FZD5* has a single-coding exon and consequently a transcript with this frameshift variant is not a canonical substrate for nonsense-mediated decay. *FZD5* encodes a transmembrane receptor with a conserved extracellular cysteine rich domain for ligand binding. The frameshift mutation results in the production of a truncated protein, which retains the Wingless-type MMTV integration site family member-ligand-binding domain, but lacks the transmembrane domain. The truncated protein was secreted from cells, and behaved as a dominant-negative FZD5 receptor, antagonizing both canonical and non-canonical WNT signaling. Expression of the resultant mutant protein caused coloboma and microphthalmia in zebrafish, and disruption of the apical junction of the retinal neural epithelium in mouse, mimicking the phenotype of *Fz5/Fz8* compound conditional knockout mutants. Our studies have revealed a conserved role of WNT–FZD signaling in ocular development and directly implicate both in normal closure of the human optic fissure and pathogenesis of coloboma.

4.2. Results

4.2.1. *A frameshift mutation in FZD5 causes autosomal dominant coloboma*

Whole exome sequencing (WES) was performed as part of the rare disease component of UK10K (www.uk10k.org) in five members of a large family with autosomal dominant ocular coloboma (OC; Family 3483; Fig. 4.2A–C). The affected individuals IV:6, V:1, VI:2 and VI:5 shared only one ultra rare variant (not present in exome aggregation consortium [ExAC], EVS, 1000G, UK10K internal databases); a frameshift mutation in *FZD5* (c.656delCinsAG; p.Ala219Glufs*49, hereafter referred to as A219Xfs*49). This variant was then shown to co-segregate with the disease in all affected individuals available for testing with one exception, IV:7 (Fig. 4.2A). IV:7 has bilateral coloboma, but is ‘married-in’ to the family, being unrelated to the affected individuals VI:2, V:1, IV:1, IV:4 and IV:6 (his wife). He has no prior family history of eye malformations and no other plausible causative variants could be identified in his exome sequence data. Two unaffected individuals (III:2 and V:8) also carried the mutation and were considered as non-penetrant. Targeted re-sequencing of *FZD5* in an additional 380 unrelated coloboma patients from the MRC Human Genetics Unit Cohort as part of UK10K revealed no other potentially pathogenic variants.

Concurrently, *FZD5* was screened as a candidate gene based on mouse studies (Liu et al., 2012; Liu and Nathans, 2008), in individuals with OC from family 111, where each individual exhibited bilateral coloboma and related phenotypes (e.g., microphthalmia, cataract) (Fig. 4.2A and B). Haplotype analysis using five microsatellite markers flanking the *FZD5* gene suggested a recent common ancestry between Family 3483 and Family 111 (Fig. 4.3). Based on the information provided by family 3483 that individual II:4 had emigrated to North America, this female represented a plausible genetic link with Family 111. In addition, both families are of Mennonite ancestry and originated from the same region in Europe. For the purpose of calculating the two-point LOD score, we designated II:4 in Family 3483 as the maternal great-grandmother of individual I:2 in Family 111, which is the closest possible link based on information from Family 111. This was a conservative approach, as it would generate a minimum possible LOD score associated with co-segregation of the disease and the mutation in the combined family. The linkage

analysis was performed using the R package paramlink. Co-segregation of the *FZD5* mutation with coloboma in the extended pedigree gave a two-point LOD score ($\theta = 0$) ranging from 3.9 to 4.2 using penetrance values between 0.1 and 1. It was not possible to obtain an accurate estimate of the penetrance for this mutation as we were not able to examine or genotype all apparently unaffected individuals in both branches of the family. However, on the basis of the genotypes, we can safely conclude a relatively high, but incomplete penetrance of the disease mutation.

FZD5 has a single coding exon with a 5' non-coding exon. As such, the mutant transcript that codes for A219Xfs*49 is not predicted to be a substrate for nonsense-mediated decay. The A219Xfs*49 mutation is thus likely to result in production of a truncated *FZD5* protein with an intact highly conserved ligand-binding domain (extracellular cysteine rich domain [CRD]), but lacking the seven transmembrane domains (Fig. 4.2D) (Fig. 4.4).

Screening a cohort of 172 unrelated individuals resulted in the identification of one additional rare missense variant (c.290A>T; p.Asp97Val (D97V); Table 4.1 and Fig. 4.5A and B). This variant is of uncertain significance as this variant was not present in the unaffected mother or brother and the father was deceased (Fig. 4.5). This variant did not significantly change the *Fzd5* protein level or its membrane localization by in vitro transfection assay (Fig. 4.5C). Atomic non-local environment assessment (ANOLEA) predicted that the D97V variant would perturb local interactions (Fig. 4.5D). Super-TOPflash (STF) reporter assays indicated a slight, but consistent increase of Wnt9b-stimulated canonical Wnt activity by the D97V mutation (Fig. 4.5E) suggesting a gain of function.

4.2.2. *Expression of FZD5 A219Xfs*49 in zebrafish results in microphthalmia and coloboma*

To elucidate the functional relevance of the human *FZD5* A219Xfs*49 mutation, zebrafish were initially used as a model system. Concordant with observations in mouse *Fzd5* mutants (Liu et al., 2012; Liu and Nathans, 2008), *Fzd5*-depleted zebrafish exhibited

coloboma and microphthalmia phenotypes (Fig. 4.6A–D). In addition, expression of the *FZD5 A219Xfs*49* mutant mRNA in zebrafish embryos also resulted in coloboma and microphthalmia (Fig. 4.6E–J). Surprisingly, these phenotypes were more prevalent when the wild type *FZD5* mRNA was expressed (Fig. 4.6K–L). We noted that the eye size was similar when either *FZD5* or *FZD5 A219Xfs*49* mutant was expressed (Fig. 4.7). These observations suggest that precise Wnt-Fzd5 signaling dosage is critical for ocular development.

*4.2.3. FZD5 A219Xfs*49 is a secreted protein that binds to Wnt ligands, but is incapable of mediating WNT signaling*

To further understand the functional consequences of the human *FZD5 A219Xfs*49* mutation, we examined mutant protein levels and localization in vitro. Transfection of *A219Xfs*49* cDNA construct into human embryonic kidney (HEK) 293 cells produced a truncated FZD5 protein as predicted, containing the entire ligand-binding domain, but not the transmembrane domains. Under non-reducing conditions, the variant FZD5 *A219Xfs*49* protein shows multiple bands in the cell extracts, including one of ~50 kDa and several ~21 kDa (Fig. 4.8A). With the addition of β -mercaptoethanol, the truncated FZD5 protein primarily migrated at a lower molecular weight in the extracellular matrix (ECM) fraction (Fig. 4.8A). Live cell surface immunofluorescence analysis confirmed that truncated FZD5 protein did not localize to the outer cell membrane (in contrast to the full length FZD5) and instead displayed punctate and/or irregular extracellular staining (Fig. 4.8B, Fig. 4.9). As predicted, the *A219Xfs*49* FZD5 protein disrupted the ability to mediate both canonical (Fig. 4.8C, based on integrated T Cell Factor [TCF]-dependent reporter) and non-canonical WNT signaling activities (Fig. 4.8D, based on pull-down assay of Wnt5a stimulated guanosine triphosphate [GTP]-RhoA). An engineered secreted FZD5-CRD protein (cysteine-rich domain; sCRD, fused with human Ig-Fc fragment) had an effect similar to the *A219Xfs*49* FZD5 mutant (Fig. 4.8C and D), suggesting that the secretion of the truncated FZD5 protein is critical for its abnormal function. To examine whether *A219Xfs*49* FZD5 binds to Wnt ligands, co-immunoprecipitation (co-IP) experiments

were conducted using cell extracts transfected with *Wnt3a-myc*, *WNT7A-HA*, *FZD5* and *FZD5 A219Xfs*49* constructs in different combinations (Carmon and Loose, 2008, 2010). We detected binding of A219Xfs*49 FZD5 to WNT7A as well as WT FZD5 (Fig. 4.10), suggesting that truncated and WT FZD5 may compete for Wnt ligands.

4.2.4. *FZD5 A219Xfs*49 antagonizes both canonical and non-canonical Wnt signaling*

Given the abnormal function of truncated A219Xfs*49, as indicated by its aberrant localization at the plasma membrane, and that A219Xfs*49 was associated with a dominant mode of inheritance in Family 3483 and Family 111, we reasoned that FZD5 A219Xfs*49 may act as a secreted FZD-related protein (Bodine et al., 2004). This acquired secretory function may allow A219Xfs*49 to act non-cell-autonomously and antagonize WNT–FZD5 activity expressed from the WT allele. To test this hypothesis, a co-culture assay was developed in which constructs encoding A219Xfs*49 and Wnt9b with FZD5 were, respectively, transfected into HEK293 and STF cells containing a built-in TCF luciferase reporter (schematically illustrated in Fig. 4.11A, left). Measurement of luciferase activity revealed dose-dependent, non-cell-autonomous inhibition of FZD5-mediated canonical WNT activity when co-cultured with A219Xfs*49 expressing cells (Fig. 4.11A, middle). Moreover, the inhibition was reversed in a dose-dependent manner by increasing FZD5 expression (Fig. 4.11A, right). Similar results were obtained in a Wnt5a/FZD5-induced RhoA activity assay (Fig. 4.11B,C), which is a measure of non-canonical WNT signaling. Taken together, these data suggest that the A219Xfs*49 FZD5 functions in a dominant, non-cell-autonomous manner to repress canonical and non-canonical WNT signaling.

4.2.5. Forced expression of *A219Xfs*49 FZD5* in mouse retina leads to apical junction defects similar to those observed in *Fzd5/Fzd8* compound mutants

Previous studies in mice demonstrated apical junction defects in the retinal pigment epithelium of *Fzd5/Fzd8* compound mutant retina, and these were likely to contribute to or cause abnormal neurogenesis and coloboma (Liu et al., 2012). To examine whether the *A219Xfs*49* mutation can mimic a *FZD5* dominant loss of function, we expressed *FZD5 A219Xfs*49* in mouse retinas and evaluated FZD5-related downstream molecular events. Mutant constructs were electroporated into E13.5 mouse retinas together with a constitutive *Ub-GFP* expression vector, and the retina was analyzed after 72 hrs of culture in vitro. Consistent with apical junction defects in *Fzd5^{-/-};Fzd8^{+/-}* compound mutant mouse retina (Liu et al., 2012), expression of the *A219Xfs*49* mutant also caused apical junction defects in cultured retinal explants, as indicated by attenuated expression of atypical protein kinase C (aPKC) (Fig. 4.12A–F) and RhoA (Fig. 4.12G–L). Both FZD5 and aPKC proteins are expressed in retinal progenitor cells (see Fig. 4.12 and (Liu et al., 2012; Liu and Nathans, 2008)). Decreased expression of these proteins likely represents the loss of concentrated apical localization of markers, which would not be demonstrated by immunoblotting. Furthermore, both human and mouse FZD5 protein show the same apical retinal localization (Fig. 4.12M–R), supporting the hypothesis that they may mediate similar molecular events during human and mouse retinal development.

4.3. Discussion

In the present study, we have identified an ultra-rare frameshift mutation in *FZD5* in a large extended family with non-syndromic coloboma segregating as an autosomal dominant disorder. The open reading frame (ORF) of *FZD5* is entirely within the second exon, which makes it unlikely that transcript would be subject to nonsense-mediated decay since there is no intron–exon boundary 3' to the premature termination codon (Popp and Maquat, 2013). The distinct location of the frameshift in the ORF suggests that the truncated protein would have an antagonistic effect on WNT signaling. This predicted

effect was demonstrated in cultured cells, the zebrafish eye and mouse retinal explants that establish *FZD5* as a strong candidate for human eye malformation(s).

FZD5 mutations with similar predicted dominant-negative effects appear to be extremely rare in human populations. A total of 18 copy number variations (CNVs) encompassing *FZD5* locus are listed in the Database of Chromosomal Imbalance and Phenotype in Humans Using Ensembl Resources database. Three patients with CNVs have eye abnormalities including cataract (one duplication case) and iris and/or chorioretinal coloboma (two deletion cases). However, a simple phenotype-genotype correlation could not be inferred since the CNV regions are large and include many genes. Only two *FZD5* ‘loss-of-function’ alleles, both frameshift, are documented in ExAC. One of these, p.E231Afs*8 is also predicted to generate a secreted WNT ligand-binding domain with no transmembrane domain. No phenotype information is available for the single individual carrying this mutation in a heterozygous state. Given that non-penetrance has been observed in at least two members of the family presented above, it is possible that this individual is non-penetrant or has microphthalmia, a disorder characterized by reduced ocular size that is closely associated with coloboma. An explanation for the rarity of such mutations may be related to the observation that *Fzd5* null mouse embryos die before E11 due to placental angiogenesis defects (Ishikawa et al., 2001). The non-penetrance of such variants may reflect rescue via genetic background effects and/or compensation by paralogs. The latter effect is prominent in *Fzd5/Fzd8* mutant mice (Liu et al., 2012) although no obvious *FZD8* mutations compatible with a digenic effect were identified in whole exome sequencing in the individuals presented here. Notably, similar non-penetrance has been observed in patients with autosomal dominant coloboma due to *YAPI* (Williamson et al., 2014) and *SHH* (Schimmenti et al., 2003) mutations.

Our results demonstrate a direct role for Wnt–FZD signaling in optic fissure closure during human eye development. The A219Xfs*49 mutation converts FZD5 from a membrane-bound Wnt receptor to a secreted FZD antagonist that, by competing with Wnt ligands or dimerization with WT FZD5 (on the cell surface), might impart dominant negative characteristics on Wnt signaling. As a result of disrupted Wnt signaling, retinal neuroblasts exhibit apical junction defects (Fig. 4.13) (Liu et al., 2012), which could

directly or indirectly impact proliferation, survival and maturation of progenitors (Fig. 4.13), leading to microphthalmia and coloboma. The dominant negative role of the A219Xfs*49 mutant is also consistent with the absence of observable ocular defects in heterozygous *Fzd5* null allelic mice.

To date, ocular disorders attributable to mutations in Wnt signaling are Norrie disease (Chen et al., 1993; Nikopoulos et al., 2010), osteoporosis-pseudoglioma syndrome (Gong et al., 2001) and familial exudative vitreoretinopathy (Chen et al., 1993; Nikopoulos et al., 2010; Poulter et al., 2012; Robitaille et al., 2002; Toomes et al., 2004). Our study directly implicates perturbed Wnt signaling in coloboma and microphthalmia and is consistent with conclusions from mouse models (Hägglund et al., 2013; Liu et al., 2012; Liu and Nathans, 2008; Zhou et al., 2008). FZD5 mediates both canonical and non-canonical Wnt signaling pathways in different organisms and tissues (Cavodeassi et al., 2005; Liu and Nathans, 2008; Van Raay et al., 2005). However, it is likely that FZD5-mediated non-canonical Wnt signaling is the predominant pathway in the developing mammalian retina, as only minimal activity from the canonical pathway has been reported in these cells (Liu et al., 2006). The retinal apical junction defects observed in *Fzd5/Fzd8* knockout mice, and retinal explants expressing the FZD5 mutant protein are likely to be the consequence of interactions between the actin cytoskeleton and components of the apical junctional complexes induced by the loss of non-canonical Wnt activity. The identification of *FZD5* as a human coloboma gene extends opportunities to elucidate disease mechanisms and treatment paradigms for ocular malformations.

4.4. Figures

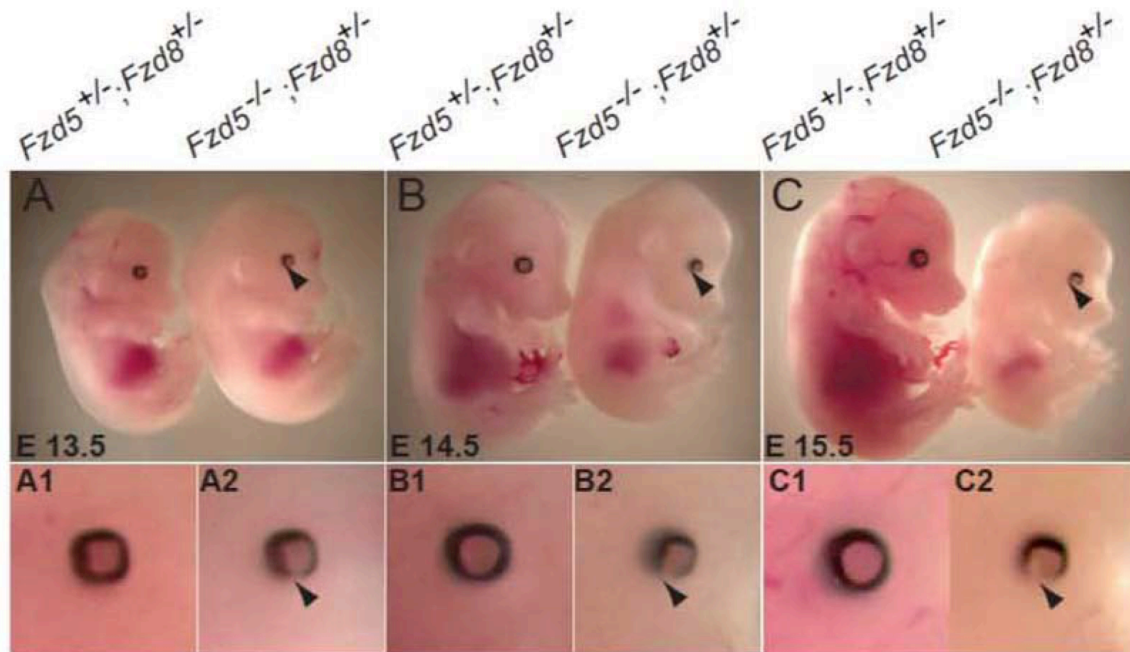


Fig. 4.1: Compound *Fzd5* conditional knockout (*Fzd5*^{-/-}) and *Fzd8* heterozygous mice have microphthalmia and coloboma. (A-C) Lateral views of compound heterozygous mutants (left) or *Fzd5*^{-/-};*Fzd5*^{+/-} mice (right). (A1-C2) Enlarged views of developing eyes corresponding to upper panels. Arrowheads indicate open optic fissures. Transgenic *Sox2*-Cre was used to excise loxP sites to generate *Fzd5* conditional mutations. Mice are E13.5 (A-A2), E14.5 (B-B2), or E15.5 (C-C2).

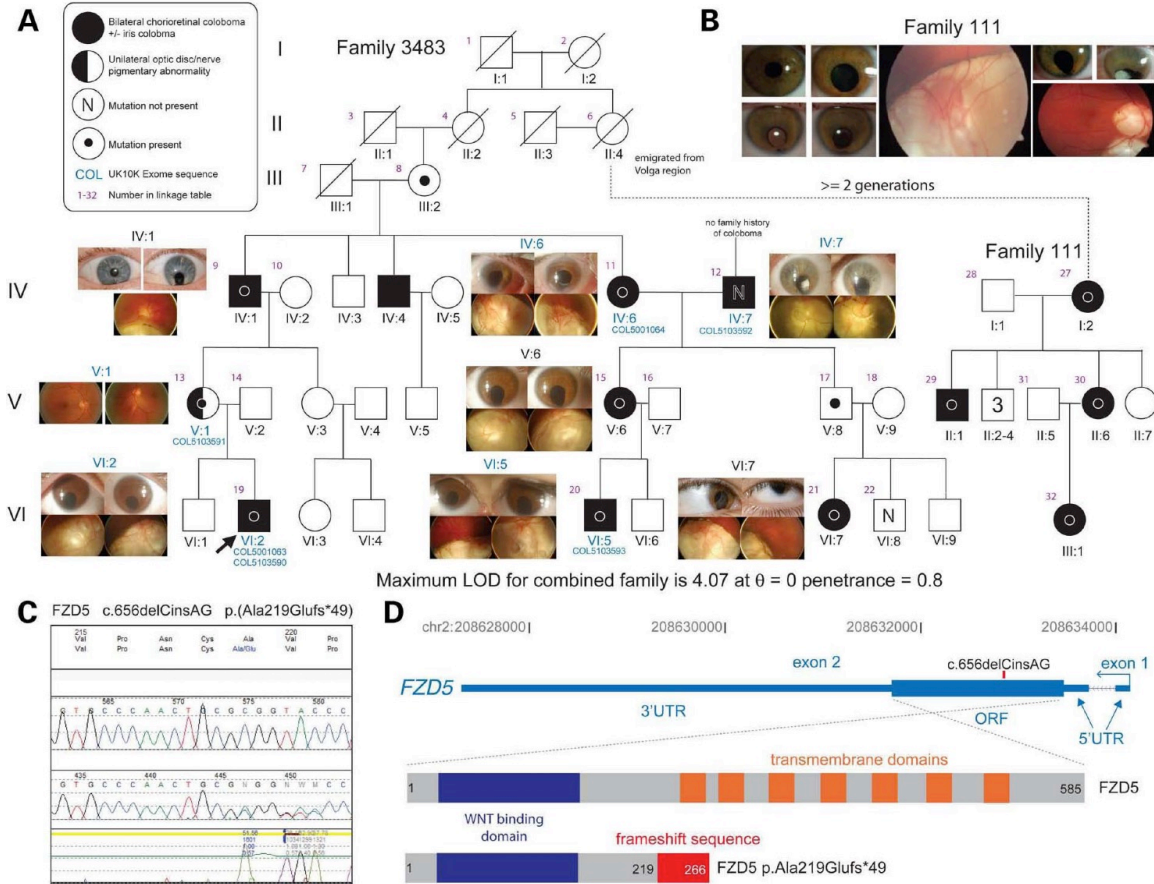


Fig. 4.2: A *FZD5* frameshift mutation identified in a family with autosomal dominant coloboma. (A) Six- and three-generation family pedigrees of Family 3483 and Family 111, respectively. The dotted line links these independently ascertained pedigrees carrying the same mutation on an identical haplotype. This link is plausible based on the history obtained from both Mennonite families, with the likely linking individual (Family 3483 II:4) having emigrated from Europe to North America. For Family 3483, ocular images from the affected individuals are shown adjacent to the cognate pedigree symbol. Coloboma patient numbers indicate individuals whose exomes were sequenced. Otherwise, Sanger sequencing was used for segregation analysis, which reveals high (0.8) but incomplete penetrance, as indicated by two obligate carriers that are unaffected. The pedigree key is in the top left corner. (B) Representative images showing eye malformations in affected individuals from Family 111. The LOD score for the combined pedigree is shown below the family tree. (C) Chromatophogram of the frameshift *FZD5* mutation (c.656delCinsAG). (D) Schematic of the human *FZD5* gene with

hg19 coordinates on chromosome 2. This gene is transcribed in the antisense direction relative to the genomic coordinate numbering. The position of the cDNA mutation is indicated in the open reading frame, which is entirely contained in the second exon. Below are diagrammatic representations of the WT and mutant FZD5 peptides. The WNT-binding domain (dark blue box) is common to both, and the seven transmembrane domains (orange boxes) are present only in the full length WT protein. The mutation results in a substitution at Ala219 (replaced with Glu) with an aberrant extension of 48 residues (red box), resulting in a truncated protein of 266 total amino acids.

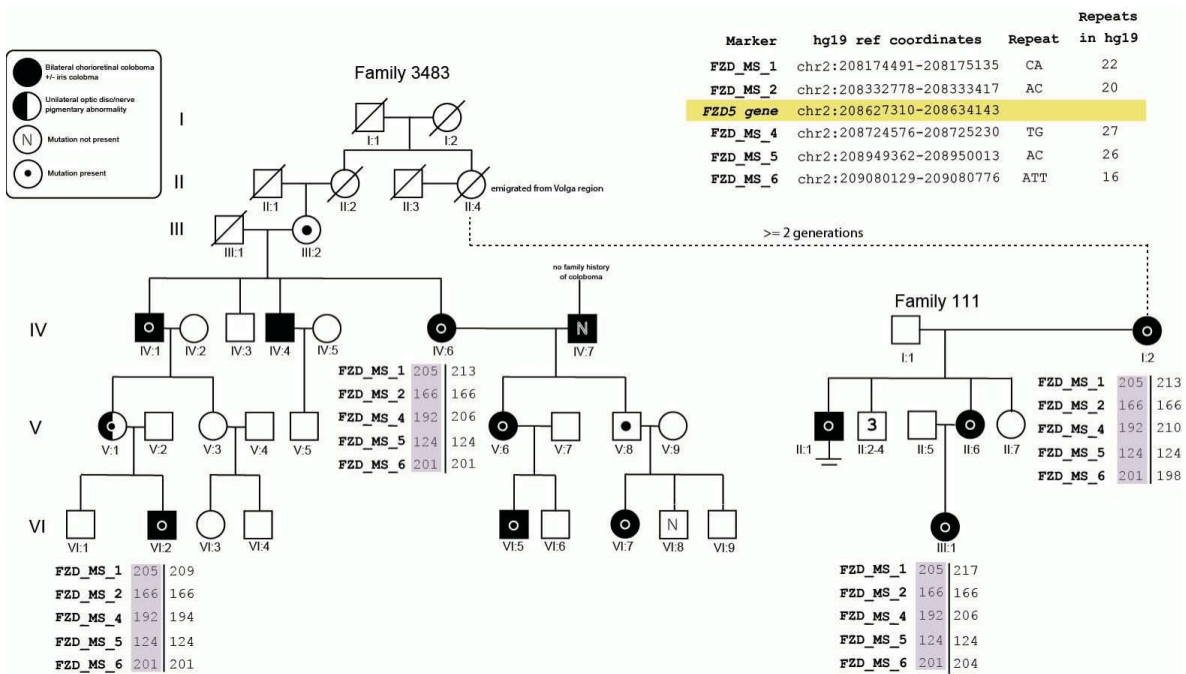


Fig. 4.3: Microsatellite markers and haplotype analysis of Families 3484 and 111. (A) Shows the same pedigree as Figure 2. (B) The absolute genomic coordinates of the five microsatellite markers used in this analysis and their position relative to the *FZD5* gene (yellow highlight). Under four affected individuals (Family 3483 IV:6 & VI:2 and Family 111 I:2 & III:1) are shown the most plausible locus haplotypes for each individual. The purple highlight indicates the identical haplotype shared by each of the affected individual suggesting recent common ancestry. It should be noted that markers FZD_MS_2 and FZD_MS_5 are not informative for haplotype construction.

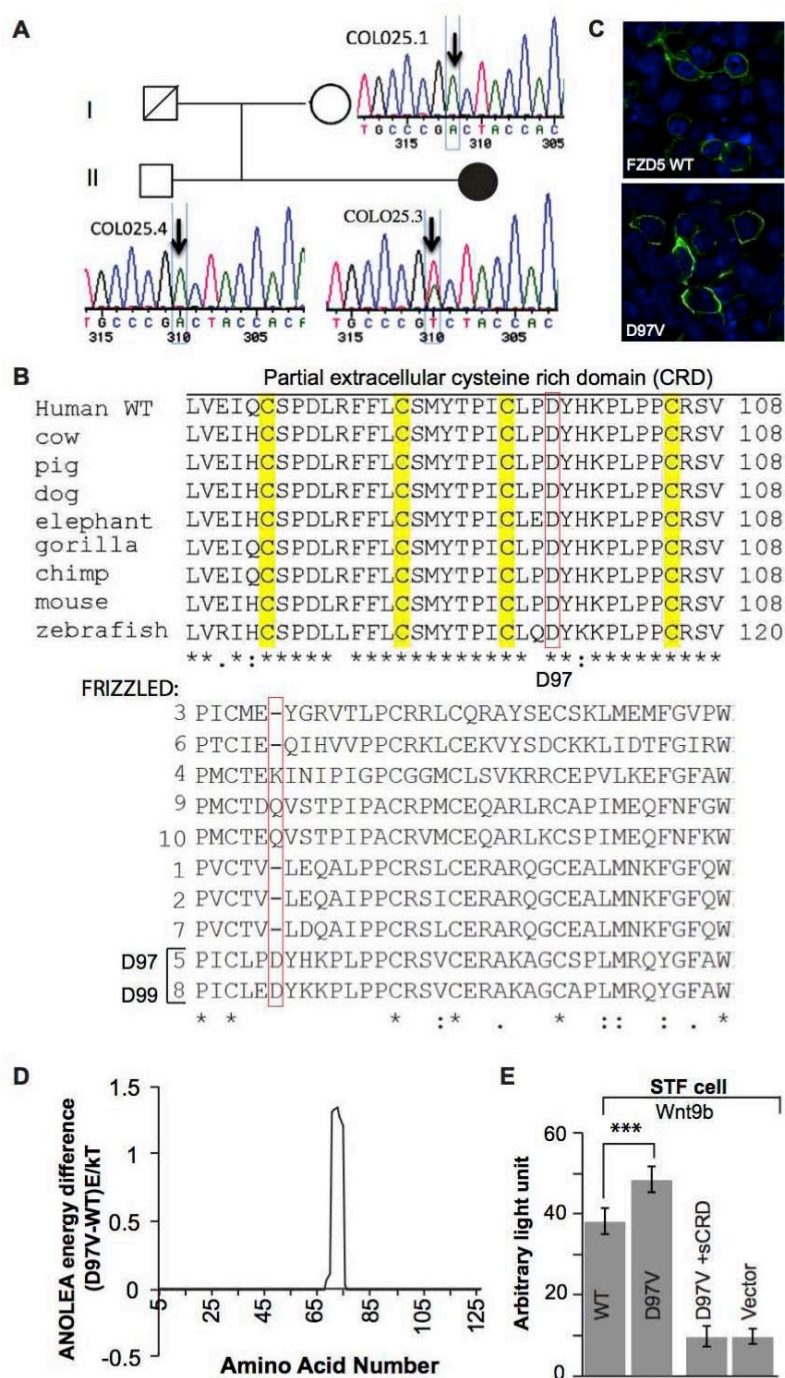


Fig. 4.5: Identification of a novel missense mutation in FZD5 (D97V). (A) Sequences of a two-generation family with a patient with ocular coloboma carrying D97V mutation. (B) Upper panel: alignment of FZD5 cysteine-rich domain (CRD) region from multiple species showing the conservation of D97. Lower panel: alignment of ten FZD CRDs shows that D97 is variable except for FZD8 and FZD5. (C) FZD5 D97V protein is correctly localized

in transfected cells. (D) Atomic non-local environment assessment (ANOLEA) predicted that the D97V variant perturbs local interactions. (E) Slight increase in Wnt9b-induced canonical Wnt activity by D97V can be abolished by FZD5 sCRD. Student t-test was used for statistical analysis. ***, $P < 0.0001$.

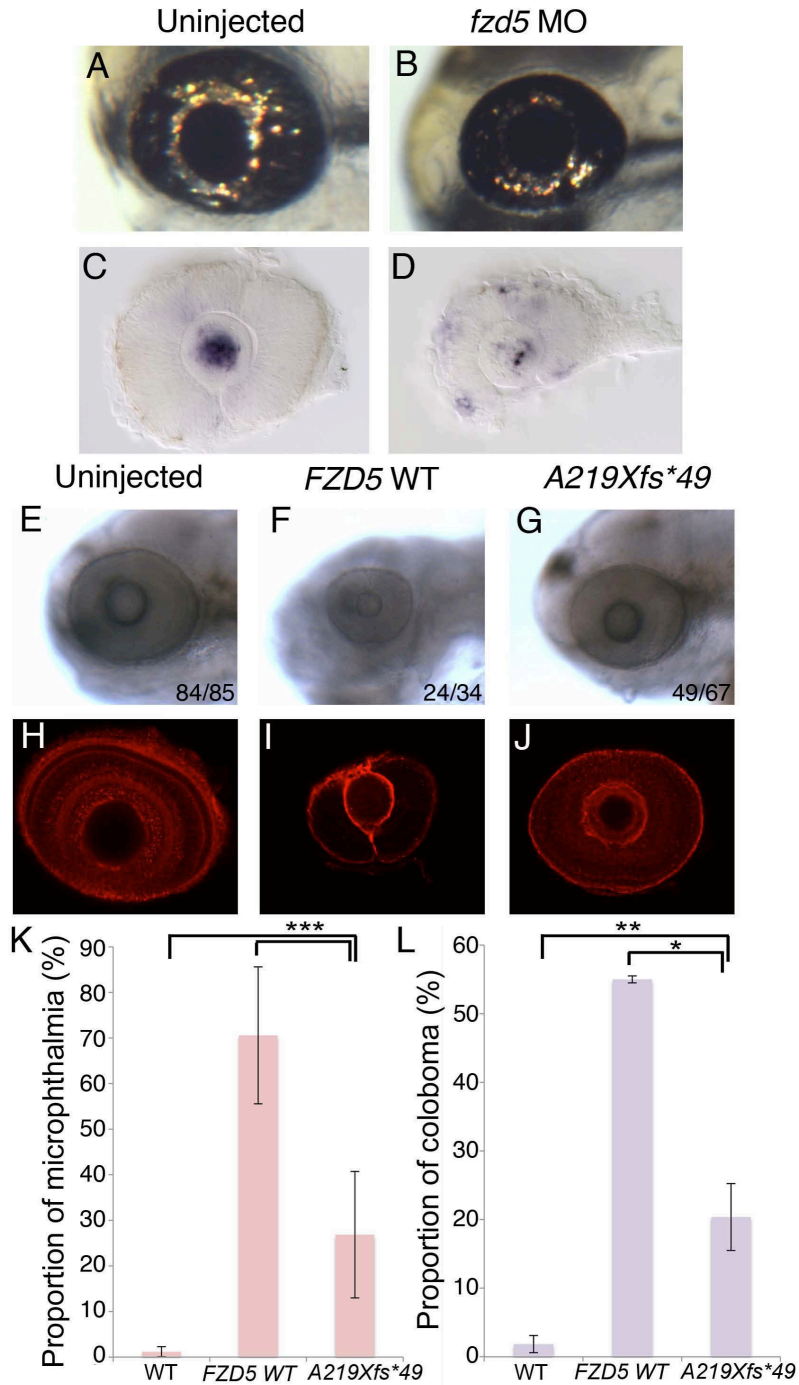


Fig. 4.6: Morpholino knockdown and expression of *FZD5* causes microphthalmia and coloboma in zebrafish. (A,B) Representative images of live embryos at 3 dpf, either uninjected (A) or injected with 1.2 pmol of *fzd5* translation blocking morpholino (MO; B). (C,D) *In situ* hybridization for *gfp* was performed at 28 hpf in *Tg(TOP:dGFP)* embryos to assess levels of canonical Wnt signaling in uninjected (C; n=26/26 eyes) or *fzd5* morphants

(D; n=23/25 eyes). Retinal *gfp* expression was increased in morphants, while lens expression was decreased (D compared with C), suggesting a tissue-specific role of Fzd5 in Wnt signaling. (E–L) Embryos were injected at the one-cell stage with either 200 pg human WT *FZD5* mRNA or *A219Xfs*49 FZD5* mRNA and imaged to analyze eye size and prevalence of coloboma. Injection of WT *FZD5* caused higher incidence of microphthalmia (K, *** $P < 0.0002$) and coloboma (L, ** $P = 0.016$; * $P = 0.008$) compared with injection of *A219Xfs*49 FZD5* mRNA. All images represent majority of observed phenotypes in each injection group. (E–G) Live images of larvae at 3 dpf; (H–J) eyes labeled with anti-laminin antibody at 3 dpf. (K,L) Quantification of ocular phenotypes seen in E–J. (E–L) The number of embryos analyzed for microphthalmia: uninjected (n=85), WT *FZD5* (n=34), *A219Xfs*49* (n=67), two experimental replicates. The number of embryos analyzed for coloboma: uninjected (n=54), WT *FZD5* (n=20), *A219Xfs*49* (n=54), two experimental replicates.

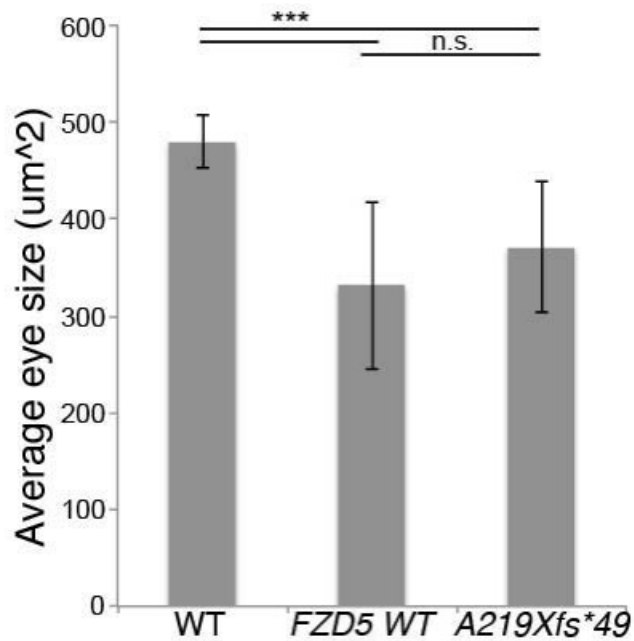


Fig. 4.7: Eye size analysis of zebrafish embryos injected with *FZD5* mRNA. Zebrafish embryos were injected at the 1-cell stage with 200 pg of either WT *FZD5* or A219Xfs*49 *FZD5* mRNA and imaged at 3 dpf. Ocular area measurements were taken 3 independent times with ImageJ and averaged for each eye. Measurements for eyes in each injection group were then averaged (uninjected, N=12 embryos; WT *FZD5*, N=20 embryos; A219Xfs*49 *FZD5*, N=30 embryos). ***, $p < 0.0003$; n.s.=not significant; t-test with Bonferroni correction for multiple comparisons.

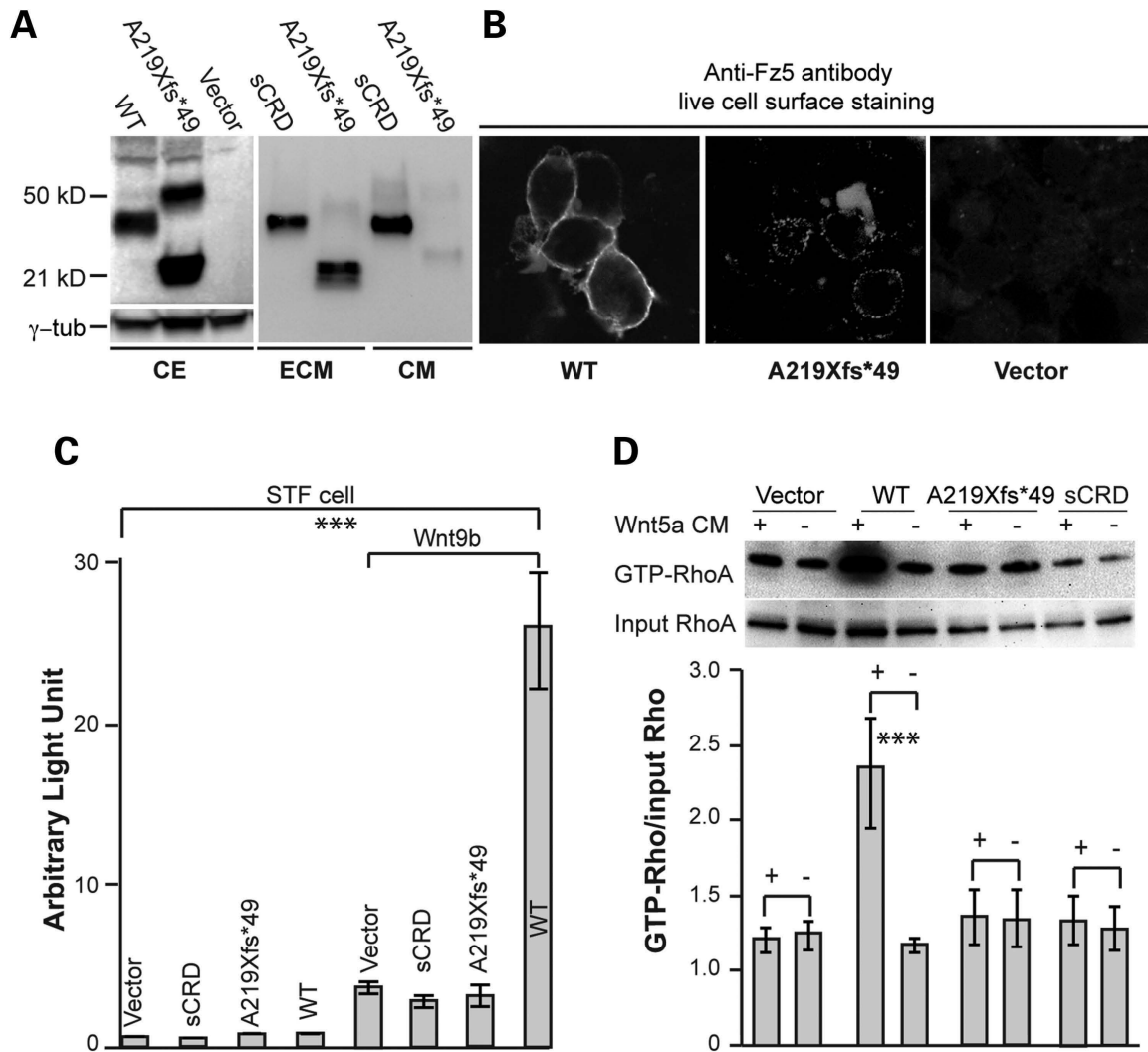


Fig. 4.8: A219Xfs*49 FZD5 is incapable of mediating Wnt signaling. (A) Immunoblot analysis of subcellular fractions from transfected HEK293 cells. FZD5 A219Xfs*49 protein is detected primarily in extracellular matrix (ECM) fraction, while secreted-cystein-rich domain (sCRD) is expressed in both the culture medium (CM) and ECM. CE, cell extract. (B) Live cell immunofluorescence detection. Immunofluorescence staining was conducted to detect FZD5 protein expression in transfected cells on coated coverslips (see methods for details). WT FZD5 is primarily present on the cell surface (left panel), while the majority of A219Xfs*49 mutant protein is detected extracellularly (middle panel), presumptively in ECM (dotted staining). Negative control with vector transfection is shown in the right panel. (C) Wnt9b-induced canonical Wnt signaling in STF reporter cell line. Cells were transfected with 0.5 μ g Wnt9b plasmid combined with 0.25 μ g other plasmids. Like sCRD,

A219Xfs*49 FZD5 protein is not able to mediate Wnt9b-induced canonical Wnt signaling. The rightmost bar represents Wnt9b-induced canonical Wnt activity by WT FZD5, which is significantly different from all other forms of FZD5. (D) Representative image for active-Rho pull-down assays for non-canonical Wnt signaling. HEK293 cells were transfected with *FZD5* WT, *A219Xfs*49* and sCRD plasmids, treated with Wnt5a recombinant protein conditioned medium. Active GTP-RhoA assays strictly followed the manufacturer instructions. Wnt5a-enhanced formation of GTP-RhoA is obtained in the presence of FZD5, but not A219Xfs*49 FZD5 or sCRD. (Student's t-test, *** $P < 0.001$).

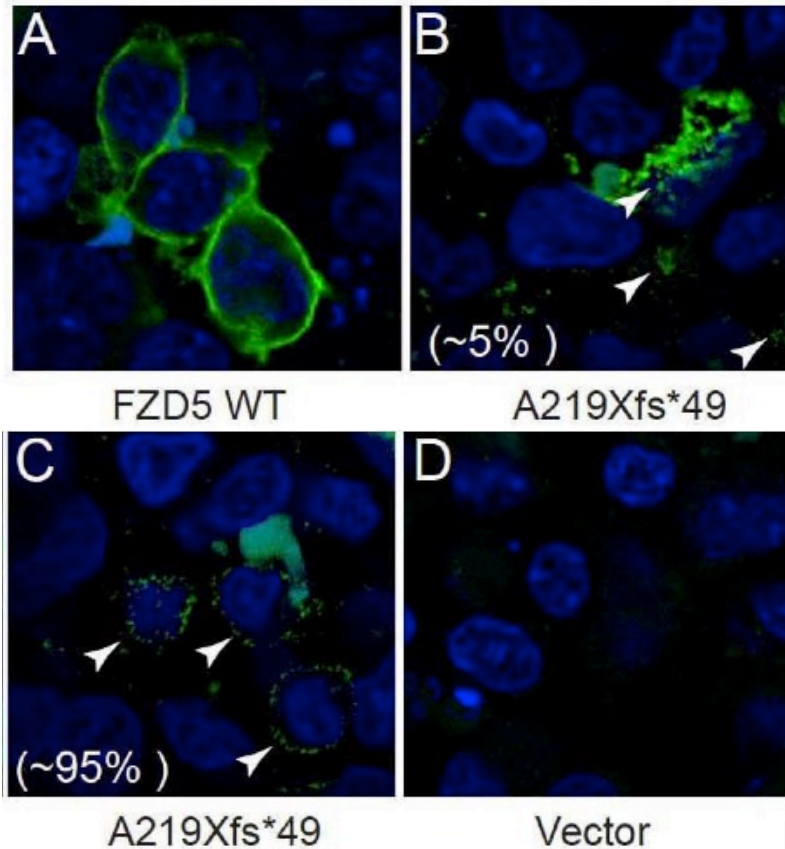


Fig. 4.9: Cellular localization of wild type and mutant FZD5 protein. Immunofluorescence detection of FZD5 proteins (green) on cell surface. Images were merged with DAPI (blue) indicating the nucleus. (A) Wild type FZD5 was localized on the cell membrane. (B,C) The majority of A219Xfs*49 mutant protein was present in extracellular space, presumptively, ECM (arrowheads). The distribution of the mutant proteins appeared to be uneven with about 5% cells showing locally heavy and/or dispersed deposition (B, arrowhead), whilst the rest (~95% C, arrowhead) showing local (near-membrane) FZD5 distribution. (D) Negative control with vector transfection. To avoid the cytoplasm staining, live cells in all samples were first incubated with anti-FZD5 antibody in cultured medium, washed with PBS, and then post-fixed with PFA for immunohistochemistry.

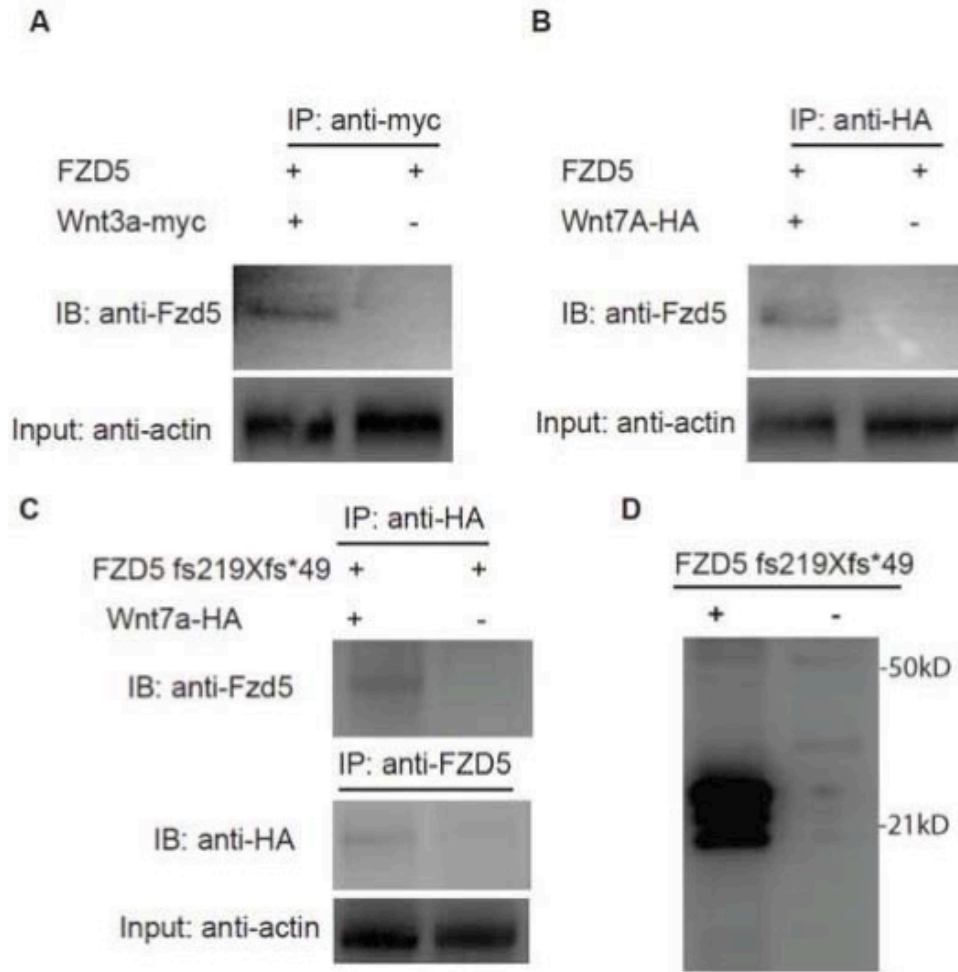


Fig. 4.10: FZD5 A219Xfs*49 binds to tagged Wnt3a and Wnt7a. (A) FZD5 binds to myc-tagged Wnt3a. HEK293T cells co-transfected with *Wnt3a-myc* and *FZD5*. Cell extracts were immunoprecipitated (IP) with anti-myc antibody, and immunoblotted (IB) with anti-FZD5 antibody. (B) FZD5 binds to HA-tagged WNT7A. HEK293T cells co-transfected with *WNT7A-HA* and *FZD5*. Cell extracts were immunoprecipitated with anti-HA antibody, and the immunoblot was probed with anti-FZD5 antibody. (C) FZD5219Xfs*49 protein binds to HA-tagged WNT7A. HEK293 cells were co-transfected with *WNT7A-HA* and *FZD5219Xfs*49* constructs. Cell extracts were immunoprecipitated with anti-HA antibody, and the protein blot was probed with anti-FZD5 antibody. Reverse IP was conducted with anti-FZD5 antibody and the blot was probed with anti-HA antibody. (D) Multiple bands of FZD5219Xfs*49 were detected under reducing conditions using FZD5 antibody.

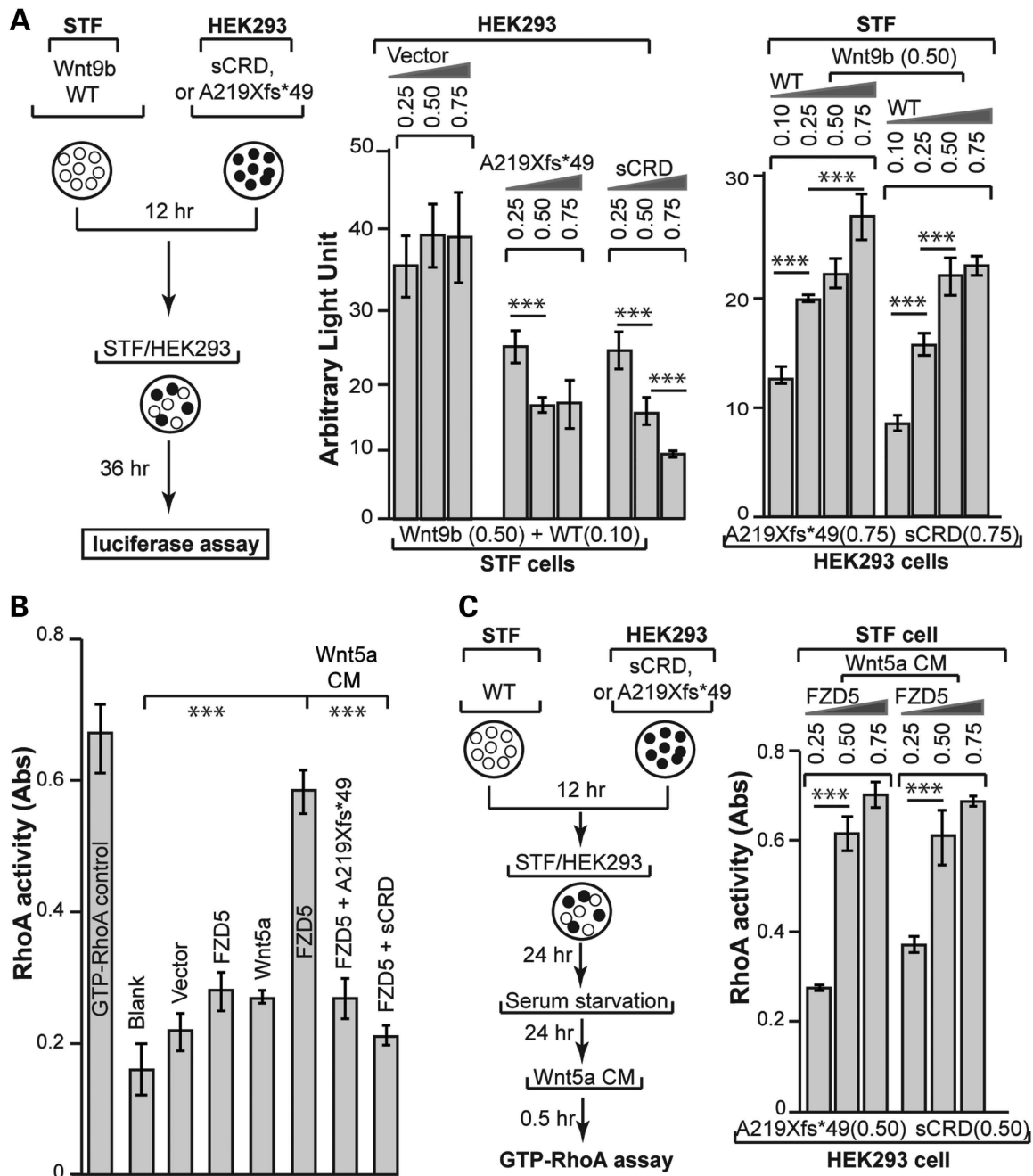


Fig. 4.11: Non-cell-autonomous dominant negative effect of A219Xfs*49 FZD5 on Wnt signaling. (A) Wnt9b–FZD5 signaling. All experiments were done in triplicates of at least three independent transfections. **Left:** illustration of the experimental scheme. A fixed amount of Wnt9b and FZD5 was co-transfected with pCAG-Renilla luciferase plasmids (RL, used for internal expression control) into STF cells. Different amounts of A219Xfs*49 FZD5 and secreted-cystein-rich domain (sCRD) plasmids were transfected into HEK293 cells. After 12 hrs, both STF and HEK293 cells were collected by trypsin-

Ethylenediaminetetraacetic acid (EDTA), mixed at 1:1 ratio and seeded into a new plate for another 36 hrs. Cell extracts were then prepared for Firefly luciferase and Renilla luciferase assay. **Middle:** inhibition of Wnt9b/FZD5 activity by either A219Xfs*49 or sCRD in a dose-dependent manner. Firefly luciferase activities were normalized against Renilla luciferase. **Right:** the inhibition of FZD5-mediated Wnt signaling by A219Xfs*49 or sCRD was reversed by increasing WT FZD5 co-expression. (B) Wnt5a–FZD5 signaling. RhoA G-lisa assay showed that Wnt5a/FZD5-stimulated accumulation of GTP-RhoA was abolished by A219Xfs*49 mutant or sCRD protein (compare the right three bars). Samples were prepared as in the previous figure and G-lisa assay followed instructions of RhoA G-lisa kit. Absorbance of horseradish peroxidase colorimetric reaction was measured by SpectraMax M. (C) Inhibition of RhoA activation by A219Xfs*49 or sCRD protein was reverted by increased FZD5 expression. **Left** panel: similar experimental scheme in (A) was used for testing non-cell-autonomous effects of A219Xfs*49 on Wnt5a/FZD5 induced RhoA activation. **Right** panel: The inhibition of RhoA activation (G-lisa assay) was reverted by increased FZD5 expression. *** $P < 0.001$, Student's t-test.

EP@ E13.5 with eGFP

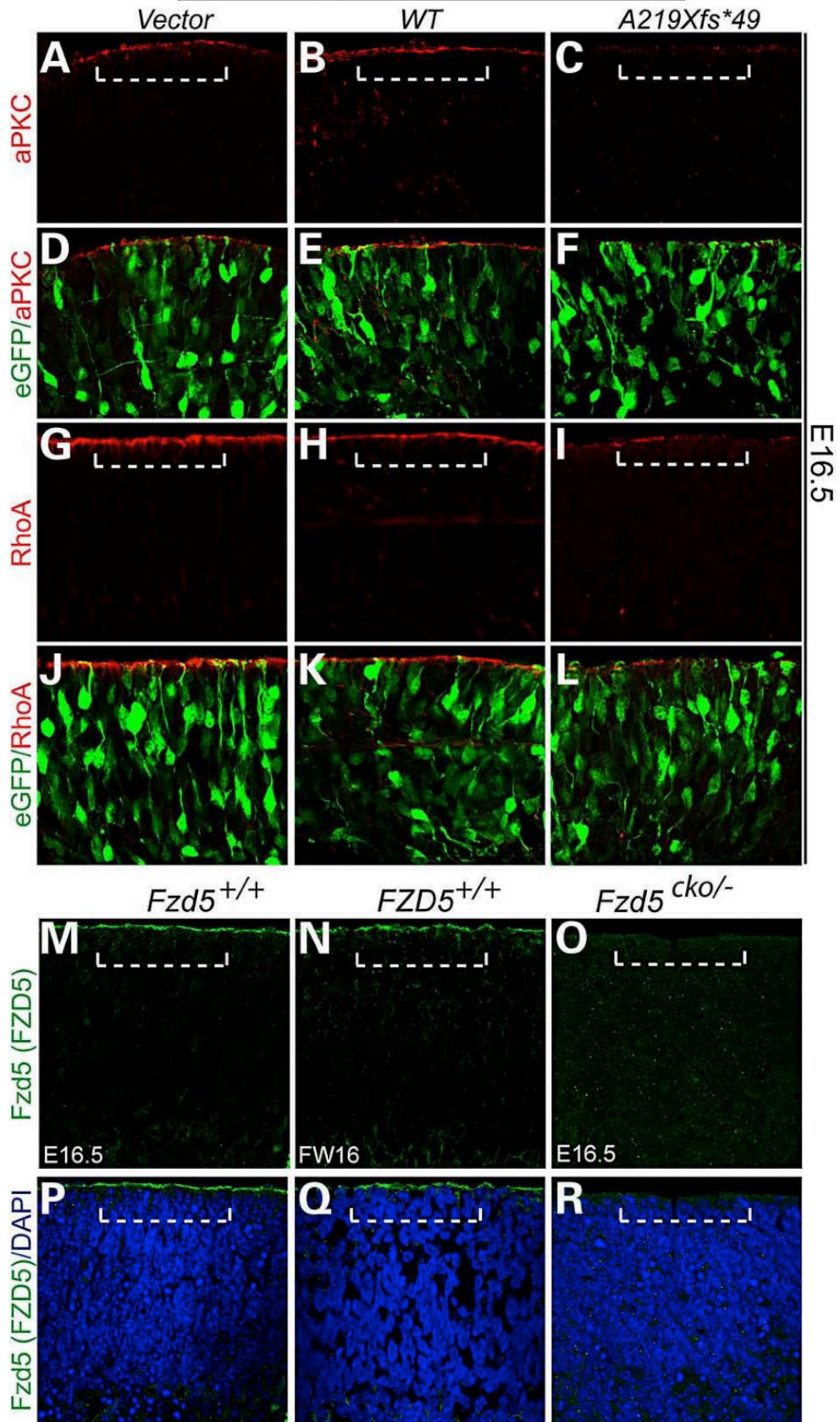


Fig. 4.12: Expression of *FZD5* A219Xfs*49 in retinas led to similar apical junction defects that were reported in mouse *Fzd5/Fzd8* compound mutants. Mouse embryonic (E13.5) retina was dissected and subjected to electroporation supplied with WT *FZD5* and A219Xfs*49 *FZD5* DNA solution. The retinae were cultured for 72 hrs and harvested for immunohistochemistry. (A–F), aPKC localization in vector (A), WT *FZD5* (B) and A219Xfs*49 *FZD5* (C) electroporated retinae. Note the loss of apical localization of aPKC in A219Xfs*49-expressing retina (C). (D–F) Images of (A–C) merged with co-electroporated eGFP, respectively. (G–I) Similar as aPKC, apical RhoA enrichment is also greatly attenuated (compared with G and H). (J–L) Images of (G–I) merged with co-electroporated eGFP, respectively. (M–R) Localization of FZD5 protein in mouse and human retina. (M) Apical localization of the FZD5 protein in WT mouse retina (above dashed bracket). (N) Same protein localization of FZD5 was detected in human retina. (O) Mouse *Fzd5* conditional mutant retina showed the absence of apical FZD5 protein. (P–R) Images from (M–O) merged with 4',6-diamidino-2-phenylindole, respectively.

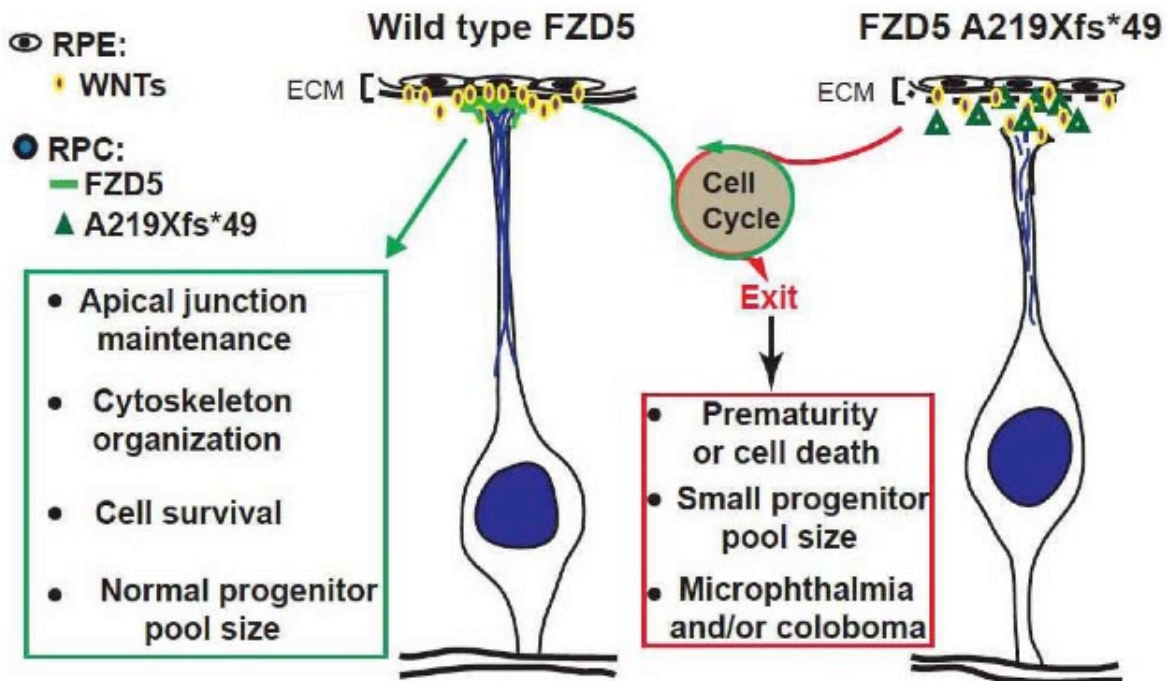


Fig. 4.13: A model of coloboma disease mechanism caused by *FZD5 A219Xfs*49*. During development, WNT signaling is crucial for maintenance of neuroblast apical junction, cell polarity, cell survival and proliferation. By competing for Wnt ligands, A219Xfs*49 mutant protein (dark green triangles) may intercept WNTs (yellow circles), which are secreted from RPE at the apical extracellular matrix (ECM) during development, preventing FZD5 (from RPC apical membrane, bright green lines) - evoked WNT signaling in the neuroblasts (blue nuclear cells). Consequently, insufficient WNT-FZD5 signaling leads to early cell cycle exit, prematurity and cell death, and reduced progenitor pool size, resulting in microphthalmia and/or coloboma. The model is modified from (Liu et al., 2012).

4.5. Tables

Table 4.1: Rare *FZD5* variant identified in coloboma patients. D97V variant has not been detected in control genomes, SNP database and 1000 Genome Project. Preliminary tests show that this variant increases FZD5-mediated canonical Wnt activity (Fig. 4.5E).

Patient ID	cDNA change	Protein change	dbSNP ID	1000G/EGS MAF	PolyPhen2 prediction	SIFT prediction
49	c.A290T	D97V	n/a	n/a	Possibly damaging	Damaging

Chapter 5

Morphogenetic defects underlie Superior Coloboma, a newly identified closure disorder of the dorsal eye

A version of this chapter is published. Jennifer C. Hocking*, Jakub K. Famulski*, Kevin H. Yoon, Sonya A. Widen, Cassidy S. Bernstein, Sophie Koch, Omri Weiss, FORGE Canada Consortium, Seema Agarwala, Adi Inbal, Ordan J. Lehmann, Andrew J. Waskiewicz. (2018). Morphogenetic defects underlie Superior Coloboma, a newly identified closure disorder of the dorsal eye. *PLoS Genetics* 14(3): e1007246 *joint first authors

**Supplemental videos referenced in this chapter may be found in online supporting information (doi: 1007246)

5.1. Introduction

Aberrant ocular morphogenesis during embryonic development frequently results in reduced visual acuity or blindness. Morphological development of the eye begins with evagination of retinal precursors from the forebrain to produce bilateral optic vesicles and subsequent invagination of the associated ectoderm to create the lens (Bazin-Lopez et al., 2015; Fuhrmann, 2010). Each optic vesicle reorganizes into a bilayered optic cup, with the distal (lens-facing) layer forming the presumptive neural retina and the proximal layer forming the retinal pigmented epithelium (RPE). To provide an entry point for vasculature and an exit pathway for axons of the optic nerve, a transient inferior (choroid) fissure forms along the ventral/inferior side of the optic cup and stalk. In cases where the inferior fissure fails to close, gaps remain within tissues of the eye (iris, retina, choroid and/or occasionally lens) (Chang et al., 2006; Onwochei et al., 2000). This congenital anomaly, referred to as ocular coloboma, is estimated to occur in 1 out of 4-5,000 live births and cause 3-11% of pediatric blindness (Onwochei et al., 2000; Williamson and FitzPatrick, 2014). Ocular coloboma has a complex causality encompassing mutations in over 20 genes (Gregory-Evans et al., 2004; Williamson and FitzPatrick, 2014). Although both clinically and genetically heterogeneous, coloboma predominantly affects the inferior aspect of the eye.

The posterior segment of the developing eye receives two vascular supplies (Saint-Geniez and D'Amore, 2004). The transient hyaloid vasculature is a plexus between the retina and lens, and is connected to the hyaloid artery, which enters the eye via the inferior fissure. A second circulatory system, the choroidal vasculature, grows over the surface of the optic cup to nourish the RPE and the light-sensing photoreceptor cells in the outer retina. Although development of the choroidal vessels is poorly understood, zebrafish studies demonstrated that the complex choroidal vascular plexus is preceded by a simple set of pioneer vessels (Kaufman et al., 2015; Kitambi et al., 2009). To form this so-called superficial vascular system (distinct from the superficial retinal vessels and also known as the ciliary vasculature), three radial vessels grow over the optic cup and anastomose to create an annular vessel encircling the lens. The highly stereotypical formation of the superficial vessels suggests precise developmental regulation, but the mechanisms that guide their growth are currently unknown.

In the context of studying a large cohort of patients with ocular coloboma, we identified five local patients with a novel ocular anomaly characterized by gaps in tissues of the superior eye. Although it is logical that such an anomaly represents another fissure disorder, common models of vertebrate eye development do not feature a division in the embryonic dorsal/superior eye. However, a careful examination of zebrafish, chick, and mouse eye development did reveal a transient groove, or sulcus, bisecting the dorsal optic cup. Moreover, we utilized patient exome sequencing and zebrafish models to define the importance of dorsal-ventral patterning in morphogenesis of this ocular sulcus. Functionally, the superior ocular sulcus serves as a conduit for the advancing first vessel of the superficial vasculature, and we note profound errors in vascular growth and connectivity in embryos with abnormal sulci.

5.1.1. Summary

The eye primordium arises as a lateral outgrowth of the forebrain, with a transient fissure on the inferior side of the optic cup providing an entry point for developing blood vessels. Incomplete closure of the inferior ocular fissure results in coloboma, a disease characterized by gaps in the inferior eye and recognized as a significant cause of pediatric blindness. Here, we identify eight patients with defects in tissues of the superior eye, a congenital disorder that we term *superior coloboma*. The embryonic origin of superior coloboma could not be explained by conventional models of eye development, leading us to reanalyze morphogenesis of the dorsal eye.

Our studies revealed the presence of the *superior ocular sulcus* (SOS), a transient division of the dorsal eye conserved across fish, chick, and mouse. Exome sequencing of superior coloboma patients identified rare variants in a Bone Morphogenetic Protein (BMP) receptor (*BMPRIA*) and T-box transcription factor (*TBX2*). Consistent with this, we find sulcus closure defects in zebrafish lacking BMP signaling or Tbx2b. In addition, loss of dorsal ocular BMP is rescued by concomitant suppression of the ventral-specific Hedgehog pathway, arguing that sulcus closure is dependent on dorsal-ventral eye patterning cues. The superior ocular sulcus acts as a conduit for blood vessels, with altered sulcus closure

resulting in inappropriate connections between the hyaloid and superficial vascular systems. Together, our findings explain the existence of superior coloboma, a congenital ocular anomaly resulting from aberrant morphogenesis of a developmental structure.

5.2. Results

5.2.1. Identification of patients with superior coloboma

Over a six-year period (2007-2012), we identified five local patients with superior ocular defects affecting the iris, lens, retina, optic nerve and/or sclera (Fig. 5.1 and Table 5.1); notably, these were not associated with a family history of such anomalies. On the basis of apparent similarity to coloboma (gaps in inferior/ventral ocular tissue), yet inverse orientation, we propose the term *superior coloboma* to describe this disorder. The first patient, with tuberous sclerosis attributable to a rare *TSC2* (c.C5026T; p.R1676W) mutation, exhibited a prominent unilateral iris coloboma situated at 12 o'clock. Bilateral disease was present in a single patient (#2), and involved both iris and lens (Fig. 5.1, images 2 and 3). Two of the five patients were diagnosed in infancy, and for one (#4), examination under anesthesia was required to fully characterize pathology. As is evident from Fig. 5.1, the diversity of tissue involvement in superior colobomata recapitulates that present in inferior colobomata. We subsequently received, from pediatric ophthalmologists at US and UK tertiary referral centers, clinical data on three further patients with superior colobomata. These cases extended the range of associated phenotypes to include additional structural ocular malformations (microphthalmia, or small eye; #8). All eight patients in our cohort had profoundly reduced visual acuity, precluding normal stereopsis.

5.2.2. Exome sequencing of superior coloboma patients

To identify candidate genetic variants carried by superior coloboma patients, exome sequencing was performed on the initial five probands (**Error! Reference source not found.**). Identified variants were prioritized by comparison to SNP databases (frequency

<1%), *in silico* prediction algorithms (MutationTaster >0.95) and expression within the developing eye or previously identified connections to coloboma. We focused our efforts on understanding genetic alterations in the single patient with bilateral superior coloboma (#2, Table 5.3). In particular, we noticed that patient #2 carries compound heterozygous variants in the Retinoic Acid (RA) synthesis gene *CYP11B1* (Chambers et al., 2007) (Fig. 5.2A) as well as a rare (dbSNP: 1 in 60,706; NHLBI and 1000 Genomes: 0 in 14,000) missense variant in Bone Morphogenetic Protein (BMP) Receptor 1A (*BMPRIA*, Fig. 5.2B,C). As RA and BMPs are morphogens with essential roles in eye development, including regulation of inferior fissure closure (Behesti et al., 2006; French et al., 2009; Gosse and Baier, 2009; Kruse-Bend et al., 2012; Lupo et al., 2011; Sasagawa et al., 2002; Valdivia et al., 2016), we hypothesized that the identified mutations contributed to the patient's ocular disorders. In order to examine how disruption of eye patterning genes could lead to superior coloboma, we next turned to animal models and conducted an in depth analyses of dorsal eye morphogenesis.

5.2.3. *Vertebrate studies of dorsal ocular morphogenesis*

Inferior coloboma arises from failed closure of the choroid fissure located in the ventral eye. Given the comparable phenotype despite opposite orientation seen in superior coloboma patients, we hypothesized a similar etiology. Although the standard model of eye development describes an uninterrupted dorsal retina, two older studies of fish eye development identified a groove present in this space (Nordquist and McLoon, 1991; Schmitt and Dowling, 1999). To determine if such a structure exists broadly across vertebrates and whether it is a Laminin-lined space, we chose to revisit the study of dorsal eye morphogenesis in fish, chick and mouse. Using multiple microscopy methods, we identified a transient groove/sulcus in the dorsal zebrafish eye (dorsal in fish and superior in human are equivalent; for consistency with superior coloboma, we describe this structure as the *superior ocular sulcus* [SOS]) (Fig. 5.3A-D). The sulcus is visible by stereoscope but more obvious in compound or confocal observations of live embryos (Fig. 5.3A), and most easily discernible from 21-25 hpf. When imaged under an electron microscope, the SOS

can be seen to transect the distal portion of the dorsal retina (Fig. 5.3B), while single confocal optical slices reveal the SOS as a distinct space (Fig. 5.3C) lined by basal lamina (Fig. 5.3D).

To ascertain whether a similar structure exists in chick, we examined tissue sections immunostained for Laminin and counterstained with DAPI. At stage HH16, we observed the presence of a Laminin-lined division in the distal portion of the chick dorsal optic cup (n=6/8 eyes; Fig. 5.3E, Fig. 5.4). For evidence of a comparable structure in mammals, we next examined mice and found a Laminin-lined separation across the inferior portion of the dorsal optic cup at embryonic day 10.5 (Fig. 5.3F). A collaborator also shared older SEM studies of newt (*Taricha tarosa*) development, which similarly demonstrate the presence of a division across the dorsal embryonic eye (Fig. 5.5, personal communication, A. Jacobson). Thus, we present clear evidence for the existence of an evolutionarily conserved, Laminin-lined sulcus in the dorsal optic cup of multiple vertebrate species.

The inferior fissure temporarily bisects the ventral retina prior to closing through progressive fusion of the nasal and temporal margins of the ventral optic cup (Chang et al., 2006). The SOS similarly extends across the dorsal zebrafish retina (Fig. 5.3A-2D) to partially separate the nasal and temporal retinal lobes, and is also present only transiently. To determine the mechanism of SOS closure, we followed ocular morphogenesis over time. The SOS arises soon after optic cup formation (19-20 hpf) as a distinct and narrow structure (S1 Video and Fig. 5.3A,B). Notably, formation of the sulcus occurs at a time when the developing retinal pigmented epithelium is spreading around the optic cup, but is not associated with significant cell movement or apoptosis in the forming dorsal retina (S2 Video). Unexpectedly, the edges of the narrow SOS do not migrate toward one another and fuse, but instead the SOS transitions at 22-24 hpf to a shallow and wide trough and gradually disappears after 26 hpf (S3-S5 Videos and Fig. 5.6). Both phases are visible in representative SEM images (Fig. 5.3B). As we observed the transition from narrow to wide, and never detected an epithelial fusion event, it is logical to propose that the sulcus closes via cell rearrangement or shape modification, mechanisms distinct from the epithelial fusion that occurs within the choroid fissure.

5.2.4. *CYP1B1 and the superior ocular sulcus*

CYP1B1 mutations cause ocular malformation and are a major cause of congenital and adult glaucoma (Chang et al., 2006). Patient #2 carries one of the known disease-causing alleles (p.R368H) while the second allele is a truncation (p.A287Pfs6), and so both alleles are expected to be pathogenic. Retinoic acid can be synthesized through both the Cyp1b1 and Aldehyde dehydrogenase (Aldh) pathways (Chambers et al., 2007; Das et al., 2014), and mRNA encoding both types of RA synthesis enzyme is expressed in the dorsal zebrafish eye (Fig. 5.7A) (French et al., 2009; Williams and Bohnsack, 2015). In order to test whether Cyp1b1 is necessary for SOS closure, we used TALEN mutagenesis to create zebrafish carrying a 13 bp frameshift deletion within the P450 domain, resulting in an early stop codon and a truncated protein. Surprisingly, the zebrafish *cyp1b1* mutants did not display defects in SOS closure, even when the Aldh pathway was additionally inhibited (Fig. 5.7B) (Morgan et al., 2015). Given the lack of a phenotype with reduced RA signaling, we next investigated the *BMPRIA* variant and BMP-dependent regulation of SOS closure.

5.2.5. *Bmp signaling regulates closure of the superior ocular sulcus*

BMP ligands (Gdf6/Bmp13 and Bmp 2, 4, and 7) pattern the eye at the time of SOS closure (Behesti et al., 2006; French et al., 2009; Gosse and Baier, 2009; Heermann et al., 2015; Kruse-Bend et al., 2012; Murali et al., 2005) and the identified *BMPRIA* patient variant alters a highly conserved residue in the kinase domain (p.Arg471His, Fig. 5.2); therefore, we tested whether reduced BMP receptor activity affects closure of the SOS. The small molecule DMH1 is an inhibitor of type IA BMP receptors, with robust and specific activity in zebrafish (Hao et al., 2010; Paul et al., 2008). Embryos were treated with DMH1 either just after gastrulation or just prior to optic cup invagination (10 and 18 hpf, respectively) and evaluated for SOS presence at 28 hpf, a time point when the sulcus is no longer visible in wild type embryos. Exposure to DMH1 prevented SOS closure in a dose-

dependent manner (Fig. 5.8A,B), establishing that BMP signaling regulates sulcus morphogenesis.

We next used a zebrafish overexpression assay to evaluate whether the patient variant disrupts BMPR1A function. As injection of one-cell stage embryos with wild type human *BMPR1A* mRNA failed to elicit alterations to dorsal-ventral axis specification, we used site-directed mutagenesis to introduce a Q233D mutation previously shown to render BMPR1A constitutively active (Zou et al., 1997). Injection of mRNA encoding the constitutively active BMPR1A receptor (caBMPR1A) efficiently induced ventralization of whole zebrafish embryos, while *caBMPR1A* carrying the patient variant (*R471H-caBMPR1A*) showed mildly reduced activity (Fig. 5.8C and Fig. 5.9). The patient variant therefore does not completely inactivate the protein, but this assay does suggest that it could be a hypomorphic allele and may have been one of multiple factors contributing to the development of superior coloboma. Overall, our data support a role for BMP signaling in regulating SOS closure.

Within the zebrafish eye, *Bmpr1a* mediates signaling from the *Gdf6a* (Growth Differentiation Factor 6a, *Bmp13*) ligand (Wang et al., 2013) and absence of *Gdf6a* results in almost complete loss of dorsal (superior) ocular gene expression, expansion of ventral (inferior) gene expression, and a small eye phenotype (den Hollander et al., 2010; French et al., 2009; Gosse and Baier, 2009). Knockdown of *Gdf6a* signaling in wild type embryos by injection of antisense morpholinos oligonucleotides caused a highly penetrant SOS closure defect, very similar to that seen with DMH1 exposure (Fig. 5.10A-C). Recapitulation of the persistent sulcus phenotype in both homozygous (French et al., 2009; Gosse and Baier, 2009) and a subset of heterozygous *gdf6a* embryos (Fig. 5.10D,E) shows that SOS closure is sensitive to the precise level of BMP signaling. A lack of *Gdf6a* also affected formation of the SOS, as seen by the deeper sulcus in a representative SEM image (Fig. 5.10D, bottom right panel) and in animations showing the surface morphology of the dorsal eye in 22 hpf wild type (S6 Video), *gdf6a* heterozygous (S7 Video) and *gdf6a* homozygous (S8 Video) embryos. While the sulcus eventually closes in most *Gdf6a*-deficient embryos, two adult *gdf6a*^{-/-} fish displayed superior colobomata (Fig. 5.10F), demonstrating that an early closure defect can lead to the disease phenotype.

There are diverse outputs of Gdf6a signaling, regulating cellular functions such as apoptosis, cell proliferation, and dorsal-ventral retinal patterning (French et al., 2009; French et al., 2013; Gosse and Baier, 2009; Valdivia et al., 2016). Because proliferative defects are visible after sulcus closure and apoptotic cells are not concentrated near the SOS (French et al., 2013), we reasoned that dorsal-ventral retinal patterning is the Gdf6a function most essential for SOS closure. During development, dorsal ocular BMP signaling is balanced by midline Sonic Hedgehog (Shh) activity (Sasagawa et al., 2002; Zhang and Yang, 2001), and *gdf6a*^{-/-} mutants exhibit an expansion of the Shh downstream gene *vax2* into the dorsal retina (Gosse and Baier, 2009). We therefore tested whether increased Shh signaling in BMP-deficient embryos underlies the persistent SOS phenotype. Indeed, treatment of *gdf6a*^{-/-} and *gdf6a*^{+/-} embryos with the Shh inhibitor cyclopamine significantly rescued the delayed closure phenotype (Fig. 5.11A,B). Cyclopamine treatment also partially rescued patterning in the dorsal retina, as it restored the *tbx5a* expression domain in *gdf6a* heterozygotes (Fig. 5.11C,D). These data support the idea that SOS closure is dependent on proper pattern formation within the developing retina and that sulcus morphogenesis is regulated by a balance of ventral Shh and dorsal BMP signaling pathways.

5.2.6. Analysis of a second superior coloboma patient

Transcriptome analyses of Gdf6a-depleted retinas have highlighted critical regulators of dorsal-ventral patterning within the zebrafish eye (French et al., 2013). Using this dataset, we interrogated the superior coloboma patient exome data, and identified a variant in *TBX2* (p.Pro329His). Zebrafish *tbx2b* is expressed in the dorsal eye in a Gdf6a- and BMP-dependent manner (Fig. 5.12A) (Gosse and Baier, 2009). To analyze the function of zebrafish *tbx2b* in regulating sulcus morphogenesis, we compared dorsal eye morphology between wild type embryos and *tbx2b*^{fbv} (*from beyond*) mutants (Snelson et al., 2008). We note a statistically significant increase in the proportion of embryos displaying an open SOS in *tbx2b*^{fbv} mutants compared to wild type embryos at 28 hpf (Fig. 5.12B,C). Such experimental results support a model in which dorsal-ventral patterning within the embryonic eye provides essential cues for morphogenesis of the SOS.

5.2.7. *Superior ocular sulcus functions as a conduit for superficial vasculature*

The inferior fissure demarcates the boundary between nasal and temporal retinal lobes and allows for ingrowth of blood vessels into the developing eye, both of which are also logical functions for the SOS. Alignment of the SOS with nasal-temporal markers was examined in *gdf6a*^{+/-} embryos because of their easily visualized sulcus and undisturbed nasal-temporal patterning. In situ hybridization with probes for *foxg1a* (nasal retina) and *foxd1* (temporal retina) demonstrates that the expression boundaries align with the position of the sulcus (Fig. 5.13A). Although the SOS lies at the division between nasal and temporal retina, its significance in separating retinal domains or, conversely, the role of nasal-temporal patterning in establishing the location of the sulcus remain to be tested.

Vascular inputs to the developing zebrafish eye include both the hyaloid artery that extends through the inferior fissure to form a plexus behind the lens, and the superficial vasculature that grows over the eye and encircles the lens (Snelson et al., 2008). The two systems are connected ventrally by the hyaloid vein. We hypothesized that the SOS forms a channel for the dorsal radial vessel (DRV; the first vessel of the superficial vasculature) as it grows over the dorsal retina and toward the lens. Indeed, SEM imaging shows a vessel extending into the SOS, and both DIC and confocal time-lapse imaging demonstrate that the nascent DRV grows through the sulcus (S3 and S9 Videos and Fig. 5.13B-D).

If the SOS functions to direct the DRV toward the lens, then altered sulcus morphology and dynamics would be expected to modify vascular development. Since our data demonstrate that BMP signaling regulates SOS closure, we therefore evaluated development of the superficial vasculature in embryos lacking Gdf6a. The DRV does form in *gdf6a*^{-/-} mutants and extends through the abnormally deep SOS; however, compared to control embryos, the DRV is of reduced calibre and unbranched at 26 hpf (*gdf6a*^{-/-}: 0±0 branch points [n=11] vs. siblings: 1.3±1.0 branch points [n=24]) (Fig. 5.14A,C,D). The *gdf6a* mutants always form a single DRV, compared to approximately half of control embryos where two DRV converge in the SOS (see control 41 hpf embryo in Fig. 5.14A,D). Moreover, instead of its normal course around the lens, the DRV in *gdf6a*^{-/-}

embryos projects deeply and ectopically travels dorsal to the lens to connect with the hyaloid vasculature (Fig. 5.14A,B,E). The DRV subsequently degenerates in most *gdf6a* mutants, but the ectopic vessel remains as a dorsal connection between the superficial annular vessel and the hyaloid plexus (Fig. 5.14A,E,F). Imaging of *Tg(rx3:GFP;kdrl:mCherry)* embryos revealed that the deep sulcus in *gdf6a*^{-/-} mutants creates a notable divot in the optic cup immediately dorsal to the lens (Fig. 5.15A). In all cases (n=8), the forming ectopic vessels grew directly into this space between the dorsal edge of the lens and the retina. Given the defects observed for the DRV in BMP-deficient embryos, we conclude that dorsal retinal patterning is necessary for superficial vascular pathfinding.

Patterning of the ventral retina is regulated by Shh (Sasagawa et al., 2002; Zhang and Yang, 2001), and our earlier data suggest a balance between Bmp and Shh signaling impacts SOS morphogenesis. In contrast to loss of BMP signaling, cyclopamine inhibition of Shh signaling in wild type embryos resulted in a shallow SOS that closes early (Fig. 5.15B), and an increased proportion of embryos with multiple DRVs spread across the dorsal retina (Fig. 5.15B and Fig. 5.16). A similar change in growth of the DRV was noted previously in embryos where the Shh receptor Smoothed is non-functional (Weiss et al., 2017). In summary, disrupted dorsal-ventral patterning of the retina leads to profound alteration of the superficial vasculature.

Aberrant vasculature in *gdf6a*^{-/-} mutants or cyclopamine-treated embryos could result either from a direct role of the morphogens in regulating vascular pathfinding or from altered SOS dynamics. To determine whether the SOS itself directly influences growth of the superficial vasculature, we prevented the Gdf6a-dependent sulcus defects by manipulating Hedgehog signaling. Indeed, cyclopamine treatment of *gdf6a*^{-/-} mutants both rescues SOS closure defects and precludes ectopic connection with the hyaloid vasculature (Fig. 5.11 and Fig. 5.16). Similarly, loss of Gdf6 rescues the DRV overgrowth phenotype observed in cyclopamine-treated embryos (Fig. 5.16). Therefore, the data support a model in which proper SOS formation and closure are necessary for correct DRV pathfinding.

5.3. Discussion

In this manuscript, we classify superior coloboma as a separate disease with a developmental origin distinct from, but comparable to, inferior coloboma. Eight patients display gaps in tissues of the superior eye, including retina, lens, and iris. We demonstrated the existence of a transient dorsal/superior groove in vertebrate eye development that is conserved among fish, chick, newt and mouse. Failure to close the superior ocular sulcus (SOS) can result in adult zebrafish displaying a phenotype that resembles superior coloboma. Furthermore, it supports the evolutionary conservation of the SOS amongst vertebrates, an evolutionary distance of some 450 million years.

There are rare reports in the scientific literature of patients with “atypical” coloboma (Abouzeid et al., 2009; Jethani et al., 2009; Mann and Ross, 1929; Ramirez-Miranda and Zenteno, 2006; Villarroel et al., 2008), ocular anomalies contrasting with the position of the known inferior embryonic fissure. The vast majority of such cases (macular coloboma, aniridia, or nasally/temporally oriented iris coloboma) are unlikely to arise from defects of sulcus closure. However, at least two of the described atypical coloboma patients display iris colobomata with a superior orientation (Abouzeid et al., 2009; Mann and Ross, 1929). Although the embryonic mechanism was originally considered anomalous, our identification of the SOS provides a likely explanation for the unusual coloboma identified in these two patients.

Exome sequencing of our superior coloboma patients identified rare variants in the genes encoding the type 1 BMP receptor and transcription factor T-box 2. In the absence of multigenerational pedigrees of affected patients, we are unable to causally link such variants to the incidence of disease. However, the connection between BMP signaling and inferior fissure morphogenesis is well established. Indeed, variants in *GDF6* (*BMP13*), *BMP4*, and *SMOC1* are linked to inferior coloboma and microphthalmia (Abouzeid et al., 2011; Asai-Coakwell et al., 2007; Bakrania et al., 2008; Gregory-Evans et al., 2004; Williamson and FitzPatrick, 2014). Furthermore, zebrafish, *Xenopus*, chick, and mouse studies have demonstrated a key role for BMP signaling in optic cup morphogenesis, apoptosis, proliferation, and dorsal-ventral eye patterning (Abouzeid et al., 2011; Adler and Belecky-Adams, 2002; Asai-Coakwell et al., 2007; Asai-Coakwell et al., 2013; Behesti et

al., 2006; French et al., 2009; Gosse and Baier, 2009; Weston et al., 2003). Consistently, abrogating BMP signaling either by DMH1 treatment or loss of Gdf6a results in profound SOS closure defects. Beyond the *gdf6a* homozygous mutant phenotype, we also detected a partially penetrant sulcus closure defect in the otherwise morphologically normal *gdf6a* heterozygotes, arguing that the sulcus is particularly sensitive to the levels of BMP signaling. Further, loss of Tbx2b function in zebrafish *fbv* mutants leads to comparable aberrations in SOS morphogenesis. Such data, taken together with the detrimental nature of the patient *BMPRIA* variant, support a model whereby BMP signaling modulates SOS closure via regulation of target genes such as *tbx2*.

Research on ocular BMP signaling defines roles in regulating eye precursor cell number, apoptosis, proliferation, and dorsal-ventral gene expression (Asai-Coakwell et al., 2013; Bielen and Houart, 2012; French et al., 2009; French et al., 2013; Gosse and Baier, 2009; Pant et al., 2013; Valdivia et al., 2016). However, apoptotic cell populations are not localized to the SOS, and proliferative defects are present only after SOS closure (French et al., 2013; Pant et al., 2013). Furthermore, we note that *gdf6a* heterozygotes display aberrant sulcus closure, yet lack apoptotic or proliferative defects. In contrast, *gdf6a*^{+/-} embryos display detectable alterations to dorsal-ventral gene expression, providing a correlation between patterning and SOS closure defects. To further test the role of dorsal-ventral patterning in sulcus dynamics, we asked whether rescue of the patterning defects in *gdf6a*^{-/-} embryos would also promote SOS closure. Given the expansion of inferior markers into the superior retina of *gdf6a* mutants (French et al., 2009; Gosse and Baier, 2009), and the rescue of SOS defects with Shh inhibition, we conclude that the aberrant closure of the SOS in Gdf6- and Tbx2-depleted embryos is linked to dorsal-ventral patterning defects of the vertebrate eye.

The identification of a patient with two variants in *CYP11B1* prompted us to carefully examine retinoid signaling in SOS closure. A role in ocular morphogenesis is well established for the retinoid signaling pathway, with mutations in the RA synthesis gene *ALDH1A3* known to cause inferior coloboma (Abouzeid et al., 2014). Furthermore, RA regulates proliferation and migration of periocular mesenchyme (POM), a neural crest- and mesoderm-derived cell population that modulates inferior fissure closure (Chawla et al.,

2016; Chawla et al., 2018; Lupo et al., 2011). The inability of extensive zebrafish experiments to reveal a role for *cyp11b1* in SOS closure, even in the context of Gdf6a deficiency (Fig. 5.17) may reflect the greater complexity of the family of retinoid synthesis enzymes in humans and their distinct expression patterns compared to zebrafish. Given the proximity of RA signaling to the SOS and known roles for RA in regulating morphogenesis in other systems, it remains plausible that RA signaling contributes to the causality of human superior coloboma. Eye morphogenesis and patterning are dependent on multiple signaling pathways, in addition to BMP and RA. For example, overexpression of the Wnt inhibitor Dkk1 results in loss of dorsal ocular gene expression (Veien et al., 2008), and mutation of the Wnt receptor *FZD5* (thought to function as a receptor for both canonical and non-canonical Wnts in a context-dependent manner) causes inferior coloboma (Liu et al., 2016). In examining the prioritized list of rare variants identified in superior coloboma patients, we note rare variants in *NKDI*, *CELSR2*, *FZD4*, *SCRIB*, and *WNT9B* (components of canonical or non-canonical Wnt pathways). The rare *TSC2* (Tuberous Sclerosis Complex 2/Tuberin) variant in patient #1 plausibly implicates other cellular mechanisms in the induction of superior coloboma. *TSC2* complexes with *TSC1* to regulate the mTOR signaling pathway (Henske et al., 2016), and loss of either gene leads to unregulated cell growth and proliferation.

The rare incidence of superior coloboma argues that the disorder is unlikely caused by simple, single-gene inheritance. Rather, a model incorporating multi-gene inheritance or incomplete penetrance is more plausible. Seven of the eight patients with superior coloboma in the current study display unilateral disease, also a common characteristic of inferior coloboma (Nakamura et al., 2011). The highly penetrant defects found in zebrafish *gdf6a* mutant larvae, which only infrequently result in an adult superior coloboma phenotype (Fig. 5.10F), are consistent with an impressive ability of the developing eye to recover from embryonic defects. However, the absence of an obvious coloboma does not preclude abnormal SOS morphogenesis generating more subtle abnormalities, such as vascular misrouting. Although defining the relative contribution of heritability and environment is challenging, other disorders offer potential insight. Characterized by appreciable globe enlargement, high myopia represents an ocular disorder with substantial genetic and environmental components, where unilateral cases account for up to one third

of the total (FitzGerald et al., 2005). Anisometropia represents a second example of an asymmetric developmental ocular phenotype (Barrett et al., 2013), and the pattern apparent in the current cases (Fig. 5.1) corresponds with such examples.

The parallels with the inferior ocular fissure, which provides a passageway for the hyaloid vasculature (Hartsock et al., 2014; Kitambi et al., 2009; Saint-Geniez and D'Amore, 2004), are strong. The close coordination between the development of both structures is highlighted by the ability of the dilated hyaloid vein in zebrafish *lmo2* mutants to disrupt fissure closure and cause inferior coloboma (Weiss et al., 2012). The tight association between the superficial vasculature's DRV and the SOS provides convincing evidence that the SOS serves a similar retinal vascular guidance function. While developing blood vessels follow guidance cues in the same manner as growing axons (Siemerink et al., 2010), our data argues that the physical landscape of a tissue can also direct angiogenesis. First, the DRV in wild type embryos travels directly through the SOS to reach the lens, whereas only a thin and unbranched DRV grows through the particularly deep sulci of *gdf6a*^{-/-} mutants. Second, the shallow or absent SOS in cyclopamine-treated embryos correlates with the appearance of multiple DRVs spread across the dorsal retina. Finally, the divot above the lens in *gdf6a*^{-/-} mutants aligns with the position of the ectopic connection between hyaloid and superficial vasculature. Taken together, these data support a model in which the SOS provides a path for directing and restraining DRV growth (Fig. 5.18).

Here, we have characterized a previously unrecognized developmental structure with a significant disease connection. Further studies will be needed to discern the exact mechanisms of sulcus formation and resolution, and to more deeply analyze the causes of superior coloboma.

5.4. Figures

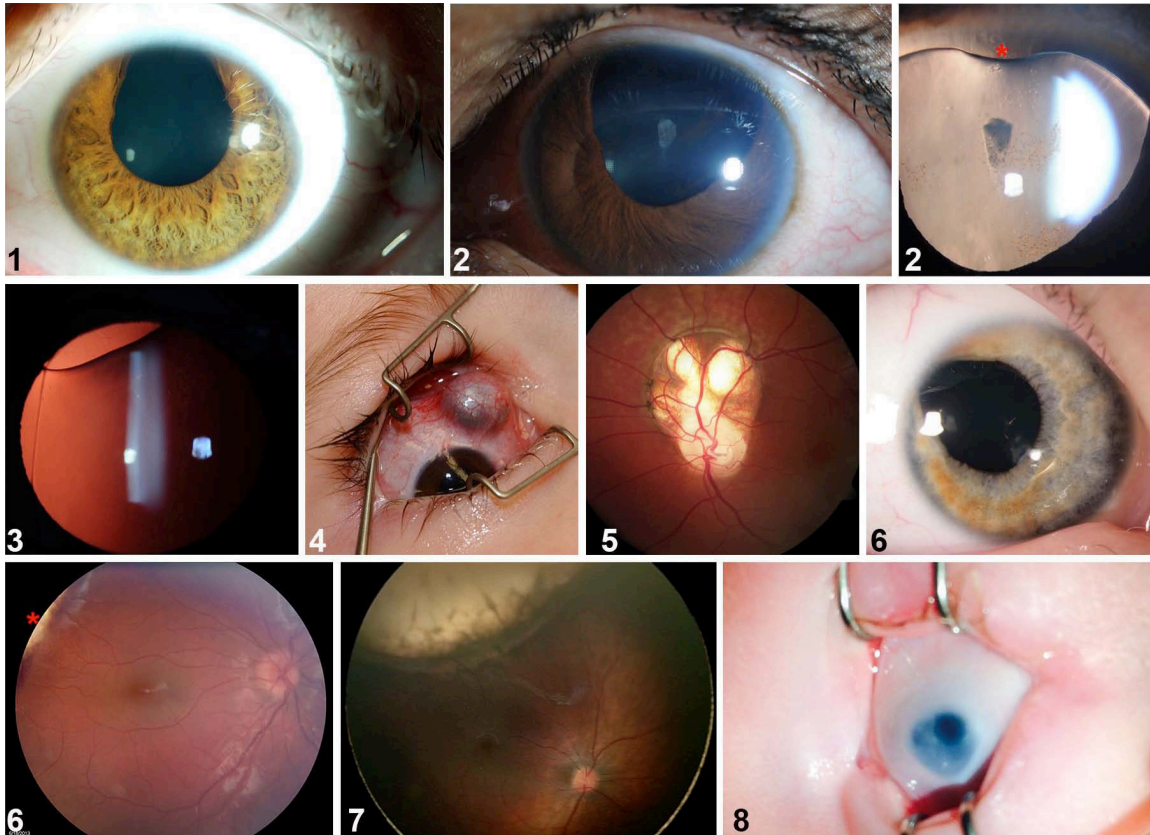


Fig. 5.1: Superior Coloboma montage from patients with superior coloboma (numbers correspond to patients described in Table 5.1). #1: unilateral superior iris coloboma. #2: first panel, asymmetrically sized iris defects with bilateral pupil involvement, left eye shown; second panel, superior lenticular coloboma (asterisk) associated with a lens zonule defect. #3: lenticular coloboma, lens edge visible with retro-illumination. #4: superior scleral defect with uveal (choroid) protrusion. #5: superior retino-choroidal coloboma extending from optic disc in a patient with Dandy-Walker Syndrome. #6: first panel, iris coloboma; second panel, edge of retino-choroidal coloboma (asterisk). #7: extensive retino-choroidal coloboma. #8: intra-operative photograph of a superior iris coloboma in a microphthalmic eye.

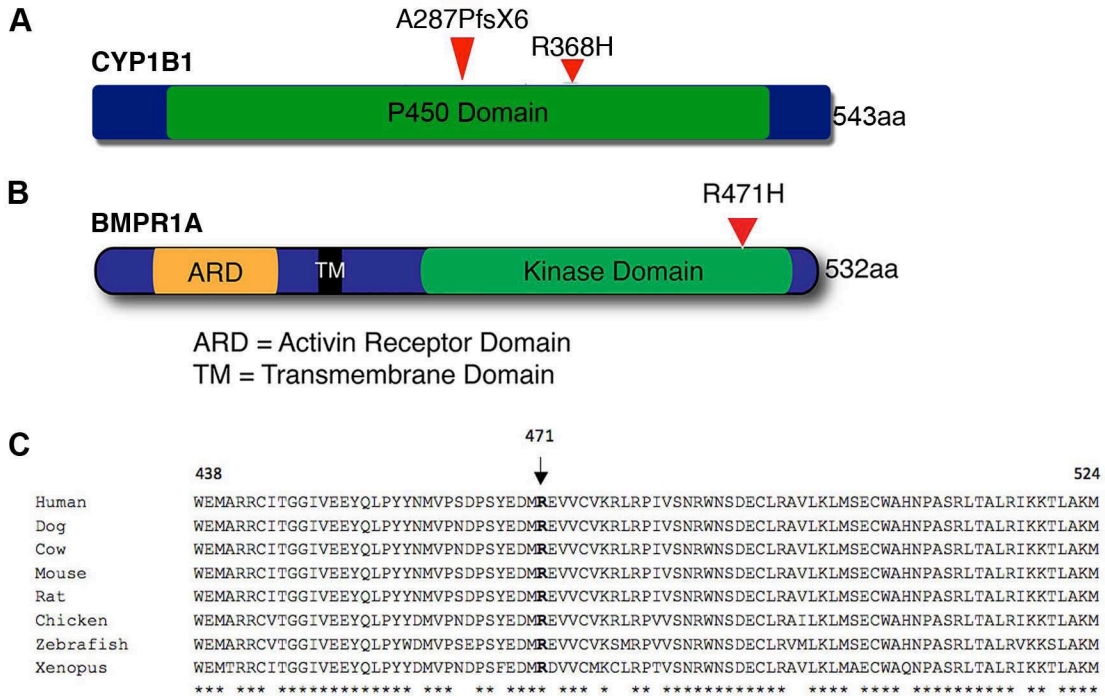


Fig. 5.2: Genetic variants identified in bilateral superior coloboma patient. (A) Diagram of the human CYP1B1 protein, with the compound heterozygous mutations carried by patient #2 indicated. (B) Diagram of the human BMPR1A protein showing rare variant present in patient #2. (C) Alignment illustrating the evolutionary conservation of the BMPR1A protein kinase domain. The altered residue (p.R471H) is depicted in bold, with invariant residues denoted by *.

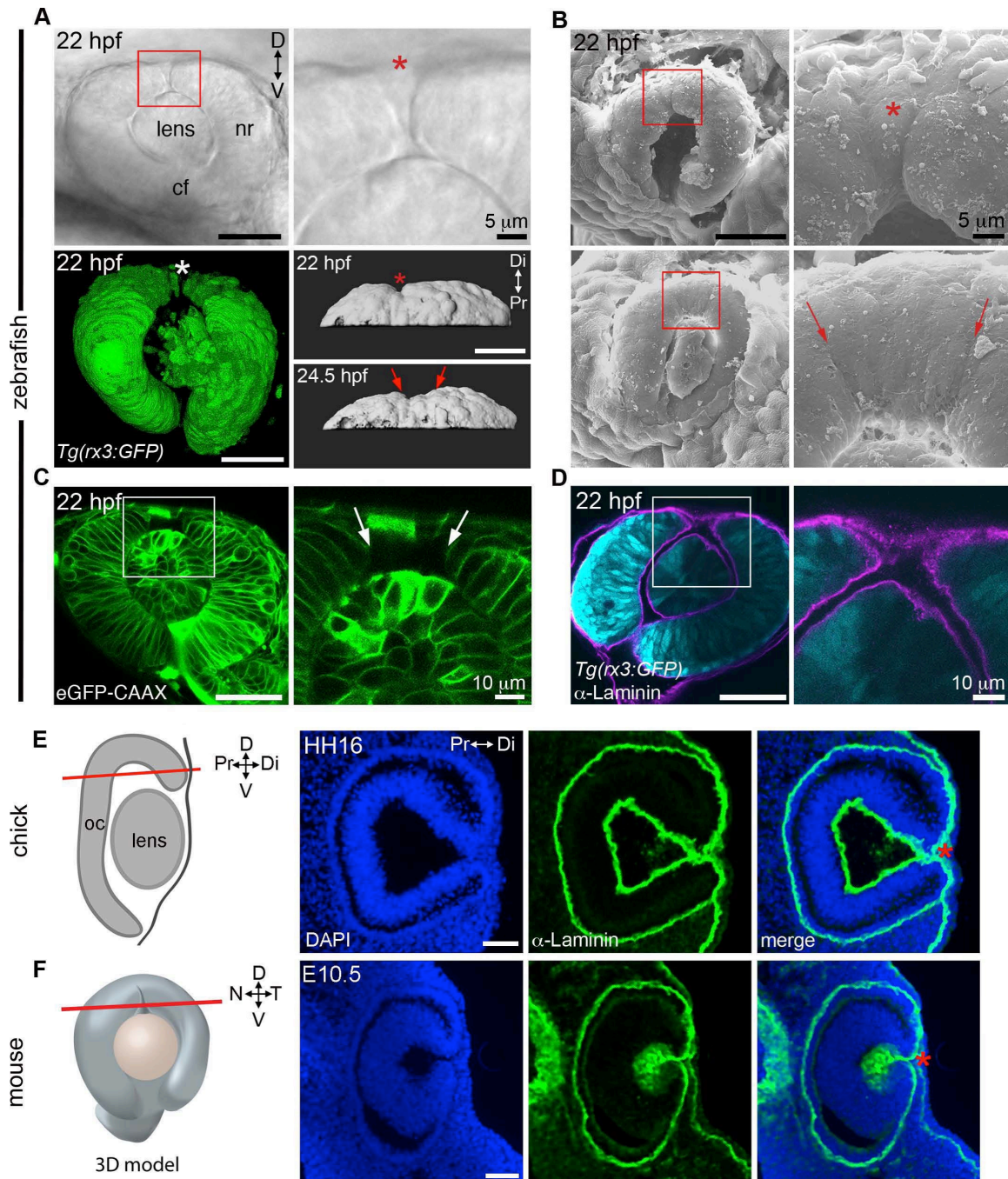


Fig. 5.3: The superior ocular sulcus in zebrafish, chick and mouse. (A) Zebrafish eyes displaying superior ocular sulci (SOS) marked by an asterisk or arrows. Top row: lateral view DIC image of the eye of a live embryo, photographed on a compound microscope. Enlarged view is shown in panel on right. Bottom row: Left, lateral view surface projection of the eye of a live *Tg(rx3:GFP)* embryo; right, surface projection dorsal views of eyes from a *Tg(rx3:GFP)* embryo. (B) Scanning electron micrographs showing SOS at narrow

(top row) and wide (bottom row) phases. Red boxes denote regions enlarged in panels on the right. (C) Single optical section, lateral view, through the eye of an embryo injected with *eGFP-CAAX* mRNA to label the cell membranes, with right panel showing enlarged view of boxed area. (D) Single optical section, lateral view, through eye of *Tg(rx3:GFP)* embryo (cyan) immunolabelled for Laminin to highlight the basal lamina (magenta). (E) Diagram showing chick eye with red line demonstrating the plane of section employed on the right. Representative horizontal section through the dorsal eye of a HH16 chick, stained with a Laminin antibody (green) and DAPI (blue). A dorsal, Laminin-lined space is evident in the distal portion of optic cup (asterisk). (F) Diagram showing 3D model of an embryonic eye with red line demonstrating plane of section for both mouse and chick sections. Right three panels are a representative horizontal section through the dorsal eye of an embryonic day 10.5 (E10.5) mouse, stained with a Laminin antibody (green) and DAPI (blue). A dorsal, Laminin-lined space is evident in the distal portion of optic cup (asterisk). Except where noted, scale bars are 50 μm . cf, choroid fissure; D-V, dorsal-ventral; HH, Hamburger Hamilton embryonic stage; hpf, hours post fertilization; N-T, nasal-temporal; nr, neural retina; Pr-Di, proximal-distal.

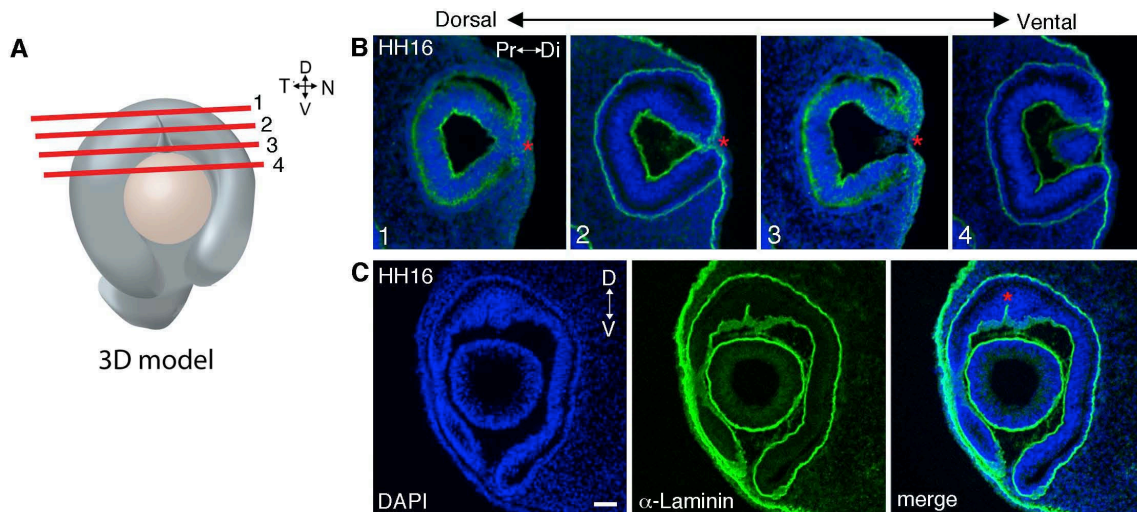


Fig. 5.4: Superior ocular sulcus in chick. (A) 3D Model of the eye depicting where the eye was sectioned to create the serial horizontal sections shown in B. (B) Serial cryostat sections of a chick HH16 stage eye stained with DAPI (blue) and α -Laminin antibody (green). First three sections are dorsal to the lens and the fourth is through the lens. (C) Tangential section of HH16 chick eye labeled with DAPI (blue) and α -Laminin antibody (green). D, dorsal; V, ventral; Di, distal; Pr, proximal; HH, Hamburger Hamilton. Red asterisks indicate superior ocular sulcus. Scale bar is 50 μ m.

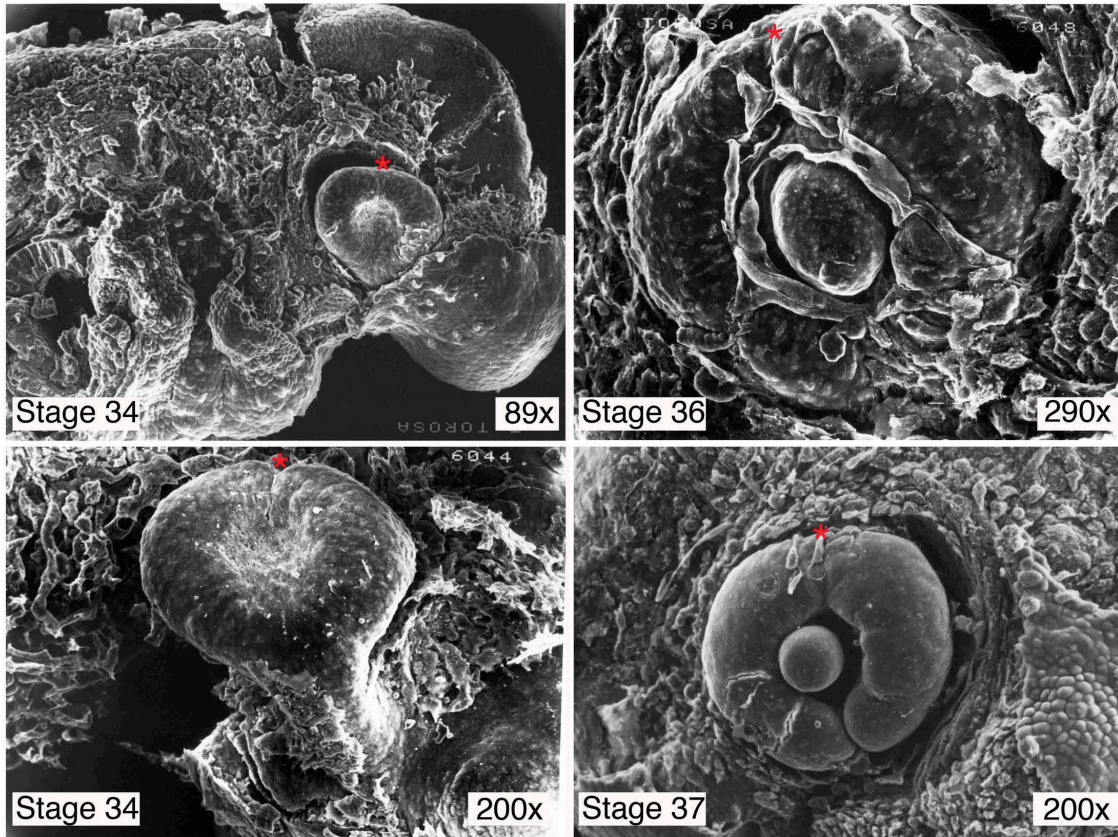


Fig. 5.5: Superior ocular sulcus in newt. Scanning electron microscopy images of newt (*Taricha tarosa*) ocular development. Panels on left display SEM images of stage 34 embryos after partial dissection of surface tissues. Panels on right show slightly older embryos (stage 36–37), with vasculature intact in the stage 36 example. Red asterisks indicate superior ocular sulcus.

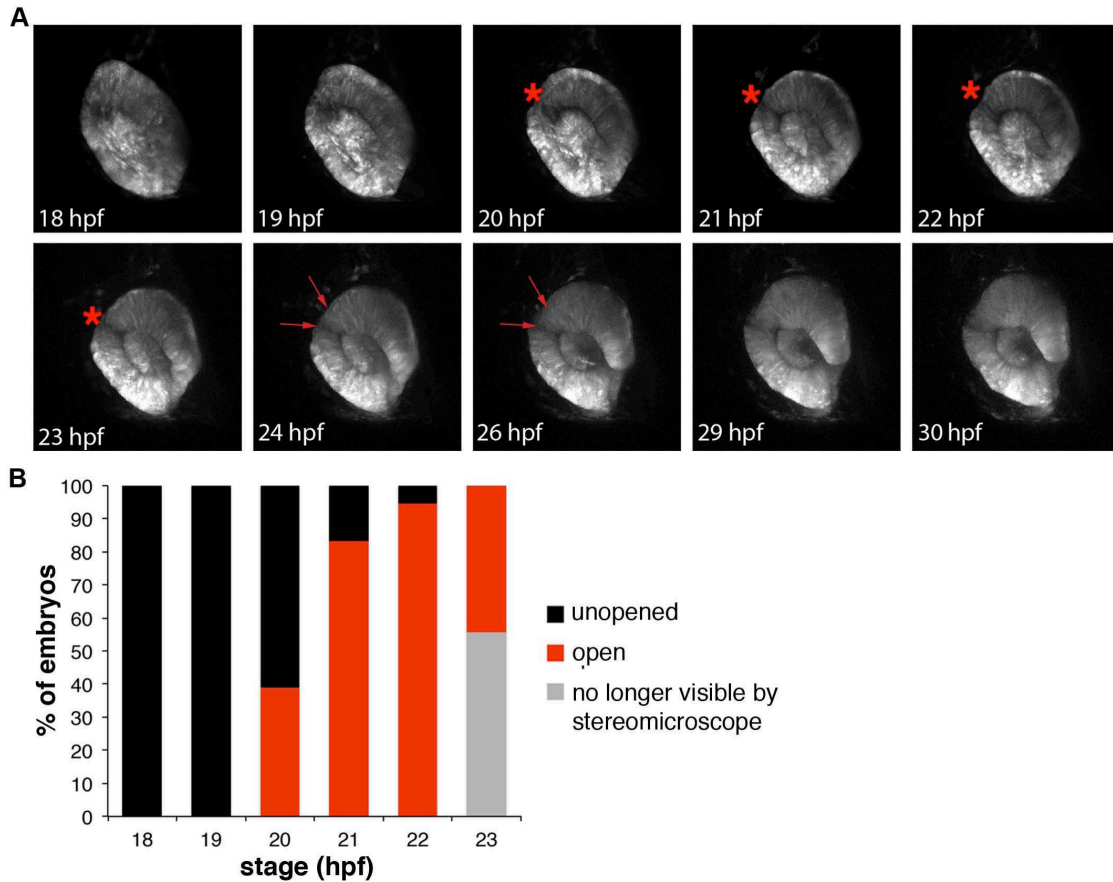


Fig. 5.6: Dynamics of the zebrafish superior ocular sulcus. (A) Time-lapse images showing lateral views of the eye of a *Tg(rx3:GFP)* embryo. The superior ocular sulcus appears as a narrow groove across the dorsal retina at ~20 hpf (red asterisk), becomes wider by 24 hpf (red arrows) and disappears after 26 hpf. (B) Timing of SOS as viewed under a stereomicroscope. The wide and shallow phase is not visible by stereomicroscope, so the red bars indicate the percentage of embryos with a narrow and distinct sulcus.

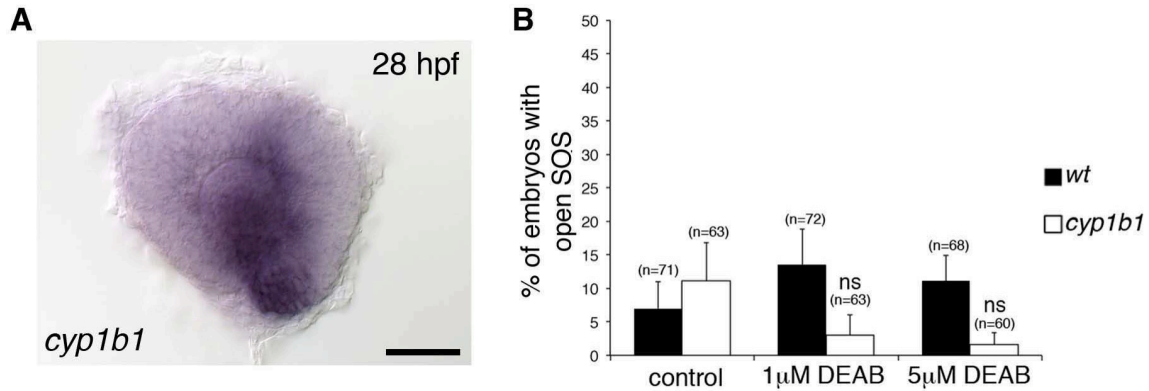


Fig. 5.7: Reduced RA signaling does not impair closure of the superior ocular sulcus.

(A) Lateral view of a 28 hpf zebrafish eye following in situ hybridization for *cyp1b1*. Note that expression extends into the dorsal eye. (B) Quantification of open SOS in 28 hpf embryos from *cyp1b1*^{+/-} incrosses treated from 10 hpf with control solution or the Aldh inhibitor, DEAB. N=3 experiments, n=number of embryos. Data are means ± SEM. Statistics is two-way ANOVA with Tukey's test. Scale bar is 50 μm. ns, not significant.

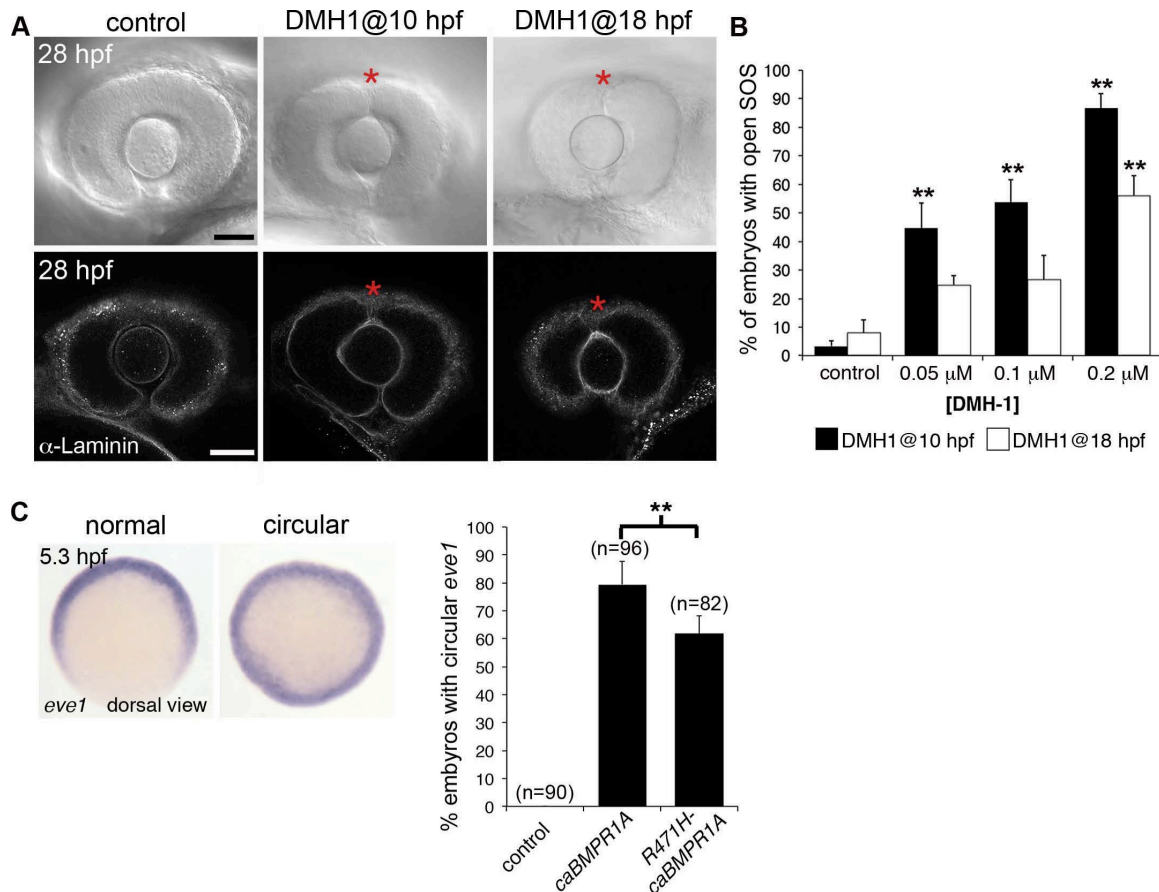


Fig. 5.8: The role of BMPR1 signaling in closure of the superior ocular sulcus. (A-B) Effect of BMPR1 antagonist DMH1 on SOS closure. Lateral view DIC images of eyes from live embryos (first row) and single optical slices of eyes processed for anti-Laminin immunofluorescence (second row) following exposure to control media or 0.02 μ M DMH1, starting at either 10 or 18 hpf (A). SOS is marked by red asterisk. Quantification of delayed sulcus closure in DMH1-treated embryos (B). N=3 experiments, n=89 or 90 embryos for each condition. Data are means \pm SEM. Statistics is a one-way ANOVA for each time series with Tukey's post-hoc test: **p<0.01. (C) Injection of *caBMPR1A* mRNA into one-cell stage zebrafish embryos caused expansion of *eve1* gene expression into a circular ring in whole embryos at 50% epiboly (5.3 hpf). Significantly fewer embryos exhibited circular *eve1* expression when injected with *R471H-caBMPR1A*. N=3 experiments. Data are means \pm SEM. Statistics is a two-tailed t-test: *p<0.05. Scale bars are 50 μ m.

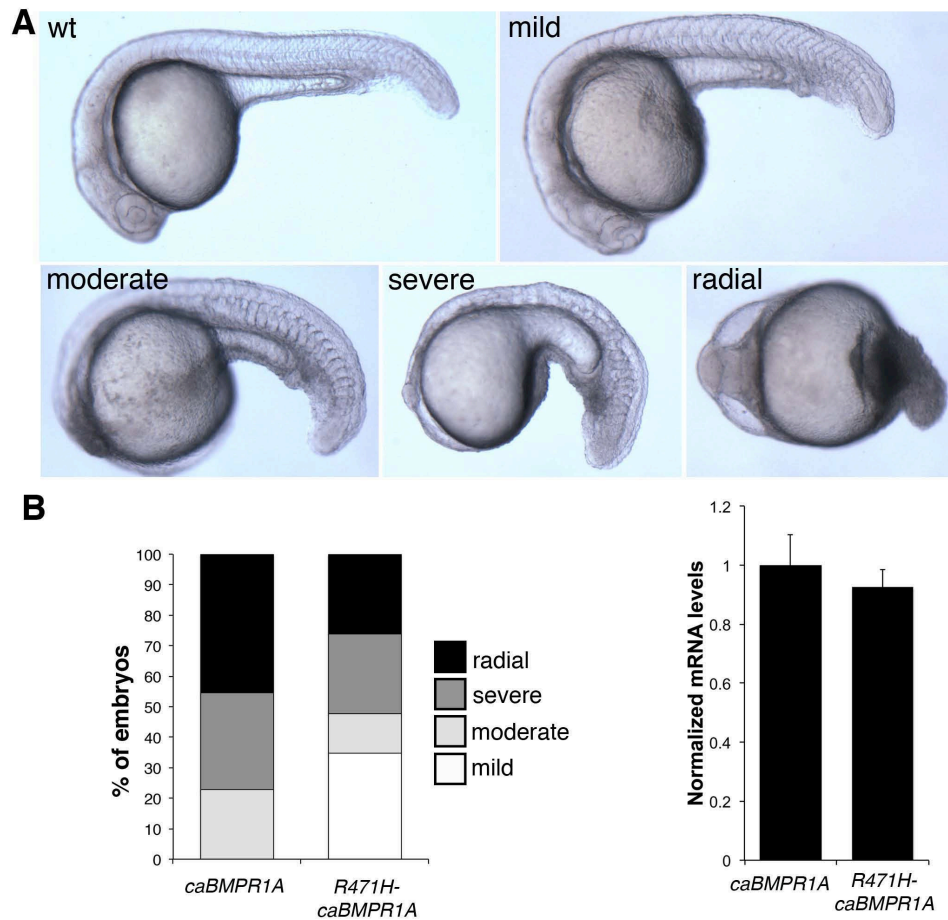


Fig. 5.9: Patient variant in BMPR1A reduces protein function. (A) One cell-stage zebrafish embryos were injected with mRNA for a constitutively active form of BMPR1A (*caBMPR1A*) or *caBMPR1A* combined with the patient's variant (*R471H-caBMPR1A*), and assessed at 24 hpf for morphological abnormalities by categorization according to the pictures shown. (B) Graph showing percentage of embryos injected with *caBMPR1A* (n=22 embryos) or *R471H-caBMPR1A* (n=23 embryos) that fit into each category of morphological abnormality. (C) qPCR showing equal amounts of injected RNA for each condition. Statistics is two-tailed t-test.

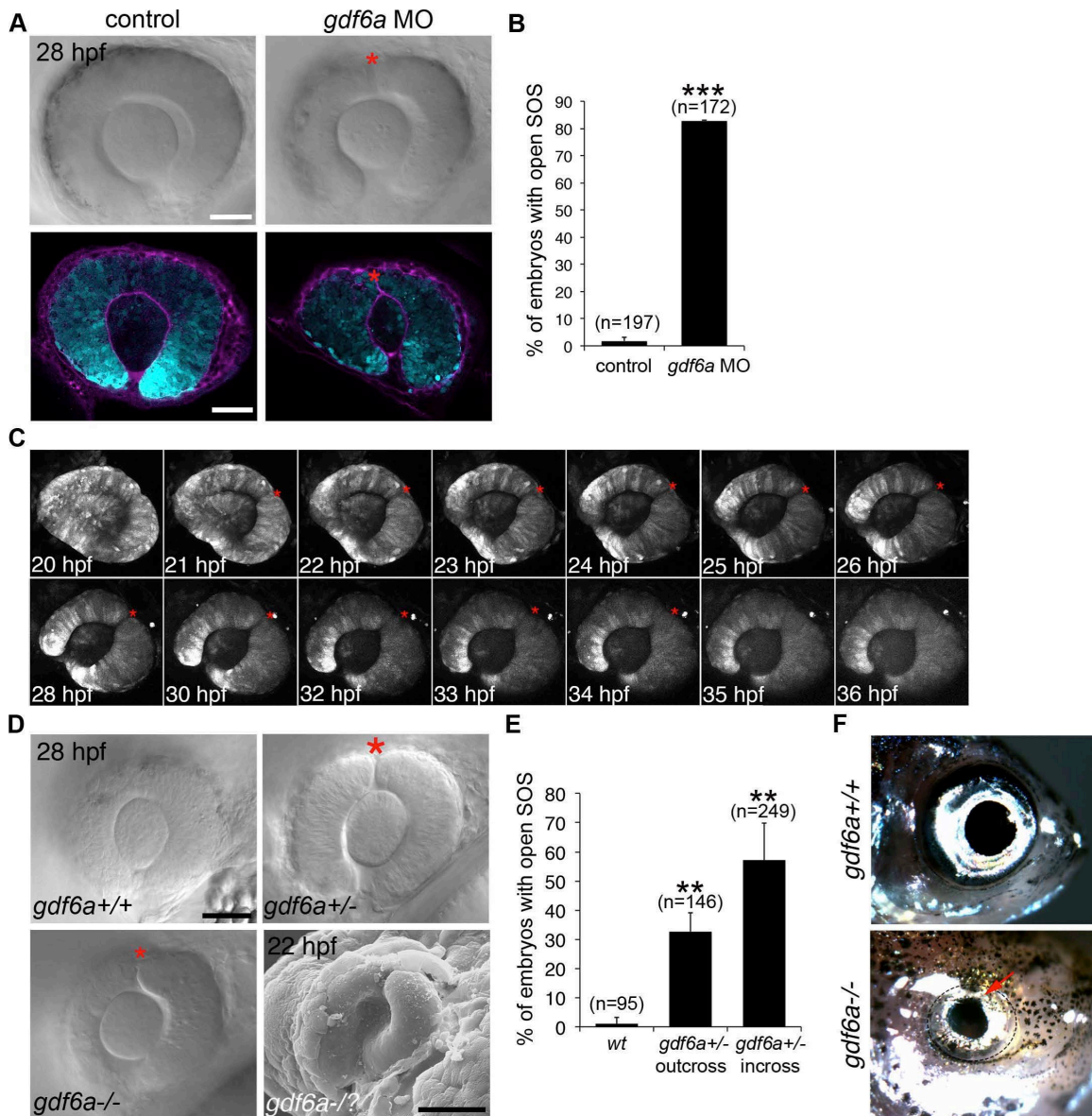


Fig. 5.10: The role of Gdf6a signaling in superior ocular sulcus morphogenesis. (A) Delayed SOS closure caused by Gdf6a knockdown. *Tg(rx3:GFP)* zebrafish eyes (cyan) from uninjected and Gdf6a morpholino-injected embryos shown as DIC images of live embryos and single optical slices following anti-Laminin antibody staining (magenta). SOS marked by red asterisk. (B) Quantification of embryos with delayed sulcus closure, as assessed at 28 hpf. (C) Time series of maximum projection confocal images of a *Tg(rx3:GFP)* embryo injected with *gdf6a* morpholino. (D) DIC images of wild type, *gdf6a*^{+/-} and *gdf6a*^{-/-} eyes (SOS marked by red asterisk). Bottom right panel shows SEM image of a Gdf6a-deficient eye with a pronounced sulcus. (E) Quantification of *gdf6a*^{-/-}

mutants (or siblings) with delayed SOS closure. (F) Adult wild type zebrafish (top panel) showing normal eye morphology and a *gdf6a*^{-/-} zebrafish (bottom panel) with superior coloboma (red arrow). N=3 experiments for graphs in B and E. n=number of embryos. Data are means ± SEM. Statistics in B is a two-tailed t-test, and in E is one-way ANOVA with Tukey's test: **p<0.01, *** p<0.001. Scale bars are 50 μm.

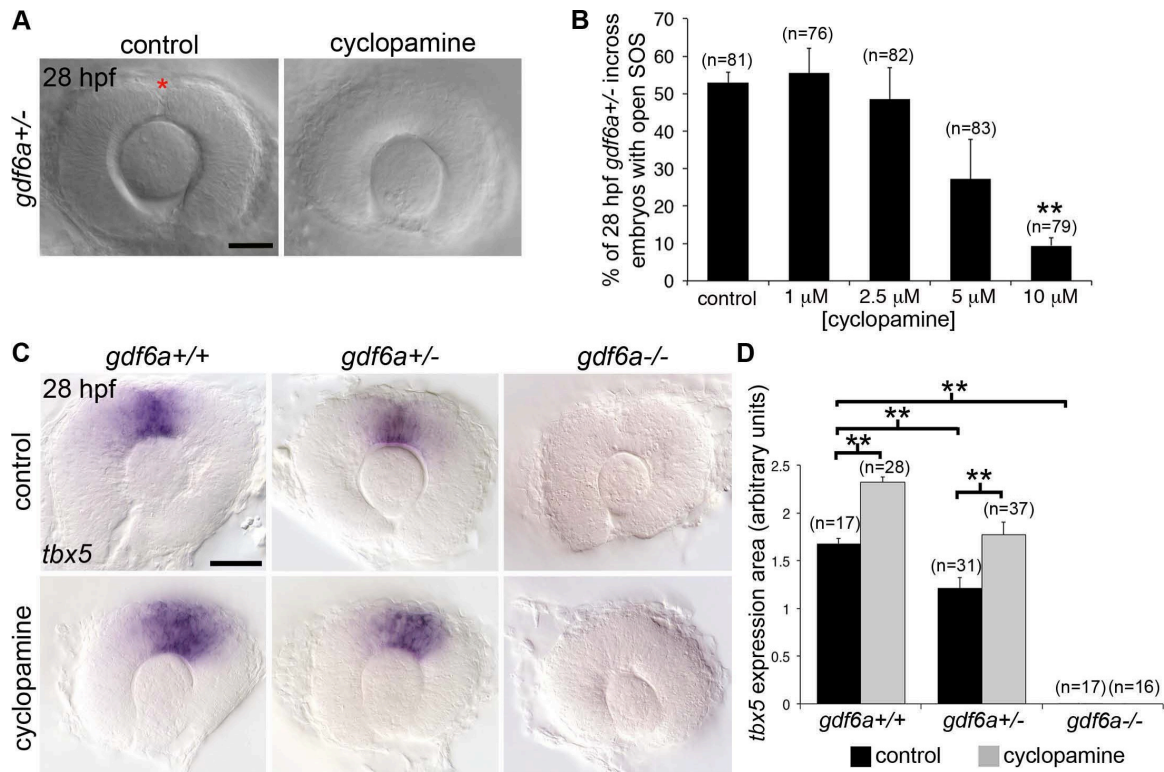


Fig. 5.11: Inhibition of Hedgehog signaling rescues closure of the superior ocular sulcus in *Gdf6a*-deficient embryos. (A-B) Effect of Hedgehog inhibition (cyclopamine treatment) on SOS closure in *Gdf6a*-deficient embryos. DIC images of *gdf6a*^{+/-} eyes, treated with either control solution (left) or 10 μ M cyclopamine (right) (A). SOS marked by red asterisk. Quantification of effect of cyclopamine treatment on SOS closure in *gdf6a*^{+/-} incross embryos (B). (C-D) Effect of cyclopamine on dorsal retinal patterning in *Gdf6a*-deficient embryos. *tbx5a* RNA expression in eyes from 28 hpf *gdf6a*^{+/+}, *gdf6a*^{+/-}, and *gdf6a*^{-/-} embryos with or without cyclopamine treatment (C). Quantification of effect of cyclopamine treatment on area of *tbx5a* expression (D). n=number of embryos, N=4 (B) or 3 (D) experiments. Data in B and D are means \pm SEM; Statistics in B is a one-way ANOVA with Tukey's test, D is two-way ANOVA with Tukey's test: **p<0.01. Scale bars are 50 μ m.

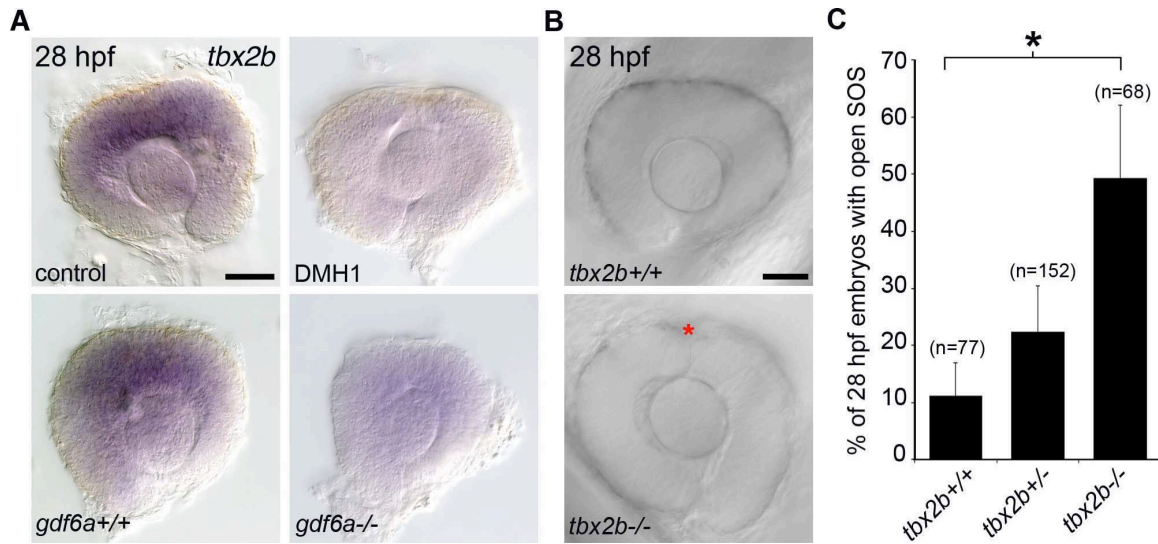


Fig. 5.12: *tbx2b* mutant zebrafish have delayed closure of the superior ocular sulcus.

(A) Whole-mount in situ hybridization for zebrafish *tbx2b* in control and BMP-depleted embryos. Top panels are eyes dissected from control and DMH1-treated embryos; bottom panels are from *gdf6a*^{+/+}, and *gdf6a*^{-/-} embryos. (B-C) Analysis of SOS closure in *tbx2b*-mutant embryos. DIC images of eyes from live *tbx2b*^{+/+} (top panel) and *tbx2b*^{by} (bottom panel) embryos (B). Quantification of SOS closure in wild type and *tbx2b*^{by} mutant zebrafish eyes (C). Data are means ± SEM; one-way ANOVA with Tukey's test: *p<0.05. Scale bars are 50 μm.

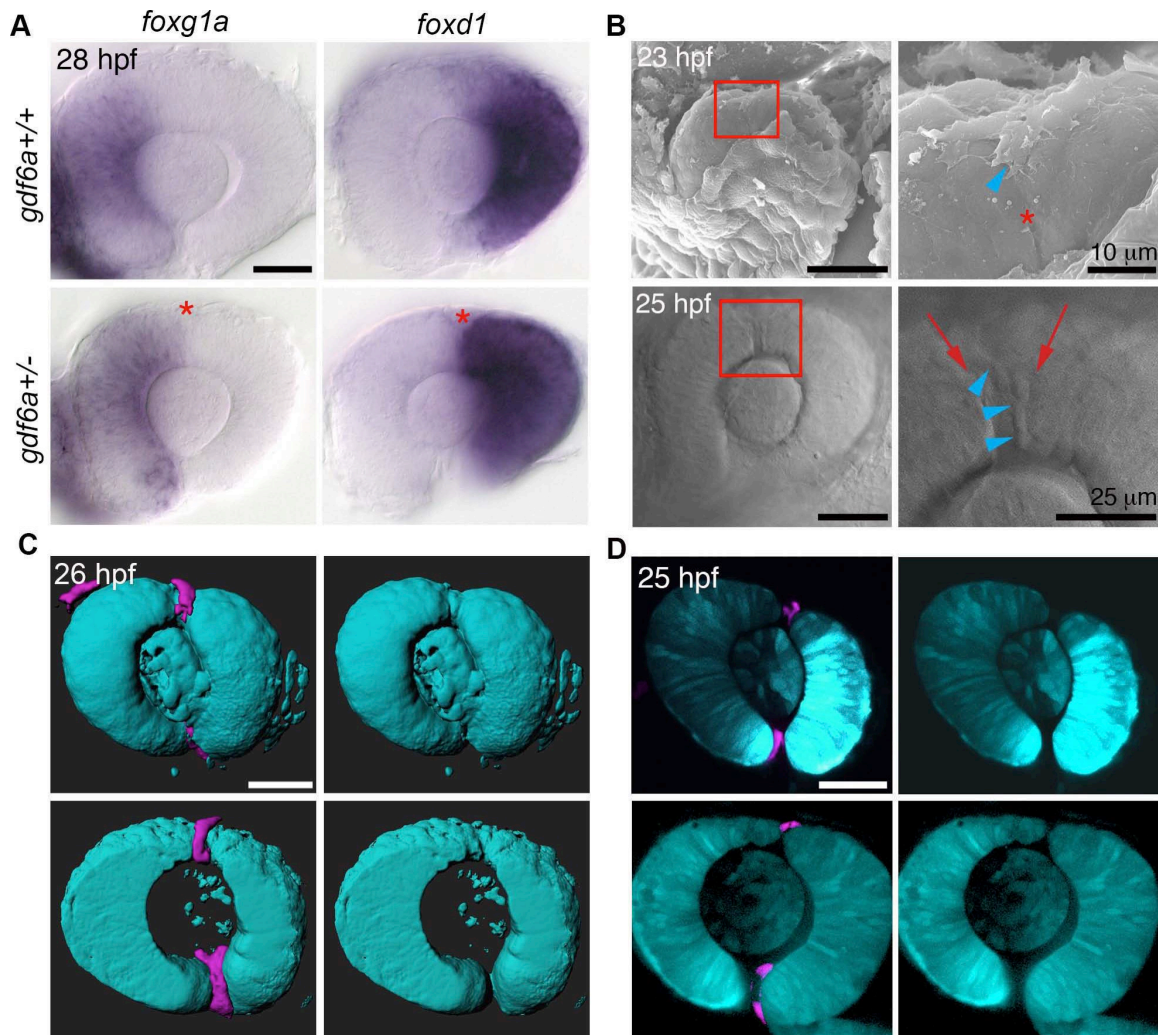


Fig. 5.13: Developmental functions of the superior ocular sulcus. (A) The prominent and persistent SOS (red asterisk) present in *gdf6a*^{+/-} embryos aligns with the boundary between the nasal marker *foxg1a* and temporal marker *foxd1*. Note that nasal-temporal patterning is unchanged in the *gdf6a* heterozygotes (bottom row) compared to the wild type embryos (top row). (B) SEM photographs showing the dorsal radial vessel (DRV) extending into the SOS (top row). DIC images of DRV (blue arrowheads) within a wide SOS (red arrows; bottom row). Right panels are magnified views of boxed regions. (C-D) Surface projections (C) and single optical slices (D) from confocal images of *Tg(rx3:GFP;kdr1:mCherry)* embryos show the DRV (magenta) extending through the SOS (optic cup and lens are cyan). Scale bars are 50 μm unless otherwise noted.

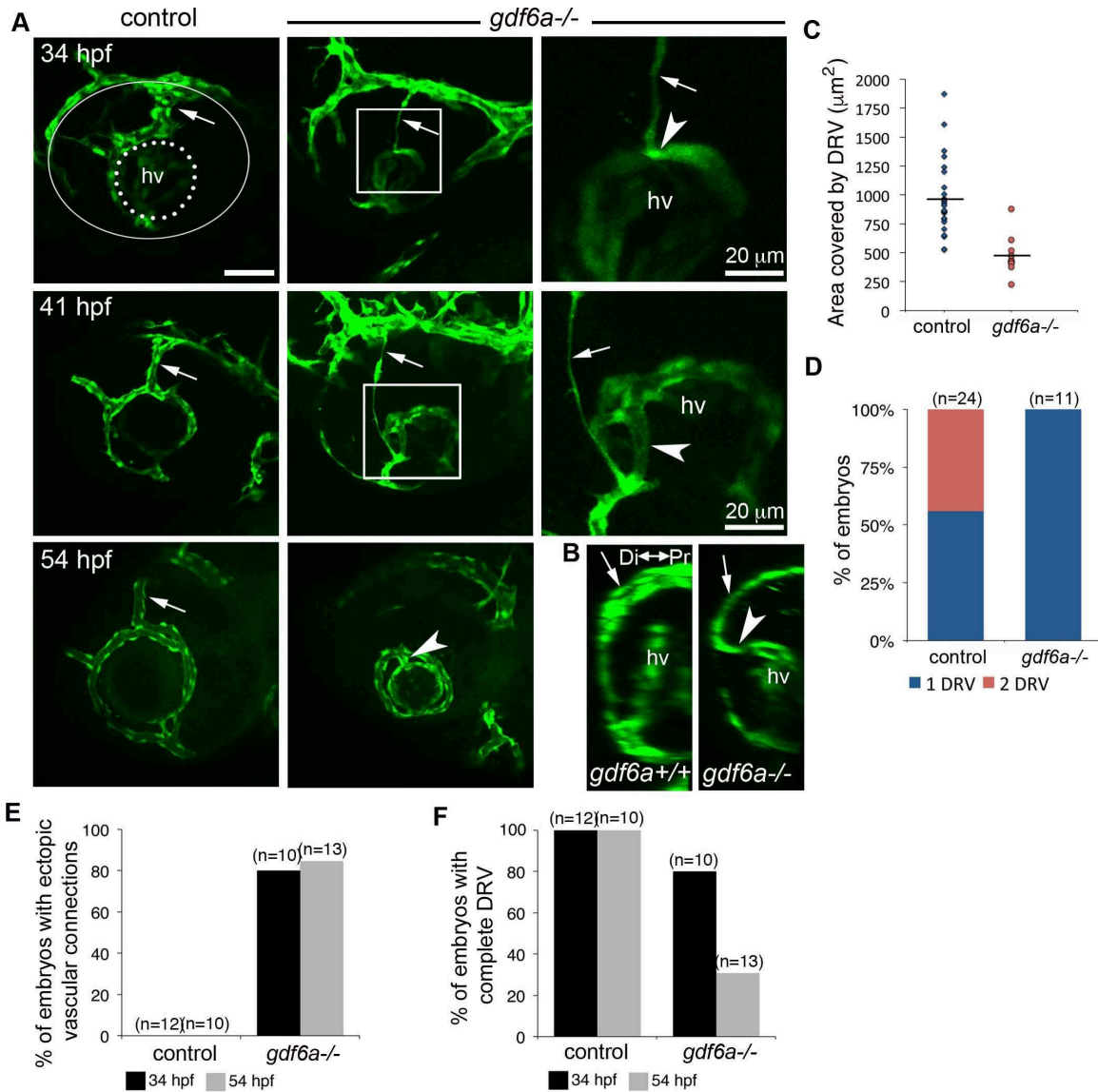


Fig. 5.14: Abnormal ocular vasculature in *gdf6a* homozygous mutants. (A-B) Growing blood vessels (green) in the developing eyes of *gdf6a*^{-/-} or control (sibling) embryos are highlighted by the *kdr1:eGFP* transgene and shown as maximum projections of confocal z-stacks (A) or 90° lateral rotations thereof (B). Dorsal radial vessels (DRVs) are indicated by arrows. In the top left panel, the lens is outlined with a dotted line and the entire eye with a white line. The DRV forms in most *gdf6a*^{-/-} mutants (shown at 34 hpf), can be observed degrading in 41 hpf embryos, and is often absent by 54 hpf. Ectopic connections (arrowheads) between DRV and hyaloid vasculature (hv) are visible in *gdf6a*^{-/-} embryos. Right panels are enlarged views of boxed regions. (B) Laterally rotated images showing ectopic connection to hyaloid vasculature in a *gdf6a*^{-/-} embryo, but not in a wild type

embryo at 41 hpf. (C-D) Quantification of area and number of DRV vessel(s) in 26 hpf control and *gdf6a*^{-/-} embryos. (E-F) Quantification showing percentage of control and *gdf6a*^{-/-} embryos with an ectopic connection between the hyaloid and superficial vascular systems (E) and a complete DRV (F) as assessed at 34 and 54 hpf. n=number of embryos. Scale bar is 50 μm.

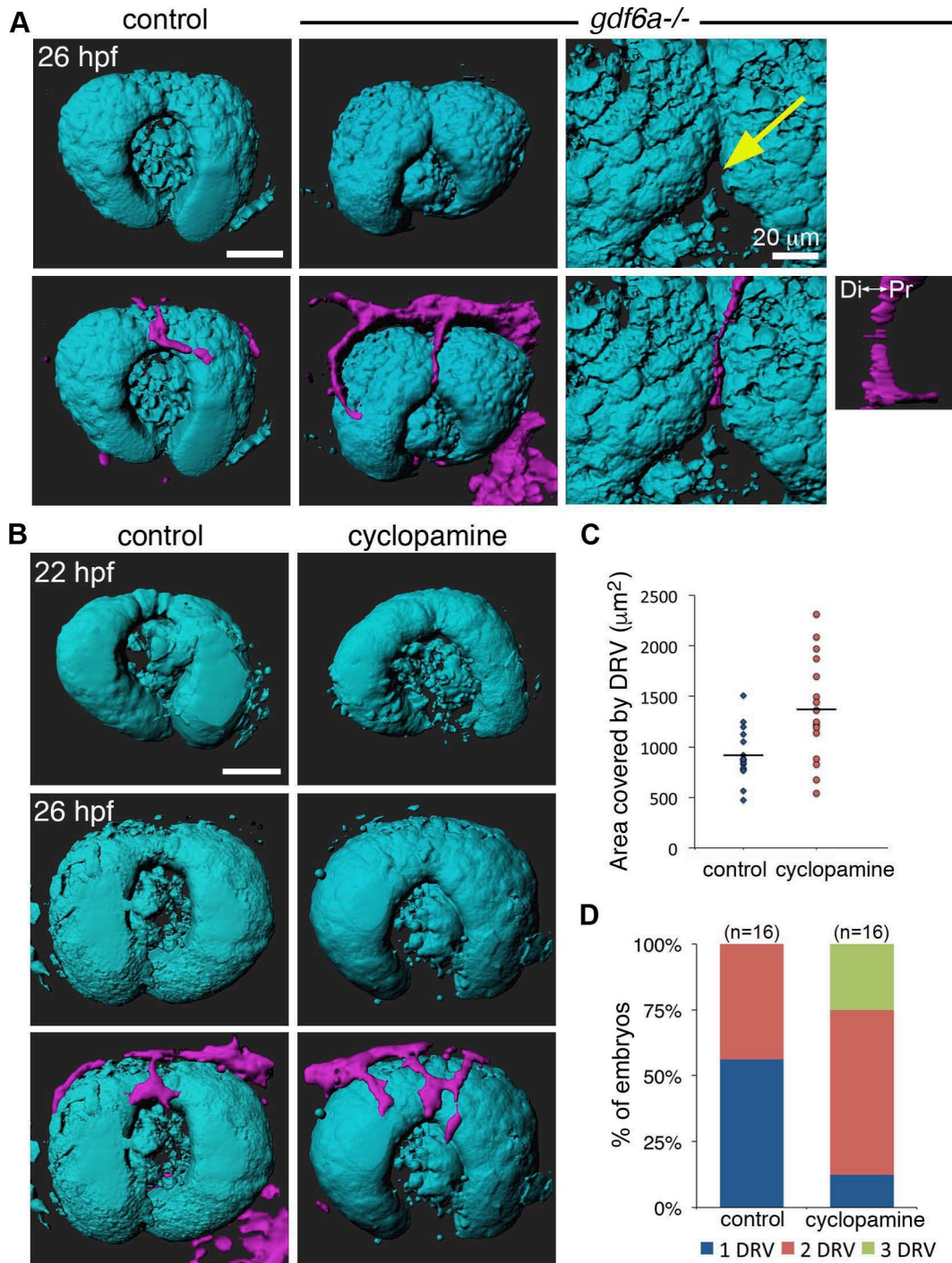


Fig. 5.15: Aberrant SOS closure leads to abnormal vasculature. (A) Surface projections of 26 hpf *Tg(rx3:GFP;kdr1:mCherry)* wild type and *gdf6a*^{-/-} embryos, shown without vessels (top row) and with vessels (bottom row). Last column shows expanded views of same *gdf6a*^{-/-} eye, highlighting the divot in the dorsal retina at the inferior edge of the superior ocular sulcus (yellow arrow). Small panel is 90° lateral rotation of vessel in

adjacent panel, showing the DRV turn and extend toward the hyaloid vasculature. (B) Surface projections of *Tg(rx3:GFP;kdr1:mCherry)* embryos before (22 hpf) and after (26 hpf) DRV formation, with and without cyclopamine treatment. (C-D) Quantification of the area and number of DRV vessel(s) in control and cyclopamine-treated 26 hpf embryos. n=number of embryos. Scale bars are 50 μm unless otherwise noted. Di-Pr, distal-proximal.

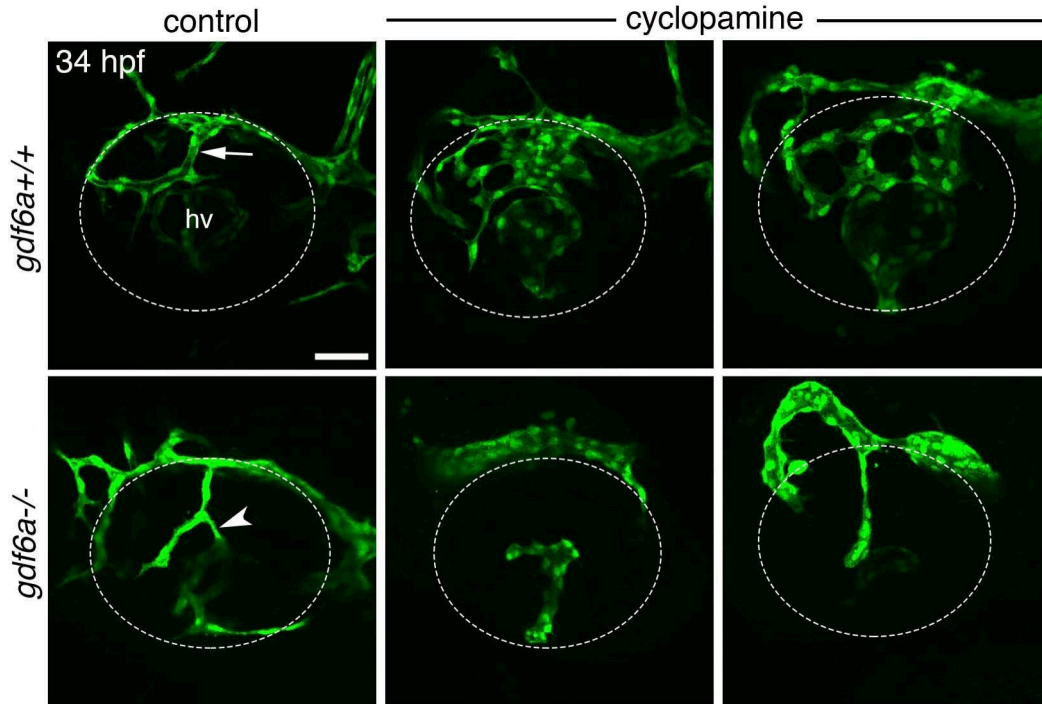


Fig. 5.16: Interaction between Hedgehog and Bone Morphogenetic Protein signaling in formation of the dorsal radial vessel. Maximum projection confocal images of 34 hpf eyes from *Tg(kdrl:eGFP)* wild type and *gdf6a*^{-/-} zebrafish embryos following treatment with control solution or 10 μ M cyclopamine from 10 hpf. Blood vessels fluoresce green and the eye is outlined by dotted lines. DRV is indicated by arrow. Ectopic connection between superficial and hyaloid vasculatures indicated by arrowhead. Top row, right two panels are two examples of vessel overgrowth phenotype in cyclopamine-treated wild type embryos. Bottom row, middle and right panels show the eyes of cyclopamine-treated *gdf6a*^{-/-} embryos that either failed to form a DRV (n=3/6 embryos) or grew a simple DRV that did not make an ectopic connection to the hyaloid vasculature (n=3/6 embryos), respectively. hv, hyaloid vasculature. Scale bar is 50 μ m.

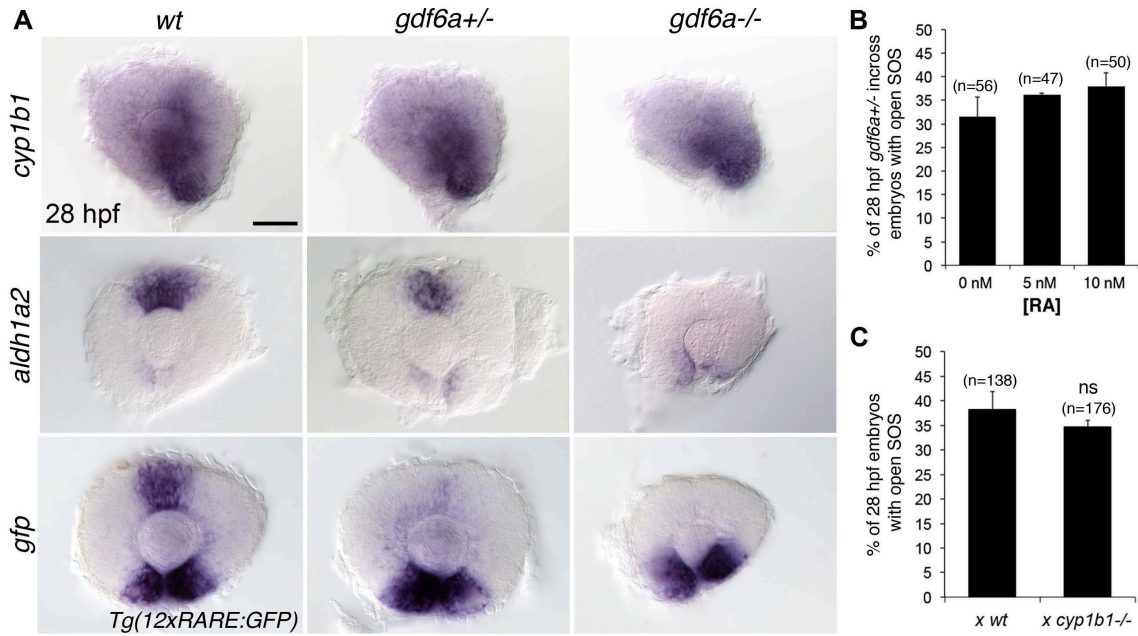


Fig. 5.17: Retinoic acid signaling and the superior ocular sulcus. (A) Lateral views of eyes from 28 hpf zebrafish embryos that are *gdf6a*^{+/+}, *gdf6a*^{+/-}, or *gdf6a*^{-/-} and have been processed for in situ hybridization. The top two rows show expression of the retinoic acid synthesis genes *cyp1b1* and *aldh1a2*. The bottom row shows expression of *gfp* in transgenic zebrafish carrying a reporter for RA signaling *Tg(12xRARE:GFP)* and are also *gdf6a*^{+/+}, *gdf6a*^{+/-}, or *gdf6a*^{-/-}. Note reduced RA signaling in the superior retina of *gdf6a*^{+/-} and *gdf6a*^{-/-} embryos. (B) Graph showing no effect of retinoic acid treatment on SOS closure. Embryos from *gdf6a*^{+/-} incrosses were grown from 10 hpf in control media, 5 nM retinoic acid, or 10 nM retinoic acid, and assessed at 28 hpf for an open SOS. (C) Graph showing no effect of the *cyp1b1* mutation on SOS closure in *gdf6a* heterozygotes. *gdf6a*^{+/-};*cyp1b*^{+/-} fish were crossed to wild type or *cyp1b*^{-/-} fish and the percentage of embryos with an open SOS was assessed at 28 hpf. n=number of embryos, N=2 (B) or 3 experiments (C). Data are means ± SEM. ns, not significant.

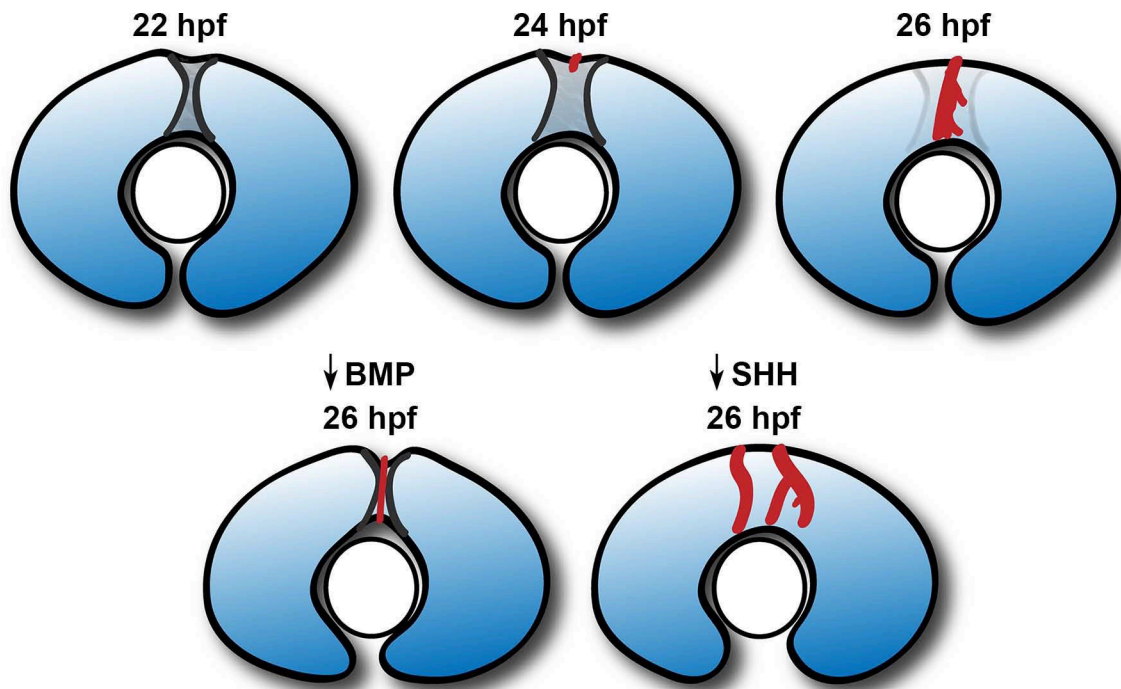


Fig. 5.18: Model of superior ocular sulcus morphogenesis and function. The superior ocular sulcus appears as a narrow groove in the dorsal retina soon after optic cup formation (22 hpf), and subsequently becomes wider (24 hpf). The dorsal radial vessel (DRV) grows through the wide sulcus as it travels across the dorsal retina towards the lens (24–26 hpf). If BMP signaling is reduced, the sulcus persists as a deep and narrow structure, through which the DRV still travels. However, in low BMP conditions, the DRV has a thin and unbranched morphology as it traverses the deeper fissure, and then enters the divot at the inferior edge of the sulcus and forms an ectopic connection with the hyaloid vessels behind the lens. If Hedgehog signaling is reduced, the SOS is absent at the time of DRV growth, resulting in the formation of more DRV vessels spread across the dorsal retina.

5.5. Tables

Table 5.1: Superior coloboma patient information.

Patient #	Age at diagnosis	Laterality and eye(s) affected	Ocular Phenotype	Other findings	Clinical Center
#1	23 years	Unilateral, OS	Iris coloboma, with anomalous retinal vasculature and localized sheathing of retinal arteries	Tuberous Sclerosis	Edmonton, Canada
#2	21 years	Bilateral	Asymmetric phenotypic severity: OD. Two small superior iris lesions, with pupillary distortion OS. Large superior iris coloboma, small superior lenticular (lens) coloboma with a small defect in the lens zonule	Congenital glaucoma, Parental consanguinity	Edmonton, Canada
#3	8 months	Unilateral, OS	Unilateral lenticular coloboma	Nil	Edmonton, Canada
#4	14 months	Unilateral, OD	Superior scleral defect with superior retinal colobomatous changes, Situs inversus (displaced vessels)	Nil	Edmonton, Canada
#5	23 years	Unilateral, OS	Unilateral superior retinal and optic nerve coloboma	Dandy-Walker syndrome	Edmonton, Canada
#6	5 years	Unilateral, OD	Iris and retino-choroidal coloboma	Tri-atrial heart	National Eye Institute, USA
#7	2 years	Unilateral, OD	Retino-choroidal coloboma and mild microphthalmia	Ovarian torsion in infancy	Cambridge, UK
#8	2 months	Unilateral, OS	Iris coloboma with microphthalmia. Right eye is microphthalmic with complete corneal opacity.	Cardiac and renal anomalies. Epilepsy	University of Michigan, USA

Table 5.2: Genetic variants in superior coloboma patients. Exome sequencing of superior coloboma patients identified rare variants (<1% frequency in general population) that were subsequently prioritized on the basis of high MutationTaster score (>0.95).

Patient #	Gene Name	Type	Variant	MutationTaster
1	AARS	nonsynonymous SNV	NM_001605:c.G2791A:p.G931S	0.999887
	ACACB	nonsynonymous SNV	NM_001093:c.G764T:p.G255V	0.99999
	ACOT2	nonsynonymous SNV	NM_006821:c.G688A:p.G230S	0.990961
	ADARB1	nonsynonymous SNV	NM_001112:c.A1582G:p.I528V	0.999823
	AGAP1	nonsynonymous SNV	NM_014914:c.G2343C:p.M781I	0.996577
	AGRN	nonsynonymous SNV	NM_198576:c.G1528A:p.G510S	0.998726
	AKAP11	nonsynonymous SNV	NM_016248:c.C2009T:p.T670M	0.99034
	ALG12	nonsynonymous SNV	NM_024105:c.C727T:p.L243F	0.985411
	AMBP	nonsynonymous SNV	NM_001633:c.A575G:p.E192G	0.986294
	ANUBL1	nonsynonymous SNV	NM_001128324:c.C2173T:p.P725S	0.999547
	ARHGAP6	nonsynonymous SNV	NM_013423:c.A2245G:p.R749G	0.994809
	ARNTL2	nonsynonymous SNV	NM_001248003:c.A1267G:p.K423E	0.994232
	ARPC4-	nonsynonymous SNV	NM_001025930:c.C766T:p.R256W	0.999629
	ASB16,C17orf65	nonsynonymous SNV	NM_080863:c.A668G:p.E223G	0.99505
	ASPH	nonsynonymous SNV	NM_001164750:c.G968A:p.R323H	0.99961
	B3GNTL1	nonsynonymous SNV	NM_001009905:c.G103A:p.E35K	0.999444
	C18orf1	nonsynonymous SNV	NM_004338:c.G122A:p.R41H	0.999923
	C18orf8	nonsynonymous SNV	NM_013326:c.C596G:p.A199G	0.971201
	CACHD1	nonsynonymous SNV	NM_020925:c.A1168G:p.T390A	0.994878
	CAD	nonsynonymous SNV	NM_004341:c.T2297C:p.M766T	0.999554
	CALCA	nonsynonymous SNV	NM_001033952:c.T197C:p.L66P	0.971328
	CD101	nonsynonymous SNV	NM_004258:c.C605T:p.S202F	0.985083
	CEBPZ	nonsynonymous SNV	NM_005760:c.T1801A:p.F601I	0.997209
	CLRN1	nonsynonymous SNV	NM_001195794:c.A20T:p.K7I	0.990343
	COG1	nonsynonymous SNV	NM_018714:c.C1049T:p.T350M	0.9989
	CSAD	nonsynonymous SNV	NM_001244706:c.G445A:p.D149N	0.999049
	CSPG4	nonsynonymous SNV	NM_001897:c.G449A:p.G150D	0.998279
	DCLK2	nonsynonymous SNV	NM_001040260:c.A1531G:p.I511V	0.998626
	DCLK3	nonsynonymous SNV	NM_033403:c.C1801T:p.R601C	0.997839
	DEPDC5	nonsynonymous SNV	NM_001242897:c.C3875T:p.A1292V	0.996425
	DHODH	nonsynonymous SNV	NM_001361:c.G890A:p.R297H	0.999256
	DNAH2	nonsynonymous SNV	NM_020877:c.G8281A:p.V2761M	0.952925
	DSE	nonsynonymous SNV	NM_001080976:c.A844G:p.I282V	0.987638
	EIF4ENIF1	nonsynonymous SNV	NM_001164502:c.G2146A:p.G716R	0.992868
	ENPP7	nonsynonymous SNV	NM_178543:c.C273G:p.H91Q	0.986687
	EPG5	nonsynonymous SNV	NM_020964:c.C3248T:p.S1083L	0.987832
	EPRS	nonsynonymous SNV	NM_004446:c.A1256G:p.Y419C	0.99985
	FAT2	nonsynonymous SNV	NM_001447:c.T1331C:p.V444A	0.999986
	FBN3	nonsynonymous SNV	NM_032447:c.G3932C:p.G1311A	0.999294
	FBXO43	nonsynonymous SNV	NM_001029860:c.C1708T:p.R570W	0.987168
	FGL1	nonsynonymous SNV	NM_004467:c.A419T:p.Y140F	0.950515
	FHL1	nonsynonymous SNV	NM_001159699:c.A161G:p.N54S	0.998281
	FKTN	nonsynonymous SNV	NM_006731:c.A1336G:p.N446D	0.999963
FRK	nonsynonymous SNV	NM_002031:c.C1358T:p.P453L	0.993664	
FZD4	nonsynonymous SNV	NM_012193:c.G477A:p.M159I	0.998516	
GALNT7	nonsynonymous SNV	NM_017423:c.T973A:p.C325S	0.999886	
GDAP2	nonsynonymous SNV	NM_001135589:c.G368A:p.R123Q	0.999557	
GDF9	nonsynonymous SNV	NM_005260:c.C307T:p.P103S	0.98725	
GNGT1	nonsynonymous SNV	NM_021955:c.G148A:p.E50K	0.961805	

Patient #	Gene Name	Type	Variant	MutationTaster
	GPT	nonsynonymous SNV	NM_005309:c.G320A:p.R107K	0.982595
	GRK4	nonsynonymous SNV	NM_001004056:c.T1274C:p.L425P	0.999994
	HPSE2	nonsynonymous SNV	NM_001166245:c.G1282C:p.V428L	0.993032
	HSPG2	nonsynonymous SNV	NM_005529:c.G8848A:p.G2950R	0.99999
	HSPG2	nonsynonymous SNV	NM_005529:c.G8422T:p.V2808F	0.987389
	HTRA2	nonsynonymous SNV	NM_013247:c.G1195A:p.G399S	0.999242
	IGFBP5	nonsynonymous SNV	NM_000599:c.C412T:p.R138W	0.992419
	ITGB4	nonsynonymous SNV	NM_001005619:c.G1544A:p.R515H	0.999921
	JUB	nonsynonymous SNV	NM_032876:c.C131T:p.P44L	0.999441
	KATNB1	nonsynonymous SNV	NM_005886:c.C1319G:p.P440R	0.980114
	KIAA0564	nonsynonymous SNV	NM_015058:c.A5297C:p.D1766A	0.99998
	KIAA0564	nonsynonymous SNV	NM_001009814:c.G2693A:p.R898K	0.994132
	KIAA1109	nonsynonymous SNV	NM_015312:c.C11129T:p.P3710L	0.993222
	KIAA1524	nonsynonymous SNV	NM_020890:c.C877A:p.P293T	0.997155
	LGI2	nonsynonymous SNV	NM_018176:c.A1355G:p.Q452R	0.965635
	LIG1	nonsynonymous SNV	NM_000234:c.G1226A:p.R409H	0.968591
	LRRC30	nonsynonymous SNV	NM_001105581:c.G604A:p.A202T	0.973978
	MBD5	nonsynonymous SNV	NM_018328:c.G1382A:p.R461H	0.998132
	MCL1	nonsynonymous SNV	NM_021960:c.C680T:p.A227V	0.962198
	MET	nonsynonymous SNV	NM_000245:c.A901G:p.T301A	0.992353
	MICALCL	stopgain SNV	NM_032867:c.C1717T:p.R573X	1
	MINA	nonsynonymous SNV	NM_001042533:c.C419T:p.P140L	0.999992
	MOGS	nonsynonymous SNV	NM_006302:c.G2062A:p.A688T	0.999989
	MPP5	nonsynonymous SNV	NM_022474:c.C422A:p.S141Y	0.988384
	MRPS9	nonsynonymous SNV	NM_182640:c.G790A:p.E264K	0.981068
	NKD1	nonsynonymous SNV	NM_033119:c.G1224C:p.E408D	0.99079
	NPC1	nonsynonymous SNV	NM_000271:c.C709T:p.P237S	0.973584
	NT5DC2	nonsynonymous SNV	NM_001134231:c.G1460A:p.R487H	0.999999
	OR4C3	stopgain SNV	NM_001004702:c.G522A:p.W174X	1
	PDZRN3	nonsynonymous SNV	NM_015009:c.C454T:p.H152Y	0.956837
	PKP1	nonsynonymous SNV	NM_001005337:c.C2050T:p.R684W	0.992554
	PLK3	nonsynonymous SNV	NM_004073:c.C1841T:p.T614I	0.999553
	POLE	nonsynonymous SNV	NM_006231:c.G6418A:p.E2140K	0.960716
	PRPF4B	nonsynonymous SNV	NM_003913:c.G857A:p.R286H	0.974959
	RAD51D	nonsynonymous SNV	NM_133629:c.A362G:p.E121G	0.996905
	RANGRF	stopgain SNV	NM_001177801:c.G181T:p.E61X	1
	RBPM5	nonsynonymous SNV	NM_194272:c.G385A:p.A129T	0.999946
	RCL1;RCL1	nonsynonymous SNV	NM_005772:c.G385A:p.V129I	0.999999
	RFX6	nonsynonymous SNV	NM_173560:c.C718T:p.L240F	0.954539
	ROPN1L	stopgain SNV	NM_031916:c.T135A:p.Y45X	1
	RPL3L	nonsynonymous SNV	NM_005061:c.C224T:p.A75V	0.99136
	RPS6	nonsynonymous SNV	NM_001010:c.G152A:p.R51Q	0.997829
	RRP7A	nonsynonymous SNV	NM_015703:c.G704A:p.R235Q	0.982204
	SCARB1	nonsynonymous SNV	NM_001082959:c.C965T:p.P322L	0.999946
	SEC24C	nonsynonymous SNV	NM_198597:c.T1160C:p.M387T	0.997577
	SEZ6L2	nonsynonymous SNV	NM_001114100:c.G1210A:p.D404N	0.970063
	SLC10A2	nonsynonymous SNV	NM_000452:c.C868T:p.P290S	0.952685
	SLIT3	nonsynonymous SNV	NM_003062:c.G4475A:p.S1492N	0.998936
	SPATA2	nonsynonymous SNV	NM_001135773:c.G878A:p.R293H	0.996562
	SRPX	nonsynonymous SNV	NM_001170750:c.G365A:p.R122Q	0.999915
	STXBP5	nonsynonymous SNV	NM_001127715:c.C1234G:p.L412V	0.999951
	SULT1C2	nonsynonymous SNV	NM_001056:c.G583A:p.E195K	1
	SYPL2	nonsynonymous SNV	NM_001040709:c.A638G:p.N213S	0.997836
	TAF1L	nonsynonymous SNV	NM_153809:c.C1909T:p.P637S	0.999501
	TCERG1	nonsynonymous SNV	NM_001040006:c.G76A:p.A26T	0.997675

Patient #	Gene Name	Type	Variant	MutationTaster
	TMED1	nonsynonymous SNV	NM_006858:c.C641T:p.T214M	0.991969
	TNFRSF10D	nonsynonymous SNV	NM_003840:c.C293G:p.P98R	0.965296
	TOE1	nonsynonymous SNV	NM_025077:c.G1022A:p.R341H	0.999761
	TPD52	nonsynonymous SNV	NM_001025252:c.G166A:p.E56K	0.989814
	TPP1	stopgain SNV	NM_000391:c.C622T:p.R208X	1
	TSC2	nonsynonymous SNV	NM_001077183:c.C5026T:p.R1676W	0.999986
	TSR1	nonsynonymous SNV	NM_018128:c.C2250A:p.H750Q	0.999775
	TUB	nonsynonymous SNV	NM_177972:c.G1126A:p.V376I	0.998975
	TULP1	nonsynonymous SNV	NM_003322:c.G797T:p.G266V	0.996546
	UGGT2	nonsynonymous SNV	NM_020121:c.A4142G:p.H1381R	0.971946
	VRK2	nonsynonymous SNV	NM_001130480:c.T104C:p.I35T	0.995967
	WDR78	nonsynonymous SNV	NM_024763:c.G1453A:p.G485S	0.974364
	WSCD1	nonsynonymous SNV	NM_015253:c.C902T:p.T301I	0.992983
	XAF1	stopgain SNV	NM_199139:c.G343T:p.E115X	1
	ZMIZ2	nonsynonymous SNV	NM_174929:c.G2404A:p.G802R	0.998878
	ZNF653	nonsynonymous SNV	NM_138783:c.G1054A:p.E352K	0.992989
	ZSWIM5	nonsynonymous SNV	NM_020883:c.G1222A:p.D408N	0.998206
2	ACTL6A	nonsynonymous SNV	NM_004301:c.T673A:p.S225T	0.994509
	ACTN1	nonsynonymous SNV	NM_001102:c.G532A:p.G178S	0.999938
	ACVRL1	nonsynonymous SNV	NM_001077401:c.C1445T:p.A482V	0.999706
	AGAP3	nonsynonymous SNV	NM_031946:c.C2419T:p.H807Y	0.998519
	AIM1L	nonsynonymous SNV	NM_001039775:c.G3252C:p.K1084N	0.99975
	ANKRD30A	stopgain SNV	NM_052997:c.G328T:p.E110X	1
	ARPP21	nonsynonymous SNV	NM_016300:c.A1055T:p.E352V	0.960229
	ASPM	nonsynonymous SNV	NM_018136:c.C4213T:p.R1405C	0.999919
	BICC1	nonsynonymous SNV	NM_001080512:c.C1462T:p.P488S	0.98711
	BLVRB	nonsynonymous SNV	NM_000713:c.G439A:p.V147M	0.998419
	BMPR1A	nonsynonymous SNV	NM_004329:c.G1412A:p.R471H	0.970915
	C16orf62	nonsynonymous SNV	NM_020314:c.C2980T:p.R994C	0.999285
	C1QTNF1	nonsynonymous SNV	NM_198594:c.A236T:p.Y79F	0.968666
	C6orf165	nonsynonymous SNV	NM_001031743:c.C1220A:p.A407E	0.979929
	CAV2	nonsynonymous SNV	NM_001206748:c.C161T:p.T54I	0.995632
	CBFA2T2	nonsynonymous SNV	NM_001032999:c.G564C:p.K188N	0.999108
	CCDC124	nonsynonymous SNV	NM_001136203:c.G406C:p.V136L	0.963876
	CD36	stopgain SNV	NM_001127444:c.T1079G:p.L360X	1
	CHFR	nonsynonymous SNV	NM_001161347:c.A613G:p.K205E	0.997104
	CHST13	nonsynonymous SNV	NM_152889:c.C150G:p.S50R	0.978808
	CLCNKA	nonsynonymous SNV	NM_001042704:c.C935T:p.T312I	0.951936
	CLSTN1	nonsynonymous SNV	NM_014944:c.G532A:p.V178M	0.962173
	CMTM6	nonsynonymous SNV	NM_017801:c.A271G:p.T91A	0.999853
	COL10A1	nonsynonymous SNV	NM_000493:c.T23G:p.L8W	0.998959
	COL19A1	nonsynonymous SNV	NM_001858:c.C1276T:p.P426S	0.999822
	CRHR2	nonsynonymous SNV	NM_001202482:c.C1160A:p.A387D	0.999255
	CTSC	nonsynonymous SNV	NM_001814:c.A1088C:p.E363A	0.999985
	CYP1A1	nonsynonymous SNV	NM_000499:c.C712T:p.P238S	0.999742
	CYP1A1	nonsynonymous SNV	NM_000499:c.T857C:p.I286T	0.99848
	CYP1B1	nonsynonymous SNV	NM_000104:c.G1103A:p.R368H	0.970216
	DHRS9	nonsynonymous SNV	NM_001142271:c.G856C:p.D286H	0.99818
	DHX38	nonsynonymous SNV	NM_014003:c.A2947G:p.I983V	0.999192
	DIP2B	nonsynonymous SNV	NM_173602:c.C4453T:p.R1485W	0.999991
	DLK1	nonsynonymous SNV	NM_003836:c.G352A:p.G118R	0.998927
	DLK1	nonsynonymous SNV	NM_003836:c.G366C:p.K122N	0.961886
	DNMT3L	nonsynonymous SNV	NM_013369:c.G209A:p.G70E	0.999785
	DOCK5	nonsynonymous SNV	NM_024940:c.G2698A:p.E900K	0.993012
	DPY19L4	nonsynonymous SNV	NM_181787:c.G578T:p.G193V	0.99991

Patient #	Gene Name	Type	Variant	MutationTaster
	DPY19L4	nonsynonymous SNV	NM_181787:c.G560T:p.S187I	0.999307
	DSCAM	nonsynonymous SNV	NM_001389:c.G701A:p.R234H	0.979737
	EAF1	nonsynonymous SNV	NM_033083:c.G619A:p.D207N	0.976956
	ECE2	nonsynonymous SNV	NM_001037324:c.G1879A:p.G627S	0.999355
	EIF1AD	nonsynonymous SNV	NM_001242481:c.G173T:p.R58L	0.999981
	EPB41	nonsynonymous SNV	NM_001166005:c.G640A:p.V214I	0.999983
	ETV4	nonsynonymous SNV	NM_001079675:c.C1309T:p.R437C	0.999087
	EXOC3L1	nonsynonymous SNV	NM_178516:c.C724G:p.R242G	0.996994
	FIBIN	nonsynonymous SNV	NM_203371:c.G287A:p.R96H	0.999931
	FMN2	nonsynonymous SNV	NM_020066:c.C4123A:p.L1375I	0.998708
	FMNL1	nonsynonymous SNV	NM_005892:c.C655T:p.R219C	0.998201
	FURIN	nonsynonymous SNV	NM_002569:c.G1343A:p.R448Q	0.997805
	GPAA1	nonsynonymous SNV	NM_003801:c.A863G:p.Q288R	0.992603
	GRHPR	nonsynonymous SNV	NM_012203:c.G488A:p.R163H	1
	GRIA1	nonsynonymous SNV	NM_000827:c.T707C:p.M236T	0.989621
	HHIP;HHIP	nonsynonymous SNV	NM_022475:c.C1762T:p.P588S	0.999972
	IFT57	nonsynonymous SNV	NM_018010:c.A1232G:p.N411S	0.991636
	IGHMBP2	nonsynonymous SNV	NM_002180:c.C46G:p.L16V	0.984176
	INCA1	stopgain SNV	NM_001167985:c.C64T:p.R22X	1
	ISOC2	nonsynonymous SNV	NM_001136202:c.G193A:p.A65T	0.95843
	ITGB6	nonsynonymous SNV	NM_000888:c.G871A:p.G291R	0.998767
	JAGN1	nonsynonymous SNV	NM_032492:c.A244G:p.I82V	0.971736
	KCND1	nonsynonymous SNV	NM_004979:c.C1447T:p.H483Y	0.997645
	KDM4B	nonsynonymous SNV	NM_015015:c.G2968A:p.G990S	0.987827
	KIAA0196	nonsynonymous SNV	NM_014846:c.G50A:p.R17K	0.999465
	KIAA1199	nonsynonymous SNV	NM_018689:c.C3625T:p.H1209Y	0.96181
	KIAA1524	nonsynonymous SNV	NM_020890:c.G823C:p.E275Q	0.95502
	KIAA1609	nonsynonymous SNV	NM_020947:c.C1061T:p.T354M	0.999949
	KIF18A	nonsynonymous SNV	NM_031217:c.C725T:p.T242I	0.987023
	KRR1	nonsynonymous SNV	NM_007043:c.A184G:p.T62A	0.99983
	LAMA4	nonsynonymous SNV	NM_001105206:c.G3239A:p.R1080Q	0.997947
	LAMA5	nonsynonymous SNV	NM_005560:c.G10411A:p.G3471S	0.999959
	LAMB4	nonsynonymous SNV	NM_007356:c.C575G:p.P192R	0.999177
	LAMC2	nonsynonymous SNV	NM_005562:c.C2080T:p.R694C	0.994374
	LAS1L	nonsynonymous SNV	NM_031206:c.C1082G:p.P361R	0.988139
	LRP2	nonsynonymous SNV	NM_004525:c.G13803A:p.M4601I	0.999811
	LTV1	nonsynonymous SNV	NM_032860:c.A1121C:p.K374T	0.999935
	MAT1A	nonsynonymous SNV	NM_000429:c.C505T:p.R169C	0.999528
	MCM5	nonsynonymous SNV	NM_006739:c.G375C:p.Q125H	0.999992
	MIOS	nonsynonymous SNV	NM_019005:c.C1928A:p.A643D	0.999022
	MKS1	stopgain SNV	NM_001165927:c.C478T:p.R160X	1
	MMP2	nonsynonymous SNV	NM_001127891:c.C1481T:p.S494L	0.994768
	MMP9	nonsynonymous SNV	NM_004994:c.A344G:p.K115R	0.985048
	N4BP3	nonsynonymous SNV	NM_015111:c.C994T:p.R332C	0.998841
	NCOR1	nonsynonymous SNV	NM_001190440:c.G6956A:p.R2319Q	0.966004
	NEUROD1	nonsynonymous SNV	NM_002500:c.C590A:p.P197H	0.999982
	NFS1	nonsynonymous SNV	NM_021100:c.A437G:p.K146R	0.999916
	NMBR	nonsynonymous SNV	NM_002511:c.C443A:p.P148H	0.999971
	NUPL1	nonsynonymous SNV	NM_001008564:c.T460C:p.S154P	0.994282
	OR4C3	stopgain SNV	NM_001004702:c.G522A:p.W174X	1
	OR5112	nonsynonymous SNV	NM_001004754:c.G3C:p.M1I	1
	OXA1L	nonsynonymous SNV	NM_005015:c.C1246G:p.P416A	0.999007
	PCDH15	stopgain SNV	NM_001142767:c.T1283G:p.L428X	1
	PCDH18	nonsynonymous SNV	NM_019035:c.G2790C:p.Q930H	0.999055
	PCK1	nonsynonymous SNV	NM_002591:c.G512A:p.R171Q	0.999995

Patient #	Gene Name	Type	Variant	MutationTaster
	PDCD2	nonsynonymous SNV	NM_002598:c.A677G:p.E226G	0.998262
	PDE1C	nonsynonymous SNV	NM_001191056:c.G1166A:p.R389H	0.998114
	PIGU	nonsynonymous SNV	NM_080476:c.G998A:p.G333E	0.999993
	PIK3R5	nonsynonymous SNV	NM_001142633:c.G511A:p.V171M	0.991058
	PITHD1	nonsynonymous SNV	NM_020362:c.C181T:p.R61W	0.999998
	PLCG2	nonsynonymous SNV	NM_002661:c.C413T:p.T138M	0.993735
	PLCH1	nonsynonymous SNV	NM_014996:c.T3485C:p.I1162T	0.998529
	PLXNA3;PLXNA	nonsynonymous SNV	NM_017514:c.A3440G:p.K1147R	0.996782
	POLH	nonsynonymous SNV	NM_006502:c.G626T:p.G209V	0.999889
	PPYR1	nonsynonymous SNV	NM_005972:c.G767A:p.R256Q	0.99992
	PTPN14	nonsynonymous SNV	NM_005401:c.C2225T:p.A742V	0.998494
	RAB25	nonsynonymous SNV	NM_020387:c.A59G:p.E20G	0.99999
	RANBP10	nonsynonymous SNV	NM_020850:c.G925A:p.E309K	0.998698
	RNF31	nonsynonymous SNV	NM_017999:c.A2846C:p.N949T	0.985124
	RPL8	nonsynonymous SNV	NM_000973:c.A292G:p.I98V	0.999923
	RPS6KB2;RPS6K	nonsynonymous SNV	NM_003952:c.C800T:p.P267L	0.997891
	SCTR	stopgain SNV	NM_002980:c.C181T:p.Q61X	1
	SCUBE2	nonsynonymous SNV	NM_001170690:c.G2095A:p.A699T	0.991195
	SGK2	nonsynonymous SNV	NM_016276:c.G800A:p.R267Q	0.999114
	SH3RF1	nonsynonymous SNV	NM_020870:c.G2311A:p.G771S	0.984581
	SIPA1L1	nonsynonymous SNV	NM_015556:c.C3056T:p.T1019M	0.99995
	SLC26A1	nonsynonymous SNV	NM_022042:c.G1511A:p.R504H	0.997285
	SLIT2	nonsynonymous SNV	NM_004787:c.G4333C:p.D1445H	0.993067
	SMYD2	nonsynonymous SNV	NM_020197:c.A1150G:p.M384V	0.963403
	SOD2	nonsynonymous SNV	NM_000636:c.G198C:p.E66D	0.999998
	SS18	nonsynonymous SNV	NM_001007559:c.G698C:p.G233A	0.958465
	SSH2	nonsynonymous SNV	NM_033389:c.G4192A:p.G1398S	0.998872
	STK16	nonsynonymous SNV	NM_001008910:c.C262T:p.R88W	0.998665
	SYNE1	nonsynonymous SNV	NM_033071:c.G12229C:p.D4077H	0.990532
	TLR10	nonsynonymous SNV	NM_001017388:c.T1255C:p.W419R	0.989287
	TMEM106C	nonsynonymous SNV	NM_001143841:c.T319C:p.F107L	0.999314
	TMEM181	nonsynonymous SNV	NM_020823:c.C1006T:p.R336W	0.999997
	TRH	nonsynonymous SNV	NM_007117:c.G248A:p.R83H	0.999936
	TRIM45	nonsynonymous SNV	NM_001145635:c.G1495A:p.G499R	0.999972
	TRPM5	nonsynonymous SNV	NM_014555:c.G2755A:p.G919S	0.992174
	TSPAN31	nonsynonymous SNV	NM_005981:c.C276G:p.I92M	0.955662
	TWF1	nonsynonymous SNV	NM_002822:c.C1028T:p.A343V	0.998383
	UBE2D4	nonsynonymous SNV	NM_015983:c.G79A:p.G27S	0.99998
	ULK2	nonsynonymous SNV	NM_001142610:c.C724T:p.P242S	0.995306
	USP25	nonsynonymous SNV	NM_013396:c.C1622G:p.T541R	0.999824
	VASH2	nonsynonymous SNV	NM_024749:c.G851A:p.R284Q	0.960635
	WDR16	nonsynonymous SNV	NM_001080556:c.C254T:p.A85V	0.999446
	XDH	stopgain SNV	NM_000379:c.A2164T:p.K722X	1
	ZNF560	stopgain SNV	NM_152476:c.C2080T:p.R694X	1
	ZSWIM5	nonsynonymous SNV	NM_020883:c.G2326A:p.D776N	0.999161
3	ABCB6	nonsynonymous SNV	NM_005689:c.G2168A:p.R723Q	0.999992
	ABCC10	nonsynonymous SNV	NM_033450:c.G1567A:p.V523M	0.999489
	ADAMTS10	nonsynonymous SNV	NM_030957:c.G217A:p.E73K	0.996312
	AFAP1	nonsynonymous SNV	NM_198595:c.C1991T:p.S664L	0.999862
	AK2	nonsynonymous SNV	NM_001199199:c.G436A:p.E146K	0.999998
	ANP32E	nonsynonymous SNV	NM_001136478:c.A564T:p.E188D	0.98776
	ATG2A	nonsynonymous SNV	NM_015104:c.G3635A:p.R1212H	0.998787
	BBS5;BBS5	nonsynonymous SNV	NM_152384:c.G620A:p.R207H	0.998605
	BCLAF1	stopgain SNV	NM_001077440:c.C886T:p.R296X	1
	BLOC1S3	nonsynonymous SNV	NM_212550:c.C322G:p.L108V	0.985367

Patient #	Gene Name	Type	Variant	MutationTaster
	BRAT1	nonsynonymous SNV	NM_152743:c.C1828T:p.R610W	0.999889
	C19orf28	nonsynonymous SNV	NM_001042680:c.G1415A:p.R472Q	0.987627
	C6orf226	nonsynonymous SNV	NM_001008739:c.G3A:p.M1I	1
	CDK7	nonsynonymous SNV	NM_001799:c.C854T:p.T285M	0.998645
	CDNF	nonsynonymous SNV	NM_001029954:c.G461C:p.W154S	0.999964
	CFHR2	nonsynonymous SNV	NM_005666:c.G215A:p.C72Y	0.970249
	CIT	nonsynonymous SNV	NM_001206999:c.C923G:p.S308C	0.986636
	CLDND1	nonsynonymous SNV	NM_001040181:c.A215G:p.N72S	0.999725
	CLSTN3	nonsynonymous SNV	NM_014718:c.G502T:p.A168S	0.999992
	COL8A2	nonsynonymous SNV	NM_005202:c.G911A:p.R304Q	0.999031
	CPEB1	nonsynonymous SNV	NM_001079535:c.G475A:p.D159N	0.999896
	CSMD2	nonsynonymous SNV	NM_052896:c.G6355A:p.E2119K	0.993159
	CTSH	nonsynonymous SNV	NM_004390:c.A479G:p.K160R	0.987819
	DNAH2	nonsynonymous SNV	NM_020877:c.C12974G:p.P4325R	0.954532
	EDEM2	nonsynonymous SNV	NM_001145025:c.T584C:p.I195T	0.999998
	ELMO1	nonsynonymous SNV	NM_001206480:c.C1042T:p.R348C	0.999927
	EPG5	nonsynonymous SNV	NM_020964:c.A3303C:p.Q1101H	0.967409
	EPHX1	nonsynonymous SNV	NM_000120:c.C387A:p.H129Q	0.999997
	EXOC3L1	nonsynonymous SNV	NM_178516:c.T223A:p.Y75N	0.999236
	FGA	stopgain SNV	NM_000508:c.C502T:p.R168X	1
	FKTN	nonsynonymous SNV	NM_006731:c.A1336G:p.N446D	0.999963
	FNDC3A	nonsynonymous SNV	NM_014923:c.A1697G:p.E566G	0.999846
	FPGS	nonsynonymous SNV	NM_001018078:c.C1246T:p.R416C	0.999863
	GAMT	nonsynonymous SNV	NM_000156:c.T79C:p.Y27H	0.999933
	GFM2	nonsynonymous SNV	NM_032380:c.C446T:p.T149I	0.999956
	GIPC3	nonsynonymous SNV	NM_133261:c.G389C:p.G130A	0.99996
	GOT1	nonsynonymous SNV	NM_002079:c.G257A:p.R86H	0.996362
	GPX4	nonsynonymous SNV	NM_001039847:c.G358A:p.A120T	0.994371
	GRHL3	nonsynonymous SNV	NM_001195010:c.C1223T:p.T408M	0.99959
	HCN3	nonsynonymous SNV	NM_020897:c.C1441T:p.R481W	0.978825
	HIVEP2	nonsynonymous SNV	NM_006734:c.A3725G:p.Y1242C	0.988015
	HYI	nonsynonymous SNV	NM_001190880:c.A287G:p.Y96C	0.997171
	IFT80;IFT80	nonsynonymous SNV	NM_001190242:c.C665T:p.S222F	0.999776
	IGFBP7	nonsynonymous SNV	NM_001553:c.G403A:p.A135T	0.989269
	IL31RA	stopgain SNV	NM_001242636:c.G466T:p.E156X	1
	ILK	nonsynonymous SNV	NM_001014795:c.G165A:p.M55I	0.999949
	ITGAV	nonsynonymous SNV	NM_001145000:c.A2735G:p.Y912C	0.999913
	ITSN2	nonsynonymous SNV	NM_019595:c.C3928T:p.R1310W	0.999215
	KIAA0907	nonsynonymous SNV	NM_014949:c.A1784G:p.Y595C	0.996422
	KLHDC4	nonsynonymous SNV	NM_001184854:c.G1345C:p.G449R	0.951719
	KRT8	nonsynonymous SNV	NM_002273:c.G1022A:p.R341H	0.999793
	KRT8	nonsynonymous SNV	NM_002273:c.G1319C:p.G440A	0.950244
	LAMB2	nonsynonymous SNV	NM_002292:c.G4307A:p.R1436H	0.979082
	LYST	nonsynonymous SNV	NM_000081:c.A10630G:p.N3544D	0.967171
	MAN1B1	nonsynonymous SNV	NM_016219:c.A1286G:p.H429R	0.998394
	MBOAT1	nonsynonymous SNV	NM_001080480:c.T1234C:p.F412L	0.999171
	MTHFD1	nonsynonymous SNV	NM_005956:c.G878A:p.R293H	0.99966
	MXRA8	nonsynonymous SNV	NM_032348:c.G1186A:p.D396N	0.989249
	MYH11	nonsynonymous SNV	NM_002474:c.C739T:p.R247C	0.999983
	NID2	nonsynonymous SNV	NM_007361:c.C2249T:p.P750L	0.961615
	NQO2;NQO2	nonsynonymous SNV	NM_000904:c.G173A:p.G58D	0.99356
	NRG2	nonsynonymous SNV	NM_001184935:c.G1508A:p.R503H	0.985524
	NUDC	nonsynonymous SNV	NM_006600:c.G661A:p.E221K	0.999543
	NUPL1	nonsynonymous SNV	NM_001008564:c.T460C:p.S154P	0.994282
	NXF1;NXF1	nonsynonymous SNV	NM_001081491:c.C640G:p.L214V	0.996002

Patient #	Gene Name	Type	Variant	MutationTaster
	P2RY4	stopgain SNV	NM_002565:c.G1043A:p.W348X	0.999358
	PAM	nonsynonymous SNV	NM_138821:c.G1861C:p.G621R	0.999999
	PLEKHG2	nonsynonymous SNV	NM_022835:c.C1358G:p.P453R	1
	POLE	nonsynonymous SNV	NM_006231:c.G6418A:p.E2140K	0.960716
	POLG	nonsynonymous SNV	NM_001126131:c.G803C:p.G268A	0.999747
	POLR3E	nonsynonymous SNV	NM_018119:c.C824T:p.T275M	0.999927
	POU4F2	nonsynonymous SNV	NM_004575:c.C417A:p.D139E	0.962715
	PRPF19	nonsynonymous SNV	NM_014502:c.A478G:p.M160V	0.996125
	RC3H1	nonsynonymous SNV	NM_172071:c.G1154A:p.R385H	0.992264
	RPS3	nonsynonymous SNV	NM_001005:c.C716A:p.P239Q	0.999438
	RTTN	nonsynonymous SNV	NM_173630:c.C5060G:p.S1687C	0.986797
	SAFB2	nonsynonymous SNV	NM_014649:c.A1369G:p.T457A	0.999961
	SHROOM3	nonsynonymous SNV	NM_020859:c.A2834T:p.D945V	0.976907
	SLC16A3	nonsynonymous SNV	NM_001042422:c.C390A:p.F130L	0.99718
	SMARCA1	nonsynonymous SNV	NM_139035:c.G2222C:p.R741P	0.999736
	SMG6	nonsynonymous SNV	NM_001170957:c.T3075G:p.D1025E	0.97331
	SMYD2	nonsynonymous SNV	NM_020197:c.A1150G:p.M384V	0.963403
	SNX30	nonsynonymous SNV	NM_001012994:c.A425C:p.K142T	0.999952
	SOX8	nonsynonymous SNV	NM_014587:c.C585A:p.H195Q	0.993473
	STEAP4	nonsynonymous SNV	NM_024636:c.G953T:p.R318L	0.995803
	STRN	nonsynonymous SNV	NM_003162:c.C1138T:p.P380S	0.999004
	SV2B	nonsynonymous SNV	NM_014848:c.T421G:p.C141G	0.999895
	TAAR1	nonsynonymous SNV	NM_138327:c.G773A:p.G258E	0.994191
	TAF1L	nonsynonymous SNV	NM_153809:c.C3046T:p.R1016C	0.999975
	TBX2	nonsynonymous SNV	NM_005994:c.C986A:p.P329H	0.973971
	THUMPD1	nonsynonymous SNV	NM_017736:c.C79A:p.R27S	0.997938
	TMEM85	nonsynonymous SNV	NM_016454:c.T413C:p.I138T	0.999363
	TRMT11	nonsynonymous SNV	NM_001031712:c.A916G:p.I306V	0.99581
	TSHZ3	nonsynonymous SNV	NM_020856:c.C1054T:p.L352F	0.99999
	TST	nonsynonymous SNV	NM_003312:c.C853G:p.P285A	0.999865
	TTC14	nonsynonymous SNV	NM_001042601:c.C515T:p.S172F	0.997118
	TTC30B	nonsynonymous SNV	NM_152517:c.G856A:p.D286N	0.999989
	UGGT2	nonsynonymous SNV	NM_020121:c.A3802T:p.N1268Y	0.999321
	ULK2	nonsynonymous SNV	NM_001142610:c.C724T:p.P242S	0.995306
	UNC79	nonsynonymous SNV	NM_020818:c.C298G:p.L100V	0.97198
	USP48;USP48	nonsynonymous SNV	NM_032236:c.A2386G:p.I796V	0.98697
	USP8	nonsynonymous SNV	NM_001128610:c.T802A:p.L268I	0.997561
	VPS13D	nonsynonymous SNV	NM_015378:c.G4831A:p.E1611K	1
	WDR35	nonsynonymous SNV	NM_020779:c.C3019T:p.R1007C	0.999912
	WSCD1	nonsynonymous SNV	NM_015253:c.C902T:p.T301I	0.992983
	ZCCHC4	nonsynonymous SNV	NM_024936:c.G214C:p.D72H	0.997358
4	AADAC	nonsynonymous SNV	NM_001086:c.G1070A:p.R357H	0.968956
	ABCA4	nonsynonymous SNV	NM_000350:c.C6721G:p.L2241V	0.990942
	ACACB	nonsynonymous SNV	NM_001093:c.A4442T:p.D1481V	0.999998
	ADAMTS15	nonsynonymous SNV	NM_139055:c.T1324C:p.Y442H	0.999918
	ADAT1	nonsynonymous SNV	NM_012091:c.C1129T:p.R377C	0.997996
	ADCY6	nonsynonymous SNV	NM_015270:c.G413A:p.R138H	0.996328
	ADRA1A	nonsynonymous SNV	NM_000680:c.T599G:p.I200S	0.957852
	AGL	nonsynonymous SNV	NM_000645:c.G1430A:p.R477H	0.99234
	ALG6	nonsynonymous SNV	NM_013339:c.T391C:p.Y131H	0.999939
	ARHGAP21	nonsynonymous SNV	NM_020824:c.C2908G:p.L970V	0.999912
	ARPP21	nonsynonymous SNV	NM_016300:c.G2220C:p.Q740H	0.956551
	ATF5	nonsynonymous SNV	NM_001193646:c.C421T:p.L141F	0.964918
	CC2D1B	nonsynonymous SNV	NM_032449:c.C2038T:p.H680Y	0.967756
	CDH3	nonsynonymous SNV	NM_001793:c.G1285A:p.V429I	0.997145

Patient #	Gene Name	Type	Variant	MutationTaster
	CDH4	nonsynonymous SNV	NM_001794:c.G1607A:p.R536Q	0.998951
	CDKN1B	nonsynonymous SNV	NM_004064:c.G187T:p.D63Y	0.996651
	CHRNA10	nonsynonymous SNV	NM_020402:c.G598A:p.V200M	0.990703
	CLCNKB	nonsynonymous SNV	NM_001165945:c.G1370A:p.C457Y	0.996654
	CLN5	stopgain SNV	NM_006493:c.C694T:p.Q232X	1
	COL9A3;COL9A	nonsynonymous SNV	NM_001853:c.C1547T:p.P516L	0.999969
	CPS1	nonsynonymous SNV	NM_001122634:c.G2773A:p.G925S	0.995938
	CPVL	nonsynonymous SNV	NM_019029:c.C1043G:p.T348S	0.981603
	CSMD2	nonsynonymous SNV	NM_052896:c.A7997G:p.N2666S	0.999988
	DDR2	nonsynonymous SNV	NM_006182:c.C1474T:p.P492S	0.96065
	DIP2B	nonsynonymous SNV	NM_173602:c.C1450T:p.R484W	0.99997
	DNAH9	nonsynonymous SNV	NM_001372:c.T3926G:p.I1309S	0.980987
	EFCAB4A	nonsynonymous SNV	NM_173584:c.A200T:p.Q67L	0.999781
	EME1	nonsynonymous SNV	NM_001166131:c.G1640A:p.R547H	0.998638
	EPX	nonsynonymous SNV	NM_000502:c.G437A:p.R146H	0.997289
	FERMT1	nonsynonymous SNV	NM_017671:c.T722C:p.V241A	0.97774
	FMN2	nonsynonymous SNV	NM_020066:c.G3542A:p.G1181E	0.999142
	GCAT	nonsynonymous SNV	NM_001171690:c.C1237T:p.R413W	1
	GFM2	nonsynonymous SNV	NM_170691:c.C2089G:p.R697G	0.999995
	GPI	stopgain SNV	NM_000175:c.G937T:p.E313X	1
	GPR17	nonsynonymous SNV	NM_001161417:c.G223A:p.V75M	0.988762
	GRIK4	nonsynonymous SNV	NM_014619:c.C500G:p.A167G	0.999321
	HEATR5B	nonsynonymous SNV	NM_019024:c.T245C:p.I82T	0.962443
	HOXC11	nonsynonymous SNV	NM_014212:c.C726G:p.F242L	0.972933
	HPS1	nonsynonymous SNV	NM_000195:c.C1718G:p.P573R	0.998361
	IGFBP5	nonsynonymous SNV	NM_000599:c.C412T:p.R138W	0.992419
	INPP4B	nonsynonymous SNV	NM_001101669:c.T1781C:p.V594A	0.999598
	IQGAP2	nonsynonymous SNV	NM_006633:c.G2905A:p.V969I	0.975348
	IQGAP2;IQGAP2	nonsynonymous SNV	NM_006633:c.C2681T:p.T894I	0.999897
	KAZALD1	nonsynonymous SNV	NM_030929:c.G707A:p.G236D	0.997013
	LMCD1	nonsynonymous SNV	NM_014583:c.C913T:p.R305W	0.965828
	LRBA	nonsynonymous SNV	NM_001199282:c.A4261G:p.S1421G	0.992564
	LRRK1	nonsynonymous SNV	NM_024652:c.C1246A:p.L416M	0.962459
	LUC7L2	nonsynonymous SNV	NM_016019:c.A861C:p.E287D	0.990717
	MANBA	nonsynonymous SNV	NM_005908:c.G2482A:p.V828I	0.977631
	MAPRE1	nonsynonymous SNV	NM_012325:c.G389C:p.R130T	0.999991
	MICAL1	nonsynonymous SNV	NM_001159291:c.G293A:p.R98Q	0.994186
	MINA	nonsynonymous SNV	NM_001042533:c.C419T:p.P140L	0.999992
	MON2	nonsynonymous SNV	NM_015026:c.A2518G:p.T840A	0.999978
	MPP3	nonsynonymous SNV	NM_001932:c.C617A:p.S206Y	0.999494
	MYH1	nonsynonymous SNV	NM_005963:c.T1303C:p.Y435H	0.995119
	MYH10	nonsynonymous SNV	NM_005964:c.C2894T:p.A965V	0.992154
	NALCN	nonsynonymous SNV	NM_052867:c.C2305T:p.H769Y	0.996386
	NARS2	nonsynonymous SNV	NM_001243251:c.A218G:p.K73R	0.97168
	NEDD9	nonsynonymous SNV	NM_006403:c.G784A:p.D262N	0.999807
	NUDT16	nonsynonymous SNV	NM_001171905:c.C67G:p.L23V	0.998334
	PARK2	nonsynonymous SNV	NM_013988:c.G733A:p.D245N	0.998566
	PMPCA	nonsynonymous SNV	NM_015160:c.T1307C:p.M436T	0.999929
	PRKCE	nonsynonymous SNV	NM_005400:c.T896C:p.I299T	0.999162
	PSMD1	nonsynonymous SNV	NM_001191037:c.A1051G:p.M351V	0.998558
	PTPN21	nonsynonymous SNV	NM_007039:c.A2983G:p.M995V	0.991544
	PTPN22	nonsynonymous SNV	NM_012411:c.A2077G:p.R693G	0.972937
	PTPRH	nonsynonymous SNV	NM_001161440:c.G1958A:p.G653D	0.999508
	PUS7	nonsynonymous SNV	NM_019042:c.C367T:p.H123Y	0.999092
	RAB40B	nonsynonymous SNV	NM_006822:c.C788G:p.P263R	0.998892

Patient #	Gene Name	Type	Variant	MutationTaster
	RFWD3	nonsynonymous SNV	NM_018124:c.C1082T:p.S361F	0.984736
	RICTOR	nonsynonymous SNV	NM_152756:c.T1989G:p.I663M	0.963034
	RPS6KB2;RPS6K	nonsynonymous SNV	NM_003952:c.C800T:p.P267L	0.997891
	SBF1	nonsynonymous SNV	NM_002972:c.G1918C:p.E640Q	0.998315
	SCRIB	nonsynonymous SNV	NM_015356:c.G571A:p.D191N	0.956013
	SDK1	nonsynonymous SNV	NM_152744:c.C6590G:p.P2197R	0.99838
	SERPIND1	nonsynonymous SNV	NM_000185:c.G623A:p.R208H	0.999998
	SFXN4	nonsynonymous SNV	NM_213649:c.A795T:p.E265D	1
	SLC35E3	nonsynonymous SNV	NM_018656:c.G182C:p.C61S	0.9996
	SPAG5	nonsynonymous SNV	NM_006461:c.A1G:p.M1V	0.994842
	TAGLN	nonsynonymous SNV	NM_001001522:c.G437A:p.R146H	0.957856
	TBC1D5	nonsynonymous SNV	NM_001134380:c.A1124G:p.Y375C	0.999883
	TBX21	nonsynonymous SNV	NM_013351:c.C1421G:p.P474R	0.99529
	THAP6	nonsynonymous SNV	NM_144721:c.A419C:p.H140P	0.959775
	TRIM36	nonsynonymous SNV	NM_018700:c.A1283G:p.K428R	0.958679
	TRIM45	nonsynonymous SNV	NM_001145635:c.G1253A:p.G418E	0.999999
	TRIM69	stopgain SNV	NM_182985:c.C145T:p.R49X	1
	UTP20;UTP20	nonsynonymous SNV	NM_014503:c.G325A:p.D109N	0.991391
	VAX2	nonsynonymous SNV	NM_012476:c.C415A:p.L139M	0.999972
	ZC3H10	nonsynonymous SNV	NM_032786:c.C380T:p.P127L	0.99827
	ZSWIM1	stopgain SNV	NM_080603:c.G26A:p.W9X	0.999992
	ZSWIM5	nonsynonymous SNV	NM_020883:c.C793T:p.R265C	0.999991
	DNAH3	nonsynonymous SNV	NM_020877:c.G8281A:p.V2761M	0.99179448
	DSE	nonsynonymous SNV	NM_001080976:c.A844G:p.I282V	0.991794732
	EIF4ENIF2	nonsynonymous SNV	NM_001164502:c.G2146A:p.G716R	0.991794983
	ENPP8	nonsynonymous SNV	NM_178543:c.C273G:p.H91Q	0.991795234
	EPG6	nonsynonymous SNV	NM_020964:c.C3248T:p.S1083L	0.991795486
	EPRS	nonsynonymous SNV	NM_004446:c.A1256G:p.Y419C	0.991795737
	FAT3	nonsynonymous SNV	NM_001447:c.T1331C:p.V444A	0.991795988
	FBN4	nonsynonymous SNV	NM_032447:c.G3932C:p.G1311A	0.99179624
	FBXO44	nonsynonymous SNV	NM_001029860:c.C1708T:p.R570W	0.991796491
	FGL2	nonsynonymous SNV	NM_004467:c.A419T:p.Y140F	0.991796742
	FHL2	nonsynonymous SNV	NM_001159699:c.A161G:p.N54S	0.991796994
	FKTN	nonsynonymous SNV	NM_006731:c.A1336G:p.N446D	0.991797245
	FRK	nonsynonymous SNV	NM_002031:c.C1358T:p.P453L	0.991797496
	FZD5	nonsynonymous SNV	NM_012193:c.G477A:p.M159I	0.991797748
	GALNT8	nonsynonymous SNV	NM_017423:c.T973A:p.C325S	0.991797999
	GDAP3	nonsynonymous SNV	NM_001135589:c.G368A:p.R123Q	0.991798251
	GDF10	nonsynonymous SNV	NM_005260:c.C307T:p.P103S	0.991798502
	GNGT2	nonsynonymous SNV	NM_021955:c.G148A:p.E50K	0.991798753
	GPT	nonsynonymous SNV	NM_005309:c.G320A:p.R107K	0.991799005
	GRK5	nonsynonymous SNV	NM_001004056:c.T1274C:p.L425P	0.991799256
	HPSE3	nonsynonymous SNV	NM_001166245:c.G1282C:p.V428L	0.991799507
	HSPG2	nonsynonymous SNV	NM_005529:c.G8848A:p.G2950R	0.991799759
	HSPG2	nonsynonymous SNV	NM_005529:c.G8422T:p.V2808F	0.99180001
	HTRA3	nonsynonymous SNV	NM_013247:c.G1195A:p.G399S	0.991800261
	IGFBP6	nonsynonymous SNV	NM_000599:c.C412T:p.R138W	0.991800513
	ITGB5	nonsynonymous SNV	NM_001005619:c.G1544A:p.R515H	0.991800764
	JUB	nonsynonymous SNV	NM_032876:c.C131T:p.P44L	0.991801016
	KATNB2	nonsynonymous SNV	NM_005886:c.C1319G:p.P440R	0.991801267
	KIAA0564	nonsynonymous SNV	NM_015058:c.A5297C:p.D1766A	0.991801518
	KIAA0564	nonsynonymous SNV	NM_001009814:c.G2693A:p.R898K	0.99180177
	KIAA1109	nonsynonymous SNV	NM_015312:c.C11129T:p.P3710L	0.991802021
	KIAA1524	nonsynonymous SNV	NM_020890:c.C877A:p.P293T	0.991802272
	LGI3	nonsynonymous SNV	NM_018176:c.A1355G:p.Q452R	0.991802524

Patient #	Gene Name	Type	Variant	MutationTaster
	LIG2	nonsynonymous SNV	NM_000234:c.G1226A:p.R409H	0.991802775
	LRRC31	nonsynonymous SNV	NM_001105581:c.G604A:p.A202T	0.991803026
	MBD6	nonsynonymous SNV	NM_018328:c.G1382A:p.R461H	0.991803278
	MCL2	nonsynonymous SNV	NM_021960:c.C680T:p.A227V	0.991803529
	MET	nonsynonymous SNV	NM_000245:c.A901G:p.T301A	0.99180378
	MICALCL	stopgain SNV	NM_032867:c.C1717T:p.R573X	0.991804032
	MINA	nonsynonymous SNV	NM_001042533:c.C419T:p.P140L	0.991804283
	MOGS	nonsynonymous SNV	NM_006302:c.G2062A:p.A688T	0.991804535
	MPP6	nonsynonymous SNV	NM_022474:c.C422A:p.S141Y	0.991804786
	MRPS10	nonsynonymous SNV	NM_182640:c.G790A:p.E264K	0.991805037
	NKD2	nonsynonymous SNV	NM_033119:c.G1224C:p.E408D	0.991805289
	NPC2	nonsynonymous SNV	NM_000271:c.C709T:p.P237S	0.99180554
	NT5DC3	nonsynonymous SNV	NM_001134231:c.G1460A:p.R487H	0.991805791
	OR4C4	stopgain SNV	NM_001004702:c.G522A:p.W174X	0.991806043
	PDZRN4	nonsynonymous SNV	NM_015009:c.C454T:p.H152Y	0.991806294
	PKP2	nonsynonymous SNV	NM_001005337:c.C2050T:p.R684W	0.991806545
	PLK4	nonsynonymous SNV	NM_004073:c.C1841T:p.T614I	0.991806797
	POLE	nonsynonymous SNV	NM_006231:c.G6418A:p.E2140K	0.991807048
	PRPF4B	nonsynonymous SNV	NM_003913:c.G857A:p.R286H	0.9918073
	RAD51D	nonsynonymous SNV	NM_133629:c.A362G:p.E121G	0.991807551
	RANGRF	stopgain SNV	NM_001177801:c.G181T:p.E61X	0.991807802
	RBPMS3	nonsynonymous SNV	NM_194272:c.G385A:p.A129T	0.991808054
	RCL1;RCL2	nonsynonymous SNV	NM_005772:c.G385A:p.V129I	0.991808305
	RFX7	nonsynonymous SNV	NM_173560:c.C718T:p.L240F	0.991808556
	ROPN1L	stopgain SNV	NM_031916:c.T135A:p.Y45X	0.991808808
	RPL3L	nonsynonymous SNV	NM_005061:c.C224T:p.A75V	0.991809059
	RPS7	nonsynonymous SNV	NM_001010:c.G152A:p.R51Q	0.99180931
	RRP7A	nonsynonymous SNV	NM_015703:c.G704A:p.R235Q	0.991809562
	SCARB2	nonsynonymous SNV	NM_001082959:c.C965T:p.P322L	0.991809813
	SEC24C	nonsynonymous SNV	NM_198597:c.T1160C:p.M387T	0.991810064
	SEZ6L3	nonsynonymous SNV	NM_001114100:c.G1210A:p.D404N	0.991810316
	SLC10A3	nonsynonymous SNV	NM_000452:c.C868T:p.P290S	0.991810567
	SLIT4	nonsynonymous SNV	NM_003062:c.G4475A:p.S1492N	0.991810819
	SPATA3	nonsynonymous SNV	NM_001135773:c.G878A:p.R293H	0.99181107
	SRPX	nonsynonymous SNV	NM_001170750:c.G365A:p.R122Q	0.991811321
	STXBP6	nonsynonymous SNV	NM_001127715:c.C1234G:p.L412V	0.991811573
	SULT1C3	nonsynonymous SNV	NM_001056:c.G583A:p.E195K	0.991811824
	SYPL3	nonsynonymous SNV	NM_001040709:c.A638G:p.N213S	0.991812075
	TAF1L	nonsynonymous SNV	NM_153809:c.C1909T:p.P637S	0.991812327
	TCERG2	nonsynonymous SNV	NM_001040006:c.G76A:p.A26T	0.991812578
	TMED2	nonsynonymous SNV	NM_006858:c.C641T:p.T214M	0.991812829
	TNFRSF10D	nonsynonymous SNV	NM_003840:c.C293G:p.P98R	0.991813081
	TOE2	nonsynonymous SNV	NM_025077:c.G1022A:p.R341H	0.991813332
	TPD53	nonsynonymous SNV	NM_001025252:c.G166A:p.E56K	0.991813584
	TPP2	stopgain SNV	NM_000391:c.C622T:p.R208X	0.991813835
	TSC3	nonsynonymous SNV	NM_001077183:c.C5026T:p.R1676W	0.991814086
	TSR2	nonsynonymous SNV	NM_018128:c.C2250A:p.H750Q	0.991814338
	TUB	nonsynonymous SNV	NM_177972:c.G1126A:p.V376I	0.991814589
	TULP2	nonsynonymous SNV	NM_003322:c.G797T:p.G266V	0.99181484
	UGGT3	nonsynonymous SNV	NM_020121:c.A4142G:p.H1381R	0.991815092
	VRK3	nonsynonymous SNV	NM_001130480:c.T104C:p.I35T	0.991815343
	WDR79	nonsynonymous SNV	NM_024763:c.G1453A:p.G485S	0.991815594
	WSCD2	nonsynonymous SNV	NM_015253:c.C902T:p.T301I	0.991815846
	XAF2	stopgain SNV	NM_199139:c.G343T:p.E115X	0.991816097
	ZMIZ3	nonsynonymous SNV	NM_174929:c.G2404A:p.G802R	0.991816348

Patient #	Gene Name	Type	Variant	MutationTaster
	ZNF654	nonsynonymous SNV	NM_138783:c.G1054A:p.E352K	0.9918166
	ZSWIM6	nonsynonymous SNV	NM_020883:c.G1222A:p.D408N	0.991816851
5	AADAC	nonsynonymous SNV	NM_001086:c.G1070A:p.R357H	0.992603765
	ABCA5	nonsynonymous SNV	NM_000350:c.C6721G:p.L2241V	0.992621922
	ACACB	nonsynonymous SNV	NM_001093:c.A4442T:p.D1481V	0.992640078
	ADAMTS16	nonsynonymous SNV	NM_139055:c.T1324C:p.Y442H	0.992658235
	ADAT2	nonsynonymous SNV	NM_012091:c.C1129T:p.R377C	0.992676392
	ADCY7	nonsynonymous SNV	NM_015270:c.G413A:p.R138H	0.992694549
	ADRA1A	nonsynonymous SNV	NM_000680:c.T599G:p.I200S	0.992712706
	AGL	nonsynonymous SNV	NM_000645:c.G1430A:p.R477H	0.992730863
	ALG7	nonsynonymous SNV	NM_013339:c.T391C:p.Y131H	0.99274902
	ARHGAP22	nonsynonymous SNV	NM_020824:c.C2908G:p.L970V	0.992767176
	ARPP22	nonsynonymous SNV	NM_016300:c.G2220C:p.Q740H	0.992785333
	ATF6	nonsynonymous SNV	NM_001193646:c.C421T:p.L141F	0.99280349
	CC2D1B	nonsynonymous SNV	NM_032449:c.C2038T:p.H680Y	0.992821647
	CDH5	nonsynonymous SNV	NM_001793:c.G1285A:p.V429I	0.992839804
	CDH6	nonsynonymous SNV	NM_001794:c.G1607A:p.R536Q	0.992857961
	CDKN1B	nonsynonymous SNV	NM_004064:c.G187T:p.D63Y	0.992876118
	CHRNA11	nonsynonymous SNV	NM_020402:c.G598A:p.V200M	0.992894274
	CLCNKB	nonsynonymous SNV	NM_001165945:c.G1370A:p.C457Y	0.992912431
	CLN6	stopgain SNV	NM_006493:c.C694T:p.Q232X	0.992930588
	COL9A3;COL9A	nonsynonymous SNV	NM_001853:c.C1547T:p.P516L	0.992948745
	CPS2	nonsynonymous SNV	NM_001122634:c.G2773A:p.G925S	0.992966902
	CPVL	nonsynonymous SNV	NM_019029:c.C1043G:p.T348S	0.992985059
	CSMD3	nonsynonymous SNV	NM_052896:c.A7997G:p.N2666S	0.993003215
	DDR3	nonsynonymous SNV	NM_006182:c.C1474T:p.P492S	0.993021372
	DIP2B	nonsynonymous SNV	NM_173602:c.C1450T:p.R484W	0.993039529
	DNAH10	nonsynonymous SNV	NM_001372:c.T3926G:p.I1309S	0.993057686
	EFCAB4A	nonsynonymous SNV	NM_173584:c.A200T:p.Q67L	0.993075843
	EME2	nonsynonymous SNV	NM_001166131:c.G1640A:p.R547H	0.993094
	EPX	nonsynonymous SNV	NM_000502:c.G437A:p.R146H	0.993112157
	FERMT2	nonsynonymous SNV	NM_017671:c.T722C:p.V241A	0.993130313
	FMN3	nonsynonymous SNV	NM_020066:c.G3542A:p.G1181E	0.99314847
	GCAT	nonsynonymous SNV	NM_001171690:c.C1237T:p.R413W	0.993166627
	GFM3	nonsynonymous SNV	NM_170691:c.C2089G:p.R697G	0.993184784
	GPI	stopgain SNV	NM_000175:c.G937T:p.E313X	0.993202941
	GPR18	nonsynonymous SNV	NM_001161417:c.G223A:p.V75M	0.993221098
	GRIK5	nonsynonymous SNV	NM_014619:c.C500G:p.A167G	0.993239255
	HEATR5B	nonsynonymous SNV	NM_019024:c.T245C:p.I82T	0.993257411
	HOXC12	nonsynonymous SNV	NM_014212:c.C726G:p.F242L	0.993275568
	HPS2	nonsynonymous SNV	NM_000195:c.C1718G:p.P573R	0.993293725
	IGFBP6	nonsynonymous SNV	NM_000599:c.C412T:p.R138W	0.993311882
	INPP4B	nonsynonymous SNV	NM_001101669:c.T1781C:p.V594A	0.993330039
	IQGAP3	nonsynonymous SNV	NM_006633:c.G2905A:p.V969I	0.993348196
	IQGAP2;IQGAP3	nonsynonymous SNV	NM_006633:c.C2681T:p.T894I	0.993366353
	KAZALD2	nonsynonymous SNV	NM_030929:c.G707A:p.G236D	0.993384509
	LMCD2	nonsynonymous SNV	NM_014583:c.C913T:p.R305W	0.993402666
	LRBA	nonsynonymous SNV	NM_001199282:c.A4261G:p.S1421G	0.993420823
	LRRK2	nonsynonymous SNV	NM_024652:c.C1246A:p.L416M	0.99343898
	LUC7L3	nonsynonymous SNV	NM_016019:c.A861C:p.E287D	0.993457137
	MANBA	nonsynonymous SNV	NM_005908:c.G2482A:p.V828I	0.993475294
	MAPRE2	nonsynonymous SNV	NM_012325:c.G389C:p.R130T	0.99349345
	MICAL2	nonsynonymous SNV	NM_001159291:c.G293A:p.R98Q	0.993511607
	MINA	nonsynonymous SNV	NM_001042533:c.C419T:p.P140L	0.993529764
	MON3	nonsynonymous SNV	NM_015026:c.A2518G:p.T840A	0.993547921

Patient #	Gene Name	Type	Variant	MutationTaster
	MPP4	nonsynonymous SNV	NM_001932:c.C617A:p.S206Y	0.993566078
	MYH19	nonsynonymous SNV	NM_005963:c.T1303C:p.Y435H	0.993584235
	MYH28	nonsynonymous SNV	NM_005964:c.C2894T:p.A965V	0.993602392
	NALCN	nonsynonymous SNV	NM_052867:c.C2305T:p.H769Y	0.993620548
	NARS3	nonsynonymous SNV	NM_001243251:c.A218G:p.K73R	0.993638705
	NEDD10	nonsynonymous SNV	NM_006403:c.G784A:p.D262N	0.993656862
	NUDT17	nonsynonymous SNV	NM_001171905:c.C67G:p.L23V	0.993675019
	PARK3	nonsynonymous SNV	NM_013988:c.G733A:p.D245N	0.993693176
	PMPCA	nonsynonymous SNV	NM_015160:c.T1307C:p.M436T	0.993711333
	PRKCE	nonsynonymous SNV	NM_005400:c.T896C:p.I299T	0.99372949
	PSMD2	nonsynonymous SNV	NM_001191037:c.A1051G:p.M351V	0.993747646
	PTPN23	nonsynonymous SNV	NM_007039:c.A2983G:p.M995V	0.993765803
	PTPN24	nonsynonymous SNV	NM_012411:c.A2077G:p.R693G	0.99378396
	PTPRH	nonsynonymous SNV	NM_001161440:c.G1958A:p.G653D	0.993802117
	PUS8	nonsynonymous SNV	NM_019042:c.C367T:p.H123Y	0.993820274
	RAB40B	nonsynonymous SNV	NM_006822:c.C788G:p.P263R	0.993838431
	RFWD4	nonsynonymous SNV	NM_018124:c.C1082T:p.S361F	0.993856588
	RICTOR	nonsynonymous SNV	NM_152756:c.T1989G:p.I663M	0.993874744
	RPS6KB2;RPS6K	nonsynonymous SNV	NM_003952:c.C800T:p.P267L	0.993892901
	SBF2	nonsynonymous SNV	NM_002972:c.G1918C:p.E640Q	0.993911058
	SCRIB	nonsynonymous SNV	NM_015356:c.G571A:p.D191N	0.993929215
	SDK2	nonsynonymous SNV	NM_152744:c.C6590G:p.P2197R	0.993947372
	SERPIND2	nonsynonymous SNV	NM_000185:c.G623A:p.R208H	0.993965529
	SFXN5	nonsynonymous SNV	NM_213649:c.A795T:p.E265D	0.993983685
	SLC35E4	nonsynonymous SNV	NM_018656:c.G182C:p.C61S	0.994001842
	SPAG6	nonsynonymous SNV	NM_006461:c.A1G:p.M1V	0.994019999
	TAGLN	nonsynonymous SNV	NM_001001522:c.G437A:p.R146H	0.994038156
	TBC1D6	nonsynonymous SNV	NM_001134380:c.A1124G:p.Y375C	0.994056313
	TBX22	nonsynonymous SNV	NM_013351:c.C1421G:p.P474R	0.99407447
	THAP7	nonsynonymous SNV	NM_144721:c.A419C:p.H140P	0.994092627
	TRIM36	nonsynonymous SNV	NM_018700:c.A1283G:p.K428R	0.994110783
	TRIM45	nonsynonymous SNV	NM_001145635:c.G1253A:p.G418E	0.99412894
	TRIM69	stopgain SNV	NM_182985:c.C145T:p.R49X	0.994147097
	UTP20;UTP21	nonsynonymous SNV	NM_014503:c.G325A:p.D109N	0.994165254
	VAX3	nonsynonymous SNV	NM_012476:c.C415A:p.L139M	0.994183411
	ZC3H11	nonsynonymous SNV	NM_032786:c.C380T:p.P127L	0.994201568
	ZSWIM9	stopgain SNV	NM_080603:c.G26A:p.W9X	0.994219725
	ZSWIM13	nonsynonymous SNV	NM_020883:c.C793T:p.R265C	0.994237881
	DNAH4	nonsynonymous SNV	NM_020877:c.G8281A:p.V2761M	0.994256038
	DSE	nonsynonymous SNV	NM_001080976:c.A844G:p.I282V	0.994274195
	EIF4ENIF3	nonsynonymous SNV	NM_001164502:c.G2146A:p.G716R	0.994292352
	ENPP9	nonsynonymous SNV	NM_178543:c.C273G:p.H91Q	0.994310509
	EPG7	nonsynonymous SNV	NM_020964:c.C3248T:p.S1083L	0.994328666
	EPRS	nonsynonymous SNV	NM_004446:c.A1256G:p.Y419C	0.994346823
	FAT4	nonsynonymous SNV	NM_001447:c.T1331C:p.V444A	0.994364979
	FBN5	nonsynonymous SNV	NM_032447:c.G3932C:p.G1311A	0.994383136
	FBXO45	nonsynonymous SNV	NM_001029860:c.C1708T:p.R570W	0.994401293
	FGL3	nonsynonymous SNV	NM_004467:c.A419T:p.Y140F	0.99441945
	FHL3	nonsynonymous SNV	NM_001159699:c.A161G:p.N54S	0.994437607
	FKTN	nonsynonymous SNV	NM_006731:c.A1336G:p.N446D	0.994455764
	FRK	nonsynonymous SNV	NM_002031:c.C1358T:p.P453L	0.99447392
	FZD6	nonsynonymous SNV	NM_012193:c.G477A:p.M159I	0.994492077
	GALNT9	nonsynonymous SNV	NM_017423:c.T973A:p.C325S	0.994510234
	GDAP4	nonsynonymous SNV	NM_001135589:c.G368A:p.R123Q	0.994528391
	GDF11	nonsynonymous SNV	NM_005260:c.C307T:p.P103S	0.994546548

Patient #	Gene Name	Type	Variant	MutationTaster
	GNGT3	nonsynonymous SNV	NM_021955:c.G148A:p.E50K	0.994564705
	GPT	nonsynonymous SNV	NM_005309:c.G320A:p.R107K	0.994582862
	GRK6	nonsynonymous SNV	NM_001004056:c.T1274C:p.L425P	0.994601018
	HPSE4	nonsynonymous SNV	NM_001166245:c.G1282C:p.V428L	0.994619175
	HSPG2	nonsynonymous SNV	NM_005529:c.G8848A:p.G2950R	0.994637332
	HSPG2	nonsynonymous SNV	NM_005529:c.G8422T:p.V2808F	0.994655489
	HTRA4	nonsynonymous SNV	NM_013247:c.G1195A:p.G399S	0.994673646
	IGFBP7	nonsynonymous SNV	NM_000599:c.C412T:p.R138W	0.994691803
	ITGB6	nonsynonymous SNV	NM_001005619:c.G1544A:p.R515H	0.99470996
	JUB	nonsynonymous SNV	NM_032876:c.C131T:p.P44L	0.994728116
	KATNB3	nonsynonymous SNV	NM_005886:c.C1319G:p.P440R	0.994746273
	KIAA0564	nonsynonymous SNV	NM_015058:c.A5297C:p.D1766A	0.99476443
	KIAA0564	nonsynonymous SNV	NM_001009814:c.G2693A:p.R898K	0.994782587
	KIAA1109	nonsynonymous SNV	NM_015312:c.C11129T:p.P3710L	0.994800744
	KIAA1524	nonsynonymous SNV	NM_020890:c.C877A:p.P293T	0.994818901
	LGI4	nonsynonymous SNV	NM_018176:c.A1355G:p.Q452R	0.994837058
	LIG3	nonsynonymous SNV	NM_000234:c.G1226A:p.R409H	0.994855214
	LRRC32	nonsynonymous SNV	NM_001105581:c.G604A:p.A202T	0.994873371
	MBD7	nonsynonymous SNV	NM_018328:c.G1382A:p.R461H	0.994891528
	MCL3	nonsynonymous SNV	NM_021960:c.C680T:p.A227V	0.994909685

Table 5.3: Select genetic variants identified in superior coloboma patient #2.
Candidates were prioritized by expression within the developing eye or previously identified connections to coloboma.

Gene	Type	Variant	Mutation Taster
ACVRL1	nonsynonymous SNV	NM_001077401:c.C1445T;p.A482V	0.999706
ASPM	nonsynonymous SNV	NM_018136:c.C4213T;p.R1405C	0.999919
SYNE1	nonsynonymous SNV	NM_033071:c.G12229C;p.D4077H	0.990532
TLR10	nonsynonymous SNV	NM_001017388:c.T1255C;p.W419R	0.989287
CD36	stopgain SNV	NM_001127444:c.T1079G;p.L360X	1
COL10A1	nonsynonymous SNV	NM_000493:c.T23G;p.L8W	0.998959
CTSC	nonsynonymous SNV	NM_001814:c.A1088C;p.E363A	0.999985
CYP1A1	nonsynonymous SNV	NM_000499:c.C712T;p.P238S	0.999742
CYP1A1	nonsynonymous SNV	NM_000499:c.T857C;p.L286T	0.99848
CYP1B1	nonsynonymous SNV	NM_000104:c.G1103A;p.R368H	0.970216
DHRS9	nonsynonymous SNV	NM_001142271:c.G856C;p.D286H	0.99818
DHX38	nonsynonymous SNV	NM_014003:c.A2947G;p.I983V	0.999192
DOCK5	nonsynonymous SNV	NM_024940:c.G2698A;p.E900K	0.993012
DSCAM	nonsynonymous SNV	NM_001389:c.G701A;p.R234H	0.979737
EAF1	nonsynonymous SNV	NM_033083:c.G619A;p.D207N	0.976956
FURIN	nonsynonymous SNV	NM_002569:c.G1343A;p.R448Q	0.997805
HHIP	nonsynonymous SNV	NM_022475:c.C1762T;p.P588S	0.999972
IFT57	nonsynonymous SNV	NM_018010:c.A1232G;p.N411S	0.991636
LAMA4	nonsynonymous SNV	NM_001105206:c.G3239A;p.R1080Q	0.997947
LAMA5	nonsynonymous SNV	NM_005560:c.G10411A;p.G3471S	0.999959
LAMC2	nonsynonymous SNV	NM_005562:c.C2080T;p.R694C	0.994374
LRP2	nonsynonymous SNV	NM_004525:c.G13803A;p.M460I	0.999811
MCM5	nonsynonymous SNV	NM_006739:c.G375C;p.Q125H	0.999992
MKS1	stopgain SNV	NM_001165927:c.C478T;p.R160X	1
MMP2	nonsynonymous SNV	NM_001127891:c.C1481T;p.S494L	0.994768
MMP9	nonsynonymous SNV	NM_004994:c.A344G;p.K115R	0.985048
NCOR1	nonsynonymous SNV	NM_001190440:c.G6956A;p.R2319Q	0.966004
NEUROD1	nonsynonymous SNV	NM_002500:c.C590A;p.P197H	0.999982
PCDH15	stopgain SNV	NM_001142767:c.T1283G;p.L428X	1
PLXNA3	nonsynonymous SNV	NM_017514:c.A3440G;p.K1147R	0.996782
SIPA1L1	nonsynonymous SNV	NM_015556:c.C3056T;p.T1019M	0.99995
SLIT2	nonsynonymous SNV	NM_004787:c.G4333C;p.D1445H	0.993067
SOD2	nonsynonymous SNV	NM_000636:c.G198C;p.E66D	0.999998
SYNE1	nonsynonymous SNV	NM_033071:c.G12229C;p.D4077H	0.990532
TLR10	nonsynonymous SNV	NM_001017388:c.T1255C;p.W419R	0.989287

Chapter 6

Bmp3 is a novel regulator of ocular fissure closure

6.1. Introduction

Ocular coloboma is a congenital blinding disorder characterized by gaps in iris, lens, retina and/or optic nerve tissue. Estimated to occur in 1 out of 4,000 live births, it represents the second leading cause of pediatric blindness worldwide (Onwochei et al., 2000; Williamson and FitzPatrick, 2014). The characteristic tissue gaps result from the incomplete fusion of a conserved developmental fissure that runs the length of the developing eye; as such, this incurable disorder can affect almost any ocular tissue layer, and can affect one (unilateral) or both eyes (bilateral).

The choroid/optic fissure transiently forms in the ventral eye during induction of the lens vesicle and formation of the bilayered optic cup, allowing invasion of periorcular mesenchyme (POM) to give rise to the hyaloid vessel. As the optic cup growth continues, the two sides of the fissure extend towards each other until they are apposed. This aligns the tissue for subsequent fusion of the two lobes, which begins centrally and progresses proximally down the optic stalk and distally towards the lens, thereby completing the continuous globe of the eye.

Studies of coloboma patients have implicated close to 40 genes in the genetic causality of this disorder (Patel and Sowden, 2017; Williamson and FitzPatrick, 2014) with experimental analyses of animal models validating the key function of many such genes in regulating optic fissure closure (reviewed in (Patel and Sowden, 2017)). For example, members of the bone morphogenetic protein (BMP) pathway regulate dorsal-ventral patterning of the developing eye, retinal progenitor proliferation and other aspects that impact ocular fissure closure (Asai-Coakwell et al., 2007; Asai-Coakwell et al., 2013; French et al., 2009; French et al., 2013; Huang et al., 2015; Huillard et al., 2005; Zhang et al., 2013). As such, mutations in *BMP7* (Wyatt et al., 2010), *BMP4* (Reis et al., 2011), *GDF3* (Ye et al., 2010), *GDF6* (Asai-Coakwell et al., 2007; Asai-Coakwell et al., 2009; Ye et al., 2010), *SMOC1* (Rainger et al., 2011) and *CRIMI* (Beleggia et al., 2015) can cause pleiotropic eye malformations, including coloboma. Despite the significant research effort aimed at understanding the molecular underpinnings of ocular coloboma and identifying pathogenic genetic alterations, the majority of cases cannot be attributed to lesions in genes already implicated.

In addition to the clear role of BMP signaling, there is strong evidence from animal model studies that the transforming growth factor beta (TGF β) pathway also regulates ocular fissure closure. Recent work in zebrafish has characterized a population of ventral retinal cells surrounding the optic fissure during its formation that are labeled by a transgenic reporter line sensitive to Smad3 activation, an intracellular effector protein in the TGF β pathway (Knickmeyer et al., 2018). Additionally, temporally precise pharmacological inhibition of Smad3 caused failed optic fissure closure. This suggests that TGF β signaling is required in this process (Knickmeyer et al., 2018), though it is unclear which ligands activate TGF β signaling in the ventral retina.

Here, we report the identification of a novel heterozygous mutation in *BMP3* in four members of an autosomal dominant pedigree displaying coloboma. We further identify two additional *BMP3* mutations using targeted Sanger sequencing of a large cohort of patients with coloboma and/or the etiologically related ocular disorders microphthalmia and anophthalmia (collectively referred to as MAC). All identified variants are predicted to disrupt protein function. BMP3 is an atypical ligand with known function as an activator of Smad3, thereby resembling a TGF β ligand. We used a combination of cultured cells and zebrafish to investigate the functions of Bmp3 and the nature of detected variants. We provide evidence that BMP3 functions as a critical regulator of choroid fissure closure and is a coloboma-causing locus.

6.2. Results and discussion

6.2.1. Patients with coloboma and/or microphthalmia have mutations in *BMP3*

Exome sequencing was conducted on five patients in an autosomal dominant pedigree displaying coloboma (4 affected and 1 unaffected; see Fig. 6.1A). These patients display either bilateral chorioretinal coloboma (Fig. 6.1B) or unilateral iris coloboma with microphthalmia (Fig. 6.1C). Analysis of the sequencing resulted in the identification of 48 variants shared amongst those four affected individuals and absent in the unaffected individual. SIFT and PolyPhen2, online tools used to predict whether an amino acid substitution is likely to affect protein function, prioritized ten loci for further evaluation. The candidate gene names, variants identified and their SIFT and PolyPhen2 scores can be found in Table 6.1.

Based on the crucial roles previously characterized for BMPs in eye development and fissure closure, one of the candidate genes particularly stood out: *BMP3* (p.A470P). In order to look for additional rare variants in *BMP3*, 192 patients from a cohort of unrelated MAC cases were Sanger sequenced to ascertain whether *BMP3* was a locus associated with ocular disease. We identified two additional rare variants located within the highly conserved mature ligand domain that are predicted to cause detrimental effects to the encoded protein: p.S393F and p.F450Y. All three variants are either not found in control databases or are extremely rare. Additional information about each *BMP3* variant can be found in Table 6.2, and they will be referred to as S393F, F450Y and A470P from here onwards.

The online tools that were used to analyze the *BMP3* variants take into consideration aspects of the protein such as the degree of conservation at the amino acid location and differences in physical properties of the original and substituted amino acid. However, they are not able to give detailed predictions regarding changes within the protein structure. Previous studies have used *in silico* modeling of wild type compared to variant proteins and subsequent analysis of the energy requirements that would be needed to maintain proper protein folding (Footz et al., 2011; Ye et al., 2010). Termed atomic non-local environment assessment (ANOLEA), this predictive algorithm gives an estimated

energy requirement at each amino acid position within the protein. Since the crystal structure of mature BMP3 is solved (Allendorph et al., 2007), we used ANOLEA to analyze the identified BMP3 variants. We see that each substitution disrupts protein folding at multiple locations along the peptide (Fig. 6.2). While S393F and F450Y show energy values close or equal to GDF3 variants previously shown to cause eye disease (Ye et al., 2010), A470P is predicted to be more severely destabilizing at two different locations within the protein.

6.2.2. *BMP3 variant proteins have altered secretion in vitro*

Online tools and *in silico* modeling are predictive in nature. As such, we sought to test whether BMP3 variants had altered protein function *in vivo*. To test this question, we first attempted an mRNA overexpression approach in zebrafish. Single-cell stage embryos were injected with 100 pg of WT *BMP3* mRNA or an equal amount of *mCherry* mRNA as a control, and embryos were analyzed for morphological defects at 28-30 hpf. Embryos injected with *BMP3* do not display detectable phenotypes compared to both uninjected embryos and *mCherry* injected embryos (Fig. 6.3). Additionally, a very high dose of 300 pg *BMP3* still results in morphologically normal embryos (Fig. 6.3). From this, we conclude that *BMP3* does not cause overt phenotypes when overexpressed in zebrafish, or that human *BMP3* does not have activity *in vivo* in zebrafish. It is possible that overexpression of *BMP3* at later time points could cause a phenotype, but the short half-life of mRNA generally prohibits reliable phenotypic analysis past the first day of development. As such, overexpressing *BMP3* in zebrafish is not currently a viable way to test biological function of wild type and variant proteins.

In order to address this question with a different approach, we instead turned to cell culture. It is not uncommon for mutant proteins to be targeted for degradation within the cell; as such, we hypothesized that variant *BMP3* protein levels may be reduced. Additionally, since BMP ligands must be secreted from the cells in which they are produced in order to relay a signal, we hypothesized that *BMP3* variants may instead alter protein secretion from cells. To test this, we transfected Cos cells with constructs encoding

WT or variant BMP3, and then performed western blots on protein isolates from both cell lysates and culture medium. Our constructs encode V5-tagged BMP3 proteins to enable us to probe for the presence of the tag, since antibodies for BMP ligands tend to have significant cross reactivity given that the mature ligands are so similar in amino acid sequence. V5-tagged BMP3 is detected equally within the cell lysates (Fig. 6.4), indicating that none of the variants affect translation or degradation of the protein. However, we see that S393F and A470P are completely or nearly absent from the culture media (Fig. 6.4), indicating that secretion of these variant proteins is altered *in vitro*.

The reduced BMP3 protein secretion that we observe in this experiment represents a plausible disease causing mechanism for S393F and A470P. BMP3 is a morphogen and as such, its effect is concentration-dependent. S393F is detected in the culture medium at extremely low levels compared to WT, while A470P is not detected at all, suggesting that a BMP3 morphogen gradient would be altered significantly in patients carrying these variants. It is perhaps not surprising that A470P shows more complete loss of secretion, given how severely it is predicted to disrupt protein structure (Fig. 6.3). Additionally, Hinck et al. (2016) performed an alignment of all TGF β superfamily ligands and showed that BMP3 amino acid 470 is not only well conserved itself, it is positioned directly between two cysteine residues that are perfectly conserved in all 33 TGF β ligands analyzed. Both of these cysteine residues are known to form disulfide bridges that make up part of the cysteine-knot domain that characterizes TGF β superfamily ligands. Additionally, A470 is entirely invariant from fish to human BMP3, spanning 450 million years of evolutionary time, strongly suggesting that it is crucial to protein function. We therefore suggest that substitution of a proline at position 470 could disrupt the cysteine knot shape or prevent the correct formation of disulfide bridges, and therefore impair the ability of the protein to activate signaling properly.

The third BMP3 variant, F450Y, is not detected at lower levels in the culture medium compared to WT, suggesting that this allele likely does not cause disease due to defects in protein secretion. However, F450 is one of the predicted receptor-interface residues that directly interact with the receptor upon ligand binding (Allendorph et al., 2007). Though F450 is conserved in all BMP3 proteins, suggesting it is important for

BMP3 function, tyrosine (Y) is more commonly seen at this position in TGF β superfamily ligands (Hinck et al., 2016), suggesting it is likely tolerated at this position. It may, however, affect how BMP3 forms ligand dimers, or alter affinity for or interaction with its receptor. BMP3 binds with high affinity to ACVR2B (Allendorph et al., 2007). There is evidence for two different mechanisms by which BMP3 is thought to affect signaling through ACVR2B. First, it can stimulate an intracellular cascade through Smad2/3 to activate TGF β signaling and/or antagonize BMP signaling within target cells, as the two pathways are known to be able to inhibit one another (Bahamonde and Lyons, 2001; Faucheux et al., 1997; Stewart et al., 2010). Second, BMP3 is thought to interact with or block BMP2/4 from binding at the receptor to prevent activation of BMP signaling (Kokabu et al., 2012). Therefore, F450Y may have altered or decreased ability to activate TGF β signaling or inhibit BMP signaling, due to changes in interactions with ACVR2B or ligands that it is thought to bind and inhibit.

Taken together, the three BMP3 protein variants that we have identified appear to have defects in protein secretion from cells or have alterations to amino acids likely to be crucial for interactions with the receptor or other ligands, suggesting they are plausible disease-causing alleles of *BMP3*.

6.2.3. *Creation of bmp3 mutant zebrafish*

Eye development is both morphologically and genetically conserved across vertebrates (Heavner and Pevny, 2012) and zebrafish have been successfully used to model structural eye disease previously, including MAC spectrum disorders (for example, (Asai-Coakwell et al., 2007); reviewed in (Patel and Sowden, 2017)). Therefore, in order to investigate a requirement for Bmp3 in vertebrate eye development, we created a line of zebrafish carrying a deleterious mutation in *bmp3* using CRISPR-Cas9. By targeting regions upstream of the TGF β domain, we generated a 5bp deletion (c.887_891delCATGG), causing a frameshift that introduces a premature stop codon upstream of the mature ligand (p.Thr296GlyfsX2). Because the P0 fish were co-injected with three different sgRNAs, this line also carries two additional 3bp deletions upstream of the frameshift

(c.544_546delCAG and c.840_842delGCA; Fig. 6.5) that each result in the deletion of a single amino acid (p.Q182del and p.Q281del, respectively; Fig. 6.6).

Given that this mutation (hereafter referred to as *bmp3*^{ua1020}) codes for a truncated protein lacking the entire mature ligand (from amino acids 350-452), *bmp3*^{ua1020} is very likely a functional null. Additionally, we do not anticipate genomic compensation in response to the mutation, as we see no evidence for nonsense-mediated decay in mutants (Fig. 6.7), the cellular response thought to mediate genomic compensatory mechanisms in many fish carrying engineered mutations (El-Brolosy and Stainier, 2017). This is supported by a previous study that used morpholino oligonucleotides to analyze the craniofacial phenotype of Bmp3-depleted zebrafish and saw deficiencies in jaw development, where multiple craniofacial cartilage elements were reduced (Schoenebeck et al., 2012). Adult *bmp3*^{ua1020} homozygotes display craniofacial defects (Fig. 6.8) that likely correspond to the *bmp3* morphant larval defect previously characterized, further suggesting that the *bmp3*^{ua1020} allele results in at least a strong hypomorph.

Lastly, phenotypes in zygotic mutant zebrafish embryos and larvae can sometimes be masked by maternally inherited wild type transcript. This is one advantage of analysis using translation-blocking morpholinos, as they are able to inhibit both maternal and zygotic transcript. For mutant analysis of maternally inherited genes, it is often necessary to create maternal-zygotic mutants in order to see a phenotype. The earliest published expression for zebrafish *bmp3* detected by in situ hybridization is at approximately 19.5 hours post fertilization (hpf) (Mueller et al., 2010), and detected by RT-PCR at 8-9 hpf (Ito-Amano et al., 2014), both of which are hours after the activation of the zygotic genome. We confirmed by both RT-PCR and in situ hybridization that *bmp3* is not detectable before the activation of the zygotic genome (Fig. 6.9A-D) and therefore do not anticipate phenotypic masking by maternal transcript.

6.2.4. *bmp3*^{ua1020} homozygous larvae have optic fissure closure defects

Our analyses of BMP3 variants identified in patients with MAC spectrum anomalies have provided strong evidence that BMP3 may play a role in optic fissure closure. Based on

these data, we hypothesized that *bmp3*^{ua1020} larvae would display fissure closure defects. In wild type zebrafish, the optic fissure begins to form around 18 hpf and is readily visible by stereoscope within a few hours. The two fissure lobes are apposed and beginning to fuse before 48 hpf, and fusion is fully complete by 60 hpf (Schmitt and Dowling, 1994). To assess the ability of *bmp3*^{ua1020} zebrafish to undergo optic fissure fusion, we stained embryos using an antibody against Laminin alpha-1 (α -Lam) at 48 hpf and 65 hpf to visualize retained basement membrane in the fissure space. α -Lam immunohistochemistry has been shown to be a reliable method to visualize retained fissures (for example, (James et al., 2016)). Wild type and *bmp3*^{ua1020} eyes do not appear morphologically different at 48 hpf (Fig. 6.10A,C). As expected, optic fissures are labeled with α -Lam and the fissure lobes are in close apposition (WT: 55/56 larvae, *bmp3*^{ua1020}: 58/59 larvae). However, well after fissure closure should be complete at 65 hpf, 17.7% of *bmp3*^{ua1020} larvae showed persisting Laminin-labeled fissures (n=23/130 *bmp3*^{ua1020}, n=0/38 WT; Fig. 6.10B,E,F) suggesting a perturbed ability to undergo correct tissue fusion in mutants.

The fissure closure defects that we observe in *bmp3*^{ua1020} larvae support our hypothesis that Bmp3 is a novel regulator of vertebrate optic fissure closure. Furthermore, the nature of their ocular phenotype hints at additional clues regarding the underlying mechanism of their fissure closure defect. While there is some natural variability in zebrafish eye size, the *bmp3*^{ua1020} eyes are not smaller than that of wild type at 48 or 65 hpf (Fig. 6.10A-D show representative images), suggesting that loss of Bmp3 activity in zebrafish does not cause microphthalmia. Because we see apposition of fissure lobes and lack of overt morphological differences in *bmp3*^{ua1020} compared to wild type eyes at 48 hpf, this suggests that Bmp3 likely does not regulate an early process in eye development, such as optic vesicle evagination, fissure formation or lobe apposition, as perturbing these early steps usually results in microphthalmia and/or more severe coloboma (reviewed in (Patel and Sowden, 2017)). Instead, coloboma seen in *bmp3*^{ua1020} mutants much more closely resembles those published in other zebrafish models with underlying defects in failed basement membrane degradation or tissue fusion between fissure lobes (James et al., 2016).

It should be noted that only *bmp3*^{ua1020} larvae with bilateral fissure closure defects were considered to have coloboma, making 17.7% closure defects in *bmp3*^{ua1020} zebrafish a

stringent estimation. Nevertheless, ocular phenotypes in *bmp3*^{ua1020} fish are incompletely penetrant. This is not uncommon in the literature; in fact, incomplete penetrance of MAC in humans is seen in the majority of cases (see (Williamson and FitzPatrick, 2014)). This is perhaps reflected in the control database prevalence for F450Y; while its existence is very rare (0.03%, see Table 6.2), it is not zero. It is also possible that unaffected relatives in the pedigree (Fig. 6.1A) carry the A470P variant, as DNA was only analyzed from one control individual.

Interestingly, each identified BMP3 variant has at least one individual with inclusion of microphthalmia in their disease presentation (see Table 6.2). This phenotype does not appear to recapitulate in *bmp3*^{ua1020} fish. This may simply be a reflection of the non-equivalent alleles in humans and zebrafish; while we believe that no mature Bmp3 ligand is produced in *bmp3*^{ua1020} mutants due to the upstream frameshift, this is not the case in patients with BMP3 variants. It is certainly a plausible hypothesis that the zebrafish truncated protein lacking the mature peptide could interact differently *in vivo* than BMP3 missense variants. Another possibility for this discrepancy in phenotypes is that zebrafish and human *BMP3* may have additional or partially overlapping roles and therefore, when mutated, cause similar but not identical phenotypes.

6.2.5. *bmp3* is expressed in head mesenchyme during eye morphogenesis in zebrafish

To begin elucidating a possible mechanism through which Bmp3 regulates optic fissure closure, we examined where *bmp3* is expressed during zebrafish eye development. In situ hybridization for *bmp3* at 22 hpf shows *bmp3* mRNA is readily detected in a domain immediately anterior and medial to the eye (Fig. 6.11A). In whole mount, it was difficult to determine exactly which cells were expressing *bmp3*; to visualize expression more precisely, we performed sectioning on paraffin-embedded embryos after *bmp3* in situ and find that expression is localized to head mesenchyme between the anterior forebrain and eye, but is not detected within either neural epithelium (Fig. 6.11B,D). Additionally, embryos in cross section show that *bmp3* expression between the eyes is extremely ventral, restricted to a one cell-thick layer ventral to the forebrain (Fig. 6.11C). As such, *bmp3* is

expressed in close proximity to the nasal and ventral retina, and therefore the developing optic fissure.

The *bmp3* expression pattern that we observe is highly reminiscent of *tbx15*, also described as staining head mesenchyme separating the brain and eye (compare Fig. 6.11A and Fig. 2H in (Begemann et al., 2002)). Head mesenchyme is primarily populated by cells of cranial neural crest origin, but also has contributions from the paraxial and splanchnic mesoderm. *bmp3* expression has been previously detected in tail paraxial mesoderm in zebrafish (Mueller et al., 2010), suggesting that perhaps head mesenchyme expressing *bmp3* may be of paraxial mesodermal origin as well. However, we cannot rule out other origins without a detailed analysis of *bmp3* expression over time and mRNA co-localization experiments to compare *bmp3* transcript with that of known markers for cranial neural crest, paraxial mesoderm and splanchnic mesoderm.

Given that Bmp3 is a secreted molecule, we conclude from these data that expression in tissues adjacent to the developing eye optimally positions the ligand to regulate fissure closure.

6.2.6. *Bmp3 may be a novel ligand in retinal TGF β signaling*

Bmp3 has been shown to signal through Smad3, acting much more like a TGF β ligand than a canonical BMP ligand (Bahamonde and Lyons, 2001; Faucheux et al., 1997; Stewart et al., 2010). Evidence from animal models suggests that TGF β signaling regulates ocular fissure closure (Ittner et al., 2005; Zhang et al., 2013). Recently, Knickmeyer et al. (2018) characterized a population of ventral retinal cells surrounding the optic fissure that are labeled by a Smad3 reporter transgene. Although these authors highlight the expression of *tgfb2* and *tgfb3* in ventral-medial periocular tissue and lens respectively, it is unknown what TGF β ligands are acting in the ventral retina. However, pharmacological inhibition of Smad3 using Specific Inhibitor of Smad3 (SIS3) specifically between 24-30 hpf caused failed optic fissure closure at 72 hpf (Knickmeyer et al., 2018), suggesting that local TGF β signaling at the fissure site is required for its closure.

Based on these data and the expression pattern of *bmp3*, we hypothesize that Bmp3 activates TGF β signaling in the ventral retina to facilitate optic fissure fusion. We have optimized a pSmad3 antibody that labels the specific population of cells in the zebrafish ventral retina described by (Knickmeyer et al., 2018). Serial optical sections highlights the ventral-proximal position in the fissure that pSmad3-expressing cells occupy (Fig. 6.12A-C). To test our hypothesis, it will be especially important to visualize ventral retinal TGF β signaling in a *bmp3*^{ua1020} background compared to wild type, where we anticipate reduced pSmad3 staining in *bmp3*^{ua1020} mutants. It is unlikely that pSmad3 staining will be lost completely, since total loss of retinal TGF β signaling would most likely result in a more severe and penetrant phenotype than is observed in *bmp3*^{ua1020} mutants (similar to the effect of SIS3 treatment). It is also likely that more than one TGF β ligand is acting in the ventral retina. Both *tgfb2* and *tgfb3* are expressed nearby, and *Tgfb2* KO mice display fissure closure defects (Knickmeyer et al., 2018), suggesting a role for at least Tgfb2 in fissure closure.

If Bmp3 is one of two or more TGF β ligands acting at the fissure, we reasoned that *bmp3*^{ua1020} mutations would sensitize embryos to a suboptimal dose of SIS3. We therefore hypothesize that fissure defects seen in *bmp3*^{ua1020} mutants would synergize with a low dose of SIS3, causing greater than additive effects seen in each condition independently. To test this, we performed SIS3 treatments from 24-30 hpf using 9 μ M, the dose published in Knickmeyer et al. (2018), a lower dose of 6 μ M, and a DMSO control. We visually scored for open fissure in embryos at 65 hpf for consistency with *bmp3*^{ua1020} mutant analyses. Our preliminary findings show that, consistent with previous studies, 9 μ M SIS3 results in 100% of wild type larvae failing to close their optic fissures, as it did in *bmp3*^{ua1020} heterozygote incrosses (n=45 each, Fig. 6.12F,I,J). However, at 6 μ M SIS3, we find almost triple the prevalence of open fissures in *bmp3*^{ua1020} heterozygote incrosses (31.1%, n=14/45) compared to wild type (11.1%, n=5/45; Fig. 6.12E,H,J). If the combined effect on fissure defects was additive instead of synergistic, we would only predict approximately 7/45 affected embryos in a *bmp3*^{ua1020} heterozygote incross treated with 6 μ M SIS3. We therefore preliminarily conclude that *bmp3*^{ua1020} and SIS3 act synergistically to perturb fissure closure.

Without evidence that pSmad3 staining at the fissure is reduced in *bmp3*^{ua1020} mutants, we cannot yet conclude that Bmp3 acts as a TGF β ligand in the ventral retina. However, our low dose SIS3 treatments preliminarily show promising results that support our hypothesis. Wild type larvae treated with 6 μ M SIS3 showed 5/45 individuals with closure defects. Our previous findings showing that 17.7% of *bmp3*^{ua1020} homozygous larvae have retained fissures (Fig. 6.10) would predict approximately 2/45 additional larvae with open fissures in a *bmp3*^{ua1020} heterozygote incross (assuming Mendelian ratios of 25% homozygotes) if Bmp3 and TGF β signaling act in parallel to regulate optic fissure closure. Instead, these data suggest that their phenotypes synergize and thus likely act in the same pathway.

An alternative hypothesis for the role of Bmp3 in fissure closure is that it instead inhibits BMP signaling in the ventral retina to maintain proper dorsal-ventral patterning, a process crucial for eye morphogenesis. The inhibitory effect of Bmp3 on BMP signaling is well documented (Gamer et al., 2009; Gamer et al., 2005; Stewart et al., 2010; Sun et al., 2010), but this has largely been attributed to the reciprocally antagonistic nature of TGF β and BMP signaling in most studies. However, work in cell culture implicates Bmp3 as a “decoy ligand” where it binds Activin Type-2 Receptor (Acvr2b) with extremely high affinity (Allendorph et al., 2007) and blocks Bmp2/4-mediated BMP signaling through this receptor (Kokabu et al., 2012). Plausibly, Bmp3 emanating from the ventral head mesenchyme could act as a ventral inhibitor of Bmp2/4-mediated BMP signaling through Acvr2ba (one of two zebrafish paralogs of mammalian Acvr2b), which is enriched in the brain but broadly expressed in the zebrafish head at 24 hpf (Albertson et al., 2005). However, this seems unlikely, as we do not see expanded dorsal marker gene expression (Fig. 6.13A-B,E-F) or reduced ventral marker gene expression (Fig. 6.13C-D,G-H) in *bmp3*^{ua1020} mutants that would be expected with the loss of a ventral BMP inhibitor.

6.2.7. Summary and future directions

Taken together, the work described in this chapter provides strong evidence that *BMP3* is a coloboma-causing locus and implicates Bmp3 in vertebrate eye development for

the first time. Two of the three BMP3 variant proteins identified in patients with coloboma and/or microphthalmia are secreted from cells in dramatically decreased levels compared to wild type (S393F and A470P) (Fig. 6.4). This represents a plausible mechanism through which these missense variants could cause disease. Secretion of the third variant (F450Y) is not altered, but the location of the amino acid substitution is a predicted receptor-interface residue and could plausibly alter or decrease signaling ability of BMP3. We attempted to demonstrate that BMP3 variant proteins have altered biological function by overexpressing *BMP3* mRNA in zebrafish but this does not appear to cause detectable phenotypes, even at relatively high levels of mRNA (Fig. 6.3). As such, it will be key to test the activity of variant BMP3 proteins compared to wild type using luciferase assays in cell culture. *Bmp3* has been shown to activate TGFB signaling through pSmad3 (Stewart et al., 2010) or inhibit BMP signaling by antagonizing *Bmp2/4* at the receptor level (Kokabu et al., 2012) depending on the context. Robust *Bmp3*-mediated responses in luciferase activity have been previously described to test both of these mechanisms, and should be performed to test the alterations in the ability of BMP variant proteins to regulate TGFB and/or BMP signaling.

Strong evidence of associations between BMP3 mutations and MAC in humans led us to generate zebrafish *bmp3* mutants to test our hypothesis that *Bmp3* has a critical function in vertebrate optic fissure closure. We characterize an incompletely penetrant fissure closure defect phenotype in *bmp3*^{ua1020} mutants (Fig. 6.10), thereby providing evidence for a novel role for *Bmp3* in vertebrate eye development. We detect expression of *bmp3* in head mesenchyme both ventral/medial and anterior to the developing eye (Fig. 6.11), suggesting that *Bmp3* is optimally positioned to modulate TGFB or BMP signaling to regulate optic fissure closure. Future research efforts should be focused on determining the mechanism of *Bmp3* regulation in eye development. It is plausible that *Bmp3* could act as a ventral inhibitor of BMP signaling in the retina but we find this unlikely based on the absence of changes to dorsal-ventral patterning that would be expected in this case (Fig. 6.13). Instead, it seems more likely that *Bmp3* activates TGFB signaling in the ventral eye, as fissure closure defects in *bmp3*^{ua1020} and a low dose of pSmad3 inhibitor appear to synergize (Fig. 6.12).

The BMP signaling gradient across the dorsal-ventral axis of the eye must be precisely regulated to restrict BMP activity to the dorsal hemisphere of the retina. Knickmeyer et al. (2018) present evidence that TGFB signaling surrounding the fissure induces local expression of the secreted BMP antagonist *grem2b* in order to preserve the expression of TGFB-regulated genes that will subsequently facilitate optic fissure fusion. Though the interactions leading to BMP inhibition of TGFβ-dependent ECM modification is poorly understood, it has been demonstrated in multiple contexts (Izumi et al., 2006; Zeisberg et al., 2003). We hypothesize that *Bmp3* is one of the ligands that activate TGFβ signaling in the ventral retina to ultimately facilitate TGFβ-mediated tissue fusion in the optic fissure. If this model is correct, we would predict that both pSmad3 antibody staining and subsequent *grem2b* expression in the ventral retina would be reduced. To more definitively demonstrate this, future experiments should test the genetic interaction between *bmp3*^{ua1020} mutants and *grem2b* mutants. Not only would we expect *grem2b* mutants to phenocopy *bmp3*^{ua1020} fissure defects, but also that overexpression of *grem2b* should rescue *bmp3*^{ua1020} mutants and not the other way around.

Interestingly, this also plausibly represents a common mechanism between the larval fissure closure defects and the reduced upper jaw phenotypes observed in *bmp3*^{ua1020} adults (Fig. 6.8). Work from Zuniga et al. (2011) shows that *Grem2b* patterns the facial skeleton by dorsally inhibiting BMP signaling in the pharyngeal arches from which the facial skeleton is derived. They show that Endothelin-1 (*Edn1*) induces expression of *grem2b*, but mutations in *edn1* do not completely abolish *grem2b* expression, nor do they cause complete ventralization of the arches, suggesting an additional upstream factor. Expression of *bmp3* ventral to the developing brain (see Fig. 6.11C) positions it immediately dorsal to where the pharyngeal arches will form and express *grem2b* by 36 hpf (Zuniga et al., 2011). Therefore, mutations in *bmp3* could result in optic fissure closure defects and reduced dorsal craniofacial skeleton due to impaired *grem2b* expression in the ventral eye and dorsal pharyngeal arches, respectively. Of note, the resulting structure of the facial skeleton in *grem2b* morphants is remarkably similar to that seen in *bmp3* morphants (compare Fig. 7J in (Zuniga et al., 2011) and Fig. 4M in (Schoenebeck et al., 2012)).

6.3. Figures

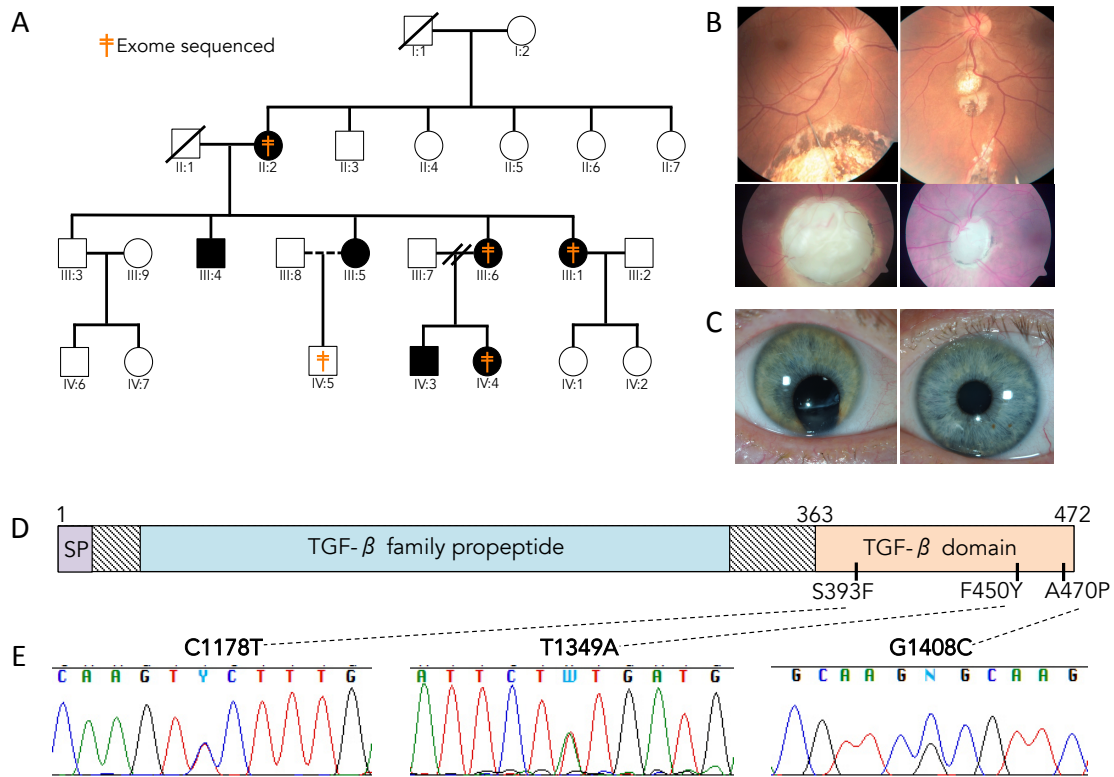


Fig. 6.1: A *BMP3* missense mutation identified in a family with autosomal dominant coloboma and/or microphthalmia. (A) Simplified pedigree of the family with indicated individuals who were exome sequenced denoted with a symbol. (B-C) Fundus (B) and iris (C) images from patients, showing bilateral retino-choroidal coloboma or bilateral iris coloboma with microphthalmia. (D) Schematic of the *BMP3* protein structure. Domains within the peptide are labeled, where the TGF β domain is the mature ligand. Numbers above indicate amino acid number of the pro-peptide. Amino acid changes labeled below the diagram indicate novel variants identified in the pedigree in A (A470P) or after targeted Sanger sequencing for *BMP3* in a cohort with coloboma and/or microphthalmia (S393F and F450Y, 192 patients in cohort). SP, signal peptide. (E) Chromatograms showing DNA sequence variants indicated by their base change within the coding sequence of *BMP3*.

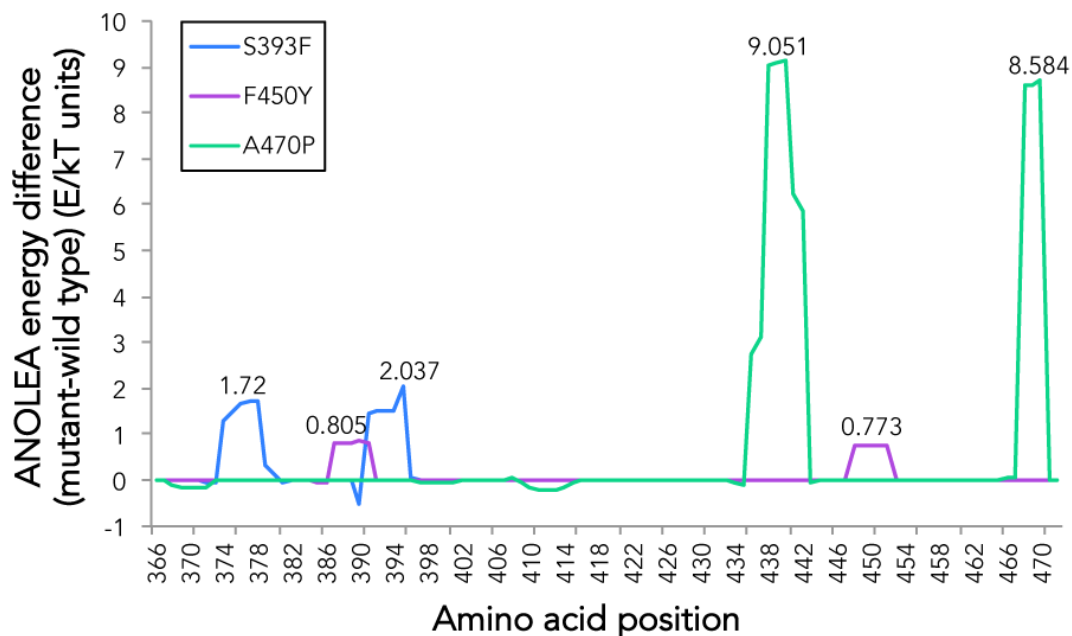


Fig. 6.2: BMP3 amino acid substitutions are predicted to destabilize protein structure at multiple points within the peptide. The wild type and variant protein models (produced using Swiss-pdbViewer, based on solved crystal structure of BMP3) were submitted to an Atomic Non Local Environment Assessment (ANOLEA) server to compute folding energy. Energy differences are in E/kT units, where E represents energy; k , the Boltzmann constant; and T , absolute temperature. Increased energy values are seen at two different locations in each BMP3 variant, indicating a less energetically favourable conformation in the model compared to wild type. Values displayed above each peak are the largest value changes around that position.

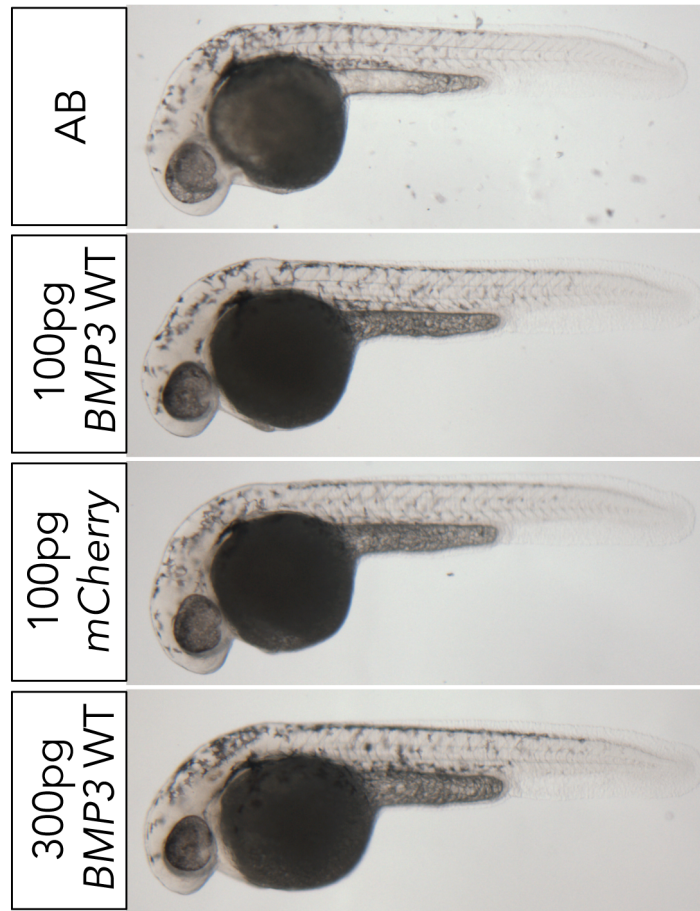


Fig. 6.3: Expression of wild type *BMP3* mRNA in zebrafish embryos does not cause detectable morphological phenotypes at 28-30 hpf. Wild type (AB) single-cell embryos were injected with 100 pg of either *BMP3* or *mCherry* mRNA to control for non-specific injection effects, allowed to develop to 28-30 hpf, anesthetized and laterally imaged to assess overall morphology. A large dose of 300 pg *BMP3* mRNA similarly does not cause detectable phenotypes. Representative embryos for each group are shown (n=15 minimum per group, N=1).

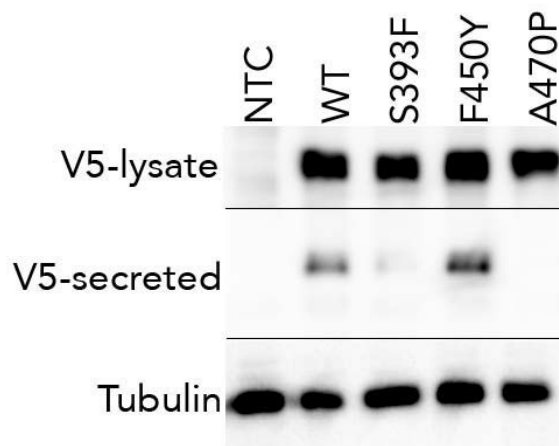


Fig. 6.4: Two of three identified BMP3 variant proteins show reduced or lost secretion from cells *in vitro*. Cos7 cells were transfected with equal amounts of plasmid DNA encoding V5-tagged BMP3 wild type or variant proteins. Protein isolates from cell lysates (top; V5-lysate) were probed for the V5 tag and indicate all BMP3 proteins are made in approximately equal amounts. Protein isolates from culture media (middle; V5-secreted), however, indicate S393F secretion is markedly reduced and secretion of A470P is not detectable. Tubulin, loading control; NTC, no transfection control. All experiments were performed at least three times.

```

ATGGATCGCTGTCAGCGGGCTGTTGTCCTCCTGGGATCGGGTATCTGTGCTGTGGA 60
ATGGATCGCTGTCAGCGGGCTGTTGTCCTCCTGGGATCGGGTATCTGTGCTGTGGA 60
*****

TACTGTGCTGTGCTTAAACGCCTGTTCATGGGTTCTCTAAAGATGTGCAACTTGGACAA 120
TACTGTGCTGTGCTTAAACGCCTGTTCATGGGTTCTCTAAAGATGTGCAACTTGGACAA 120
*****

AARGCAGAAGGCCAGAGAGCAGCAAGTGAAGAGAGCGAGCAGGATACGCTGTCTAGAG 180
AARGCAGAAGGCCAGAGAGCAGCAAGTGAAGAGAGCGAGCAGGATACGCTGTCTAGAG 180
*****

CACATGCAGATGCTTACGCCAAATACACCAGCGGGGATTCCTCTCAAAGACGGAAC 240
CACATGCAGATGCTTACGCCAAATACACCAGCGGGGATTCCTCTCAAAGACGGAAC 240
*****

ACTGTCCGAGCTTCAAGGGCCATTTGGGAACCATCAACAATAGGCAGTTGCAGATCTTT 300
ACTGTCCGAGCTTCAAGGGCCATTTGGGAACCATCAACAATAGGCAGTTGCAGATCTTT 300
*****

AACCTCACATCCCTCACCAGTCTGAAGATGTTCTCTCAGCGACGCTGCACACTACTATT 360
AACCTCACATCCCTCACCAGTCTGAAGATGTTCTCTCAGCGACGCTGCACACTACTATT 360
*****

GGTATCTTCAACAGCAGCCACAGATGCTCAAAACACAAGAGCTGTGCTCAACACAAC 420
GGTATCTTCAACAGCAGCCACAGATGCTCAAAACACAAGAGCTGTGCTCAACACAAC 420
*****

CTCAGAAGACAAGCTCACGTTACCTTGACGCTGGAGCTTCAGCTTAGTGAAAAACACA 480
CTCAGAAGACAAGCTCACGTTACCTTGACGCTGGAGCTTCAGCTTAGTGAAAAACACA 480
*****

ACTAGAACCATCGGCCATTTTCCAATCAACATCTCCACGATGCACCTGGGACTTCATATCA 540
ACTAGAACCATCGGCCATTTTCCAATCAACATCTCCACGATGCACCTGGGACTTCATATCA 540
*****

TGCGAGTGGAAAGACATCACTCGTGTGGTCAACCAAGCCAAGCATCACGACCAGCTCCTC 600
TGG---GGAAAGACATCACTCGTGTGGTCAACCAAGCCAAGCATCACGACCAGCTCCTC 597
***

ATAGGCATTAACATCAACTCCAGAGGGCCACCAACCCTGGAAGAACTCTTGTCTAGACCGA 660
ATAGGCATTAACATCAACTCCAGAGGGCCACCAACCCTGGAAGAACTCTTGTCTAGACCGA 657
*****

TCCACCCCTCAGAGACACAAAAGCAGACTGTTGCCAATCTTCATATGCTGGAATCGCAT 780
TCCACCCCTCAGAGACACAAAAGCAGACTGTTGCCAATCTTCATATGCTGGAATCGCAT 777
*****

AACCACAAGCATCCGCACAACATCGAAGCAGAGTCCACCAACATCCTCCTCCACTG 840
AACCACAAGCATCCGCACAACATCGAAGCAGAGTCCACCAACATCCTCCTCCACTG 836
*****

CAGAACATGAGCTCCAGGTCCAGAGTACCCCTTATGAGATCCCACATGGGATGAGGCC 900
---GAACAATGAGCTCCAGGTCCAGAGTACCCCTTATGAGATCCCACATGGGATGAGGCC 889
*****

AGCCCTTATGATCCGATGGAGAGCAAACCTGCAAGCGGCCCCCAAGAAGCCTCGCAAG 960
AGCCCTTATGATCCGATGGAGAGCAAACCTGCAAGCGGCCCCCAAGAAGCCTCGCAAG 949
*****

AACCACGACACAAGAACCCTCCTGCAGTTCGATGAGCAGACCATTAATAAAGCTCGC 1020
AACCACGACACAAGAACCCTCCTGCAGTTCGATGAGCAGACCATTAATAAAGCTCGC 1009
*****

AAGAAGCAGTGGAAACGAGCCAGGAAGTGTCTCGCAGATATTTAAAGTGGACTTCGCT 1080
AAGAAGCAGTGGAAACGAGCCAGGAAGTGTCTCGCAGATATTTAAAGTGGACTTCGCT 1069
*****

GATATCGGCTGGAGCGAGTGGATTATCTCACCAAGCTGTTTATGCGTATTACTGTTCT 1140
GATATCGGCTGGAGCGAGTGGATTATCTCACCAAGCTGTTTATGCGTATTACTGTTCT 1129
*****

GGATCATGTCAGTTCCTCCATGCCAAGTCTCTGAAACCTTCCAATCACGCCACCATTAG 1200
GGATCATGTCAGTTCCTCCATGCCAAGTCTCTGAAACCTTCCAATCACGCCACCATTAG 1189
*****

AGCATCGTGGGGCAGTGGTGTGGTCCGGGCATCCCGAGCCCTGTGTGCCCCGAA 1260
AGCATCGTGGGGCAGTGGTGTGGTCCGGGCATCCCGAGCCCTGTGTGCCCCGAA 1249
*****

AAGATGTCATCCCTAAGCATTCTCTCTTCGACGAGACAAGAAGTGGTCTCCTAAGGTC 1320
AAGATGTCATCCCTAAGCATTCTCTCTTCGACGAGACAAGAAGTGGTCTCCTAAGGTC 1309
*****

TACCCATAACATGACAGTGGACTCCTGCGCCTGTCGGTAA 1359
TACCCATAACATGACAGTGGACTCCTGCGCCTGTCGGTAA 1348
*****

```

Fig. 6.5: Zebrafish *bmp3*^{ua1020} coding sequence alignment with wild type. Mutants were generated by co-injecting three single guide RNAs (sgRNAs); all three sgRNA target sequences are shown with either a purple underline (if on the forward strand) or a green underline (if on the reverse strand). Alignment shows wild type *bmp3* sequence (top) and *bmp3*^{ua1020} mutant sequence (middle) with the nucleotide number within the coding sequence to the right. Orange boxes highlight each of the three deletions (c.544_546delCAG, c.840_842delGCA and c.887_891delCATGG). All additional single base changes were confirmed to be published polymorphisms with Ensembl. Alignments were generated using the ClustalOmega pair-wise alignment tool. *indicates invariant bases between the two sequences.



Fig. 6.6: The *bmp3*^{ua1020} mutation encodes a prematurely truncated peptide that lacks the entire TGFβ ligand domain. Mutants were generated by co-injecting Cas9 protein and three single guide RNAs (sgRNAs), shown in Fig. 6.5. The alignment shows wild type Bmp3 sequence (top) and Bmp3 p.Thr296GlyfsX2 mutant sequence (middle) and amino acid number of the pro-peptide to the right. Orange boxes highlight each of the upstream single residue deletions (p.Q182del, p.Q281del). The frameshift at T296 (blue box) results in an aberrant glycine, immediately followed by a stop codon. The TGFβ ligand domain is highlighted in purple. Alignments were generated using the ClustalOmega pair-wise alignment tool. *indicates invariant residues between the two peptide sequences.

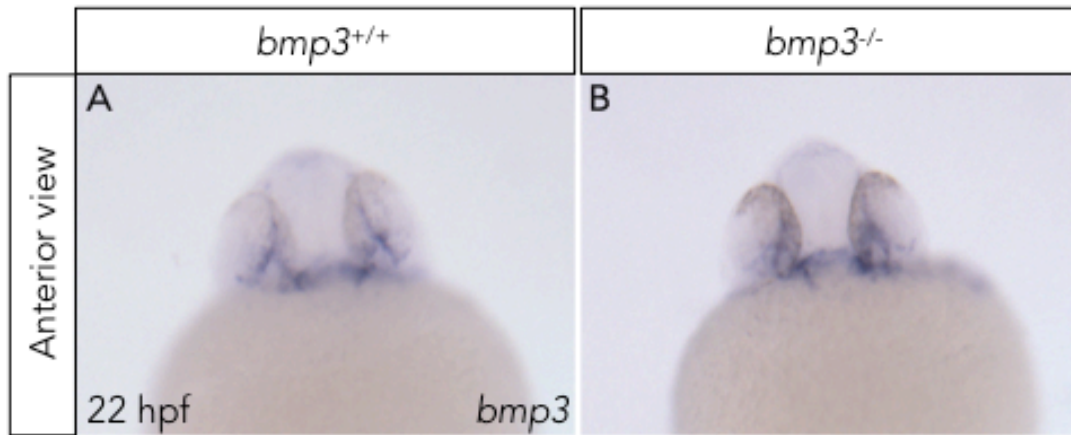


Fig. 6.7: *bmp3*^{ua1020} mutant transcript does not undergo nonsense-mediated decay. (A-B) In situ hybridization for *bmp3* mRNA was performed on 22 hpf embryos from a *bmp3*^{ua1020} heterozygous incross. Genomic DNA was extracted from each embryo after imaging and they were genotyped for *bmp3*. Embryos on the yolk were imaged in 3% methylcellulose on a dissecting microscope and are seen in anterior view. Representative images are shown; wild type, n=12; *bmp3*^{ua1020}, n=13.

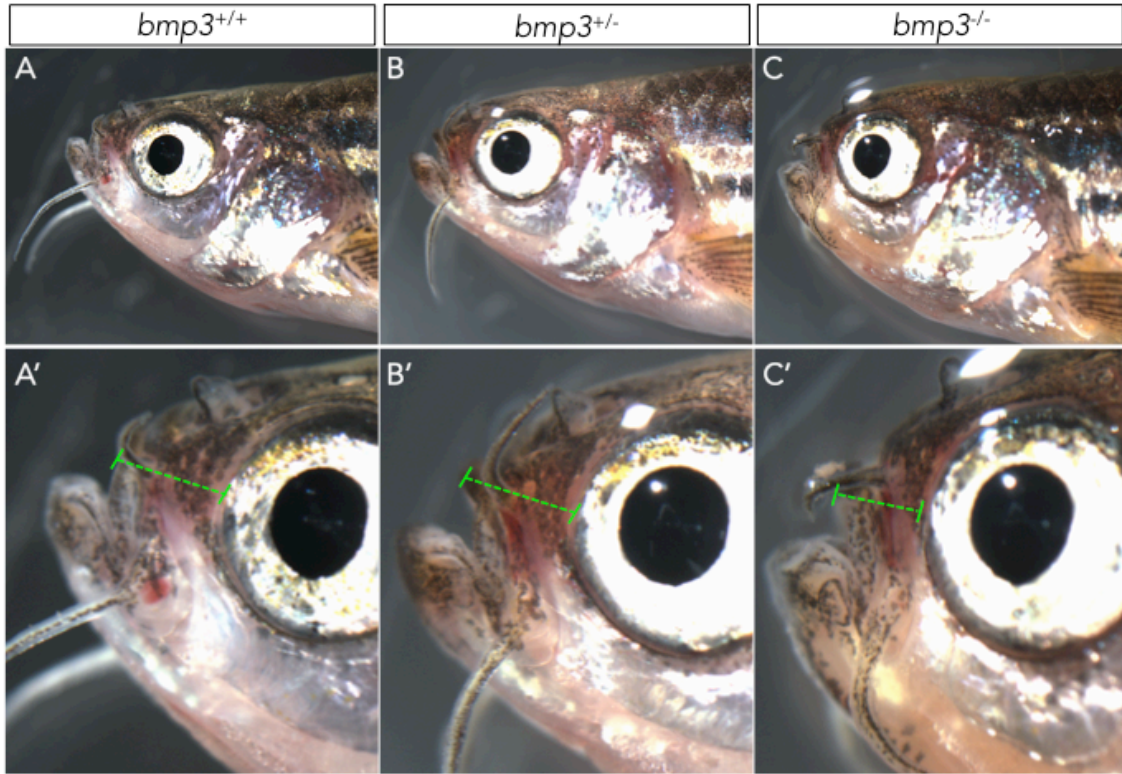


Fig. 6.8: Adult *bmp3^{ua1020}* mutant zebrafish display aberrant craniofacial shape. Representative adult that were previously fin clipped and genotyped as wild type (A,A'), *bmp3^{ua1020}* heterozygous (B,B') and *bmp3^{ua1020}* mutant (C,C') siblings. Fish were anesthetized at approximately 18 months old and imaged laterally on a dissecting microscope in fish water. The overall shape of the head appears to be less tapered in mutants compared to heterozygotes and wild type siblings (C, compare to A and B) and the length of the upper jaw is shortened (C', compare to A' and B'). The dotted line illustrates distance from the anterior margin of the eye to the distal tip of the upper jaw.

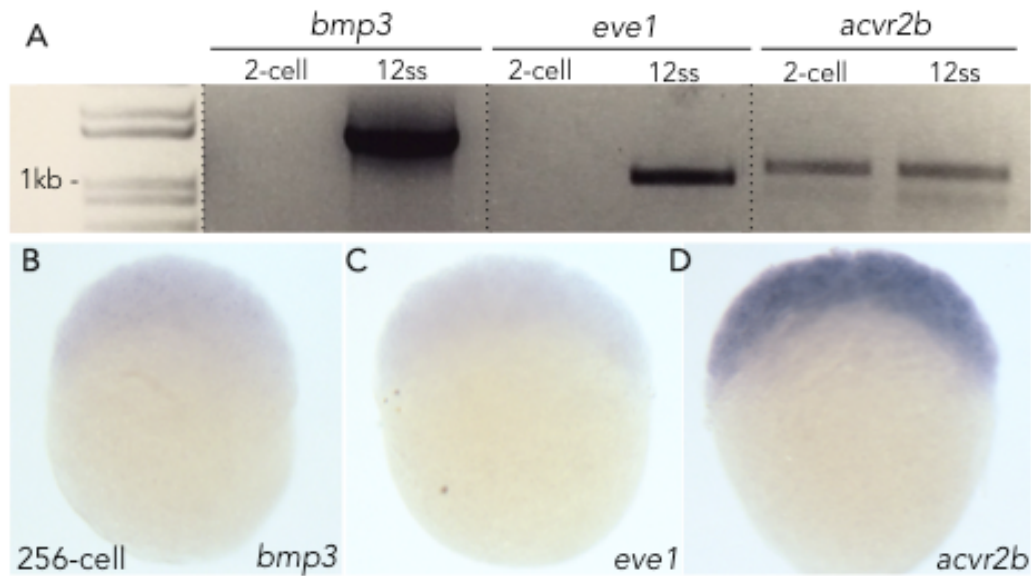


Fig. 6.9: *bmp3* is not maternally expressed in zebrafish. (A) RT-PCR was performed for *bmp3*, *even-skipped* (*eve1*; not maternally inherited control), and *activin receptor 2b* (*acvr2b*; maternally inherited control) using total RNA isolated from pools of either 2-cell or 12 somite stage (ss) wild type embryos. *bmp3* transcript is not detected in 2-cell RNA (before activation of the zygotic genome). (B-D) In situ hybridization for *bmp3* (B), *eve1* (C) or *acvr2b* (D) in 256-cell wild type embryos, confirming that *bmp3* is not expressed before the maternal to zygotic transition. In situs were performed on a minimum of 20 embryos for each probe.

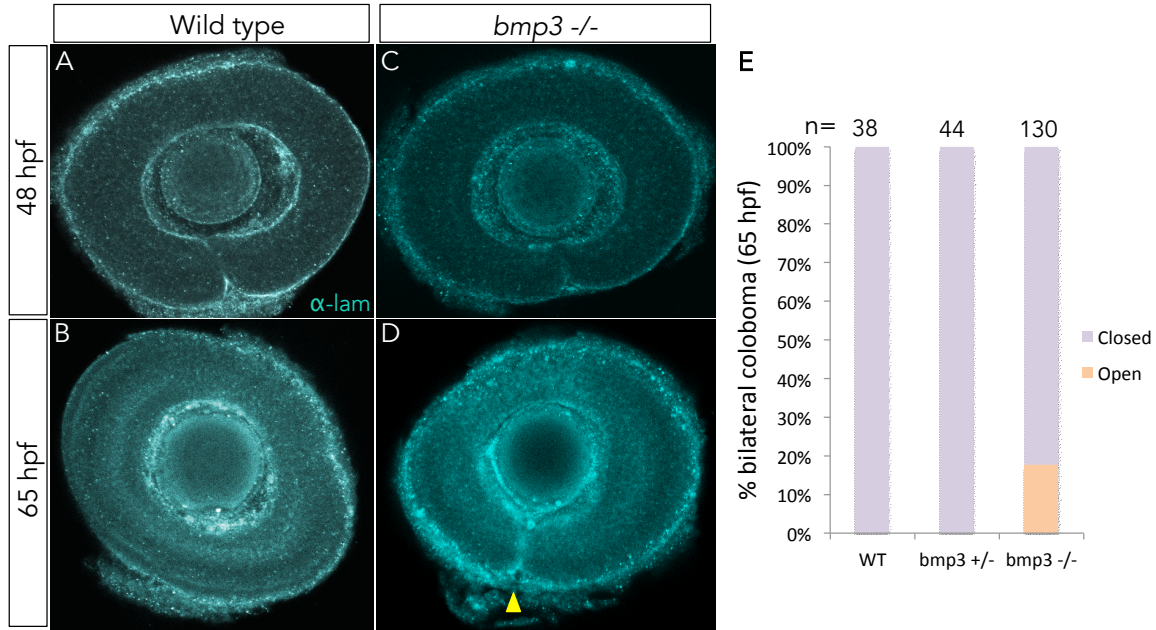


Fig. 6.10: *bmp3*^{ua1020} mutants show incompletely penetrant fissure closure defects. (A-D) Embryos from a *bmp3*^{ua1020} heterozygous incross were fixed at 48 hpf (A,C) and 65 hpf (B,D) and stained with anti-alpha-Laminin antibody. Eyes were dissected off and slide mounted in pairs and remaining tissue was used to extract genomic DNA for genotyping. Both wild type and *bmp3*^{ua1020} mutant eyes show apposed lobes but not fused fissures at 48 hpf (wild type, n=75/76; *bmp3*^{ua1020}, n=76/77). (E) At 65 hpf, 23/130 mutant larvae show bilateral fissures still present (yellow arrowhead), compared to 0/38 wild type and 0/44 heterozygous larvae.

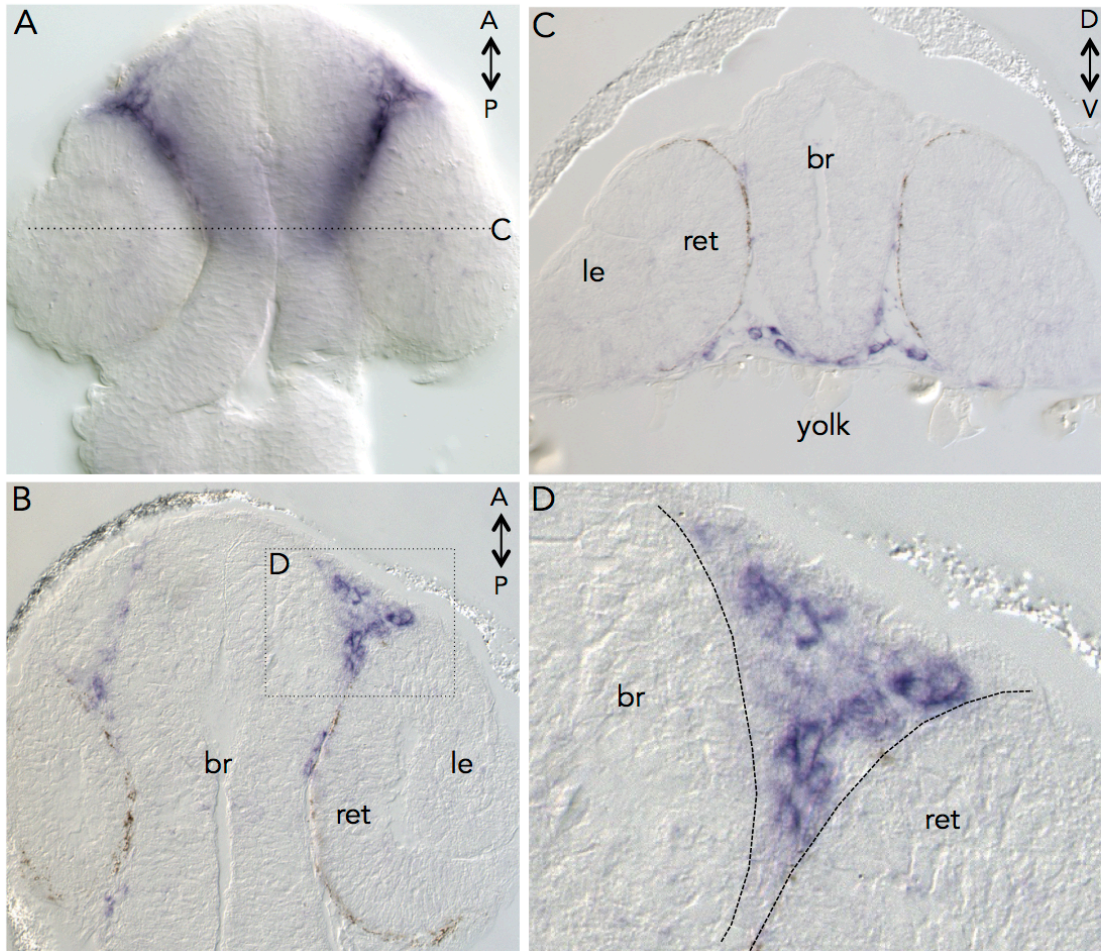


Fig. 6.11: Zebrafish *bmp3* is expressed in head mesenchyme during optic fissure formation. (A) DIC image of de-yolked and ventral mounted embryo in dorsal view, showing in situ hybridization for *bmp3* at 22 hpf. (B-D) DIC images of paraffin wax embedded and sectioned embryos at 22 hpf after in situ hybridization for *bmp3*. Staining can be seen in the head mesenchyme between the brain and eye in longitudinal section (B,D) and medial/ventral to the eye and ventral to the forebrain in cross section (C). Approximate location of the section plane in C is indicated in A, while boxed area in B indicates the enlarged area seen in D. Dotted lines in D indicate edges of the forebrain (left) and eye (right) epithelia where *bmp3* expression is absent. In all images, anterior or dorsal is up. br, brain; ret, retina; le, lens. Sections are 8 μ m thick.

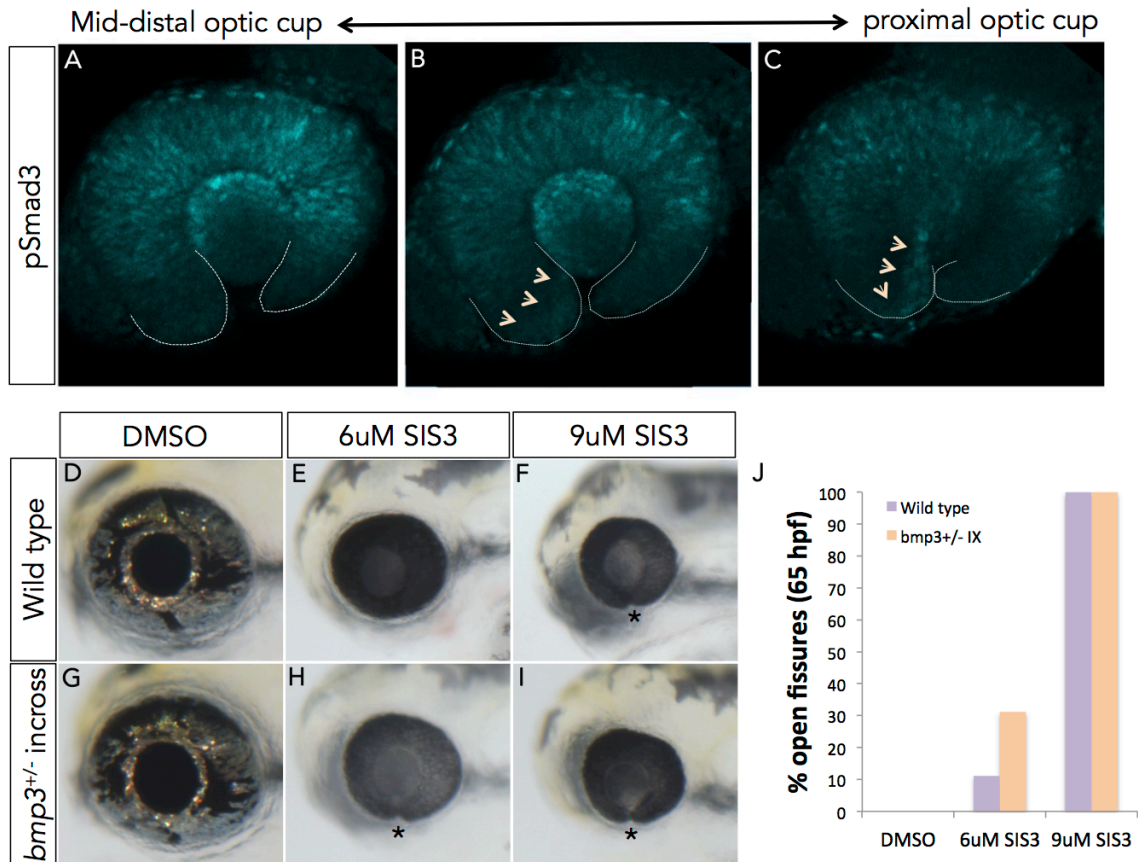


Fig. 6.12: pSmad3 signaling is active in the proximal ventral retina and partial pSmad3 inhibition synergizes with *bmp3^{ua1020}* mutant fissure closure phenotypes. (A-C) Representative wild type eye at 28 hpf stained for phosphorylated Smad3 (pSmad3; active form) showing optical slices through the mid-distal optic cup (A; through the anterior lens), mid-optic cup (B; through middle of lens) and proximal optic cup (C; through retina behind lens) in lateral view. Margins of the fissure lobes are outlined in white and arrowheads highlight faint beginnings of pSmad3 staining in (B) and pSmad3-labeled cells in the proximal nasal fissure lobe. (D-J) Pharmacological inhibition of pSmad3 in wild type (D-F) or *bmp3^{ua1020}* incross (G-I) embryos. Embryos were stage matched at tailbud, dechorionated and treated with the indicated solution from 24-30 hpf, and fixed at 65 hpf. Larvae were then visually scored for fissures on a dissecting microscope. Percent of embryos with bilateral coloboma is quantified in J (n=45 for each group; n=5/45 wild type larvae in 6 μM group with open fissures; n=14/45 *bmp3^{ua1020}* incross larvae in 6 μM group with open fissures). Error bars are not shown, as the experiment was only performed once. * = retained fissure present.

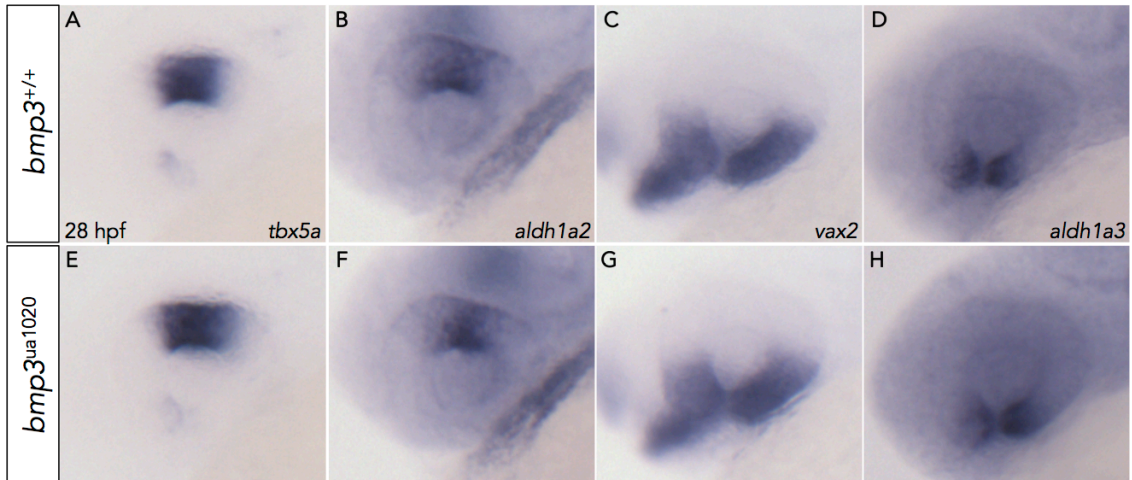


Fig. 6.13: *bmp3*^{ua1020} mutants do not have altered expression of dorsal or ventral marker genes. (A-H) In situ hybridization was performed for dorsal marker (*tbx5a* and *aldh1a2*) and ventral marker (*vax2* and *aldh1a3*) gene expression in wild type (A-D) and *bmp3*^{ua1020} mutant embryos (F-H) at 28 hpf. Embryos were imaged laterally in 3% methylcellulose on a dissecting microscope and then used for genomic DNA extraction and genotyping. Representative images are shown (n=25 for each probe).

6.4. Tables

Table 6.1: Candidate genes identified in a pedigree with coloboma. Exome sequencing of four affected and one unaffected family members was analyzed to include only non-synonymous variants that were not detected in control exome databases. SIFT and PolyPhen2 scores predict the likelihood that the listed variant disrupts protein function (most damaging score = 0 in SIFT, 1 in PolyPhen2).

Gene name	Amino acid variant	SIFT score	PolyPhen2 score
<i>BMP3</i>	A470P	0	1
<i>VPS72</i>	Y89C	0	0.992
<i>NLRC3</i>	R51W	0	0.998
<i>SARM1</i>	R230C	0	1
<i>SEMA5B</i>	R273H	0	0.992
<i>PDZD9</i>	Q104*	n/a	n/a
<i>TTC3</i>	P1239S	n/a	0.999
<i>ZNF658</i>	P657L	0	0.999
<i>MYH3</i>	D1178N	0.01	0.994
<i>CRYAA</i>	R96C	0	1

Table 6.2: BMP3 variants identified in a pedigree with coloboma and microphthalmia, and an unrelated cohort of patients with variable MAC. All affected individuals in the pedigree outlined in Fig. 6.1 were found to be heterozygous for G1408C (A470P). Additional variants (C1178T and T1349A, S393F and F450Y) were found in unrelated patients in the cohort. **(Top)** PolyPhen2 scores are shown (most damaging score = 1) and are recapitulated by MutationTaster predictions, suggesting all three variants are likely to cause disease (p-values close to one indicate high security of prediction). M=microphthalmia, BC=bilateral coloboma, UCM=unilateral colobomatous microphthalmia, BCM=bilateral colobomatous microphthalmia, severe. **(Bottom)** The identified sequence variants are rare or not detected in control individuals, as well as genome databases combined from NHLBI (n=6503), 1000G (n=2504) and ExAC (n-values vary; 60145 minimum). n-values given represent number of individuals, not total number of alleles. All individuals in genome databases with T1349A (F450Y) were heterozygous.

CDS	Protein	PolyPhen	MutationTaster	Ocular phenotype
C1178T	S393F	1	Disease causing (p=0.99)	M
T1349A	F450Y	0.995	Disease causing (p=0.99)	BCM
G1408C	A470P	1	Disease causing (p=0.99)	UCM, BC

Prevalence of detection

CDS	Protein	Affected	Controls	Genome Databases
C1178T	S393F	1/154	0/192	0%
T1349A	F450Y	1/130	0/268	0.03%
G1408C	A470P	4/4	0/257	0%

Chapter 7

General discussion and future directions

7.1. Summary of findings

Work in this thesis has contributed to our understanding of how the Wnt and BMP signaling pathways contribute to, and are regulated during, vertebrate eye development. We defined a role for the known Wnt modulators secreted frizzled-related protein 1 and 5 (Sfrp1/5) in dose-dependent regulation of retinal canonical Wnt signaling. I performed analyses of embryos injected with both low and high doses of *sfrp5* mRNA that unexpectedly showed that at least Sfrp5 appears to have a Wnt-independent role directly regulating retinal BMP signaling. Sfrp1/5 regulate dorsal-ventral (DV) patterning of the developing eye, as we see changes to DV marker genes that suggest they somewhat surprisingly function to facilitate Wnt/BMP activity in the dorsal eye (Chapter 3).

We also expand our limited understanding of the roles of non-canonical Wnt/PCP signaling in eye morphogenesis by investigations of Frizzled-5 (Fzd5). Predominantly thought of as a receptor for Wnt/PCP signaling, we showed that Fzd5 may act on both the PCP and canonical Wnt pathways in the eye in a tissue-dependent context. We characterize a novel *FZD5* frameshift mutation in a large pedigree with coloboma that encodes a resulting protein that acts as a dominant negative receptor, able to bind ligands but not transduce a signal. This mutation represents the first report of a Wnt pathway member in a structural ocular disease (Chapter 4).

Through genetic analysis of patients with atypical coloboma and subsequent work in both model and non-model organisms, we describe a novel and highly transient structure in the dorsal eye termed the superior ocular sulcus, or superior fissure, and a rare disease that results from its failed closure, superior coloboma. We show that altering the carefully regulated balance between BMP and Shh signaling across the dorsal-ventral axis of the eye can interfere with timely formation and closure of the superior fissure, as well as the resulting vasculature that may use the superior fissure as a conduit to direct its growth (Chapter 5).

Lastly, we begin the characterization of a novel regulator of eye development, *Bmp3*. We identify three rare missense mutations in *BMP3* in a pedigree with coloboma and an unrelated cohort of patients with coloboma and/or microphthalmia and

anophthalmia. Our initial studies in *bmp3* mutant zebrafish suggest that Bmp3 function in eye development is at least partly conserved through evolution, and Bmp3 is likely acting through activation of TGF β signaling in the ventral retina (Chapter 6).

7.2. The complex nature of MAC disorders

Almost 40 genes have been implicated in human ocular coloboma, microphthalmia and anophthalmia (MAC) (reviewed in (Patel and Sowden, 2017)). However, fewer than half of patients with MAC have mutations in genes already implicated in causing this spectrum of diseases, which implies that many additional MAC-causing loci are yet to be identified. As we continue to expand this list of genes and investigate their various roles in eye development, we also gain an appreciation for the complexity and seemingly stochastic nature of MAC. The vast majority of implicated mutations have incomplete penetrance and variable expressivity; that is, the mutations do not always cause disease and when they do, the nature and severity may often vary. The variable expressivity is almost certainly in part due to the fact that MAC disorders have related etiology and exist on a spectrum of severity. Given that MAC commonly presents unilaterally (one eye, not both), there is very likely also an element of stochasticity in determining whether an eye in any given genetic and/or environmental context will develop disease or not.

A contributing factor to the variable expressivity and complexity of disease presentation is that some cases of MAC are likely multigenic (caused by a combination of multiple genetic lesions). For example, multiple *GDF3* missense variants have been associated with microphthalmia and coloboma (Ye et al., 2010). However, patients carrying the same *GDF3* allele may present with MAC or skeletal anomalies independently, or a combination of both. One explanation for cases such as this is that different phenotypes may reflect the presence or absence of mutations in the genetic background that create a patient who is “sensitized” to certain phenotypes. In support of this, one patient shown to have both MAC and skeletal phenotypes has family members in previous generations who share the same *GDF3* variant, but only present with skeletal anomalies (Ye et al., 2010). In an unrelated pedigree in the same study, both a patient and her mother carry the same *GDF3* variant, but the mother is asymptomatic. Situations such as these may be cases

where the patients with MAC carry additional sensitizing background mutations, while their relatives with the same *GDF3* variant do not.

In Chapter 5, we characterize a novel transient structure during eye development, the superior fissure, and a rare type of coloboma that results from its persistence past embryogenesis, superior coloboma. The occurrence of this disease is almost certainly multigenic, given its extreme rarity and the absence of genetic lesions shared across patients. The patient who was the primary focus of our study had promising compound heterozygous mutations in a gene encoding a retinoic acid synthesis enzyme (*CYP11B1*), but a lack of defects in the superior fissure in *cyp11b1* mutant zebrafish suggests that this alone is not causative of superior coloboma. This patient is also heterozygous for a mutation in a BMP receptor (*BMPRIA*), and while our analyses suggest that dorsal patterning cues in the eye such as BMP signaling do have roles in superior fissure formation and closure, reports of *BMPRIA* mutations in the literature do not describe any ocular phenotypes. However, given the known roles of BMP and retinoic acid signaling in eye development, it is plausible that mutations in both *CYP11B1* and *BMPRIA* could contribute to an embryo that is more sensitive than normal to superior fissure defects. In fact, this patient also carries variants in *FURIN* (able cleave BMP ligands prior to secretion), *HHIP* (interacts with Shh, which is crucial to oppose BMP signals during eye patterning), and several components of the extracellular matrix, which may require remodeling in order to close the superior fissure, as it does in the inferior fissure. These variants almost certainly do not cause superior coloboma individually, but the combined effect of the total mutational load may very well be causative.

Another layer of complexity in determining a genetic cause of MAC in humans is that studies in animal models tell us that vertebrates have an enormous capacity to overcome embryonic defects. For example, we show in Chapter 5 that delayed superior fissure closure is prevalent in *gdf6a* heterozygous zebrafish embryos, and even more so in homozygotes. However, very rarely do we see superior coloboma in *gdf6a* mutant adults. This exemplifies genes with strict requirements in the developing eye and, when mutated, cause highly penetrant embryonic or larvae ocular phenotypes that much less frequently manifest in disease. A similar pattern is seen in many animal models with inferior fissure

closure defects. For example, zebrafish with mutations in *talin1* (which encodes an actin cytoskeletal scaffold) were recently shown to have deficient breakdown of the basement membrane during choroid fissure fusion, similar to what is observed in *cloche* mutants, but neither mutation results in robust persistent fissures (James et al., 2016). As such, there is an important distinction that should be made between a *delay in* versus a *failure of* choroid and superior fissure closure that may be seen in animal models. This is likely also reflected in *bmp3*^{ua1020} mutant zebrafish described in Chapter 6, where partially penetrant fissure closure defects in homozygous larvae are seen, but no *bmp3*^{ua1020} adults have yet been observed with coloboma phenotypes.

7.3. The importance of redundancy in development

There are many examples in the literature of multiple factors acting redundantly to accomplish a task during development. Because the main signaling pathways discussed in this thesis are used repeatedly to control the development of essentially every organ within the vertebrate body, it is perhaps unsurprising how frequently it is seen that multiple BMP and Wnt ligands act redundantly, as do their inhibitors. For example, BMP antagonists expressed in the mouse pharynx (*Chordin* and *Noggin*) are essential for proper development of structures derived from the first branchial arch, such as the jaws and multiple skull bones. Mice with mutations in either gene only have subtle changes in phenotype, but when even one copy of *Noggin* is mutant in a *Chordin* homozygous mutant background, phenotypes as severe as a complete lack of jaws are observed (Stottmann et al., 2001). This strategy of redundancy supports a more robust system that likely provides the animal a layer of insulation against disadvantageous embryonic phenotypes.

Work in this thesis adds to our understanding of how components of morphogen signaling pathways contribute to proper eye morphogenesis, as well as highlighting the importance of redundancy in this process. In Chapter 3, we tackle the question of how dorsal signals (Wnt and BMP signaling) are inhibited in the ventral eye in order to preserve proper balance of cellular identity across the dorsal-ventral (DV) axis in the retina. Alterations to DV patterning can cause incorrect retinotectal mapping, and are also

associated with ocular fissure closure defects (French et al., 2009; Gosse and Baier, 2009), but factors involved in effecting DV patterning are incompletely understood. Based on their known roles as Wnt modulators, we used zebrafish to investigate two secreted frizzled-related proteins (Sfrps) that are expressed in the ventral eye, *sfrp1* and *sfrp5*. Morpholino-mediated depletion of Sfrp1 or Sfrp5 independently fails to produce detectable eye phenotypes, but simultaneous Sfrp1/5 depletion results in strongly ventralized eyes and obvious fissure closure defects. While this result surprisingly suggests that Sfrp1/5 facilitate Wnt signaling instead of acting as ventral inhibitors, it highlights a tag-team effort of two proteins that appears to establish a backup of sorts if the activity of either one is lost. Cooperation of Sfrps in eye development appears to be important, as Sfrp1 instead acts redundantly with Sfrp2 in patterning the mouse optic cup (Esteve et al., 2011). We additionally show that at least Sfrp5 also has a novel, dose-dependent effect on regulating retinal BMP signaling, but it is unclear if this is a separate or redundant function with Sfrp1.

Multiple Wnt ligands are expressed in the developing zebrafish eye. Expression of *wnt11r* is found in the lens, while *wnt2* and *wnt8b* are expressed in the RPE and both signal to the dorsal eye to activate the canonical Wnt pathway, thereby maintain dorsal retinal identity (Veien et al., 2008). Depletion of *wnt2* and *wnt8b* alone or together causes mild decreases in dorsal marker gene expression, but multiple different methods of broadly inhibiting Wnt signaling (overexpression of an inhibitor, *Dkk1*, or expression of a dominant-repressive *TCF*) in the eye provide a more extreme response. This suggests that there are as yet unidentified Wnt ligands that can act redundantly with Wnt2/8b to pattern the eye. The number of redundantly-acting Wnt ligands has the potential to be quite high, as evidence from mouse suggests that surface ectoderm adjacent to the developing optic cup expresses at least 12 different Wnts (Carpenter et al., 2015).

The Frizzled (Fzd) receptors that Wnt ligands bind to activate signaling are not well characterized in the developing eye. Fzd5 is known to mediate Wnt/PCP signaling in specification of the eye field and formation of the optic vesicles (Cavodeassi et al., 2005) but PCP signaling is not thought to have a role in DV eye patterning. In Chapter 4, we describe a novel frameshift mutation in *FZD5* that encodes a truncated protein that can bind

Wnt ligands, but lacks the transmembrane and intracellular domains required to transmit a signal. Our cell culture experiments show the ability of truncated FZD5 to act as a secreted dominant negative receptor, its likely mechanism of pathogenicity, but interestingly it is able to do so on both the non-canonical and canonical Wnt pathways. This suggests that FZD5 has the capacity to bind at least one canonical Wnt ligand. If vertebrate Fzd5 does play a role in canonical Wnt signaling and DV patterning in the eye, it almost certainly does so redundantly with other receptors, as *fzd5* morphant zebrafish do not fully phenocopy a strong reduction in dorsal identity (for example, we do not see a prolonged superior fissure, like in *Sfrp1/5* depleted embryos).

Mutations in Wnt ligands or receptors have not previously been described to cause MAC. It is possible that the *FZD5* mutation we identify in Chapter 4 causes a disease phenotype in large part due to its potential ability to overwhelm ligand redundancy in the Wnt pathway during eye development. Dominant negative receptors in general frequently cause more extreme phenotypes since they can actively prevent signaling of multiple different ligands at once. Truncated FZD5 protein not only acts in a dominant negative fashion, but also may be able to do so to antagonize both canonical and non-canonical Wnt ligands. Therefore, the potential effect of a dominant negative FZD5 is astronomically high compared to mutations in one or two pathway components at a time.

In some cases, the redundancy can also exist between two or more tissues or cell types to control an important developmental step, though genetic/protein/tissue redundancies are certainly not mutually exclusive. This can be seen in *cloche* mutant zebrafish that entirely lack all periorbital mesenchyme (POM)-derived eye vasculature. Strong evidence suggests POM cells are required for tissue degradation, and the lack of POM consequently results in aberrant breakdown of the basal lamina between optic fissure lobes (Dhakal et al., 2015; James et al., 2016). Notably, despite the complete absence of POM, *cloche* mutants eventually recover and only suffer a delay in fissure closure. This suggests that POM or eye vasculature is not the only cell type or tissue required for basal lamina breakdown, and that POM-independent mechanisms exist with functionally redundant roles in tissue fusion.

Many zebrafish mutations fail to illicit a phenotype because the mutant transcript undergoes nonsense-mediated decay, thereby triggering a genomic compensatory response where related genes are upregulated and mask any role of the mutated gene (El-Brolosy and Stainier, 2017; Rossi et al., 2015). For mutations that do not undergo nonsense-mediated decay, and are therefore not likely candidates for genomic compensation, redundancy during development may account for absent or mild phenotypes. In Chapter 6, we describe the creation and initial characterization of *bmp3*^{ua1020} mutants with incompletely penetrant fissure closure defects that present as retained basal lamina at various positions along the ventral fissure. Importantly, *bmp3*^{ua1020} mutant transcript is not degraded in these animals. The nature of coloboma in these fish, in that the overall eye morphology appears to be normal when the fissure margins are fully apposed, suggests the underlying defect lies in the fusion process itself. In support of this, *bmp3*^{ua1020} mutants phenocopy the loss of genes such as *talin1*, which have been implicated in basement membrane breakdown at the fissure (James et al., 2016). Recent work describes specific requirements of a TGFβ signaling domain localized at the fissure margins for correct tissue fusion (Knickmeyer et al., 2018). Not only does Bmp3 predominantly act as a TGFβ ligand (Bahamonde and Lyons, 2001; Stewart et al., 2010), but a low dose of a pharmacological TGFβ inhibitor has synergistic effects with *bmp3*^{ua1020} mutants on fissure phenotypes. Taken together, we predict that Bmp3 activates TGFβ signaling at the ventral fissure to facilitate tissue fusion between the two lobes. If this model is correct, Bmp3 is very likely acting with at least partial redundancy with Tgfb2 and Tgfb3 (Knickmeyer et al., 2018). This could account for the low penetrance of retained fissures in *bmp3*^{ua1020} mutant larvae, the synergy with a low SIS3 dose, and the much more extreme ocular phenotype seen in larvae treated with a high SIS3 dose, as this would mimic the loss of all TGFβ ligands involved.

7.4. The importance of identifying factors downstream of morphogens

Significant research efforts across multiple decades have provided us a strong basis for understanding the roles of morphogen signaling pathways during eye development. While our understanding is far from complete, the major morphogen pathways involved in tissue specification, patterning and morphogenesis have largely been identified. In

comparison, our understanding of downstream factors is much more lacking. Research going forward should place a large emphasis on identification of the specific molecular regulators that carry out instructions imparted by precisely balanced morphogen signals. This will not only improve our understanding of vertebrate eye development but also give insights to the development of other organs, and subsequently disease, that involve common mechanisms.

Of particular relevance to this thesis, there is a need for the identification of factors that act to maintain boundaries between opposing morphogen gradients across axes within the eye. For example, BMP and/or Wnt activity is restricted to the dorsal eye, and likewise Shh to the ventral eye. A logical explanation is that regionally restricted transcription factors activated by BMPs and Shh, *tbx5a* and *vax2* respectively, mutually repress each other's expression, similar to what is seen in patterning of the nasal-temporal retina. Nasally expressed *foxg1* directly inhibits *foxd1* expression in the temporal retina and vice versa; as such, loss of one transcription factor causes a subsequent expansion of the other (Picker et al., 2009). However, this is not the case with *tbx5a* and *vax2*, as loss of either one does not cause expansion of the other suggesting that they do not reciprocally repress each other (French et al., 2009). A significant distance between ventral-most *tbx5a* and dorsal-most *vax2* expression, unlike *foxg1/d1* expression, also indicates an absence of direct interaction. Modifying the levels of BMP ligands expressed in the dorsal eye causes corresponding reduction/expansion in *vax2* expression, suggesting that factors downstream of BMP signaling, but upstream or independent of *tbx5a*, carry out repression of ventral identity.

Perhaps even more poorly understood are the molecular events leading to tissue fusion at the ocular fissure. Many studies implicate the inability to degrade the basal lamina between fissure lobes in delayed/failed fissure closure (Barbieri et al., 2002; See and Clagett-Dame, 2009) but few molecules have been directly implicated in the degradation process. Similarly, the molecular mechanisms of subsequent tissue fusion are incompletely understood, although probable roles for adhesion regulators such as N-cadherin (Erdmann et al., 2003; Masai et al., 2003) and Alpha-catenin (Chen et al., 2012) have been described. Such adhesion molecules may be regulated by TGF β signaling in the fissure margins

(Knickmeyer et al., 2018), but this is only speculation. Recently, the contribution of extraocular cells in mediating breakdown and fusion has gained attention. Matrix metalloproteinases secreted from macrophages in the mouse optic fissure may play an active role in basal lamina degradation (Tsuji et al., 2018). The direct requirement of periorbital mesenchyme (POM) in basal lamina breakdown has been inferred by the correlation of POM with degradation foci (Hero, 1990; Hero et al., 1991). Developments in zebrafish refine the model to specific POM-derived vascular endothelial cells (James et al., 2016) but specific factors involved are almost entirely unknown.

Future studies should examine the specific molecules at play in processes such as direct regulation of cell identity, basal lamina breakdown and tissue fusion. This will not only improve our understanding of eye development and disease, but that of structures that form through similar mechanisms. For example, the association between ocular and skeletal disease in patients with deficient BMP signaling has been discussed in the previous sections. Another such example is found in patients with Marfan syndrome (which results from an increase in TGF β signaling that pleiotropically affects connective tissues in the body) who also occasionally present with coloboma (LeBlanc et al., 2014). Most commonly (though not exclusively), patients with Marfan syndrome display lens coloboma; given that the developing lens does not form a ventral fissure, it is presently unclear whether this could represent a common TGF β deficiency in extracellular matrix regulation. In zebrafish, *tgfb2* and *tgfb3* are expressed in close proximity to the ventral retinal TGF β signaling domain and are also required in other models for fusion events in the palate that mechanistically resemble ocular fissure closure (Proetzel et al., 1995; Sanford et al., 1997; Taya et al., 1999). Unsurprisingly, cleft palate and lip are one of the more common extraocular phenotypes associated with coloboma, and work in one system will therefore likely inform the other. Mechanistically, podosomes and invadosomes are involved in basal lamina breakdown in a number of different contexts (Murphy and Courtneidge, 2011; van den Dries et al., 2014) and therefore warrant future study in regulation of the ocular fissure.

7.5. Future analysis of combined effects in specific mutation cocktails

As discussed in previous sections, complex and variable presentation of MAC disease is at least partly rooted in their multifactorial and/or multigenic nature, as well as the prevalence of redundancy in developmental checks and balances. Any genes that have strong association with MAC have likely been identified since their detection is much more straightforward. Logically, we can assume that the majority of coloboma-causing loci that remain to be identified will have more subtle influences and therefore require more precise analyses.

One approach to take is to analyze the combined effects of multiple mutations that do not cause disease individually, but together perturb the biological system enough to result in MAC. Improvements in our ability to generate large datasets aimed at identifying loci that correlate with a particular disease will facilitate the identification of candidate variants. But perhaps more importantly, the advances made in targeted genome editing could allow for *in vivo* testing of the combined effect of specific alleles detected in patients of interest. The CRISPR-Cas9 system in zebrafish has seen so much optimization in recent years that targeted knock-ins are now almost commonplace (Albadri et al., 2017; Prykhozhij and Berman, 2018; Prykhozhij et al., 2018), including introducing specific point mutations to recapitulate those found in a patient. The lack of evolutionary conservation at the amino acid level in many proteins may present challenges in trying to model specific mutations in the endogenous zebrafish genome, but functional conservation may still be high enough in many cases to test the effects of point mutations *in vivo* by using CRISPRs to instead perform whole gene replacement with and without inclusion of the variant.

A greater appreciation for more subtle contributions to MAC disorders will be crucial in implicating additional genes in this disease spectrum. It will also likely have subsequent applications in future treatments of diseases both within and outside of the eye with common underlying mechanisms, as well as recurrence predictions and prevention.

Literature Cited

Ablain, J., Zon, L.I., 2013. Of fish and men: using zebrafish to fight human diseases. *Trends in Cell Biology* 23, 584-586.

Abouzeid, H., Boisset, G., Favez, T., Youssef, M., Marzouk, I., Shakankiry, N., Bayoumi, N., Descombes, P., Agosti, C., Munier, F.L., 2011. Mutations in the SPARC-related modular calcium-binding protein 1 gene, SMOC1, cause waardenburg anophthalmia syndrome. *The American Journal of Human Genetics* 88, 92-98.

Abouzeid, H., Favez, T., Schmid, A., Agosti, C., Youssef, M., Marzouk, I., El Shakankiry, N., Bayoumi, N., Munier, F.L., Schorderet, D.F., 2014. Mutations in ALDH 1 A 3 Represent a Frequent Cause of Microphthalmia/Anophthalmia in Consanguineous Families. *Human mutation* 35, 949-953.

Abouzeid, H., Meire, F.M., Osman, I., ElShakankiri, N., Bolay, S., Munier, F.L., Schorderet, D.F., 2009. A new locus for congenital cataract, microcornea, microphthalmia, and atypical iris coloboma maps to chromosome 2. *Ophthalmology* 116, 154-162. e151.

Adler, R., Belecky-Adams, T.L., 2002. The role of bone morphogenetic proteins in the differentiation of the ventral optic cup. *Development* 129, 3161.

Adler, R., Canto-Soler, M.V., 2007. Molecular mechanisms of optic vesicle development: Complexities, ambiguities and controversies. *Developmental Biology* 305, 1-13.

Ahmed, M.I., Mardaryev, A.N., Lewis, C.J., Sharov, A.A., Botchkareva, N.V., 2011. MicroRNA-21 is an important downstream component of BMP signalling in epidermal keratinocytes. *J Cell Sci* 124, 3399-3404.

Albadri, S., Del Bene, F., Revenu, C., 2017. Genome editing using CRISPR/Cas9-based knock-in approaches in zebrafish. *Methods* 121, 77-85.

Albertson, R.C., Payne-Ferreira, T.L., Postlethwait, J., Yelick, P.C., 2005. Zebrafish *acvr2a* and *acvr2b* exhibit distinct roles in craniofacial development. *Developmental Dynamics* 233, 1405-1418.

Aldahmesh, M., Khan, A., Hijazi, H., Alkuraya, F., 2013. Mutations in ALDH1A3 cause microphthalmia. *Clinical genetics* 84, 128-131.

Allendorph, G.P., Isaacs, M.J., Kawakami, Y., Izpisua Belmonte, J.C., Choe, S., 2007. BMP-3 and BMP-6 Structures Illuminate the Nature of Binding Specificity with Receptors^{†,‡}. *Biochemistry* 46, 12238-12247.

Amarnath, S., Agarwala, S., 2017. Cell-cycle-dependent TGFβ–BMP antagonism regulates neural tube closure by modulating tight junctions. *J Cell Sci* 130, 119-131.

Andreazzoli, M., Gestri, G., Angeloni, D., Menna, E., Barsacchi, G., 1999. Role of *Xrx1* in *Xenopus* eye and anterior brain development. *Development* 126, 2451-2460.

Asai-Coakwell, M., French, C.R., Berry, K.M., Ye, M., Koss, R., Somerville, M., Mueller, R., van Heyningen, V., Waskiewicz, A.J., Lehmann, O.J., 2007. GDF6, a novel locus for a spectrum of ocular developmental anomalies. *The American Journal of Human Genetics* 80, 306-315.

Asai-Coakwell, M., French, C.R., Ye, M., Garcha, K., Bigot, K., Perera, A.G., Staehling-Hampton, K., Mema, S.C., Chanda, B., Mushegian, A., 2009. Incomplete penetrance and phenotypic variability characterize Gdf6-attributable oculo-skeletal phenotypes. *Human molecular genetics* 18, 1110-1121.

Asai-Coakwell, M., March, L., Dai, X.H., DuVal, M., Lopez, I., French, C.R., Famulski, J., De Baere, E., Francis, P.J., Sundaresan, P., 2013. Contribution of growth differentiation factor 6-dependent cell survival to early-onset retinal dystrophies. *Human molecular genetics* 22, 1432-1442.

Avsian-Kretchmer, O., Hsueh, A.J., 2004. Comparative genomic analysis of the eight-membered ring cystine knot-containing bone morphogenetic protein antagonists. *Molecular endocrinology* 18, 1-12.

Azuma, N., Yamaguchi, Y., Handa, H., Tadokoro, K., Asaka, A., Kawase, E., Yamada, M., 2003. Mutations of the PAX6 gene detected in patients with a variety of optic-nerve malformations. *The American Journal of Human Genetics* 72, 1565-1570.

Bahamonde, M.E., Lyons, K.M., 2001. BMP3: To Be or Not To Be a BMP. *The Journal of Bone & Joint Surgery* 83, S56-S62.

Bakrania, P., Efthymiou, M., Klein, J.C., Salt, A., Bunyan, D.J., Wyatt, A., Ponting, C.P., Martin, A., Williams, S., Lindley, V., Gilmore, J., Restori, M., Robson, A.G., Neveu, M.M., Holder, G.E., Collin, J.R.O., Robinson, D.O., Farndon, P., Johansen-Berg, H., Gerrelli, D., Ragge, N.K., 2008. Mutations in BMP4 Cause Eye, Brain, and Digit Developmental Anomalies: Overlap between the BMP4 and Hedgehog Signaling Pathways. *The American Journal of Human Genetics* 82, 304-319.

Barbieri, A.M., Broccoli, V., Bovolenta, P., Alfano, G., Marchitello, A., Mochetti, C., Crippa, L., Bulfone, A., Marigo, V., Ballabio, A., 2002. Vax2 inactivation in mouse determines alteration of the eye dorsal-ventral axis, misrouting of the optic fibres and eye coloboma. *Development* 129, 805-813.

Barbieri, A.M., Lupo, G., Bulfone, A., Andreazzoli, M., Mariani, M., Foucherousse, F., Consalez, G.G., Borsani, G., Beckmann, J.S., Barsacchi, G., 1999. A homeobox gene, vax2, controls the patterning of the eye dorsoventral axis. *Proceedings of the National Academy of Sciences* 96, 10729-10734.

Bardakjian, T., Krall, M., Wu, D., Lao, R., Tang, P.L.-F., Wan, E., Kopinsky, S., Schneider, A., Kwok, P.-y., Slavotinek, A., 2017. A recurrent, non-penetrant sequence variant, p. Arg266Cys in Growth/Differentiation Factor 3 (GDF3) in a female with unilateral anophthalmia and skeletal anomalies. *American journal of ophthalmology case reports* 7, 102-106.

Barrett, B.T., Bradley, A., Candy, T.R., 2013. The relationship between anisometropia and amblyopia. *Progress in retinal and eye research* 36, 120-158.

Bazin-Lopez, N., Valdivia, L.E., Wilson, S.W., Gestri, G., 2015. Watching eyes take shape. *Current opinion in genetics & development* 32, 73-79.

Beaulieu, C.L., Majewski, J., Schwartzenuber, J., Samuels, M.E., Fernandez, B.A., Bernier, F.P., Brudno, M., Knoppers, B., Marcadier, J., Dyment, D., 2014. FORGE Canada Consortium: outcomes of a 2-year national rare-disease gene-discovery project. *The American Journal of Human Genetics* 94, 809-817.

Begemann, G., Gibert, Y., Meyer, A., Ingham, P.W., 2002. Cloning of zebrafish T-box genes *tbx15* and *tbx18* and their expression during embryonic development. *Mechanisms of Development* 114, 137-141.

Behesti, H., Holt, J.K.L., Sowden, J.C., 2006. The level of BMP4 signaling is critical for the regulation of distinct T-box gene expression domains and growth along the dorso-ventral axis of the optic cup. *BMC Developmental Biology* 6, 62.

Beleggia, F., Li, Y., Fan, J., Elcioğlu, N.H., Toker, E., Wieland, T., Maumenee, I.H., Akarsu, N.A., Meitinger, T., Strom, T.M., Lang, R., Wollnik, B., 2015. CRIM1 haploinsufficiency causes defects in eye development in human and mouse. *Human molecular genetics* 24, 2267-2273.

Bhanot, P., Brink, M., Samos, C.H., Hsieh, J.-C., Wang, Y., Macke, J.P., Andrew, D., Nathans, J., Nusse, R., 1996. A new member of the frizzled family from *Drosophila* functions as a Wingless receptor. *Nature* 382, 225.

Bielen, H., Houart, C., 2012. BMP signaling protects telencephalic fate by repressing eye identity and its *Cxcr4*-dependent morphogenesis. *Developmental cell* 23, 812-822.

Billin, A.N., Thirlwell, H., Ayer, D.E., 2000. β -Catenin–histone deacetylase interactions regulate the transition of LEF1 from a transcriptional repressor to an activator. *Molecular and cellular biology* 20, 6882-6890.

Bodine, P.V., Zhao, W., Kharode, Y.P., Bex, F.J., Lambert, A.-J., Goad, M.B., Gaur, T., Stein, G.S., Lian, J.B., Komm, B.S., 2004. The Wnt antagonist secreted frizzled-related protein-1 is a negative regulator of trabecular bone formation in adult mice. *Molecular endocrinology* 18, 1222-1237.

Bogdanović, O., Delfino-Machín, M., Nicolás-Pérez, M., Gavilán, M.P., Gago-Rodrigues, I., Fernández-Miñán, A., Lillo, C., Ríos, R.M., Wittbrodt, J., Martínez-Morales, J.R., 2012. Numb/Numbl-Opo antagonism controls retinal epithelium morphogenesis by regulating integrin endocytosis. *Developmental cell* 23, 782-795.

Borello, U., Buffa, V., Sonnino, C., Melchionna, R., Vivarelli, E., Cossu, G., 1999. Differential expression of the Wnt putative receptors Frizzled during mouse somitogenesis. *Mechanisms of development* 89, 173-177.

- Bovolenta, P., Esteve, P., Ruiz, J.M., Cisneros, E., Lopez-Rios, J., 2008. Beyond Wnt inhibition: new functions of secreted Frizzled-related proteins in development and disease. *J Cell Sci* 121, 737-746.
- Bragdon, B., Moseychuk, O., Saldanha, S., King, D., Julian, J., Nohe, A., 2011. Bone Morphogenetic Proteins: A critical review. *Cellular Signalling* 23, 609-620.
- Brazil, D.P., Church, R.H., Surae, S., Godson, C., Martin, F., 2015. BMP signalling: agony and antagonism in the family. *Trends in Cell Biology* 25, 249-264.
- Bueno, J.L., Ynigo, M., de Miguel, C., Gonzalo-Daganzo, R.M., Richart, A., Vilches, C., Regidor, C., García-Marco, J.A., Flores-Ballester, E., Cabrera, J.R., 2016. Growth differentiation factor 11 (GDF11) – a promising anti-ageing factor – is highly concentrated in platelets. *Vox Sanguinis* 111, 434-436.
- Burns, C.J., Zhang, J., Brown, E.C., Van Bibber, A.M., Van Es, J., Clevers, H., Ishikawa, T.o., Taketo, M.M., Vetter, M.L., Fuhrmann, S., 2008. Investigation of Frizzled-5 during embryonic neural development in mouse. *Developmental Dynamics* 237, 1614-1626.
- Butler, M.T., Wallingford, J.B., 2017. Planar cell polarity in development and disease. *Nature Reviews Molecular Cell Biology* 18, 375.
- Cai, Z., Tao, C., Li, H., Ladher, R., Gotoh, N., Feng, G.-S., Wang, F., Zhang, X., 2013. Deficient FGF signaling causes optic nerve dysgenesis and ocular coloboma. *Development* 140, 2711-2723.
- Carl, M., Loosli, F., Wittbrodt, J., 2002. Six3 inactivation reveals its essential role for the formation and patterning of the vertebrate eye. *Development* 129, 4057-4063.
- Carmon, K.S., Loose, D.S., 2008. Secreted frizzled-related protein 4 regulates two Wnt7a signaling pathways and inhibits proliferation in endometrial cancer cells. *Molecular cancer research* 6, 1017-1028.
- Carmon, K.S., Loose, D.S., 2010. Development of a bioassay for detection of Wnt-binding affinities for individual frizzled receptors. *Analytical biochemistry* 401, 288-294.
- Carpenter, A.C., Smith, A.N., Wagner, H., Cohen-Tayar, Y., Rao, S., Wallace, V., Ashery-Padan, R., Lang, R.A., 2015. Wnt ligands from the embryonic surface ectoderm regulate 'bimetallic strip' optic cup morphogenesis in mouse. *Development* 142, 972.
- Casari, A., Schiavone, M., Facchinello, N., Vettori, A., Meyer, D., Tiso, N., Moro, E., Argenton, F., 2014. A Smad3 transgenic reporter reveals TGF-beta control of zebrafish spinal cord development. *Developmental Biology* 396, 81-93.
- Cavodeassi, F., Carreira-Barbosa, F., Young, R.M., Concha, M.L., Allende, M.L., Houart, C., Tada, M., Wilson, S.W., 2005. Early Stages of Zebrafish Eye Formation Require the Coordinated Activity of Wnt11, Fz5, and the Wnt/ β -Catenin Pathway. *Neuron* 47, 43-56.

Cavodeassi, F., Ivanovitch, K., Wilson, S.W., 2013. Eph/Ephrin signalling maintains eye field segregation from adjacent neural plate territories during forebrain morphogenesis. *Development* 140, 4193-4202.

Cermak, T., Doyle, E.L., Christian, M., Wang, L., Zhang, Y., Schmidt, C., Baller, J.A., Somia, N.V., Bogdanove, A.J., Voytas, D.F., 2011. Efficient design and assembly of custom TALEN and other TAL effector-based constructs for DNA targeting. *Nucleic acids research* 39, e82-e82.

Chambers, D., Wilson, L., Maden, M., Lumsden, A., 2007. RALDH-independent generation of retinoic acid during vertebrate embryogenesis by CYP1B1. *Development* 134, 1369-1383.

Chang, C., Hemmati-Brivanlou, A., 1999. *Xenopus* GDF6, a new antagonist of noggin and a partner of BMPs. *Development* 126, 3347-3357.

Chang, L., Blain, D., Bertuzzi, S., Brooks, B.P., 2006. Uveal coloboma: clinical and basic science update. *Current opinion in ophthalmology* 17, 447-470.

Chawla, B., Schley, E., Williams Antionette, L., Bohnsack Brenda, L., 2016. Retinoic Acid and Pitx2 Regulate Early Neural Crest Survival and Migration in Craniofacial and Ocular Development. *Birth Defects Research Part B: Developmental and Reproductive Toxicology* 107, 126-135.

Chawla, B., Swain, W., Williams, A.L., Bohnsack, B.L., 2018. Retinoic Acid Maintains Function of Neural Crest-Derived Ocular and Craniofacial Structures in Adult Zebrafish. *Investigative Ophthalmology & Visual Science* 59, 1924-1935.

Chen, S., Lewis, B., Moran, A., Xie, T., 2012. Cadherin-Mediated Cell Adhesion Is Critical for the Closing of the Mouse Optic Fissure. *PLoS ONE* 7, e51705.

Chen, Z., Battinelli, E., Fielder, A., Bunday, S., Sims, K., Breakefield, X., Craig, I., 1993. A mutation in the norrie disease gene (ndp) associated with x-linked familial exudative vitreoretinopathy. *Nature genetics* 5, 180.

Chiang, C., Litingtung, Y., Lee, E., Young, K.E., Corden, J.L., Westphal, H., Beachy, P.A., 1996. Cyclopia and defective axial patterning in mice lacking Sonic hedgehog gene function. *Nature* 383, 407.

Choi, J., Dong, L., Ahn, J., Dao, D., Hammerschmidt, M., Chen, J.-N., 2007. FoxH1 negatively modulates flk1 gene expression and vascular formation in zebrafish. *Developmental biology* 304, 735-744.

Chow, R.L., Lang, R.A., 2001. Early eye development in vertebrates. *Annual review of cell and developmental biology* 17, 255-296.

Chuang, J.C., Raymond, P.A., 2001. Zebrafish genes rx1 and rx2 help define the region of forebrain that gives rise to retina. *Developmental biology* 231, 13-30.

- Collery, R.F., Link, B.A., 2011. Dynamic smad-mediated BMP signaling revealed through transgenic zebrafish. *Developmental Dynamics* 240, 712-722.
- Constam, D.B., 2014. Regulation of TGF β and related signals by precursor processing. *Seminars in Cell & Developmental Biology* 32, 85-97.
- Creuzet, S., Vincent, C., Couly, G., 2005. Neural crest derivatives in ocular and periocular structures. *International journal of Developmental Biology* 49, 161-171.
- Danno, H., Michiue, T., Hitachi, K., Yukita, A., Ishiura, S., Asashima, M., 2008. Molecular links among the causative genes for ocular malformation: Otx2 and Sox2 coregulate Rax expression. *Proceedings of the National Academy of Sciences* 105, 5408-5413.
- Das, B.C., Thapa, P., Karki, R., Das, S., Mahapatra, S., Liu, T.-C., Torregroza, I., Wallace, D.P., Kambhampati, S., Van Veldhuizen, P., 2014. Retinoic acid signaling pathways in development and diseases. *Bioorganic & medicinal chemistry* 22, 673-683.
- de Caestecker, M., 2004. The transforming growth factor- β superfamily of receptors. *Cytokine & Growth Factor Reviews* 15, 1-11.
- De Robertis, E.M., 2006. Spemann's organizer and self-regulation in amphibian embryos. *Nature reviews Molecular cell biology* 7, 296.
- Dee, C.T., Szymoniuk, C.R., Mills, P.E.D., Takahashi, T., 2013. Defective neural crest migration revealed by a Zebrafish model of Alx1-related frontonasal dysplasia. *Human molecular genetics* 22, 239-251.
- den Hollander, A.I., Biyanwila, J., Kovach, P., Bardakjian, T., Traboulsi, E.I., Ragge, N.K., Schneider, A., Malicki, J., 2010. Genetic defects of GDF6 in the zebrafish out of sight mutant and in human eye developmental anomalies. *BMC genetics* 11, 102.
- Dhakal, S., Stevens, C.B., Sebbagh, M., Weiss, O., Frey, R.A., Adamson, S., Shelden, E.A., Inbal, A., Stenkamp, D.L., 2015. Abnormal retinal development in Cloche mutant zebrafish. *Developmental Dynamics* 244, 1439-1455.
- Dorsky, R.I., Sheldahl, L.C., Moon, R.T., 2002. A Transgenic Lef1/ β -Catenin-Dependent Reporter Is Expressed in Spatially Restricted Domains throughout Zebrafish Development. *Developmental Biology* 241, 229-237.
- Dudley, A.T., Lyons, K.M., Robertson, E.J., 1995. A requirement for bone morphogenetic protein-7 during development of the mammalian kidney and eye. *Genes & development* 9, 2795-2807.
- Duester, G., 2009. Keeping an eye on retinoic acid signaling during eye development. *Chemico-biological interactions* 178, 178-181.

Echelard, Y., Epstein, D.J., St-Jacques, B., Shen, L., Mohler, J., McMahon, J.A., McMahon, A.P., 1993. Sonic hedgehog, a member of a family of putative signaling molecules, is implicated in the regulation of CNS polarity. *Cell* 75, 1417-1430.

Egeland, T., Pinto, N., Vigeland, M.D., 2014. A general approach to power calculation for relationship testing. *Forensic Science International: Genetics* 9, 186-190.

Ekker, S.C., Ungar, A.R., Greenstein, P., von Kessler, D.P., Porter, J.A., Moon, R.T., Beachy, P.A., 1995. Patterning activities of vertebrate hedgehog proteins in the developing eye and brain. *Current Biology* 5, 944-955.

El-Brolosy, M.A., Stainier, D.Y., 2017. Genetic compensation: A phenomenon in search of mechanisms. *PLoS genetics* 13, e1006780.

England, S.J., Blanchard, G.B., Mahadevan, L., Adams, R.J., 2006. A dynamic fate map of the forebrain shows how vertebrate eyes form and explains two causes of cyclopia. *Development* 133, 4613-4617.

Eom, D.S., Amarnath, S., Fogel, J.L., Agarwala, S., 2011. Bone morphogenetic proteins regulate neural tube closure by interacting with the apicobasal polarity pathway. *Development* 138, 3179-3188.

Erdmann, B., Kirsch, F.P., Rathjen, F.G., Moré, M.I., 2003. N-Cadherin is essential for retinal lamination in the zebrafish. *Developmental dynamics: an official publication of the American Association of Anatomists* 226, 570-577.

Esteve, P., Sardonis, A., Ibañez, C., Shimono, A., Guerrero, I., Bovolenta, P., 2011. Secreted frizzled-related proteins are required for Wnt/ β -catenin signalling activation in the vertebrate optic cup. *Development* 138, 4179-4184.

Evans, A.L., Gage, P.J., 2005. Expression of the homeobox gene *Pitx2* in neural crest is required for optic stalk and ocular anterior segment development. *Human Molecular Genetics* 14, 3347-3359.

Fares-Taie, L., Gerber, S., Chassaing, N., Clayton-Smith, J., Hanein, S., Silva, E., Serey, M., Serre, V., Gérard, X., Baumann, C., 2013. *ALDH1A3* mutations cause recessive anophthalmia and microphthalmia. *The American Journal of Human Genetics* 92, 265-270.

Faucheux, C., Ulysse, F., Bareille, R., Reddi, A.H., Amédée, J., 1997. Opposing Actions of BMP3 and TGF β 1 in Human Bone Marrow Stromal Cell Growth and Differentiation. *Biochemical and Biophysical Research Communications* 241, 787-793.

FitzGerald, D.E., Chung, I., Krumholtz, I., 2005. An analysis of high myopia in a pediatric population less than 10 years of age. *Optometry-Journal of the American Optometric Association* 76, 102-114.

- Footz, T., Dubois, S., Sarfarazi, M., Raymond, V., Walter, M.A., 2011. Co-variation of ST11 and WDR36/UTP21 alters cell proliferation in a glaucoma model. *Mol Vis* 17, 1957-1969.
- Freeman, M., Gurdon, J., 2002. Regulatory principles of developmental signaling. *Annual review of cell and developmental biology* 18, 515-539.
- French, C.R., Erickson, T., French, D.V., Pilgrim, D.B., Waskiewicz, A.J., 2009. Gdf6a is required for the initiation of dorsal–ventral retinal patterning and lens development. *Developmental Biology* 333, 37-47.
- French, C.R., Stach, T.R., March, L.D., Lehmann, O.J., Waskiewicz, A.J., 2013. Apoptotic and proliferative defects characterize ocular development in a microphthalmic BMP model. *Investigative ophthalmology & visual science* 54, 4636-4647.
- Fuhrmann, S., 2010. Eye morphogenesis and patterning of the optic vesicle, *Current topics in developmental biology*. Elsevier, pp. 61-84.
- Fuhrmann, S., Levine, E.M., Reh, T.A., 2000. Extraocular mesenchyme patterns the optic vesicle during early eye development in the embryonic chick. *Development* 127, 4599-4609.
- Fujimura, N., 2016. WNT/ β -Catenin Signaling in Vertebrate Eye Development. *Frontiers in Cell and Developmental Biology* 4.
- Fujimura, N., Taketo, M.M., Mori, M., Korinek, V., Kozmik, Z., 2009. Spatial and temporal regulation of Wnt/ β -catenin signaling is essential for development of the retinal pigment epithelium. *Developmental biology* 334, 31-45.
- Gage, P.J., Rhoades, W., Prucka, S.K., Hjalt, T., 2005. Fate maps of neural crest and mesoderm in the mammalian eye. *Investigative ophthalmology & visual science* 46, 4200-4208.
- Gagnon, J.A., Valen, E., Thyme, S.B., Huang, P., Ahkmetova, L., Pauli, A., Montague, T.G., Zimmerman, S., Richter, C., Schier, A.F., 2014. Efficient Mutagenesis by Cas9 Protein-Mediated Oligonucleotide Insertion and Large-Scale Assessment of Single-Guide RNAs. *PLoS ONE* 9, e98186.
- Gamer, L.W., Cox, K., Carlo, J.M., Rosen, V., 2009. Overexpression of BMP3 in the developing skeleton alters endochondral bone formation resulting in spontaneous rib fractures. *Developmental Dynamics* 238, 2374-2381.
- Gamer, L.W., Nove, J., Levin, M., Rosen, V., 2005. BMP-3 is a novel inhibitor of both activin and BMP-4 signaling in *Xenopus* embryos. *Developmental Biology* 285, 156-168.
- Gerth-Kahlert, C., Williamson, K., Ansari, M., Rainger, J.K., Hingst, V., Zimmermann, T., Tech, S., Guthoff, R.F., van Heyningen, V., FitzPatrick, D.R., 2013. Clinical and mutation

analysis of 51 probands with anophthalmia and/or severe microphthalmia from a single center. *Molecular genetics & genomic medicine* 1, 15-31.

Gestri, G., Bazin-Lopez, N., Scholes, C., Wilson, S.W., 2018. Cell Behaviors during Closure of the Choroid Fissure in the Developing Eye. *Frontiers in Cellular Neuroscience* 12.

Gestri, G., Osborne, R., Wyatt, A., Gerrelli, D., Gribble, S., Stewart, H., Fryer, A., Bunyan, D., Prescott, K., Collin, J.R., Fitzgerald, T., Robinson, D., Carter, N., Wilson, S., Ragge, N., 2009. Reduced TFAP2A function causes variable optic fissure closure and retinal defects and sensitizes eye development to mutations in other morphogenetic regulators. *Hum Genet* 126, 791-803.

Golz, S., Lantin, C., Mey, J., 2004. Retinoic acid-dependent regulation of BMP4 and Tbx5 in the embryonic chick retina. *Neuroreport* 15, 2751-2755.

Gong, Y., Slee, R.B., Fukai, N., Rawadi, G., Roman-Roman, S., Reginato, A.M., Wang, H., Cundy, T., Glorieux, F.H., Lev, D., 2001. LDL receptor-related protein 5 (LRP5) affects bone accrual and eye development. *Cell* 107, 513-523.

Gosse, N.J., Baier, H., 2009. An essential role for Radar (Gdf6a) in inducing dorsal fate in the zebrafish retina. *Proceedings of the National Academy of Sciences* 106, 2236-2241.

Gregory-Evans, C.Y., Williams, M., Halford, S., Gregory-Evans, K., 2004. Ocular coloboma: a reassessment in the age of molecular neuroscience. *Journal of medical genetics* 41, 881-891.

Guex, N., Peitsch, M.C., 1997. SWISS-MODEL and the Swiss-Pdb Viewer: an environment for comparative protein modeling. *electrophoresis* 18, 2714-2723.

Hägglund, A.-C., Berghard, A., Carlsson, L., 2013. Canonical Wnt/ β -Catenin Signalling Is Essential for Optic Cup Formation. *PLoS ONE* 8, e81158.

Halfter, W., Von Boxberg, Y., 1992. Axonal growth on solubilized and reconstituted matrix from the embryonic chicken retina inner limiting membrane. *European Journal of Neuroscience* 4, 840-852.

Halilagic, A., Ribes, V., Ghyselinck, N.B., Zile, M.H., Dollé, P., Studer, M., 2007. Retinoids control anterior and dorsal properties in the developing forebrain. *Developmental Biology* 303, 362-375.

Hammerschmidt, M., Serbedzija, G.N., McMahon, A.P., 1996. Genetic analysis of dorsoventral pattern formation in the zebrafish: requirement of a BMP-like ventralizing activity and its dorsal repressor. *Genes & development* 10, 2452-2461.

Hanel, M.L., Hensey, C., 2006. Eye and neural defects associated with loss of GDF6. *BMC developmental biology* 6, 43.

- Hao, J., Ho, J.N., Lewis, J.A., Karim, K.A., Daniels, R.N., Gentry, P.R., Hopkins, C.R., Lindsley, C.W., Hong, C.C., 2010. In vivo structure– activity relationship study of dorsomorphin analogues identifies selective VEGF and BMP inhibitors. *ACS chemical biology* 5, 245-253.
- Hartsock, A., Lee, C., Arnold, V., Gross, J.M., 2014. In vivo analysis of hyaloid vasculature morphogenesis in zebrafish: A role for the lens in maturation and maintenance of the hyaloid. *Developmental biology* 394, 327-339.
- Heavner, W., Pevny, L., 2012. Eye development and retinogenesis. *Cold Spring Harbor perspectives in biology* 4, a008391.
- Heermann, S., Schütz, L., Lemke, S., Kriegelstein, K., Wittbrodt, J., 2015. Eye morphogenesis driven by epithelial flow into the optic cup facilitated by modulation of bone morphogenetic protein.
- Heinke, J., Juschkat, M., Charlet, A., Mnich, L., Helbing, T., Bode, C., Patterson, C., Moser, M., 2013. Antagonism and synergy between extracellular BMP modulators Tsg and BMPER balance blood vessel formation. *J Cell Sci* 126, 3082-3094.
- Henske, E.P., Józwiak, S., Kingswood, J.C., Sampson, J.R., Thiele, E.A., 2016. Tuberous sclerosis complex. *Nature reviews Disease primers* 2, 16035.
- Hero, I., 1990. Optic fissure closure in the normal cinnamon mouse. An ultrastructural study. *Investigative ophthalmology & visual science* 31, 197-216.
- Hero, I., Farjah, M., Scholtz, C.L., 1991. The prenatal development of the optic fissure in colobomatous microphthalmia. *Investigative ophthalmology & visual science* 32, 2622-2635.
- Hild, M., Dick, A., Rauch, G.J., Meier, A., Bouwmeester, T., Haffter, P., Hammerschmidt, M., 1999. The smad5 mutation somitabun blocks Bmp2b signaling during early dorsoventral patterning of the zebrafish embryo. *Development* 126, 2149.
- Hinck, A.P., Mueller, T.D., Springer, T.A., 2016. Structural Biology and Evolution of the TGF- β Family. *Cold Spring Harbor Perspectives in Biology* 8.
- Holly, V.L., Widen, S.A., Famulski, J.K., Waskiewicz, A.J., 2014. Sfrp1a and Sfrp5 function as positive regulators of Wnt and BMP signaling during early retinal development. *Developmental Biology* 388, 192-204.
- Hoppler, S., Brown, J.D., Moon, R.T., 1996. Expression of a dominant-negative Wnt blocks induction of MyoD in *Xenopus* embryos. *Genes & development* 10, 2805-2817.
- Hornby, S.J., Gilbert, C.E., Rahi, J., Sil, A.K., Xiao, Y., Dandona, L., Foster, A., 2000. Regional variation in blindness in children due to microphthalmos, anophthalmos and coloboma. *Ophthalmic epidemiology* 7, 127-138.

Hornby, S.J., Ward, S.J., Gilbert, C.E., Dandona, L., Foster, A., Jones, R.B., 2002. Environmental risk factors in congenital malformations of the eye. *Annals of tropical paediatrics* 22, 67-77.

Houart, C., Caneparo, L., Heisenberg, C.-P., Barth, K.A., Take-Uchi, M., Wilson, S.W., 2002. Establishment of the telencephalon during gastrulation by local antagonism of Wnt signaling. *Neuron* 35, 255-265.

Huang, J., Liu, Y., Filas, B., Gunhaga, L., Beebe, D.C., 2015. Negative and positive auto-regulation of BMP expression in early eye development. *Developmental Biology* 407, 256-264.

Huillard, E., Laugier, D., Marx, M., 2005. Defects in chicken neuroretina misexpressing the BMP antagonist *Drm/Gremlin*. *Developmental Biology* 283, 335-344.

Hyatt, G., Schmitt, E., Marsh-Armstrong, N., McCaffery, P., Drager, U., Dowling, J., 1996. Retinoic acid establishes ventral retinal characteristics. *Development* 122, 195-204.

Hyer, J., Kuhlman, J., Afif, E., Mikawa, T., 2003. Optic cup morphogenesis requires pre-lens ectoderm but not lens differentiation. *Developmental biology* 259, 351-363.

Iemura, S.-i., Yamamoto, T.S., Takagi, C., Uchiyama, H., Natsume, T., Shimasaki, S., Sugino, H., Ueno, N., 1998. Direct binding of follistatin to a complex of bone-morphogenetic protein and its receptor inhibits ventral and epidermal cell fates in early *Xenopus* embryo. *Proceedings of the National Academy of Sciences* 95, 9337-9342.

Ishikawa, T.-o., Tamai, Y., Zorn, A.M., Yoshida, H., Seldin, M.F., Nishikawa, S.-i., Taketo, M.M., 2001. Mouse Wnt receptor gene *Fzd5* is essential for yolk sac and placental angiogenesis. *Development* 128, 25-33.

Ito-Amano, M., Nakamura, Y., Morisaki, M., He, X., Hayashi, M., Watanapokasin, R., Kato, H., 2014. Temporal and Spatial Expression Patterns of Bone Morphogenetic Protein 3 in Developing Zebrafish. *The Open Rheumatology Journal* 8, 69-72.

Ittner, L., Wurdak, H., Schwerdtfeger, K., Kunz, T., Ille, F., Leveen, P., Hjalt, T., Suter, U., Karlsson, S., Hafezi, F., Born, W., Sommer, L., 2005. Compound developmental eye disorders following inactivation of TGFbeta signaling in neural-crest stem cells. *Journal of Biology* 4, 11.

Ivanovitch, K., Cavodeassi, F., Wilson, S.W., 2013. Precocious acquisition of neuroepithelial character in the eye field underlies the onset of eye morphogenesis. *Developmental cell* 27, 293-305.

Izumi, N., Mizuguchi, S., Inagaki, Y., Saika, S., Kawada, N., Nakajima, Y., Inoue, K., Suehiro, S., Friedman, S.L., Ikeda, K., 2006. BMP-7 Opposes TGF β 1-Mediated Collagen Induction in Mouse Pulmonary Myofibroblasts through Id2. *American Journal of Physiology-Lung Cellular and Molecular Physiology*.

- Jamaiyar, A., Wan, W., Janota, D.M., Enrick, M.K., Chilian, W.M., Yin, L., 2017. The versatility and paradox of GDF 11. *Pharmacology & Therapeutics* 175, 28-34.
- James, A., Lee, C., Williams, A.M., Angileri, K., Lathrop, K.L., Gross, J.M., 2016. The hyaloid vasculature facilitates basement membrane breakdown during choroid fissure closure in the zebrafish eye. *Developmental Biology* 419, 262-272.
- Jethani, J., Sharma, V.R., Marwah, K., 2009. Superior Lens Coloboma with Superior Rectus Palsy and Congenital Ptosis. *Journal of optometry* 2, 67-69.
- Kang, H., Louie, J., Weisman, A., Sheu-Gruttadauria, J., Davis-Dusenbery, B.N., Lagna, G., Hata, A., 2012. Inhibition of microRNA-302 (miR-302) by bone morphogenetic protein 4 (BMP4) facilitates the BMP signaling pathway. *Journal of Biological Chemistry* 287, 38656-38664.
- Kaufman, R., Weiss, O., Sebbagh, M., Ravid, R., Gibbs-Bar, L., Yaniv, K., Inbal, A., 2015. Development and origins of Zebrafish ocular vasculature. *BMC Developmental Biology* 15, 18.
- Khokha, M.K., Yeh, J., Grammer, T.C., Harland, R.M., 2005. Depletion of three BMP antagonists from Spemann's organizer leads to a catastrophic loss of dorsal structures. *Developmental cell* 8, 401-411.
- Kim, H.-S., Shin, J., Kim, S.-H., Chun, H.-S., Kim, J.-D., Kim, Y.-S., Kim, M.-J., Rhee, M., Yeo, S.-Y., Huh, T.-L., 2007. Eye field requires the function of *Sfrp1* as a Wnt antagonist. *Neuroscience letters* 414, 26-29.
- Kimmel, C.B., Ballard, W.W., Kimmel, S.R., Ullmann, B., Schilling, T.F., 1995. Stages of embryonic development of the zebrafish. *Developmental dynamics* 203, 253-310.
- Kishimoto, Y., Lee, K.-H., Zon, L., Hammerschmidt, M., Schulte-Merker, S., 1997. The molecular nature of zebrafish swirl: BMP2 function is essential during early dorsoventral patterning. *Development* 124, 4457-4466.
- Kitambi, S.S., McCulloch, K.J., Peterson, R.T., Malicki, J.J., 2009. Small molecule screen for compounds that affect vascular development in the zebrafish retina. *Mechanisms of development* 126, 464-477.
- Knickmeyer, M.D., Mateo, J.L., Eckert, P., Roussa, E., Rahhal, B., Zuniga, A., Krieglstein, K., Wittbrodt, J., Heermann, S., 2018. TGF β -facilitated optic fissure fusion and the role of bone morphogenetic protein antagonism. *Open Biology* 8.
- Kokabu, S., Gamer, L., Cox, K., Lowery, J., Tsuji, K., Raz, R., Economides, A., Katagiri, T., Rosen, V., 2012. BMP3 Suppresses Osteoblast Differentiation of Bone Marrow Stromal Cells via Interaction with *Acvr2b*. *Molecular Endocrinology* 26, 87-94.

- Koshiba-Takeuchi, K., Takeuchi, J.K., Matsumoto, K., Momose, T., Uno, K., Hoepker, V., Ogura, K., Takahashi, N., Nakamura, H., Yasuda, K., 2000. Tbx5 and the retinotectum projection. *Science* 287, 134-137.
- Kruse-Bend, R., Rosenthal, J., Quist, T.S., Veien, E.S., Fuhrmann, S., Dorsky, R.I., Chien, C.-B., 2012. Extraocular ectoderm triggers dorsal retinal fate during optic vesicle evagination in zebrafish. *Developmental Biology* 371, 57-65.
- Lagna, G., Hata, A., Hemmati-Brivanlou, A., Massagué, J., 1996. Partnership between DPC4 and SMAD proteins in TGF- β signalling pathways. *Nature* 383, 832.
- Lander, A.D., Nie, Q., Wan, F.Y., 2002. Do morphogen gradients arise by diffusion? *Developmental cell* 2, 785-796.
- Langenberg, T., Kahana, A., Wszalek, J.A., Halloran, M.C., 2008. The eye organizes neural crest cell migration. *Developmental Dynamics* 237, 1645-1652.
- LeBlanc, S.K., Taranath, D., Morris, S., Barnett, C.P., 2014. Multisegment coloboma in a case of Marfan syndrome: another possible effect of increased TGF β signaling. *Journal of American Association for Pediatric Ophthalmology and Strabismus* 18, 90-92.
- Lee, H.X., Ambrosio, A.L., Reversade, B., De Robertis, E., 2006. Embryonic dorsal-ventral signaling: secreted frizzled-related proteins as inhibitors of tolloid proteinases. *Cell* 124, 147-159.
- Lemke, G., Reber, M., 2005. Retinotectal mapping: new insights from molecular genetics. *Annu. Rev. Cell Dev. Biol.* 21, 551-580.
- Levine, A.J., Brivanlou, A.H., 2006. GDF3, a BMP inhibitor, regulates cell fate in stem cells and early embryos. *Development* 133, 209.
- Leyns, L., Bouwmeester, T., Kim, S.-H., Piccolo, S., De Robertis, E.M., 1997. Frzb-1 is a secreted antagonist of Wnt signaling expressed in the Spemann organizer. *Cell* 88, 747-756.
- Li, H., Tierney, C., Wen, L., Wu, J.Y., Rao, Y., 1997. A single morphogenetic field gives rise to two retina primordia under the influence of the prechordal plate. *Development* 124, 603.
- Li, J., Ma, X., Hu, Z., 2011. Lens coloboma and associated ocular malformations. *Eye Science* 2, 108-110.
- Li, Y., Rankin, S.A., Sinner, D., Kenny, A.P., Krieg, P.A., Zorn, A.M., 2008. Sfrp5 coordinates foregut specification and morphogenesis by antagonizing both canonical and noncanonical Wnt11 signaling. *Genes & development* 22, 3050-3063.
- Lieven, O., Rütter, U., 2011. The Dkk1 dose is critical for eye development. *Developmental Biology* 355, 124-137.

Lin, K., Wang, S., Julius, M.A., Kitajewski, J., Moos, M., Luyten, F.P., 1997. The cysteine-rich frizzled domain of Frzb-1 is required and sufficient for modulation of Wnt signaling. *Proceedings of the National Academy of Sciences* 94, 11196-11200.

Liu, C., Bakeri, H., Li, T., Swaroop, A., 2012. Regulation of retinal progenitor expansion by Frizzled receptors: implications for microphthalmia and retinal coloboma. *Human molecular genetics* 21, 1848-1860.

Liu, C., Nathans, J., 2008. An essential role for frizzled 5 in mammalian ocular development. *Development* 135, 3567-3576.

Liu, C., Widen, S.A., Williamson, K.A., Ratnapriya, R., Gerth-Kahlert, C., Rainger, J., Alur, R.P., Strachan, E., Manjunath, S.H., Balakrishnan, A., Floyd, J.A., Consortium, U.K., Li, T., Waskiewicz, A., Brooks, B.P., Lehmann, O.J., FitzPatrick, D.R., Swaroop, A., 2016. A secreted WNT-ligand-binding domain of FZD5 generated by a frameshift mutation causes autosomal dominant coloboma. *Human molecular genetics* 25, 1382-1391.

Liu, H., Thurig, S., Mohamed, O., Dufort, D., Wallace, V.A., 2006. Mapping canonical Wnt signaling in the developing and adult retina. *Investigative ophthalmology & visual science* 47, 5088-5097.

Livak, K.J., Schmittgen, T.D., 2001. Analysis of relative gene expression data using real-time quantitative PCR and the $2^{-\Delta\Delta CT}$ method. *methods* 25, 402-408.

Loosli, F., Staub, W., Finger-Baier, K.C., Ober, E.A., Verkade, H., Wittbrodt, J., Baier, H., 2003. Loss of eyes in zebrafish caused by mutation of *chokh*. *EMBO reports* 4, 894.

Lopez-Rios, J., Esteve, P., Ruiz, J.M., Bovolenta, P., 2008. The Netrin-related domain of Sfrp1 interacts with Wnt ligands and antagonizes their activity in the anterior neural plate. *Neural development* 3, 19.

Lu, F.-I., Thisse, C., Thisse, B., 2011. Identification and mechanism of regulation of the zebrafish dorsal determinant. *Proceedings of the National Academy of Sciences* 108, 15876-15880.

Lupo, G., Gestri, G., O'Brien, M., Denton, R.M., Chandraratna, R.A., Ley, S.V., Harris, W.A., Wilson, S.W., 2011. Retinoic acid receptor signaling regulates choroid fissure closure through independent mechanisms in the ventral optic cup and periorbital mesenchyme. *Proceedings of the National Academy of Sciences* 108, 8698-8703.

Lupo, G., Liu, Y., Qiu, R., Chandraratna, R.A., Barsacchi, G., He, R.-Q., Harris, W.A., 2005. Dorsoventral patterning of the *Xenopus* eye: a collaboration of Retinoid, Hedgehog and FGF receptor signaling. *Development* 132, 1737-1748.

Mann, I., Ross, J.A., 1929. A case of atypical coloboma associated with abnormal retinal vessels. *The British journal of ophthalmology* 13, 608.

Martinez-Morales, J.R., Rembold, M., Greger, K., Simpson, J.C., Brown, K.E., Quiring, R., Pepperkok, R., Martin-Bermudo, M.D., Himmelbauer, H., Wittbrodt, J., 2009. Ojoplano-mediated basal constriction is essential for optic cup morphogenesis. *Development* 136, 2165-2175.

Martinez-Morales, J.R., Wittbrodt, J., 2009. Shaping the vertebrate eye. *Current opinion in genetics & development* 19, 511-517.

Masai, I., Lele, Z., Yamaguchi, M., Komori, A., Nakata, A., Nishiwaki, Y., Wada, H., Tanaka, H., Nojima, Y., Hammerschmidt, M., 2003. N-cadherin mediates retinal lamination, maintenance of forebrain compartments and patterning of retinal neurites. *Development* 130, 2479-2494.

Massague, J., 1990. The transforming growth factor-beta family. *Annual review of cell biology* 6, 597-641.

Matt, N., Dupé, V., Garnier, J.-M., Dennefeld, C., Chambon, P., Mark, M., Ghyselinck, N.B., 2005. Retinoic acid-dependent eye morphogenesis is orchestrated by neural crest cells. *Development* 132, 4789-4800.

McMahon, C., Gestri, G., Wilson, S.W., Link, B.A., 2009. *Lmx1b* is essential for survival of periorbital mesenchymal cells and influences Fgf-mediated retinal patterning in zebrafish. *Developmental Biology* 332, 287-298.

Mii, Y., Taira, M., 2009. Secreted Frizzled-related proteins enhance the diffusion of Wnt ligands and expand their signalling range. *Development* 136, 4083-4088.

Mii, Y., Taira, M., 2011. Secreted Wnt “inhibitors” are not just inhibitors: Regulation of extracellular Wnt by secreted Frizzled-related proteins. *Development, growth & differentiation* 53, 911-923.

Miyazaki, T., Miyauchi, S., Tawada, A., Anada, T., Matsuzaka, S., Suzuki, O., 2008. Oversulfated chondroitin sulfate-E binds to BMP-4 and enhances osteoblast differentiation. *Journal of Cellular Physiology* 217, 769-777.

Mizutani, C.M., Nie, Q., Wan, F.Y., Zhang, Y.-T., Vilmos, P., Sousa-Neves, R., Bier, E., Marsh, J.L., Lander, A.D., 2005. Formation of the BMP activity gradient in the *Drosophila* embryo. *Developmental cell* 8, 915-924.

Molotkov, A., Molotkova, N., Duester, G., 2006. Retinoic acid guides eye morphogenetic movements via paracrine signaling but is unnecessary for retinal dorsoventral patterning. *Development* 133, 1901.

Morcillo, J., Martínez-Morales, J.R., Trousse, F., Fermin, Y., Sowden, J.C., Bovolenta, P., 2006. Proper patterning of the optic fissure requires the sequential activity of BMP7 and SHH. *Development* 133, 3179.

Morgan, C.A., Parajuli, B., Buchman, C.D., Dria, K., Hurley, T.D., 2015. N, N-diethylaminobenzaldehyde (DEAB) as a substrate and mechanism-based inhibitor for human ALDH isoenzymes. *Chemico-biological interactions* 234, 18-28.

Morrison, D., FitzPatrick, D., Hanson, I., Williamson, K., 2002. van HV, Fleck B, Jones I, Chalmers J, Campbell H: National study of microphthalmia, anophthalmia, and coloboma (MAC) in Scotland: investigation of genetic aetiology. *J Med Genet* 39, 16-22.

Mory, A., Ruiz, F.X., Dagan, E., Yakovtseva, E.A., Kurolap, A., Parés, X., Farrés, J., Gershoni-Baruch, R., 2014. A missense mutation in *ALDH1A3* causes isolated microphthalmia/anophthalmia in nine individuals from an inbred Muslim kindred. *European Journal of Human Genetics* 22, 419.

Mueller, R.L., Huang, C., Ho, R.K., 2010. Spatio-temporal regulation of Wnt and retinoic acid signaling by *tbx16/spadetail* during zebrafish mesoderm differentiation. *BMC Genomics* 11, 492.

Mui, S.H., Kim, J.W., Lemke, G., Bertuzzi, S., 2005. *Vax* genes ventralize the embryonic eye. *Genes & Development* 19, 1249-1259.

Mullins, M.C., Hammerschmidt, M., Kane, D.A., Odenthal, J., Brand, M., Van Eeden, F., Furutani-Seiki, M., Granato, M., Haffter, P., Heisenberg, C.-P., 1996. Genes establishing dorsoventral pattern formation in the zebrafish embryo: the ventral specifying genes. *Development* 123, 81-93.

Murali, D., Yoshikawa, S., Corrigan, R.R., Plas, D.J., Crair, M.C., Oliver, G., Lyons, K.M., Mishina, Y., Furuta, Y., 2005. Distinct developmental programs require different levels of *Bmp* signaling during mouse retinal development. *Development* 132, 913-923.

Muraoka, O., Shimizu, T., Yabe, T., Nojima, H., Bae, Y.-K., Hashimoto, H., Hibi, M., 2006. Sizzled controls dorso-ventral polarity by repressing cleavage of the *Chordin* protein. *Nature cell biology* 8, 329-340.

Murphy, D.A., Courtneidge, S.A., 2011. The 'ins' and 'outs' of podosomes and invadopodia: characteristics, formation and function. *Nature reviews Molecular cell biology* 12, 413.

Nakamura, K.M., Diehl, N.N., Mohny, B.G., 2011. Incidence, ocular findings, and systemic associations of ocular coloboma: a population-based study. *Archives of ophthalmology* 129, 69-74.

Nguyen, V.H., Schmid, B., Trout, J., Connors, S.A., Ekker, M., Mullins, M.C., 1998. Ventral and lateral regions of the zebrafish gastrula, including the neural crest progenitors, are established by *abmp2b/swirl* pathway of genes. *Developmental biology* 199, 93-110.

Nikopoulos, K., Venselaar, H., Collin, R.W., Riveiro-Alvarez, R., Boonstra, F.N., Hooymans, J.M., Mukhopadhyay, A., Shears, D., van Bers, M., de Wijs, I.J., 2010. Overview of the mutation spectrum in familial exudative vitreoretinopathy and Norrie

disease with identification of 21 novel variants in FZD4, LRP5, and NDP. *Human mutation* 31, 656-666.

Noordermeer, D., Leleu, M., Splinter, E., Rougemont, J., De Laat, W., Duboule, D., 2011. The Dynamic Architecture of Hox Gene Clusters. *Science* 334, 222-225.

Nordquist, D., McLoon, S.C., 1991. Morphological patterns in the developing vertebrate retina. *Anatomy and embryology* 184, 433-440.

Nusse, R., Clevers, H., 2017. Wnt/ β -Catenin Signaling, Disease, and Emerging Therapeutic Modalities. *Cell* 169, 985-999.

Olbrich, H., Schmidts, M., Werner, C., Onoufriadis, A., Loges, N.T., Raidt, J., Banki, N.F., Shoemark, A., Burgoyne, T., Al Turki, S., 2012. Recessive HYDIN mutations cause primary ciliary dyskinesia without randomization of left-right body asymmetry. *The American Journal of Human Genetics* 91, 672-684.

Onwochei, B.C., Simon, J.W., Bateman, J.B., Couture, K.C., Mir, E., 2000. Ocular Colobomata. *Survey of Ophthalmology* 45, 175-194.

Packard, M., Mathew, D., Budnik, V., 2003. Wnts and TGF β in synaptogenesis: old friends signalling at new places. *Nature Reviews Neuroscience* 4, 113.

Pant, S.D., March, L.D., Famulski, J.K., French, C.R., Lehmann, O.J., Waskiewicz, A.J., 2013. Molecular Mechanisms Regulating Ocular Apoptosis in Zebrafish *gdf6a* Mutants Apoptosis Due to *gdf6a* Loss. *Investigative ophthalmology & visual science* 54, 5871-5879.

Pasutto, F., Sticht, H., Hammersen, G., Gillissen-Kaesbach, G., FitzPatrick, D.R., Nürnberg, G., Brasch, F., Schirmer-Zimmermann, H., Tolmie, J.L., Chitayat, D., 2007. Mutations in STRA6 cause a broad spectrum of malformations including anophthalmia, congenital heart defects, diaphragmatic hernia, alveolar capillary dysplasia, lung hypoplasia, and mental retardation. *The American Journal of Human Genetics* 80, 550-560.

Patel, A., Sowden, J.C., 2017. Genes and pathways in optic fissure closure. *Seminars in Cell & Developmental Biology*.

Paul, B.Y., Hong, C.C., Sachidanandan, C., Babitt, J.L., Deng, D.Y., Hoyng, S.A., Lin, H.Y., Bloch, K.D., Peterson, R.T., 2008. Dorsomorphin inhibits BMP signals required for embryogenesis and iron metabolism. *Nature chemical biology* 4, 33.

Peng, G., Westerfield, M., 2006. *Lhx5* promotes forebrain development and activates transcription of secreted Wnt antagonists. *Development* 133, 3191-3200.

Picker, A., Brand, M., 2005. Fgf signals from a novel signaling center determine axial patterning of the prospective neural retina. *Development* 132, 4951.

Picker, A., Cavodeassi, F., Machate, A., Bernauer, S., Hans, S., Abe, G., Kawakami, K., Wilson, S.W., Brand, M., 2009. Dynamic coupling of pattern formation and morphogenesis in the developing vertebrate retina. *PLoS biology* 7, e1000214.

Ploper, D., Lee, H.X., De Robertis, E.M., 2011. Dorsal–ventral patterning: crescent is a dorsally secreted Frizzled-related protein that competitively inhibits Tolloid proteases. *Developmental biology* 352, 317-328.

Popp, M.W.-L., Maquat, L.E., 2013. Organizing principles of mammalian nonsense-mediated mRNA decay. *Annual review of genetics* 47, 139-165.

Poulter, J.A., Davidson, A.E., Ali, M., Gilmour, D.F., Parry, D.A., Mintz-Hittner, H.A., Carr, I.M., Bottomley, H.M., Long, V.W., Downey, L.M., 2012. Recessive mutations in TSPAN12 cause retinal dysplasia and severe familial exudative vitreoretinopathy (FEVR). *Investigative ophthalmology & visual science* 53, 2873-2879.

Prince, V.E., Moens, C.B., Kimmel, C.B., Ho, R.K., 1998. Zebrafish hox genes: expression in the hindbrain region of wild-type and mutants of the segmentation gene, valentino. *Development* 125, 393-406.

Proetzel, G., Pawlowski, S.A., Wiles, M.V., Yin, M., Boivin, G.P., Howles, P.N., Ding, J., Ferguson, M.W., Doetschman, T., 1995. Transforming growth factor- β 3 is required for secondary palate fusion. *Nature genetics* 11, 409.

Proulx, K., Lu, A., Sumanas, S., 2010. Cranial vasculature in zebrafish forms by angioblast cluster-derived angiogenesis. *Developmental biology* 348, 34-46.

Prykhozhij, S.V., Berman, J.N., 2018. Zebrafish knock-ins swim into the mainstream. The Company of Biologists Ltd.

Prykhozhij, S.V., Fuller, C., Steele, S.L., Veinotte, C.J., Razaghi, B., Robitaille, J.M., McMaster, C.R., Shlien, A., Malkin, D., Berman, J.N., 2018. Optimized knock-in of point mutations in zebrafish using CRISPR/Cas9. *Nucleic acids research* 46, e102-e102.

Rahi, J., Sripathi, S., Gilbert, C., Foster, A., 1995. Childhood blindness in India: causes in 1318 blind school students in nine states. *Eye* 9, 545.

Rainger, J., van Beusekom, E., Ramsay, J.K., McKie, L., Al-Gazali, L., Pallotta, R., Saponari, A., Branney, P., Fisher, M., Morrison, H., Bicknell, L., Gautier, P., Perry, P., Sokhi, K., Sexton, D., Bardakjian, T.M., Schneider, A.S., Elcioglu, N., Ozkinay, F., Koenig, R., M egarban e, A., Semerci, C.N., Khan, A., Zafar, S., Hennekam, R., Sousa, S.B., Ramos, L., Garavelli, L., Furga, A.S., Wischmeijer, A., Jackson, I.J., Gillessen-Kaesbach, G., Brunner, H.G., Wiczorek, D., van Bokhoven, H., FitzPatrick, D.R., 2011. Loss of the BMP Antagonist, SMOC-1, Causes Ophthalmo-Acromelic (Waardenburg Anophthalmia) Syndrome in Humans and Mice. *PLoS Genet* 7, e1002114.

Ramirez-Miranda, A., Zenteno, J.C., 2006. PAX6 gene intragenic deletions in Mexican patients with congenital aniridia. *Mol Vis* 12, 318-323.

- Reis, L.M., Tyler, R.C., Schilter, K.F., Abdul-Rahman, O., Innis, J.W., Kozel, B.A., Schneider, A.S., Bardakjian, T.M., Lose, E.J., Martin, D.M., 2011. BMP4 loss-of-function mutations in developmental eye disorders including SHORT syndrome. *Hum Genet* 130, 495-504.
- Rembold, M., Loosli, F., Adams, R.J., Wittbrodt, J., 2006. Individual Cell Migration Serves as the Driving Force for Optic Vesicle Evagination. *Science* 313, 1130.
- Renström, J., Istvanffy, R., Gauthier, K., Shimono, A., Mages, J., Jardon-Alvarez, A., Kröger, M., Schiemann, M., Busch, D.H., Esposito, I., 2009. Secreted frizzled-related protein 1 extrinsically regulates cycling activity and maintenance of hematopoietic stem cells. *Cell Stem Cell* 5, 157-167.
- Rhinn, M., Dollé, P., 2012. Retinoic acid signalling during development. *Development* 139, 843-858.
- Ribeiro, L.A., Murray, J.C., Richieri-Costa, A., 2006. PTCH mutations in four Brazilian patients with holoprosencephaly and in one with holoprosencephaly-like features and normal MRI. *American journal of medical genetics Part A* 140, 2584-2586.
- Robitaille, J., MacDonald, M.L., Kaykas, A., Sheldahl, L.C., Zeisler, J., Dubé, M.-P., Zhang, L.-H., Singaraja, R.R., Guernsey, D.L., Zheng, B., 2002. Mutant frizzled-4 disrupts retinal angiogenesis in familial exudative vitreoretinopathy. *Nature genetics* 32, 326.
- Roos, L., Fang, M., Dali, C., Jensen, H., Christoffersen, N., Wu, B., Zhang, J., Xu, R., Harris, P., Xu, X., 2014. A homozygous mutation in a consanguineous family consolidates the role of ALDH1A3 in autosomal recessive microphthalmia. *Clinical genetics* 86, 276-281.
- Rossi, A., Kontarakis, Z., Gerri, C., Nolte, H., Hölper, S., Krüger, M., Stainier, D.Y., 2015. Genetic compensation induced by deleterious mutations but not gene knockdowns. *Nature* 524, 230.
- Ruiz, J.M., Rodríguez, J., Bovolenta, P., 2009. Growth and differentiation of the retina and the optic tectum in the medaka fish requires *olSfrp5*. *Developmental neurobiology* 69, 617-632.
- Saint-Geniez, M., D'Amore, P.A., 2004. Development and pathology of the hyaloid, choroidal and retinal vasculature.
- Sakuta, H., Suzuki, R., Takahashi, H., Kato, A., Shintani, T., Iemura, S.-i., Yamamoto, T.S., Ueno, N., Noda, M., 2001. Ventroptin: a BMP-4 antagonist expressed in a double-gradient pattern in the retina. *Science* 293, 111-115.
- Sanford, L.P., Ormsby, I., Gittenberger-de Groot, A.C., Sariola, H., Friedman, R., Boivin, G.P., Cardell, E.L., Doetschman, T., 1997. TGFbeta2 knockout mice have multiple developmental defects that are non-overlapping with other TGFbeta knockout phenotypes. *Development* 124, 2659-2670.

- Santoriello, C., Zon, L.I., 2012. Hooked! Modeling human disease in zebrafish. *The Journal of Clinical Investigation* 122, 2337-2343.
- Sasagawa, S., Takabatake, T., Takabatake, Y., Muramatsu, T., Takeshima, K., 2002. Axes establishment during eye morphogenesis in *Xenopus* by coordinate and antagonistic actions of BMP4, Shh, and RA. *genesis* 33, 86-96.
- Scheufler, C., Sebald, W., Hülsmeier, M., 1999. Crystal structure of human bone morphogenetic protein-2 at 2.7 Å resolution. *Journal of molecular biology* 287, 103-115.
- Schimmenti, L.A., de la Cruz, J., Lewis, R.A., Karkera, J., Manligas, G.S., Roessler, E., Muenke, M., 2003. Novel mutation in sonic hedgehog in non-syndromic colobomatous microphthalmia. *American Journal of Medical Genetics Part A* 116, 215-221.
- Schmid, B., Furthauer, M., Connors, S.A., Trout, J., Thisse, B., Thisse, C., Mullins, M.C., 2000. Equivalent genetic roles for *bmp7/snailhouse* and *bmp2b/swirl* in dorsoventral pattern formation. *Development* 127, 957-967.
- Schmitt, E.A., Dowling, J.E., 1994. Early-eye morphogenesis in the zebrafish, *Brachydanio rerio*. *Journal of Comparative Neurology* 344, 532-542.
- Schmitt, E.A., Dowling, J.E., 1999. Early retinal development in the zebrafish, *Danio rerio*: light and electron microscopic analyses. *Journal of Comparative Neurology* 404, 515-536.
- Schoenebeck, J.J., Hutchinson, S.A., Byers, A., Beale, H.C., Carrington, B., Faden, D.L., Rimbault, M., Decker, B., Kidd, J.M., Sood, R., 2012. Variation of BMP3 contributes to dog breed skull diversity. *PLoS genetics* 8, e1002849.
- Schulte, D., Furukawa, T., Peters, M.A., Kozak, C.A., Cepko, C.L., 1999. Misexpression of the *Emx*-related homeobox genes *cVax* and *mVax2* ventralizes the retina and perturbs the retinotectal map. *Neuron* 24, 541-553.
- Schwarz, M., Cecconi, F., Bernier, G., Andrejewski, N., Kammandel, B., Wagner, M., Gruss, P., 2000. Spatial specification of mammalian eye territories by reciprocal transcriptional repression of *Pax2* and *Pax6*. *Development* 127, 4325.
- Scicolone, G., Ortalli, A.L., Carri, N.G., 2009. Key roles of Ephs and ephrins in retinotectal topographic map formation. *Brain research bulletin* 79, 227-247.
- Sedykh, I., Yoon, B., Roberson, L., Moskvina, O., Dewey, C.N., Grinblat, Y., 2017. Zebrafish *zic2* controls formation of periocular neural crest and choroid fissure morphogenesis. *Developmental Biology* 429, 92-104.
- See, A.W.-M., Clagett-Dame, M., 2009. The temporal requirement for vitamin A in the developing eye: Mechanism of action in optic fissure closure and new roles for the vitamin in regulating cell proliferation and adhesion in the embryonic retina. *Developmental Biology* 325, 94-105.

Shah, S.P., Taylor, A.E., Sowden, J.C., Ragge, N.K., Russell-Eggitt, I., Rahi, J.S., Gilbert, C.E., 2011. Anophthalmos, microphthalmos, and typical coloboma in the United Kingdom: a prospective study of incidence and risk. *Investigative ophthalmology & visual science* 52, 558-564.

Sieber, C., Kopf, J., Hiepen, C., Knaus, P., 2009. Recent advances in BMP receptor signaling. *Cytokine & growth factor reviews* 20, 343-355.

Siemerink, M.J., Augustin, A.J., Schlingemann, R.O., 2010. Mechanisms of ocular angiogenesis and its molecular mediators, Anti-VEGF. Karger Publishers, pp. 4-20.

Sinn, R., Wittbrodt, J., 2013. An eye on eye development. *Mechanisms of Development* 130, 347-358.

Slavotinek, A.M., Chao, R., Vacik, T., Yahyavi, M., Abouzeid, H., Bardakjian, T., Schneider, A., Shaw, G., Sherr, E.H., Lemke, G., Youssef, M., Schorderet, D.F., 2012. VAX1 mutation associated with microphthalmia, corpus callosum agenesis, and orofacial clefting: The first description of a VAX1 phenotype in humans. *Human Mutation* 33, 364-368.

Snelson, C.D., Santhakumar, K., Halpern, M.E., Gamse, J.T., 2008. Tbx2b is required for the development of the parapineal organ. *Development* 135, 1693-1702.

Spemann, H., Mangold, H., 2001. Induction of Embryonic Primordia by Implantation of Organizers from a Different Species. *International journal of Developmental Biology* 45, 13-38.

Srour, M., Chitayat, D., Caron, V., Chassaing, N., Bitoun, P., Patry, L., Cordier, M.-P., Capo-Chichi, J.-M., Francannet, C., Calvas, P., 2013. Recessive and dominant mutations in retinoic acid receptor beta in cases with microphthalmia and diaphragmatic hernia. *The American Journal of Human Genetics* 93, 765-772.

Stafford, D.A., Brunet, L.J., Khokha, M.K., Economides, A.N., Harland, R.M., 2011. Cooperative activity of noggin and gremlin 1 in axial skeleton development. *Development* 138, 1005-1014.

Steinhart, Z., Angers, S., 2018. Wnt signaling in development and tissue homeostasis. *Development* 145, dev146589.

Stewart, A., Guan, H., Yang, K., 2010. BMP-3 promotes mesenchymal stem cell proliferation through the TGF- β /activin signaling pathway. *Journal of Cellular Physiology* 223, 658-666.

Stigloher, C., Ninkovic, J., Laplante, M., Geling, A., Tannhäuser, B., Topp, S., Kikuta, H., Becker, T.S., Houart, C., Bally-Cuif, L., 2006. Segregation of telencephalic and eye-field identities inside the zebrafish forebrain territory is controlled by Rx3. *Development* 133, 2925-2935.

Stoick-Cooper, C.L., Weidinger, G., Riehle, K.J., Hubbert, C., Major, M.B., Fausto, N., Moon, R.T., 2007. Distinct Wnt signaling pathways have opposing roles in appendage regeneration. *Development* 134, 479-489.

Stottmann, R.W., Anderson, R.M., Klingensmith, J., 2001. The BMP Antagonists Chordin and Noggin Have Essential but Redundant Roles in Mouse Mandibular Outgrowth. *Developmental Biology* 240, 457-473.

Sumanas, S., Ekker, S.C., 2001. *Xenopus* frizzled-5: a frizzled family member expressed exclusively in the neural retina of the developing eye. *Mechanisms of development* 103, 133-136.

Sun, Y., Zhang, Q.-J., Zhong, J., Wang, Y.-Q., 2010. Characterization and expression of *AmphiBMP3/3b* gene in amphioxus *Branchiostoma japonicum*. *Development, Growth & Differentiation* 52, 157-167.

Takahashi, H., Sakuta, H., Shintani, T., Noda, M., 2009. Functional mode of FoxD1/CBF2 for the establishment of temporal retinal specificity in the developing chick retina. *Developmental biology* 331, 300-310.

Take-uchi, M., Clarke, J.D., Wilson, S.W., 2003. Hedgehog signalling maintains the optic stalk-retinal interface through the regulation of *Vax* gene activity. *Development* 130, 955-968.

Tanabe, Y., Jessell, T.M., 1996. Diversity and pattern in the developing spinal cord. *Science* 274, 1115-1123.

Taya, Y., O'Kane, S., Ferguson, M., 1999. Pathogenesis of cleft palate in TGF-beta3 knockout mice. *Development* 126, 3869-3879.

Tendeng, C., Houart, C., 2006. Cloning and embryonic expression of five distinct *sfrp* genes in the zebrafish *Danio rerio*. *Gene expression patterns* 6, 761-771.

Thisse, C., Thisse, B., 2008. High-resolution in situ hybridization to whole-mount zebrafish embryos. *Nature protocols* 3, 59.

Toomes, C., Bottomley, H.M., Jackson, R.M., Towns, K.V., Scott, S., Mackey, D.A., Craig, J.E., Jiang, L., Yang, Z., Trembath, R., 2004. Mutations in *LRP5* or *FZD4* underlie the common familial exudative vitreoretinopathy locus on chromosome 11q. *The American Journal of Human Genetics* 74, 721-730.

Tsuji, N., Matsuura, T., Narama, I., Yoshiki, A., Ozaki, K., 2018. Macrophage-Associated Gelatinase Degrades Basement Membrane at the Optic Fissure Margins During Normal Ocular Development in Mice. *Investigative Ophthalmology & Visual Science* 59, 1368-1373.

Umulis, D., Connor, M.B., Blair, S.S., 2009. The extracellular regulation of bone morphogenetic protein signaling. *Development* 136, 3715.

Uren, A., Reichsman, F., Anest, V., Taylor, W.G., Muraiso, K., Bottaro, D.P., Cumberledge, S., Rubin, J.S., 2000. Secreted Frizzled-related protein-1 binds directly to Wingless and is a biphasic modulator of Wnt signaling. *The Journal of Biological Chemistry* 275, 4374-4382.

Urist, M.R., 1965. Bone: Formation by Autoinduction. *Science* 150, 893-899.

Valdivia, L.E., Lamb, D.B., Horner, W., Wierzbicki, C., Tafessu, A., Williams, A.M., Gestri, G., Krasnow, A.M., Vleeshouwer-Neumann, T.S., Givens, M., 2016. Antagonism between Gdf6a and retinoic acid pathways controls timing of retinal neurogenesis and growth of the eye in zebrafish. *Development* 143, 1087-1098.

van den Dries, K., Bolomini-Vittori, M., Cambi, A., 2014. Spatiotemporal organization and mechanosensory function of podosomes. *Cell adhesion & migration* 8, 268-272.

Van Raay, T.J., Moore, K.B., Iordanova, I., Steele, M., Jamrich, M., Harris, W.A., Vetter, M.L., 2005. Frizzled 5 signaling governs the neural potential of progenitors in the developing *Xenopus* retina. *Neuron* 46, 23-36.

Varga, Z.M., Wegner, J., Westerfield, M., 1999. Anterior movement of ventral diencephalic precursors separates the primordial eye field in the neural plate and requires cyclops. *Development* 126, 5533-5546.

Veien, E.S., Rosenthal, J.S., Kruse-Bend, R.C., Chien, C.-B., Dorsky, R.I., 2008. Canonical Wnt signaling is required for the maintenance of dorsal retinal identity. *Development* 135, 4101.

Verma, A.S., FitzPatrick, D.R., 2007. Anophthalmia and microphthalmia. *Orphanet journal of rare diseases* 2, 47.

Villarroel, C.E., Villanueva-Mendoza, C., Orozco, L., Alcántara-Ortigoza, M.A., Jiménez, D.F., Ordaz, J.C., González-del Angel, A., 2008. Molecular analysis of the PAX6 gene in Mexican patients with congenital aniridia: report of four novel mutations. *Mol Vis* 14, 1650.

Wang, R.N., Green, J., Wang, Z., Deng, Y., Qiao, M., Peabody, M., Zhang, Q., Ye, J., Yan, Z., Denduluri, S., Idowu, O., Li, M., Shen, C., Hu, A., Haydon, R.C., Kang, R., Mok, J., Lee, M.J., Luu, H.L., Shi, L.L., 2014. Bone Morphogenetic Protein (BMP) signaling in development and human diseases. *Genes Dis* 1, 87-105.

Wang, S., Krinks, M., Lin, K., Luyten, F.P., Moos Jr, M., 1997. Frzb, a secreted protein expressed in the Spemann organizer, binds and inhibits Wnt-8. *Cell* 88, 757-766.

Wang, S.S., Huang, H.Y., Chen, S.Z., Li, X., Zhang, W.T., Tang, Q.Q., 2013. Gdf6 induces commitment of pluripotent mesenchymal C3H10T1/2 cells to the adipocyte lineage. *The FEBS journal* 280, 2644-2651.

- Weiss, O., Kaufman, R., Michaeli, N., Inbal, A., 2012. Abnormal vasculature interferes with optic fissure closure in *lmo2* mutant zebrafish embryos. *Developmental Biology* 369, 191-198.
- Weiss, O., Kaufman, R., Mishani, E., Inbal, A., 2017. Ocular vessel patterning in zebrafish is indirectly regulated by Hedgehog signaling. *International Journal of Developmental Biology* 61, 277-284.
- Westenskow, P., Piccolo, S., Fuhrmann, S., 2009. β -catenin controls differentiation of the retinal pigment epithelium in the mouse optic cup by regulating *Mitf* and *Otx2* expression. *Development* 136, 2505-2510.
- Weston, C.R., Wong, A., Hall, J.P., Goad, M.E., Flavell, R.A., Davis, R.J., 2003. JNK initiates a cytokine cascade that causes *Pax2* expression and closure of the optic fissure. *Genes & development* 17, 1271-1280.
- Williams, A.L., Bohnsack, B.L., 2015. Neural crest derivatives in ocular development: Discerning the eye of the storm. *Birth Defects Research Part C: Embryo Today: Reviews*, n/a-n/a.
- Williamson, K.A., FitzPatrick, D.R., 2014. The genetic architecture of microphthalmia, anophthalmia and coloboma. *European Journal of Medical Genetics* 57, 369-380.
- Williamson, Kathleen A., Rainger, J., Floyd, James A.B., Ansari, M., Meynert, A., Aldridge, Kishan V., Rainger, Jacqueline K., Anderson, Carl A., Moore, Anthony T., Hurles, Matthew E., Clarke, A., van Heyningen, V., Verloes, A., Taylor, Martin S., Wilkie, Andrew O.M., FitzPatrick, David R., 2014. Heterozygous Loss-of-Function Mutations in *YAP1* Cause Both Isolated and Syndromic Optic Fissure Closure Defects. *The American Journal of Human Genetics* 94, 295-302.
- Wilson, P.A., Hemmati-Brivanlou, A., 1995. Induction of epidermis and inhibition of neural fate by *Bmp-4*. *Nature* 376, 331.
- Wilson, S.W., Houart, C., 2004. Early Steps in the Development of the Forebrain. *Developmental Cell* 6, 167-181.
- Winkler, S., Loosli, F., Henrich, T., Wakamatsu, Y., Wittbrodt, J., 2000. The conditional medaka mutation *eyeless* uncouples patterning and morphogenesis of the eye. *Development* 127, 1911.
- Wolpert, L., 1969. Positional information and the spatial pattern of cellular differentiation. *Journal of Theoretical Biology* 25, 1-47.
- Wyatt, A.W., Osborne, R.J., Stewart, H., Ragge, N.K., 2010. Bone morphogenetic protein 7 (*BMP7*) mutations are associated with variable ocular, brain, ear, palate, and skeletal anomalies. *Human mutation* 31, 781-787.

Ye, M., Berry-Wynne, K.M., Asai-Coakwell, M., Sundaresan, P., Footz, T., French, C.R., Abitbol, M., Fleisch, V.C., Corbett, N., Allison, W.T., Drummond, G., Walter, M.A., Underhill, T.M., Waskiewicz, A.J., Lehmann, O.J., 2010. Mutation of the bone morphogenetic protein GDF3 causes ocular and skeletal anomalies. *Human molecular genetics* 19, 287-298.

Yu, J., He, S., Friedman, J.S., Akimoto, M., Ghosh, D., Mears, A.J., Hicks, D., Swaroop, A., 2004. Altered Expression of Genes of the Bmp/Smad and Wnt/Calcium Signaling Pathways in the Cone-only *Nrl*^{-/-} Mouse Retina, Revealed by Gene Profiling Using Custom cDNA Microarrays. *Journal of Biological Chemistry* 279, 42211-42220.

Zaghloul, N.A., Yan, B., Moody, S.A., 2005. Step-wise specification of retinal stem cells during normal embryogenesis. *Biology of the Cell* 97, 321-337.

Zeisberg, M., Hanai, J.-i., Sugimoto, H., Mammoto, T., Charytan, D., Strutz, F., Kalluri, R., 2003. BMP-7 counteracts TGF- β 1-induced epithelial-to-mesenchymal transition and reverses chronic renal injury. *Nature medicine* 9, 964.

Zhang, R., Huang, H., Cao, P., Wang, Z., Chen, Y., Pan, Y., 2013. Sma- and Mad-related Protein 7 (Smad7) Is Required for Embryonic Eye Development in the Mouse. *Journal of Biological Chemistry* 288, 10275-10285.

Zhang, X., Li, S., Xiao, X., Jia, X., Wang, P., Shen, H., Guo, X., Zhang, Q., 2009. Mutational screening of 10 genes in Chinese patients with microphthalmia and/or coloboma. *Mol Vis* 15, 2911-2918.

Zhang, X.-M., Yang, X.-J., 2001. Temporal and spatial effects of Sonic hedgehog signaling in chick eye morphogenesis. *Developmental biology* 233, 271-290.

Zhou, C.-J., Molotkov, A., Song, L., Li, Y., Pleasure, D.E., Pleasure, S.J., Wang, Y.-Z., 2008. Ocular coloboma and dorsoventral neuroretinal patterning defects in *Lrp6* mutant eyes. *Developmental Dynamics* 237, 3681-3689.

Zhou, C.J., Wang, Y.-Z., Yamagami, T., Zhao, T., Song, L., Wang, K., 2010. Generation of *Lrp6* conditional gene-targeting mouse line for modeling and dissecting multiple birth defects/congenital anomalies. *Developmental Dynamics* 239, 318-326.

Zinski, J., Bu, Y., Wang, X., Dou, W., Umulis, D., Mullins, M.C., 2017. Systems biology derived source-sink mechanism of BMP gradient formation. *eLife* 6, e22199.

Zou, H., Wieser, R., Massagué, J., Niswander, L., 1997. Distinct roles of type I bone morphogenetic protein receptors in the formation and differentiation of cartilage. *Genes & development* 11, 2191-2203.

Zuber, M.E., Gestri, G., Viczian, A.S., Barsacchi, G., Harris, W.A., 2003. Specification of the vertebrate eye by a network of eye field transcription factors. *Development* 130, 5155-5167.

Zuniga, E., Rippen, M., Alexander, C., Schilling, T.F., Crump, J.G., 2011. Gremlin 2 regulates distinct roles of BMP and Endothelin 1 signaling in dorsoventral patterning of the facial skeleton. *Development* 138, 5147-5156.

Appendix A

Somite-derived retinoic acid regulates zebrafish hematopoietic stem cell formation

A version of this chapter is published. Laura M. Pillay, Kacey J. Mackowetzky, Sonya A. Widen, Andrew J. Waskiewicz. (2016) Somite-derived retinoic acid regulates zebrafish hematopoietic stem cell formation. *PLoS One* **12**(1): e0171058

A.1 Introduction

All adult vertebrate hematopoietic lineages arise from a common multipotent progenitor, the hematopoietic stem cell (HSC). This definitive hematopoietic cell type is able to self renew, differentiate into all major blood lineages, and maintain adult hematopoiesis for life. HSC transplants are used to treat a spectrum of diseases ranging from congenital blood disorders to acute leukemia. Unfortunately, these cells are present in restrictive quantities, and recent *ex vivo* methods for expanding human HSCs for clinical therapies have achieved limited success. Identifying the molecular pathways that regulate HSC formation is therefore a major goal of both basic and clinical biology.

The HSC arises intra-embryonically, in an anatomically distinct site from primitive hematopoietic cells (Davidson and Zon, 2004; Palis and Yoder, 2001). HSCs emerge from mesoderm-derived hemogenic endothelium, in close association with the dorsal aorta (Dzierzak, 2005; Palis and Yoder, 2001). In mice, this region is termed the aorta-gonad-mesonephros (AGM). Following their emergence, mammalian HSCs then migrate to the fetal liver and spleen before becoming established in the bone marrow (Cumano and Godin, 2007; Moore and Metcalf, 1970). Although much is known about the cellular and functional properties of vertebrate HSCs, the genetic regulatory mechanisms that govern HSC induction from the AGM, expansion, and homeostasis remain incompletely understood. One candidate regulator of HSC formation is the vitamin A derivative retinoic acid (RA).

RA is an extremely potent diffusible morphogen. Consequently, its levels are tightly regulated within the developing embryo. The *aldehyde dehydrogenase 1a* (*aldh1a/Raldh*) genes encode the rate-limiting enzymes in RA synthesis, and high levels of RA occur in or near tissues that express them (Begemann and Meyer, 2001; Niederreither et al., 1999; Niederreither et al., 2000). Mouse *Aldh1a2* (*Raldh2*) mutants recapitulate phenotypes associated with vitamin A deficiency, suggesting that *Aldh1a2* is the rate-limiting source of RA in the vertebrate embryo (Niederreither et al., 1999; Niederreither et al., 2000). Once synthesized, RA binds nuclear retinoic acid receptor and retinoid X receptor heterodimers to activate target gene transcription (Belandia and Parker, 2003; Glass and Rosenfeld, 2000; Xu et al., 1999).

RA has been shown to enhance the short and long-term repopulating activity of HSCs in suspension culture and serial transplantation assays (Purton et al., 1999, 2000). Conversely, treatment of HSCs with the RAR antagonist AGN 193109 reduces HSC repopulating activity (Purton et al., 2000), implicating RA signaling in HSC maintenance. *In vivo* evidence for the role of RA signaling in definitive hematopoiesis has emerged from analyses of *Aldh1a2* mutant mice. These mice exhibit decreased numbers of yolk sac hemogenic endothelial cells, and a corresponding loss of multipotent blood progenitors that give rise to myeloid and erythroid lineages (Goldie et al., 2008). At embryonic day 8.0, *Aldh1a2* mutants exhibit normal endothelial cell-specific gene expression, and normal circulation (Goldie et al., 2008; Lai et al., 2003). These data suggest that RA signaling is not required for general endothelial cell formation, but rather for vascular endothelial cells to adopt a hemogenic fate. Support for this hypothesis comes from recent analyses of mice with a conditional deletion of *Aldh1a2* in VE-cadherin-positive endothelial cells (Chanda et al., 2013), as AGM-derived endothelial cells isolated from these mice fail to contribute to the peripheral blood of recipients following transplant. Notably, *Aldh1a2* mutant mice die of severe vascular defects by embryonic day 10.5 (Niederreither et al., 1999), prior to HSC emergence. This early embryonic lethality makes mice a challenging model in which to examine the native developmental functions of RA in definitive hematopoiesis.

Zebrafish have recently become one of the most powerful model organisms with which to study embryonic hematopoiesis. Unlike mice, *Aldh1a2*-depleted zebrafish survive up to five days post fertilization (dpf) (Alexa et al., 2009). Zebrafish HSC emergence occurs by 30 hours post fertilization (hpf), making zebrafish an ideal model to study the role of RA in definitive hematopoiesis. In the present study, we provide evidence that RA is an essential regulator of zebrafish HSC specification. We demonstrate that RA regulates the formation of HSCs prior to dorsal aorta hemogenic endothelial cell formation, at a time when *aldh1a2* is expressed in the paraxial mesoderm and somites. Recent evidence suggests that these mesodermal derivatives contribute to HSC formation in a Notch and Cxcl12 chemokine-dependent fashion (Clements et al., 2011; Gering and Patient, 2010; Hadland et al., 2004; Kim et al., 2014; Kumano et al., 2003; Nguyen et al., 2014; Robert-Moreno et al., 2005; Robert-Moreno et al., 2008). We

therefore sought to determine if and how these two signaling pathways are regulated by RA signaling. To do this, we conducted a comprehensive survey of Notch and Cxcl12 pathway component gene expression in RA-depleted embryos. We find that RA-depleted embryos display altered expression of the junctional adhesion molecules *jam1a* and *jam2a*, which enhance Notch signaling in pre-hematopoietic endothelial cells (Kobayashi et al., 2014). *cxcl12b* and its receptor *cxcr4a* are initially expressed within the somites, and later within the dorsal aorta. We find that somatic *cxcr4a* expression is strongly downregulated in RA-depleted embryos. Our work reveals a novel, early role for RA in definitive hematopoiesis and suggests that RA may regulate HSC formation by modulating the expression of Notch and Cxcl12b chemokine signaling pathway components.

A.2. Methods

A.2.1 Animal care, fish lines, and morpholino injection

Care of adult and embryonic zebrafish was conducted according to standard protocols (Westerfield, 2000), in accordance with Canadian Council for Animal Care (CCAC) guidelines. This study was approved by the University of Alberta Animal Care and Use Committee for Biosciences (protocol AUP00000082). Embryos were grown at room temperature (RT), 25.5°C, 28.5°C, or 33°C in embryo media (EM) and staged according to standardized morphological criteria (Kimmel et al., 1995). EM was supplemented with 0.003%-0.006% 1-phenyl 2-thiourea (PTU) (Sigma), to prevent pigment formation in post-24 hours post fertilization (hpf) embryos.

Unless noted, AB strain zebrafish were used for all experiments. Transgenic fish lines used in experiments include *Tg(gata1:DsRed)^{sd2Tg}* (Traver et al., 2003), and *Tg(kdrl:GFP)^{la116Tg}* (Choi et al., 2007). Aldehyde dehydrogenase 1 family, member A2 (Aldh1a2)-depleted embryos were generated by injecting one-cell AB embryos with 5 ng of translation-blocking *aldh1a2* morpholino oligonucleotide (MO; Gene Tools); GCAGTTCAACTTCACTGGAG GTCAT, as previously described (Alexa et al., 2009).

A.2.2 Pharmacological treatments

A 10 μM solution of the Cxcr4 receptor antagonist AMD3100 (EMD Millipore) in EM, was used to inhibit Cxcr4 chemokine signaling (Nguyen et al., 2014). Embryos were treated with AMD3100 from 4 hpf to 24 hpf. All other compounds were dissolved in Dimethyl sulfoxide (DMSO), and diluted to a working concentration in EM. Equivalent solutions of DMSO/EM were used as solvent controls. A 1 μM , 2.5 μM or 5 μM solution of Diethylaminobenzaldehyde (DEAB; Sigma) was used to inhibit retinoic acid (RA) synthesis by aldehyde dehydrogenase enzymes (Maves and Kimmel, 2005; Perz-Edwards et al., 2001). Embryos were treated with DEAB from 4 hpf onward. A 1 nM solution of all-trans RA (Sigma) was applied to live, dechorionated embryos at various stages to activate retinoic acid signaling. All embryos were then grown at 28.5°C in the dark, and were assessed for phenotypes, washed into EM, or fixed in 4% PFA/PBS overnight at 4°C.

A.2.3 mRNA *in situ* hybridization and imaging

Examination of gene expression by whole-mount *in situ* hybridization was performed essentially as previously described (French et al., 2009; Gongal et al., 2011; Gongal and Waskiewicz, 2007; Pillay, 2010). Prior to mRNA *in situ* hybridization analyses, embryos were fixed in 4% paraformaldehyde (PFA)/phosphate-buffered saline (PBS) overnight at 4°C or 4–5 hours at RT with gentle agitation on a rotating platform. Embryos were permeabilized in 10 $\mu\text{g}/\text{ml}$ proteinase K for 10 seconds (10–12 hpf embryos), 30 seconds (14–17 hpf embryos), 3 minutes (24–32 hpf embryos), or 1 hour (3–4 days post fertilization embryos) at RT.

Following *in situ* hybridization, embryos were manually deyolked, and cleared in 30%, 50%, and 70% glycerol/PBS. Mounted *in situ* hybridized embryos and live *Tg(gata1:DsRed)^{sd2Tg}* embryos were photographed using a Zeiss AxioImager Z1 compound microscope with an AxioCam HR digital camera. Mounted *Tg(kdrl:GFP)^{la116Tg}* embryos were photographed using a Zeiss LSM510 confocal microscope. Whole embryos were photographed using an Olympus stereoscope with a QImaging

micropublisher camera. Images were assembled in ImageJ or Zen (Zeiss), and figures were assembled in Photoshop (Adobe).

A.2.4 Real-time quantitative PCR (qPCR)

mRNA was extracted from dissected (head and tail removed) embryos using RNAqueous-4PCR (Ambion) according to the manufacturer's specifications, then treated with DNase I (Ambion), 19 μ l of diethylpyrocarbonate-treated water, and 10 μ l of 10X DNase I Buffer (Ambion) for 30 min at 37°C to remove DNA. Extracted mRNA was purified using the RNeasy Mini Kit (Qiagen) according to the manufacturer's specifications. RNA quantity and quality was assessed by spectrophotometry. First-strand cDNA synthesis was performed using the AffinityScript QPCR cDNA Synthesis Kit (Agilent), with random primers, according to the manufacturer's specifications.

qPCR analysis of cDNA was performed using the Brilliant II SYBR Green QPCR Master Mix (Agilent) and the Rotor-Gene Q System (Qiagen). All cDNA samples were run in replicates of 6, and each experiment was repeated three times. The PCR cycle conditions were 95°C for 10 min (initial denaturation), then 40 cycles of 95°C for 30 s (denaturation), 55°C for 1 min (annealing), and 72°C for 30 s (extension). Fluorescence readings were taken after the 55°C annealing step. The Ct value data were analyzed using the comparative Ct method ($2^{-\Delta\Delta C_t}$ method) (Livak and Schmittgen, 2001), using *eukaryotic translation elongation factor 1 alpha 1a (ef1a)* as an endogenous control. Previously published qPCR primer sequences are *cxcr4a*-F, TGGCTTATTACGAACACATCG; *cxcr4a*-R GAGCCGAATTCAGAGCTGTT (Stückemann et al., 2012); *ef1a*-F, CCTTCGTCCCAATTCAGG; *ef1a*-R, CCTTGAACCAGCCCATGT (Pillay, 2010). Intron-spanning *her9* (*her9*-F, GAATGCCAGCGAGCATAG; *her9*-R, GCTTGACTGTCATCTCCA G) qPCR primers were selected from the Universal Probe Library Assay Design Center for Zebrafish (Roche). Prior to real-time qPCR analysis, these primer sets were validated as follows: An amplification plot was produced from a standard cDNA two-fold dilution series. This plot was used to generate a linear regression curve. The validated *her9* primer sets

produced a linear regression slope of -3.3 ± 0.1 (within 0.1 of the *efl1a* primer set), with a coefficient of determination (R^2) of 0.99.

A.2.5 Morphometric analysis

For morphometric analysis, data from three independent replicates with separate cohorts of zebrafish embryos were analyzed for the main effects of treatment. All measurements were performed using ImageJ software. Width of somatic *jam2a* expression was measured as a fraction of the length of the domain of expression along the medio-lateral axis (denoted y), divided by length of the domain of expression along the anterior-posterior axis (denoted x) of the eighth *jam2a*-expressing somite on the right side of the embryo (fraction y/x). Notably, the length of the domain of *jam2a* expression along the anterior-posterior axis (x) of the eighth *jam2a*-expressing somite did not significantly differ in control (DMSO) versus DEAB-treated embryos ($P \geq 0.2624$).

A.2.6 Statistical analyses

For *in situ* hybridization experiments, and analyses of circulation in *Tg(gata1:DsRed)^{sd2Tg}* embryos, data from two to three independent replicates with separate cohorts of zebrafish embryos were analyzed for the main effects of treatment. Homogeneity across replicates was determined using the G -test of independence, and homogenous datasets (heterogeneity G -value ≥ 0.05) were combined for statistical analysis. Heterogeneous replicate datasets were analyzed separately, and combined when statistical analyses yielded identical results for each replicate dataset. Significant differences among treatments were determined using two-tailed Fisher's exact tests on cumulative raw counts, with Bonferroni correction applied to multiple comparisons ($\alpha = 0.05$). For DEAB and AMD3100 treatment experiments, significant differences in *cmyb*-expressing dorsal aorta cell counts among treatments were determined using unpaired t-tests, with Bonferroni correction applied to multiple comparisons ($\alpha = 0.05$). For qPCR analyses and morphometric analysis, significant differences among treatments were determined using unpaired t-tests ($\alpha = 0.05$).

For analyses of dorsal aorta morphology in *Tg(kdrl:GFP)^{la116Tg}* embryos, data from three independent replicates with separate cohorts of zebrafish embryos were analyzed for the main effects of treatment. Significant differences among treatments and phenotypes were determined by two-way ANOVA with Bonferroni's post-test ($\alpha = 0.05$).

A.3 Results

A.3.1 Retinoic acid regulates hematopoietic stem cell formation

Of the known *aldh1a* genes expressed in early zebrafish development, only *aldh1a2* is expressed in pre-hematopoietic posterior mesoderm (Fig. A.1A–C; (Begemann et al., 2001; Drummond et al., 2013; Grandel et al., 2002)). Consequently, to determine if RA regulates zebrafish HSC formation, we generated RA-deficient embryos by injecting embryos with *aldh1a2* morpholino (hereafter referred to as *aldh1a2* morphants) (Begemann et al., 2001; Drummond et al., 2013; Grandel et al., 2002), or by treating them with diethylaminobenzaldehyde (DEAB), a competitive inhibitor of aldehyde dehydrogenases including Aldh1a2 (Maves and Kimmel, 2005; Perz-Edwards et al., 2001). Published analyses indicate that *aldh1a2* morphants and DEAB treatment accurately phenocopy *aldh1a2* (*nlsⁱ²⁶*) mutants (Begemann et al., 2001; Maves and Kimmel, 2005). Zebrafish HSCs first emerge from dorsal aorta hemogenic endothelium, a region analogous to the mammalian aorta-gonad-mesonephros (AGM), at 30 hours post fertilization (hpf) (Burns et al., 2002; Kalev-Zylinska et al., 2002; Thompson et al., 1998; Zhang et al., 2011). These cells express *cmyb*, a transcription factor essential for HSC emergence (Burns et al., 2002; Kalev-Zylinska et al., 2002; Thompson et al., 1998; Zhang et al., 2011). As shown by *in situ* hybridization, both *aldh1a2* morphants and DEAB-treated embryos display severely reduced dorsal aorta *cmyb* expression at 32 hpf (Fig. A.1D–F; Table A.1).

Following their emergence, zebrafish HSCs migrate posteriorly to the caudal hematopoietic tissues, before becoming established in the thymus by 3 dpf (Jin et al., 2007; Murayama et al., 2006), where they differentiate to form *rag1*- and *ikaros*-

expressing lymphoid progenitors (Jin et al., 2007; Murayama et al., 2006). Subsequently, in order to further determine if HSCs are specified in RA-deficient zebrafish embryos, we examined their *rag1* and *ikaros* expression. *aldh1a2* morphant embryos completely lack thymic *rag1* and *ikaros* expression at 3 dpf, as shown by *in situ* hybridization (Fig. A.1G and H'; Table A.2).

Thymic epithelial cells support lymphoid progenitor development and maturation. These cells differentiate from the thymus primordium, which is derived from the third pharyngeal endodermal pouch in zebrafish (Ma et al., 2013). As perturbations in RA signaling have been shown to produce defects in endodermal pouch morphogenesis (Kopinke et al., 2006), we wanted to verify that the thymic epithelium of RA-deficient embryos is correctly specified. We therefore examined the expression of the thymic epithelial cell marker *foxn1*, and find that it is expressed at wild type levels in 4 dpf *aldh1a2* morphant embryos (Fig. A.1I and I'; Table A.2). Combined, our data suggest that RA is required for the proper specification of zebrafish HSCs and their thymocyte progeny.

As HSC formation is also dependent upon intact blood flow (North et al., 2009), and HSCs originate from dorsal aorta hemogenic endothelium (Burns et al., 2002; Kalev-Zylinska et al., 2002; Thompson et al., 1998), we next wanted to determine if the hematopoietic defects that we observe in RA-deficient embryos are due to aberrant vasculogenesis. To do this, we first visualized circulating primitive erythrocytes in wild type and *aldh1a2* morphant embryos. The majority of *aldh1a2* morphants ($71\% \pm 1.0\%$) exhibit circulating blood cells by 28 hpf (Fig. A.2D; Table A.3). However, this represents a significant reduction when compared to wild type embryos ($87\% \pm 3.0\%$, $P = 0.0196$; Fig. A.2D; Table A.3). Examination of live 48 hpf, *aldh1a2* morphant *Tg(gata1:DsRed)^{sd2Tg}* (Traver et al., 2003) embryos reveals beating hearts, intact circulation, and a functional dorsal aorta (Fig. A.2A,A'). At 48 hpf, the proportion of *aldh1a2* morphants with intact circulation ($97\% \pm 3.5\%$) is not statistically different from that of wild type embryos ($97\% \pm 3.0\%$, $P = 0.5633$; Fig. A.2D; Table A.3). Combined, these data suggest that some *aldh1a2* morphants experience a mild delay in the formation of their mature circulatory system.

To determine if the hematopoietic defects of RA-deficient embryos are attributable to alterations in dorsal aorta morphogenesis and patterning, we examined dorsal aorta morphology in *Tg(kdrl:GFP)^{la116Tg}* transgenic zebrafish embryos (Choi et al., 2007) at 28 hpf, following the onset of circulation (Fig. A.2E–G; Table A.4). Compared to control embryos (Fig. A.2E; 100% ± 0%), the majority of embryos treated with 2.5 μM DEAB exhibit grossly normal vasculature (Fig. A.2F; 69% ± 20%; $P \geq 0.05$). Conversely, only 19% ± 13% of embryos treated with a higher 5 μM dose of DEAB exhibit wild type dorsal aorta morphology ($P < 0.05$; Fig. A.2G). As shown by *in situ* hybridization, RA-deficient embryos exhibit wild type *kdrl* vasculature marker expression and wild type levels of *efnb2a* arterial marker gene expression at 28 hpf (Fig. A.2B,C'; Table A.5). Our combined data therefore suggest that RA does not regulate vascular or arterial gene expression. Our data also suggest that low doses of DEAB (2.5 μM) can be used to block RA synthesis without causing gross maldevelopment of the embryonic vasculature. To avoid generating confounding hematopoietic phenotypes that result from impaired circulation, we used 2.5 μM DEAB or *aldh1a2* morpholino to deplete RA when assessing circulation-stage (26–32 hpf) embryos in all subsequent experiments.

A.3.2 RA is dispensable for zebrafish aorta Notch1 signaling

Previous studies have revealed an essential role for the Notch signaling pathway in regulating vertebrate HSC development (Bertrand et al., 2010; Burns et al., 2005; Clements et al., 2011; Gering and Patient, 2010; Robert-Moreno et al., 2008; Weinstein and Lawson, 2002). Binding of the transmembrane Notch receptor to its Delta or Jagged transmembrane ligand on a neighbouring cell induces a conformational change in Notch that renders it susceptible to cleavage by γ -secretase. This cleavage event releases the Notch intracellular domain (NICD), permitting it to enter the nucleus where it acts as a transcriptional activator (Bertrand et al., 2010; Burns et al., 2005; Clements et al., 2011; Gering and Patient, 2010; Robert-Moreno et al., 2008; Weinstein and Lawson, 2002). The basic helix-loop-helix transcription factors *Hairy* and *enhancer of split (Hes)* are

transcriptional targets of the Notch signaling pathway, and serve to mediate the majority of Notch function (Iso et al., 2003).

Previous research in both mouse and zebrafish has established a cell-autonomous function for Notch signaling in HSC specification, whereby Notch1-expressing cells within the dorsal aorta are instructed by adjacent cells to form HSCs (Gering and Patient, 2010; Hadland et al., 2004; Kim et al., 2014; Kumano et al., 2003; Robert-Moreno et al., 2005; Robert-Moreno et al., 2008). The yolk sac endothelial cells of *Aldh1a2* mutant mice exhibit downregulated *Notch1* and Notch1-target gene (*Hes1*) expression (Marcelo et al., 2013), implicating RA as a potential modulator of Notch signaling. We therefore wanted to determine if hematopoietic defects that we observe in RA-deficient zebrafish are the result of impaired Notch1 signaling. To do this, we first examined the expression of dorsal aorta Notch signaling pathway components and their downstream transcriptional targets in RA-deficient embryos. Zebrafish possess four Notch receptors: Notch1a, Notch1b, Notch2, and Notch3. Of these, only Notch2 is completely dispensable for HSC formation (Hadland et al., 2004; Kim et al., 2014; Kumano et al., 2003). *notch1a*, *notch1b*, and *notch3* are initially expressed within the somitic mesoderm, with their domain of expression expanding to include nascent endothelial cells and the dorsal aorta (Bertrand et al., 2010; Kim et al., 2014; Ma and Jiang, 2007). As shown through *in situ* hybridization, RA-deficient embryos exhibit wild type expression of *notch1a*, and *notch1b*, while the somitic expression of *notch3* is mildly increased at 26 hpf (Fig. A.3A–C'; Table A.6). Our combined data suggest that RA is dispensable for dorsal aorta Notch receptor expression in zebrafish.

Previous research has shown that both global NICD induction after 20 hpf, and vascular- (but not somite-) specific induction of the NICD rescues the HSC gene expression defects of *notch1a* and *notch1b* morphant zebrafish embryos (Kim et al., 2014). Conversely, global or somite-specific NICD induction at 14 hpf, but not 20 hpf, rescues HSC formation in *notch3* morphant embryos (Kim et al., 2014). As the dorsal aorta begins to form at 20 hpf (Ellertsdóttir et al., 2010), these combined data suggest that the definitive hematopoietic roles of zebrafish Notch1a/b and murine Notch1 are likely functionally conserved. These data also suggest that there is a distinct temporal and

spatial requirement for Notch3 in zebrafish hematopoiesis, which occurs prior to formation of the dorsal aorta. Consequently, to further determine if RA regulates zebrafish dorsal aorta Notch signaling, we next examined the expression of transcriptional targets of the Notch1 signaling pathway in RA-deficient embryos (Fig. A.3D,E'; Table A.6). Expression of the Notch ligand *deltaC* (*dlc*) is strongly reduced in the dorsal aorta of *notch1a* and *notch1b* morphant zebrafish embryos (Kim et al., 2014). We therefore examined its expression in RA-deficient embryos. *Dlc* is expressed at wild type levels in 26 hpf DEAB-treated embryos (Fig. A.3D,D'; Table A.6). We also examined the expression of *her6* (the zebrafish ortholog of mammalian *Hes1* (Gates et al., 1999; Jouve et al., 2000)), finding that it is also expressed at wild type levels in 26 hpf *aldh1a2* morphant embryos (Fig. A.3E,E'; Table A.6). These data suggest that, unlike its mammalian orthologue *Hes1*, zebrafish *her6* is not RA-responsive. These combined data also suggest that RA does not regulate the Notch1 signaling pathway in zebrafish.

A.3.3 RA signalling regulates HSC formation prior to 19 hpf

Our analyses indicate that the hematopoietic defects of RA-deficient embryos are not due to impaired dorsal aorta Notch signaling. Consequently, to gain a better understanding of how RA regulates zebrafish definitive hematopoiesis, we next wanted to elucidate the temporal requirement for RA signaling in HSC formation. To accomplish this, we treated *aldh1a2* morphant embryos with RA at different time points, and examined their *cmyb* HSC gene expression at 32 hpf through *in situ* hybridization (Fig. A.4; Table A.7). We demonstrate that RA treatment beginning at 4 hpf rescues dorsal aorta *cmyb* gene expression in *aldh1a2* morphant embryos (Fig. A.4C). Conversely, RA treatment beginning at 19 hpf (Fig. A.4E) or 24 hpf (Fig. A.4F) fails to rescue *cmyb* expression in *aldh1a2* morphants. Combined, these data suggest that RA is required prior to 19 hpf to specify HSCs. Notably, *aldh1a2* is expressed in the paraxial mesoderm and somites during this period, and the dorsal aorta has not yet formed (Ellertsdóttir et al., 2010).

A.3.4 RA does not positively regulate *Wnt16*-*Notch3* signaling within the somites

The Wingless-type MMTV integration site family, member 16 (*Wnt16*) participates in a non-canonical Wnt signaling pathway (Clements et al., 2011). Its depletion causes defects in Notch signaling and HSC formation (Clements et al., 2011). Given that RA and *Wnt16* are required for HSC formation prior to 19 hpf, and *aldh1a2* and *wnt16* are both expressed in the paraxial mesoderm and somites at this time (Clements et al., 2011), we hypothesized that perturbations in *Wnt16* or its downstream effectors may be responsible for the hematopoietic defects that we observe in RA-depleted embryos. We demonstrate that *wnt16* is expressed at wild type levels DEAB-treated embryos at 17 hpf (Fig. A.5A,B'; Table A.8). In addition to hematopoietic defects, *Wnt16*-depleted embryos exhibit reduced somitic expression of the Notch ligands *dlc* and *dld*, and *dlc/dld* overexpression rescues HSC gene expression in *wnt16* morphants (Clements et al., 2011). In comparison to wild type embryos, DEAB-treated embryos exhibit normal levels of somatic *dlc* expression (Fig. A.5C,D'; Table A.8), and mildly upregulated *dld* expression (Fig. A.5E,F'; Table A.8). *Dlc/Dld* and *Notch3* proteins cooperate as regulators of HSC formation, as partial loss of *Dlc* and *Notch3*, or *Dld* and *Notch3* produces greater HSC gene expression defects than partial loss of *Dlc*, *Dld*, or *Notch3* alone (Kim et al., 2014). When compared to wild type embryos (Fig. A.5G,G'), DEAB-treated embryos exhibit increased somatic *notch3* expression at 17 hpf (Fig. A.5H,H'; Table A.8). *her9* is partially downregulated in both *notch1a* mutant and *notch3* morphant zebrafish embryos (Liu et al., 2007; Ma and Jiang, 2007). Like *notch3*, *her9* expression is upregulated in 17 hpf DEAB-treated embryos, as shown by qPCR (Fig. A.5K). However, this upregulation in expression is not observable by *in situ* hybridization (Fig. A.5I,J'; Table A.8). Taken together, our data provide evidence that RA negatively regulates *Notch3*-mediated signal transduction, without altering somitic *Wnt16*.

A.3.5 RA regulates *jam1a* and *jam2a* expression

The dorsal aorta forms from angioblasts that arise from bilateral stripes of posterior lateral plate mesoderm. These angioblasts migrate medially and aggregate

(Ellertsdóttir et al., 2010). Recent evidence suggests that the junctional adhesion molecules Jam1a and Jam2a physically interact, and are required for zebrafish HSC formation (Kobayashi et al., 2014). *jam1a* is expressed within angioblasts that migrate across *jam2a*-, *dlc*-, and *dld*-expressing somites (Kobayashi et al., 2014). Jam1a- and Jam2a-deficient embryos exhibit impaired Notch signal transduction, and their hematopoietic defects are rescued by heat-shock induction of the NICD during angioblast migration (Kobayashi et al., 2014). Combined, the data generated by Kobayashi et al. (2014) suggest that Notch signal transduction in pre-hematopoietic angioblasts requires Jam-mediated intercellular contact.

Angioblast migration occurs between 14 and 18 hpf. We demonstrate that the diffusible morphogen RA is required prior to 19 hpf for HSC formation. Furthermore, like Jam1a- and Jam2a-depleted embryos, RA-deficient embryos do not display reduced expression of *notch1a*, *notch1b*, *notch3*, *dlc*, and *dld* (Kobayashi et al., 2014). We therefore sought to determine if RA is an upstream regulator of *jam1a* and/or *jam2a* by examining their expression in 17 hpf control and DEAB-treated embryos through *in situ* hybridization (Fig. A.6; Table A.8). DEAB-treated embryos express *jam1a* at wild type levels (Fig. A.6A,A'). However, unlike in controls, the anterior-most *jam1a*-expressing posterior lateral plate mesoderm cells do not contact the somites in DEAB-treated embryos (Fig. A.6A,A'; arrowheads). Compared to controls, 17 hpf DEAB-treated embryos display increased levels of somatic *jam2a* expression, and lateral expansion of the *jam2a* expression domain (Fig. A.B-B',C). Combined, these data suggest that RA is required for the proper expression of *jam1a* and *jam2a* within somitogenesis stage embryos.

A.3.6 RA regulates *cxcl12b* and *cxcr4a* expression

The CXC-motif chemokine receptor Cxcr4a and its ligand Cxcl12b regulate brain (Bussmann et al., 2011), coronary (Harrison et al., 2011), gastrointestinal (Ara et al., 2005; Tachibana et al., 1998), kidney (Takabatake et al., 2009), and arterial (Xu et al., 2015) vessel development, as well as lateral dorsal aorta formation (Siekmann et al., 2009). Cxcl12 signaling has also been implicated in hematopoietic cell migration (Aiuti

et al., 1997; Peled et al., 1999; Siekmann et al., 2009; Walters et al., 2010; Zou et al., 1998), engraftment (Peled et al., 1999) and hematopoietic stem cell maintenance (Peled et al., 1999). Recently, Nguyen et al. (2014) demonstrated that *Cxcl12b* is required for zebrafish HSC formation, as HSC gene expression is reduced in both *cxcl12b* morphants and embryos treated with a pharmacological inhibitor of Cxcl12 signaling from 14 to 24 hpf. Combined, these data suggest that Cxcl12b signaling within the somites contributes to zebrafish HSC formation between 14 and 24 hpf. *aldh1a2* is expressed within the somites during this period, and our data suggest that RA is required for HSC formation prior to 19 hpf. We therefore hypothesized that the HSC gene expression defects that we observe in RA-depleted embryos may be due to reduced Cxcl12 signaling, and so examined the expression of *cxc4a* and *cxcl12b* in 17 hpf control and DEAB-treated embryos through *in situ* hybridization (Fig. A.7A-C'; Table A.9). Compared to controls, 17 hpf DEAB-treated embryos exhibit narrowing of the *cxc4a* expression domain within each somite, along with an overall strong reduction in *cxc4a* expression (Fig. A.7A,A'; Table A.9). Conversely, *cxcl12b* expression is subtly upregulated within the somites of DEAB-treated embryos (Fig. A.7B,B'; Table A.9). We performed qPCR on 17 hpf control and DEAB-treated embryos to quantitatively measure the observed changes in *cxc4a* expression. Consistent with the *in situ* hybridization analyses, DEAB-treated embryos exhibit a significant reduction in *cxc4a* expression (Fig. A.7D) compared to controls.

meox1-null (*cho*) zebrafish mutants exhibit an increase in somatic *cxcl12b* expression, and a corresponding increase in HSC number (Nguyen et al., 2014). Given that we observe a subtle increase in somitic *cxcl12b* expression within RA-depleted embryos, we next wanted to determine if *meox1* expression is also affected by loss of embryonic RA. As shown by *in situ* hybridization, 17 hpf DEAB-treated embryos display a subtle decrease in somitic *meox1* expression, when compared to controls (Fig. A.7C,C'; Table A.9).

Given that RA-depleted embryos exhibit strongly decreased somitic *cxc4a* expression, we next wanted to determine if this decrease is consistent with reduced chemokine signalling. We therefore examined if RA signalling functions in association

with Cxcr4-mediated chemokine signalling to regulate HSC formation. To test this, we examined *cmyb* HSC gene expression in 36 hpf embryos treated with a suboptimal dose DEAB (1 μ M) and/or a suboptimal dose of Cxcr4 chemokine receptor antagonist AMD3100 (10 μ M) by *in situ* hybridization. Compared to DMSO-treated controls (Fig. A.7E,I), embryos treated with 1 μ M DEAB or 10 μ M AMD3100 exhibit a small reduction in *cmyb*-expressing cell numbers (Fig. A.7F,G,I). Embryos treated with both 1 μ M DEAB and 10 μ M AMD3100 exhibit a severe reduction in *cmyb*-expressing cell numbers (Fig. A.7H,I), a phenotype that resembles treatment with a higher dose of DEAB (5 μ M) alone (Fig. A.1F). Taken together, these data support a role for somitic retinoids in regulating Cxcr4-mediated chemokine signaling during the developmental period in which RA functions to regulate HSC formation.

From 28–30 hpf, *meox1* is expressed within cells found immediately adjacent to the dorsal aorta, while *cxcr4a*, and *cxcl12b* display weak, punctate expression throughout the dorsal aorta (Fig. A.8A–C; (Nguyen et al., 2014)). It is possible that Cxcl12b-Cxcr4a signaling within the dorsal aorta is required for HSC formation. We therefore wanted to determine if RA-depleted embryos exhibit alterations to *cxcr4a*, *cxcl12b*, and *meox1* expression at 28 hpf, just prior to HSC emergence. When compared to controls, DEAB-treated embryos exhibit a strong increase in dorsal aorta *cxcr4a* (Fig. A.8A,A') and *cxcl12b* (Fig. A.8B,B') expression at 28 hpf, as shown by *in situ* hybridization. DEAB-treated embryos also display a strong increase in *meox1* expression at 28 hpf, when compared to controls (Fig. A.8C,C'). Combined, these data suggest that RA negatively regulates Cxcl12b-Cxcr4a pathway component gene expression at 28 hpf.

A.4 Discussion

Previous research has shown that RA treatment of hematovascular precursors increases their ability to generate definitive hematopoietic precursors (Chanda et al., 2013; Yu et al., 2010), suggesting that RA signaling plays an instructive role in definitive hematopoiesis. This data is in line with previous analyses of RA function in mice, as *Aldh1a2* mutants fail to correctly specify yolk sac hemogenic endothelial cells (Goldie et al., 2008), and loss of *Aldh1a2* in VE-cadherin-positive endothelial cells is sufficient to

abrogate HSC formation (Chanda et al., 2013). *Aldh1a2* mutant mice die of severe vascular defects prior to HSC emergence (Niederreither et al., 1999), precluding global analyses of *Aldh1a2* function in murine definitive hematopoiesis. We therefore used zebrafish as a model to study the role of RA signaling in definitive hematopoiesis.

Our study describes a novel role for RA signaling in definitive hematopoiesis. We propose that RA functions within the paraxial mesoderm or somites to regulate hematopoietic stem cell (HSC) formation. By impairing RA synthesis in the developing zebrafish embryo, we demonstrate that RA is required for proper HSC gene expression. In the absence of RA, embryos exhibit a severe reduction in HSC number and a corresponding failure to produce thymic lymphoid progenitors.

A.4.1 RA regulates HSC formation independent of the Notch1-signaling pathway

Previous research in both mouse and zebrafish has established a model whereby Notch1-expressing cells within the dorsal aorta are instructed by adjacent cells to form HSCs (Gerety et al., 2013; Hadland et al., 2004; Kumano et al., 2003; Robert-Moreno et al., 2005; Robert-Moreno et al., 2008). *Notch1* mutant embryonic stem cells fail to contribute to the wild type adult hematopoietic system in mouse chimeras (Hadland et al., 2004), supporting this cell-autonomous role for Notch1 in definitive hematopoiesis. The yolk sac endothelial cells of *Aldh1a2* mutant mice exhibit downregulated *Notch1* and Notch target gene expression (Marcelo et al., 2013), implicating RA as a critical regulator of murine Notch1 signaling. Notch1 specifies HSCs (Gerety et al., 2013; Hadland et al., 2004; Robert-Moreno et al., 2005; Robert-Moreno et al., 2008). We, however, demonstrate that *notch1a/b* expression is unaffected by loss of RA in zebrafish. We further demonstrate that RA is required for HSC formation prior to the formation of dorsal aorta hemogenic endothelium. Our combined results therefore suggest that, unlike in mice, zebrafish RA does not regulate Notch1 signaling. We therefore propose a model whereby RA signaling acts outside of the pre-hemogenic endothelium, in a Notch1-independent fashion to regulate zebrafish HSC formation.

A.4.2 RA may indirectly regulate *Wnt16*-Notch signalling

Recently, Clements et al. (2011) demonstrated a requirement for *Wnt16* in zebrafish hematopoiesis. RA-deficient and *wnt16* morphant embryos display common hematopoietic phenotypes; both demonstrate proper vascular gene expression and produce a functional dorsal aorta, but exhibit a severe reduction in HSC and common lymphoid progenitor gene expression (Clements et al., 2011). These data suggest that both RA and *Wnt16* are required for HSC formation. Our data, and previous results, suggest that both RA and *Wnt16* function outside of dorsal aorta pre-hemogenic endothelium to regulate zebrafish HSC formation prior to 19 hpf (Clements et al., 2011). Furthermore, both *aldh1a2* and *wnt16* are expressed in the paraxial mesoderm at this time (Clements et al., 2011). In addition to hematopoietic defects, *Wnt16*-depleted embryos exhibit reduced somitic expression of the Notch ligands *dlc* and *dld* (Clements et al., 2011). HSC gene expression is lost in *dlc* mutants injected with *dld* morpholino, and *dlc/dld* overexpression rescues HSC gene expression in *wnt16* morphants (Clements et al., 2011). Notch3 is required by *Wnt16*-induced Dlc/Dld to regulate HSC formation (Kim et al., 2014). We demonstrate that the expression of *notch3*, and its transcriptional target *her9* are not downregulated in RA-deficient embryos at 17 hpf. Our data therefore indicate that, despite their similar localization, and their common temporal requirement in definitive hematopoiesis, RA does not positively regulate *wnt16*, its downstream targets *dlc*, and *dld*, or *notch3*.

Dlc/Dld-mediated Notch signal transduction within pre-hematopoietic endothelial cells relies on the junctional adhesion molecules Jam1a/Jam2a (Kobayashi et al., 2014). We demonstrate that the anterior-most *jam1a*-expressing posterior lateral plate mesoderm cells of RA-depleted embryos are improperly situated, and do not contact the somites. Furthermore, RA-depleted embryos exhibit upregulated, laterally expanded somatic *jam2a* expression. The expression domains of *jam1a/2a*, and the Notch transcriptional target *her9* do not significantly overlap at 17 hpf. Consequently, despite observing mildly upregulated *her9* expression in somitogenesis stage RA-depleted embryos, it remains possible that their *jam1a*-positive cell populations experience reduced Notch signaling. It is therefore currently unclear if the modifications to *jam1a/2a* expression that we observe

in RA-depleted embryos are sufficient to disrupt Notch signaling within migrating pre-hematopoietic endothelial cells, or serve to reduce their definitive hematopoietic potential.

A.4.3 RA differentially regulates the expression of early and late Cxcl12b signaling pathway components

Studies of Cxcl12b-signaling in zebrafish have revealed an essential role for this chemokine in definitive hematopoiesis. Targeted ablation of somitic *cxcl12b*-expressing endothelial cell precursors is sufficient to disrupt HSC formation in zebrafish, as is pharmacological or genetic inhibition of Cxcl12b signaling during somitogenesis stages (Nguyen et al., 2014). We find that *cxcl12b* expression is subtly increased in the posterior somites of RA-depleted embryos, suggesting that RA may negatively regulate its expression.

meox1-null (*cho*) zebrafish mutants exhibit an increase in somitic *cxcl12b* expression, and a corresponding increase in HSC number (Nguyen et al., 2014). Meox1-mediated chromatin immunoprecipitation of the zebrafish *cxcl12b* locus suggests that Meox1 is probably a direct inhibitor of *cxcl12b* (Nguyen et al., 2014). We demonstrate that RA-depleted zebrafish embryos exhibit a subtle decrease in the posterior somitic expression of *meox1*. This decrease likely accounts for the increased *cxcl12b* expression that we observe in RA-depleted embryos. As these modifications to *meox1/cxcl12b* gene expression would be expected to generate increased HSC numbers (Nguyen et al., 2014), they do not explain the loss of HSCs that we observe in RA-depleted embryos.

Cxcl12b signaling occurs preferentially through the Cxcr4a receptor (Boldajipour et al., 2011). During zebrafish somitogenesis, *cxcr4a* is expressed within the anterior half of each somite (Fig. A.7A). We demonstrate that this expression is nearly abolished in RA-depleted embryos. Our data therefore implicates RA as a transcriptional regulator of *cxcr4a* within the somites. Given the requirement for Cxcl12b signaling in zebrafish definitive hematopoiesis, it is possible that the HSC gene expression defects that we observe in RA-depleted embryos may be partially attributable to reduced levels of

cxcr4a. In support of this idea, we find that the RA-synthesis inhibitor DEAB and the Cxcr4-receptor antagonist AMD3100 act in concert to impair zebrafish embryonic HSC formation.

Lineage tracing experiments have shown that a proportion of *cxcl12b* and *cxcr4a*-expressing cells from the medio-lateral portion of each somite colonize the dorsal aorta and dorsal-aorta supportive cells, but do not contribute to HSC populations directly (Nguyen et al., 2014). This has led to the idea that Cxcl12b-signaling within the dorsal aorta may render endothelial cells competent to make HSCs (Nguyen et al., 2014). Surprisingly, the early reduction of *cxcr4a* expression that we observe in RA-depleted embryos is not maintained; RA-depleted embryos exhibit strongly increased *cxcr4a*, *cxcl12b*, and *meox1* expression within the dorsal aorta and surrounding tissues at 28 hpf, just prior to HSC emergence (Fig. A.8A–C'; Table A.9). Despite this increase, RA-depleted embryos do not produce HSCs. It is therefore possible that Cxcl12b/Cxcr4a signaling may regulate HSC formation earlier in development than previously thought (i.e. during somitogenesis). Alternatively, RA could act downstream of the Cxcl12b signaling pathway at 28 hpf, and *cxcl12b/cxcr4a* upregulation at this time may reflect the existence of some sort of negative-feedback loop. More stringent temporal analyses of Cxcl12b/Cxcr4a function in definitive hematopoiesis will be required to distinguish between these two possibilities.

Previous research has shown that *cxcr4a* expression is negatively regulated by hemodynamic force (Bussmann et al., 2011; Packham et al., 2009), and that dorsal aorta *cxcr4a* expression is upregulated in embryos with reduced blood flow (Packham et al., 2009). We observe mild circulatory and dorsal aorta morphology defects in a proportion of 2.5 μ M DEAB-treated embryos at 28 hpf. It is therefore possible that the increased *cxcr4a* expression that we observe in these embryos results from decreased vascular perfusion. There are currently no published accounts linking hemodynamic force to changes in *cxcl12b* expression. It is not therefore clear if the upregulated *cxcl12b* expression that we observe in 28 hpf RA-depleted embryos might also be a consequence of impaired circulation.

The majority of *aldh1a2* morphant and 2.5 μ M DEAB-treated embryos exhibit normal posterior dorsal aorta and intersegmental vessel formation. Furthermore, although some *aldh1a2* morphants exhibit delayed circulation, most possess visible circulating erythrocytes by 28 hpf. Our results further suggest that vascular and arterial gene expression is not altered in RA-depleted embryos. Nevertheless, RA-depleted embryos exhibit HSC gene expression defects. Our temporal analyses indicate that RA is required prior to the onset of dorsal aorta formation. Consequently, although previous studies have linked blood flow to HSC formation (North et al., 2009), our combined data suggest that the definitive hematopoietic phenotypes of RA-depleted embryos are not simply the consequence of reduced circulation or improper patterning of the dorsal aorta.

A.5 Figures

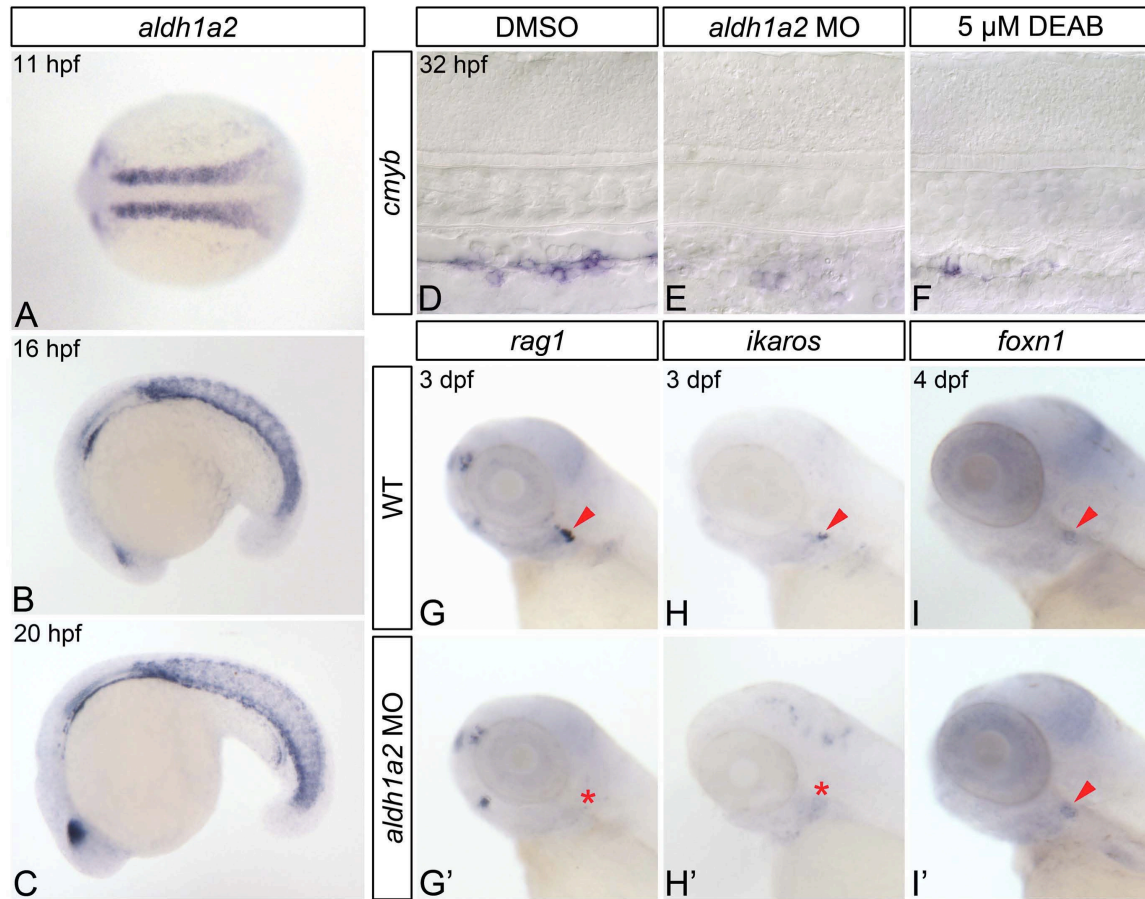


Fig. A.1: RA-deficient embryos demonstrate impaired HSC formation. (A-C) *In situ* hybridization analyses of *aldh1a2* gene expression in wild type (WT) embryos. (A) Expression within the somites at 11 hpf, shown in dorsal view with anterior to the left. Somitic expression persists in 16 hpf (B) and 20 hpf (C) embryos, shown in lateral view with anterior to the left. (D-F) Representative flat-mounted embryos following *in situ* hybridization analysis of *cmyb* gene expression at 32 hpf. Lateral view of gene expression in the dorsal aorta region of the trunk is shown with anterior to the left. Compared to DMSO-treated controls (D) *aldh1a2* morphants (E), and 5 μ M DEAB-treated embryos (F) exhibit nearly abolished *cmyb* expression. (G-H') *In situ* hybridization analyses of common lymphoid progenitor gene expression in 3 dpf embryos. Lateral view of gene expression in the head is shown with anterior to the left. Arrowheads and asterisks

indicate thymus. Compared to WT embryos (G,H), *aldh1a2* morphants exhibit nearly abolished thymic *rag1* (G') and *ikaros* (H') expression. (I,I') Representative embryos following *in situ* hybridization analysis of *foxn1* thymic epithelial cell gene expression in 4 dpf embryos. Lateral view of gene expression in the head is shown with anterior to the left. Arrowheads indicate thymus. WT embryos (I) and *aldh1a2* morphants (I') exhibit similar thymic *foxn1* expression levels.

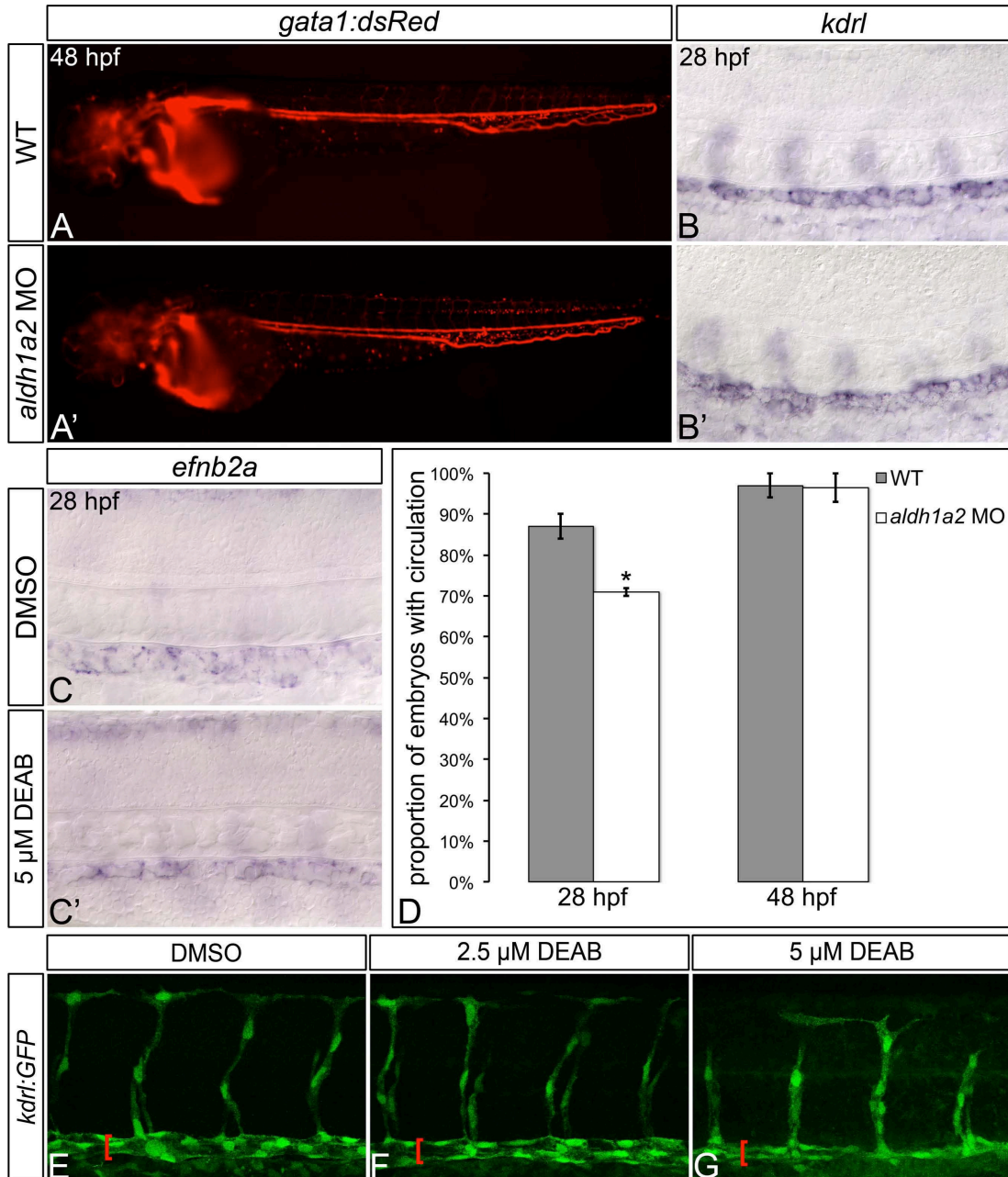


Fig. A.2: RA-deficient embryos exhibit relatively normal gross embryonic vasculogenesis. (A,A') Lateral view of live 48 hpf *Tg(gata1:DsRed)^{sd2Tg}* embryos with anterior to the left. Compared to wild type (WT) embryos (A), *aldh1a2* morphants (A') display visible circulating blood cells, and an intact dorsal aorta and posterior cardinal vein. (B-C') Representative embryos following *in situ* hybridization analysis of *kdrl* vasculature marker gene expression (B,B') or *efnb2a* arterial marker gene expression (C,C') in 28 hpf embryos. Lateral view of gene expression in the dorsal aorta region of

the trunk is shown in flat-mount embryos, with anterior to the left. Compared to WT embryos (B), *aldh1a2* morphants (B') exhibit normal dorsal aorta *kdrl* gene expression. Compared to DMSO-treated controls (C), embryos treated with 5 μ M DEAB (C') exhibit normal levels, but a reduced domain of dorsal aorta *efnb2a* gene expression. (D) Graph demonstrating the mean proportion of WT or *aldh1a2* morphant embryos with intact circulation at 28 hpf and 48 hpf. Error bars represent standard error. *=statistically significant difference compared to WT ($P = 0.0196$). See text for statistical tests. (E-G) Lateral view of dorsal aorta region of the trunk is shown in representative flat-mount *Tg(kdrl:GFP)^{la116Tg}* 28 hpf embryos, with anterior to the left. Brackets indicate dorsal aorta. Compared to DMSO-treated controls (E), 2.5 μ M DEAB-treated embryos (F) exhibit normal dorsal aorta morphology, while 5 μ M DEAB-treated embryos (G) exhibit thinning of the dorsal aorta.

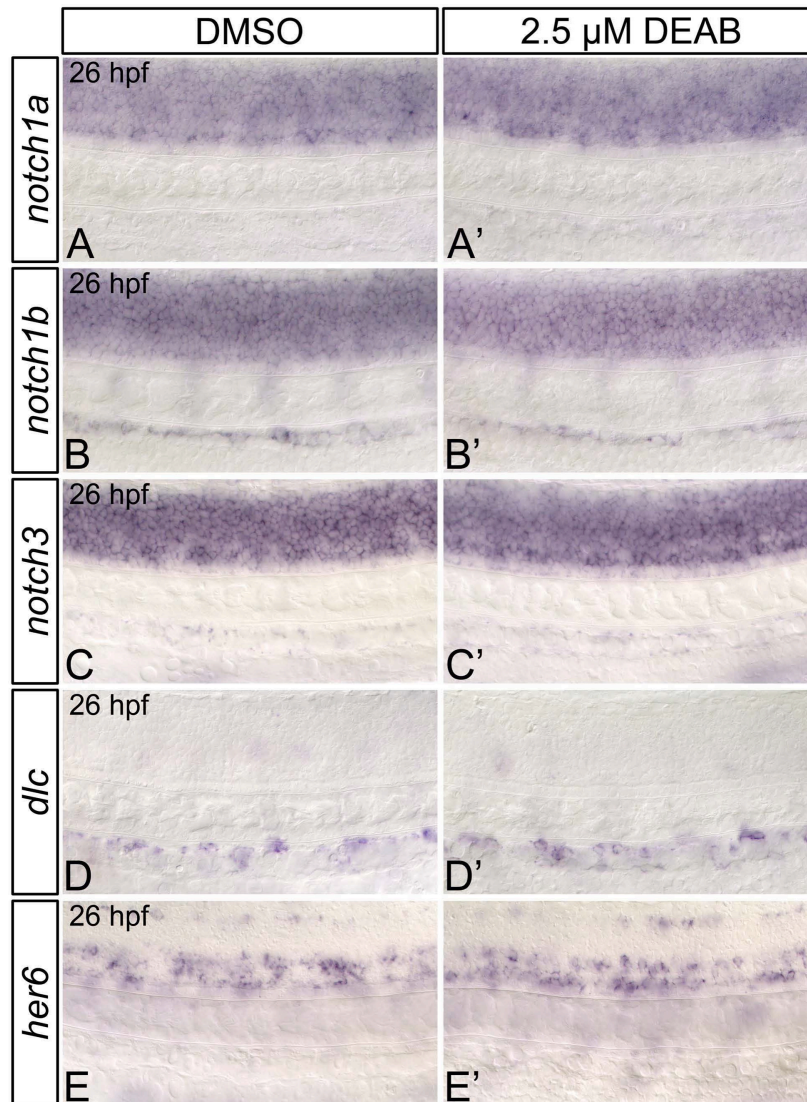


Fig. A.3: RA-deficient embryos demonstrate normal dorsal aorta *notch* and Notch1-target gene expression. Representative flat-mount 26 hpf embryos following *in situ* hybridization analyses. Lateral view of gene expression in the dorsal aorta region of the trunk is shown with anterior to the left. Compared to DMSO-treated controls (A,B), embryos treated with 2.5 μ M DEAB exhibit normal *notch1a* (A'), and *notch1b* (B') gene expression within the trunk and dorsal aorta. *notch3* is expressed at normal levels in the dorsal aorta (C,C'), but is mildly upregulated in the somites of 2.5 μ M DEAB-treated versus DMSO-treated control embryos (data not shown). Compared to DMSO-treated controls (D,E) embryos treated with 2.5 μ M DEAB exhibit normal gene expression levels of the Notch1-signaling pathway transcriptional targets *dlc* (D') and *her6* (E').

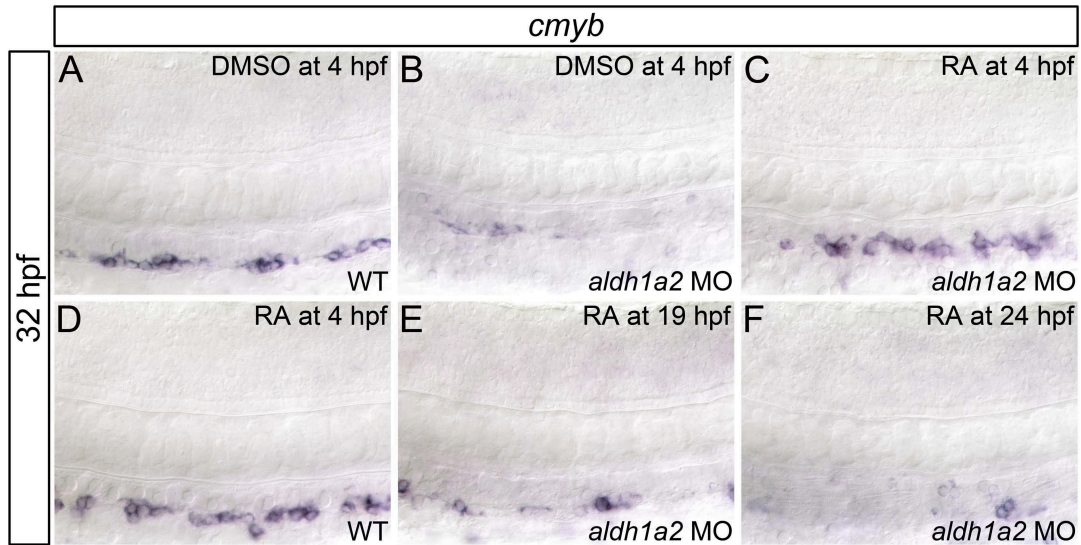


Fig. A.4: RA is required prior to 19 hpf for HSC formation. (A-F) Representative flat-mount embryos following *in situ* hybridization analyses of *cmyb* gene expression in wild type (WT; A,D) or *aldh1a2* morphant (B,C,E,F) 32 hpf embryos treated with DMSO (A,B) or 1 nM RA (C-F) at indicated time points. Lateral view of gene expression in the dorsal aorta region of the trunk is shown with anterior to the left. Compared to WT embryos (A), embryos treated with 1 nM RA (D) exhibit normal *cmyb* expression (two-tailed $P = 1.000$). *aldh1a2* morphants (B) exhibit nearly abolished *cmyb* expression compared to WT embryos (two-tailed $P = 0.01$). *cmyb* expression is significantly restored in *aldh1a2* morphant embryos treated with 1 nM RA at 4 hpf (C; two-tailed $P = 1.000$ compared to WT). *cmyb* expression is not significantly restored in *aldh1a2* morphants treated with 1 nM RA at 19 hpf (E; two-tailed $P < 0.0005$) or 24 hpf (F; two-tailed $P < 0.0005$).

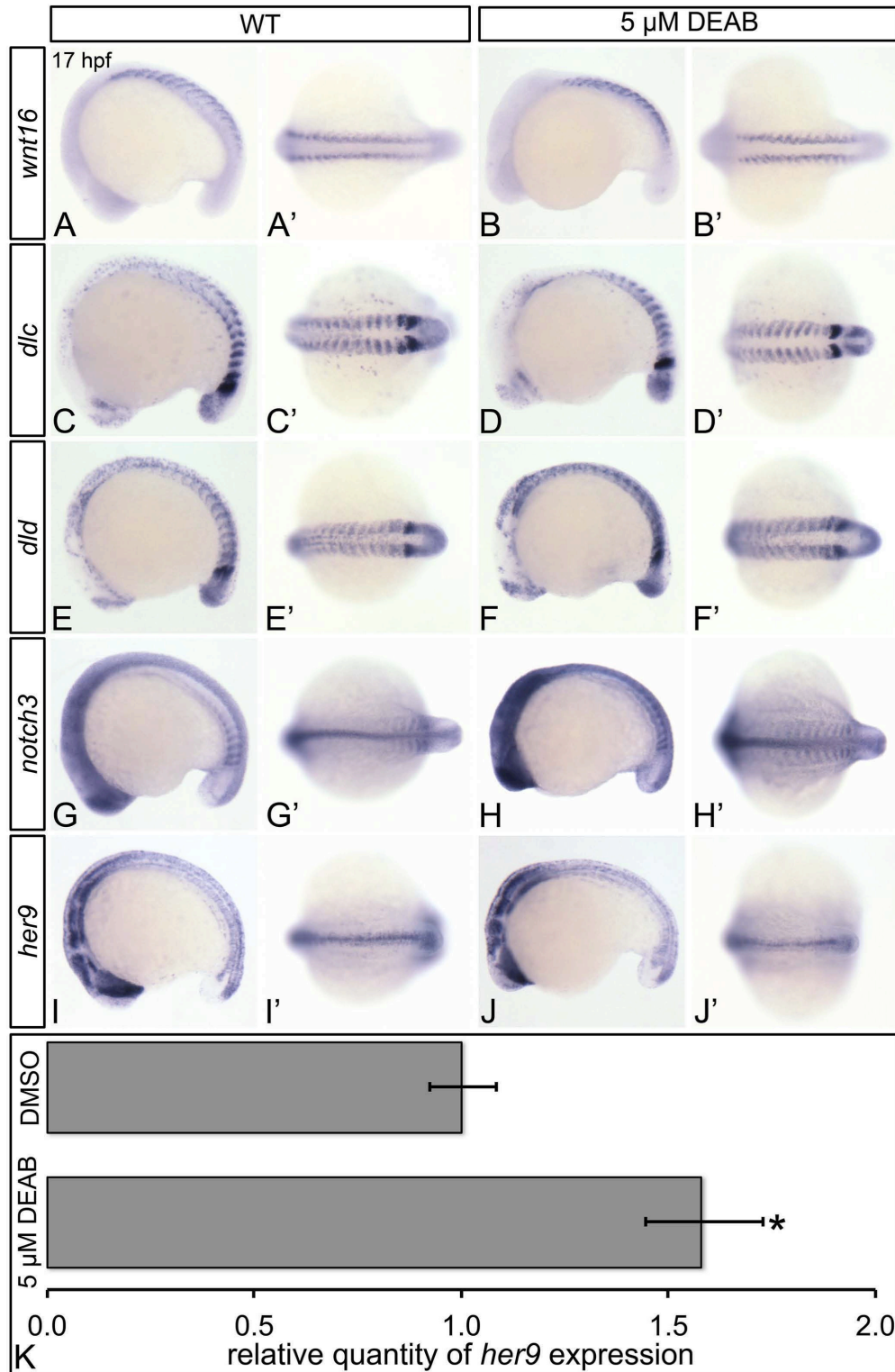


Fig. A.5: RA does not regulate the somitic expression of Wnt16-Notch3 signaling pathway components. Shown are representative 17 hpf embryos following *in situ* hybridization analyses (A-J). Lateral view (A-J) or dorsal view (A'-J') of gene expression is shown with anterior oriented to the left. A'-J' represent different views of the embryos shown in A-J. Compared to DMSO-treated controls (A-A',C-C',E-E',G-G'), DEAB-treated embryos exhibit normal somitic expression levels of *wnt16* (B,B'), and *dlc* (D,D'), mildly increased *dld* expression (F,F'), and increased *notch3* somitic gene expression (H, H'). DEAB-treated embryos also exhibit normal expression levels of the Notch3 signaling pathway transcriptional target *her9* (J,J'), when compared to DMSO-treated controls (I,I'). (K) Quantitative real-time PCR analysis of *her9* expression in 17 hpf DMSO-treated controls and embryos treated with 5 μ M DEAB. Shown is the relative quantity of *her9* expression. Samples were normalized to *efla* and DMSO-treated was set to 1. Error bars indicate standard error of the mean. *=difference compared to control is significant by Student t-test, $P = 0.0198$.

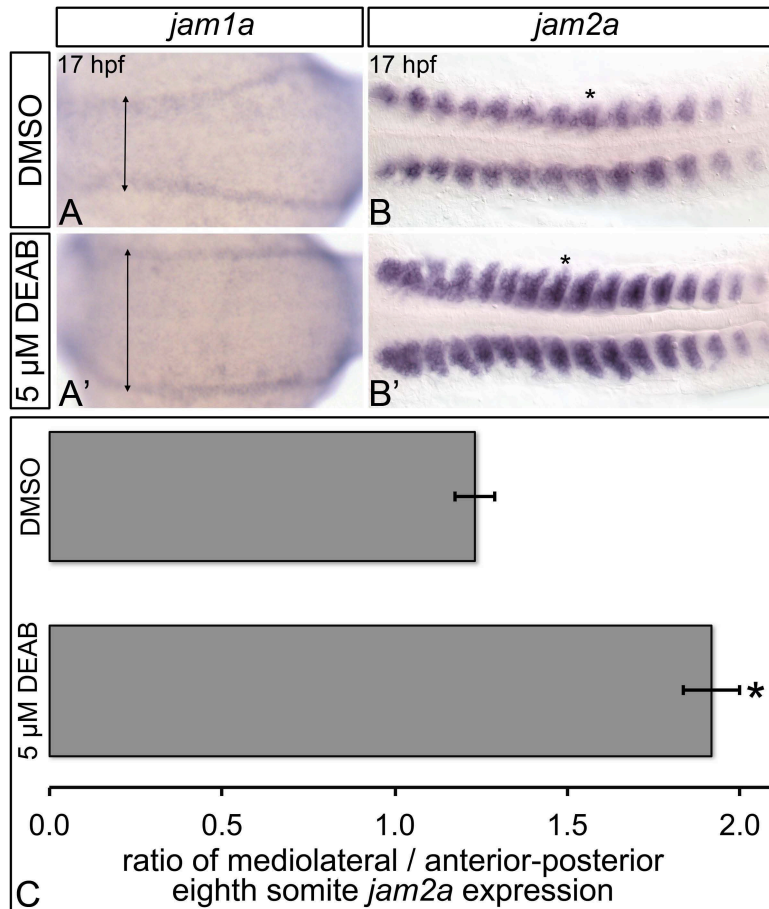


Fig. A.6: RA-deficient embryos exhibit abnormal *jam1a* and *jam2a* expression. Representative flat-mount 17 hpf embryos following *in situ* hybridization analyses. Dorsal view of gene expression is shown with anterior to the left. Compared to DMSO-treated controls (A), embryos treated with 5 μM DEAB (A') exhibit wild type levels of *jam1a* expression, and extreme lateral positioning of the anterior-most domains of *jam1a* expression (double-headed arrows). Compared to DMSO-treated controls (B), embryos treated with 5 μM DEAB (B') display strongly increased somitic *jam2a* expression, and lateral expansion of the *jam2a* expression domain. (C) Graph demonstrating length of the domain of *jam2a* expression along the medio-lateral axis, divided by length of the domain of expression along the anterior-posterior axis of the eighth *jam2a*-expressing somite on the right side of the embryo (see asterisk in B,B'). Error bars represent standard error *=statistically significant difference in ratio compared to DMSO-treated controls ($P < 0.0001$).

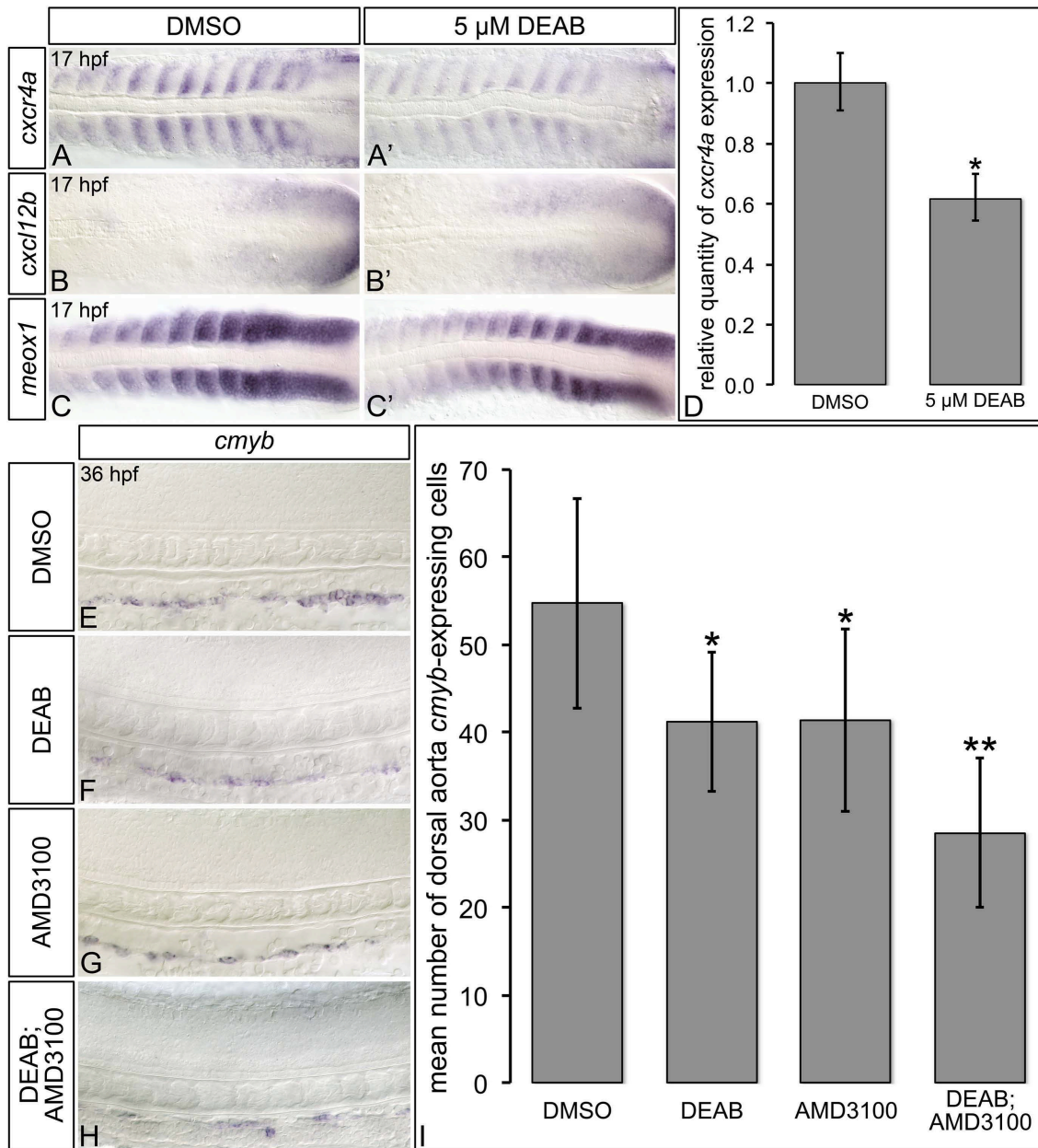


Fig. A.7: RA-deficient embryos exhibit altered Cxcl12b chemokine signaling pathway component gene expression. (A-C') Representative flat-mount 17 hpf embryos following *in situ* hybridization analyses. Dorsal of gene expression is shown with anterior to the left. Compared to DMSO-treated controls (A), embryos treated with 5 μ M DEAB (A') exhibit strongly reduced somitic *cxcr4a* gene expression, and narrowing of the *cxcr4a* expression domain within each somite. Compared to DMSO-treated controls (B, C), embryos treated with 5 μ M DEAB exhibit subtly increased levels of somitic *cxcl12b* expression (B'), and subtly decreased levels of somitic *meox1* expression (C'). (D)

Quantitative real-time PCR analysis of *cxcr4a* expression in 17 hpf DMSO-treated controls and embryos treated with 5 μ M DEAB. Shown is the relative quantity of *cxcr4a* expression. Samples were normalized to *efla* and DMSO-treated was set to 1. Error bars indicate standard error of the mean. *=difference compared to control is significant by Student t-test, $P < 0.0382$. (E-H) Representative flat-mount 36 hpf embryos following *in situ* hybridization analyses of *cmyb* gene expression. Lateral view of gene expression in the dorsal aorta region of the trunk is shown with anterior to the left. Compared to DMSO-treated controls (E), embryos treated with 1 μ M DEAB (F) or 10 μ M AMD3100 (G) exhibit a small reduction *cmyb*-expressing cell numbers. Embryos treated with both 1 μ M DEAB and 10 μ M AMD310 (H) exhibit a more severe reduction in *cmyb*-expressing cell numbers. (I) Graph demonstrating the mean number of dorsal aorta *cmyb*-expressing cells in DMSO-treated controls, embryos treated with 1 μ M DEAB, 10 μ M AMD3100, or both 1 μ M DEAB and 10 μ M AMD310. Error bars represent standard error. *=statistically significant difference compared to control ($P \leq 0.0144$). **=statistically significant difference compared to 1 μ M DEAB, and 10 μ M AMD3100 ($P \leq 0.0028$).

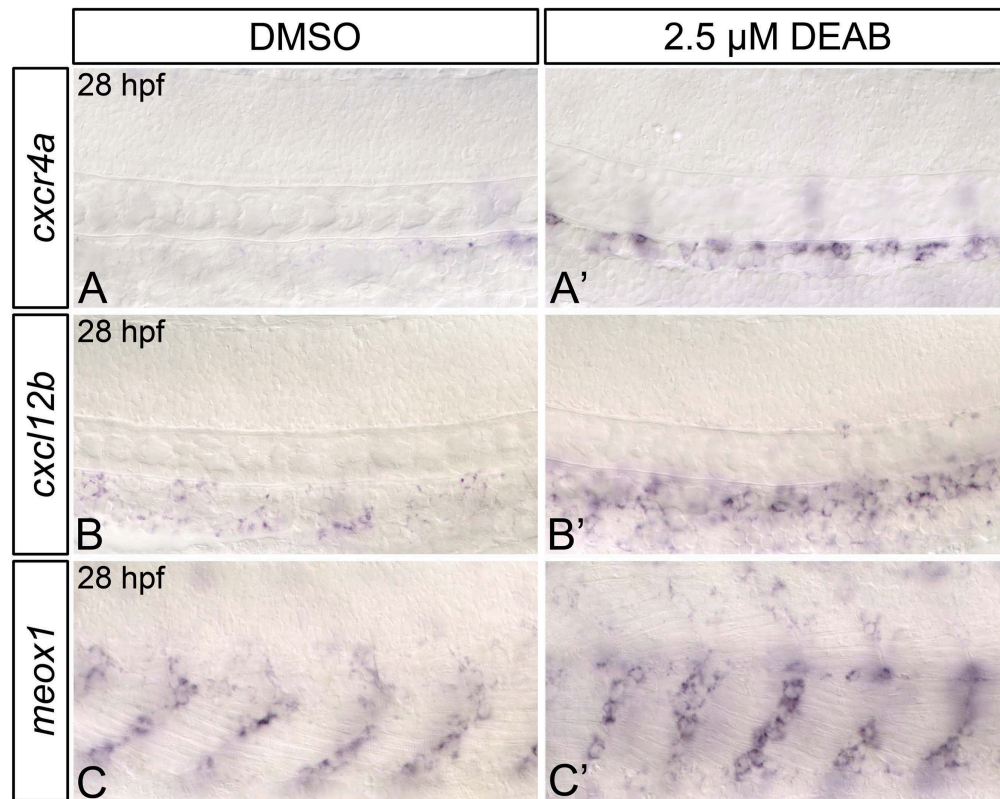


Fig. A.8: RA-deficient embryos exhibit altered Cxcl12b chemokine signaling pathway component gene expression. (A-C') Representative flat-mount 17 hpf embryos following *in situ* hybridization analyses. Dorsal of gene expression is shown with anterior to the left. Compared to DMSO-treated controls (A), embryos treated with 5 μ M DEAB (A') exhibit strongly reduced somitic *cxcr4a* gene expression, and narrowing of the *cxcr4a* expression domain within each somite. Compared to DMSO-treated controls (B, C), embryos treated with 5 μ M DEAB exhibit subtly increased levels of somitic *cxcl12b* expression (B'), and subtly decreased levels of somitic *meox1* expression (C'). (D) Quantitative real-time PCR analysis of *cxcr4a* expression in 17 hpf DMSO-treated controls and embryos treated with 5 μ M DEAB. Shown is the relative quantity of *cxcr4a* expression. Samples were normalized to *efla* and DMSO-treated was set to 1. Error bars indicate standard error of the mean. *=difference compared to control is significant by Student t-test, $P < 0.0382$. (E-H) Representative flat-mount 36 hpf embryos following *in situ* hybridization analyses of *cmyb* gene expression. Lateral view of gene expression in the dorsal aorta region of the trunk is shown with anterior to the left. Compared to DMSO-treated controls (E), embryos treated with 1 μ M DEAB (F) or 10 μ M AMD3100

(G) exhibit a small reduction *cmyb*-expressing cell numbers. Embryos treated with both 1 μM DEAB and 10 μM AMD310 (H) exhibit a more severe reduction in *cmyb*-expressing cell numbers. (I) Graph demonstrating the mean number of dorsal aorta *cmyb*-expressing cells in DMSO-treated controls, embryos treated with 1 μM DEAB, 10 μM AMD3100, or both 1 μM DEAB and 10 μM AMD310. Error bars represent standard error. *=statistically significant difference compared to control ($P \leq 0.0144$). **=statistically significant difference compared to 1 μM DEAB, and 10 μM AMD3100 ($P \leq 0.0028$).

A.6 Tables

Table A.1: Quantification of *cmyb* gene expression phenotypes in 32 hpf wild type (WT) controls and RA-deficient embryos. *Indicates significant result compared to WT, by Fisher's Exact Test with Bonferroni correction on cumulative raw counts.

Treatment	Wild type	Reduced	Total	Two-tailed <i>P</i>-value
WT; DMSO	60	7	67	
<i>aldh1a2</i> MO; DMSO	10	27	37	<0.0002*
5 μ M DEAB	12	42	54	<0.0002*

Table A.2: Quantification of thymic gene expression phenotypes in wild type (WT) and *aldh1a2*-morphant embryos. *Indicates significant result compared to WT, by Fisher's Exact Test on cumulative raw counts.

Gene	Stage	Treatment	Wild type	Reduced	Total	Two-tailed P-value
<i>rag1</i>	3 dpf	WT	65	7	72	<0.0001*
		<i>aldh1a2</i> MO	14	31	45	
<i>ikaros</i>	3 dpf	WT	62	0	62	<0.0001*
		<i>aldh1a2</i> MO	8	37	45	
<i>foxn1</i>	4 dpf	WT	45	2	47	0.6771
		<i>aldh1a2</i> MO	43	3	46	

Table A.3: Quantification of circulatory phenotypes in wild type (WT) and *aldh1a2*-morphant embryos. *Indicates significant result compared to WT, by Fisher's Exact Test on cumulative raw counts.

Stage	Treatment	Circulation	No Circulation	Total	Mean % with Circulation	SEM (%)	Two-tailed P-value
28 hpf	WT	70	9	79	87.0	3.00	0.0196*
	<i>aldh1a2</i> MO	37	15	52	71.0	1.00	
48 hpf	WT	74	1	75	97.0	3.00	0.5633
	<i>aldh1a2</i> MO	48	2	50	96.5	3.50	

Table A.4. Quantification of *Tg(kdrl:GFP)* dorsal aorta morphology phenotypes in 28 hpf wild type (WT) controls and RA-deficient embryos. *Indicates significant result ($P < 0.05$) compared to WT, by Bonferroni method post-test following two-way ANOVA. $F(4,18) = 11.18$, $P = 0.0001$.

Treatment	Mean % Wild type	SEM (%)	Mean % Thin	SEM (%)	Mean % Other	SEM (%)
WT; DMSO	100.0	0.0	0.0	0.0	0.0	0.0
2.5 μ M DEAB	69.1	19.8	30.2	16.4	0.7	0.6
5 μ M DEAB	19.1*	12.5	65.7*	13.7	15.2	1.2

Table A.5: Quantification of dorsal aorta gene expression phenotypes in wild type (WT) controls and RA-deficient embryos.

Gene	Stage	Treatment	Wild type	Reduced	Total	Two-tailed <i>P</i>-value
<i>kdrl</i>	28 hpf	WT	16	2	18	0.6581
		<i>aldh1a2</i> MO	14	3	17	
<i>efnb2a</i>	28 hpf	WT; DMSO	36	0	36	1.000
		5 μ M DEAB	37	1	38	

Table A.6: Quantification of dorsal aorta *notch* gene expression phenotypes in 26 hpf wild type (WT) controls and RA-deficient embryos. *Indicates significant result compared to WT, by Fisher's Exact Test on cumulative raw counts.

Gene	Treatment	Wild type	Abnormal	Total	Two-tailed P-value
<i>notch1a</i>	WT; DMSO	37	0	37	1.000
	2.5 μ M DEAB	49	0	49	
<i>notch1b</i>	WT; DMSO	37	0	37	1.000
	2.5 μ M DEAB	58	1	59	
<i>notch3</i>	WT; DMSO	78	2	80	<0.0001*
	2.5 μ M DEAB	9	50	59	
<i>dlc</i>	WT; DMSO	46	0	46	1.000
	2.5 μ M DEAB	56	0	56	
<i>her6</i>	WT; DMSO	25	0	25	1.000
	2.5 μ M DEAB	24	0	24	

Table A.7: Quantification of *cmyb* gene expression defects in 32 hpf wild type (WT) controls and *aldh1a2*-morphant embryos treated with 1 nM RA at indicated time points. *Indicates significant result compared to WT, DMSO-treated controls by Fisher's Exact Test with Bonferroni correction on cumulative raw counts.

Treatment	Wild type	Reduced	Total	Two-tailed P-value
WT; DMSO	40	3	43	
WT; 1 nm RA at 4 hpf	35	2	37	1.000
<i>aldh1a2</i> MO; DMSO	10	10	20	0.001*
<i>aldh1a2</i> MO; 1 nM RA at 4 hpf	22	4	26	1.000
<i>aldh1a2</i> MO; 1 nM RA at 19 hpf	7	23	30	<0.0005*
<i>aldh1a2</i> MO; 1 nM RA at 24 hpf	6	19	25	<0.0005*

Table A.8: Quantification of Wnt16-Notch3 pathway component gene expression phenotypes in 17 hpf wild type (WT) controls and RA-deficient embryos. *Indicates significant result compared to WT, by Fisher's Exact Test on cumulative raw counts.

Gene	Treatment	Wild type	Abnormal	Total	Two-tailed P-value
<i>wnt16</i>	WT; DMSO	43	0	43	1.000
	5 μ M DEAB	49	0	49	
<i>dlc</i>	WT; DMSO	53	0	53	1.000
	5 μ M DEAB	55	0	55	
<i>dld</i>	WT; DMSO	41	1	42	<0.0001*
	5 μ M DEAB	9	25	34	
<i>notch3</i>	WT; DMSO	50	0	50	<0.0001*
	5 μ M DEAB	4	36	40	
<i>her9</i>	WT; DMSO	40	0	40	1.000
	5 μ M DEAB	45	0	45	
<i>jam1a</i>	WT; DMSO	65	0	65	<0.0001*
	5 μ M DEAB	0	62	62	
<i>jam2a</i>	WT; DMSO	78	1	79	<0.0001*
	5 μ M DEAB	4	65	69	

Table A.9: Quantification of Cxcl12b chemokine pathway component gene expression phenotypes in wild type (WT) controls and RA-deficient embryos.

*Indicates significant result compared to WT, by Fisher's Exact Test on cumulative raw counts.

Gene	Stage	Treatment	Wild type	Abnormal	Total	Two-tailed P-value
<i>cxcr4a</i>	17 hpf	WT; DMSO	48	5	53	<0.0001*
		5 μ M DEAB	3	48	51	
<i>cxcl12b</i>	17 hpf	WT; DMSO	32	5	37	<0.0001*
		5 μ M DEAB	19	24	43	
<i>meox1</i>	17 hpf	WT; DMSO	50	4	54	<0.0001*
		5 μ M DEAB	12	40	52	
<i>cxcr4a</i>	28 hpf	WT; DMSO	47	0	47	<0.0001*
		2.5 μ M DEAB	2	43	45	
<i>cxcl12b</i>	28 hpf	WT; DMSO	59	3	62	<0.0001*
		2.5 μ M DEAB	49	42	91	
<i>meox1</i>	28 hpf	WT; DMSO	39	1	40	<0.0001*
		2.5 μ M DEAB	6	35	41	

A.7 References

Aiuti, A., Webb, I., Bleul, C., Springer, T., Gutierrez-Ramos, J., 1997. The chemokine SDF-1 is a chemoattractant for human CD34+ hematopoietic progenitor cells and provides a new mechanism to explain the mobilization of CD34+ progenitors to peripheral blood. *Journal of Experimental Medicine* 185, 111-120.

Alexa, K., Choe, S.-K., Hirsch, N., Etheridge, L., Laver, E., Sagerström, C.G., 2009. Maternal and zygotic *aldh1a2* activity is required for pancreas development in zebrafish. *PloS one* 4, e8261.

Ara, T., Tokoyoda, K., Okamoto, R., Koni, P.A., Nagasawa, T., 2005. The role of CXCL12 in the organ-specific process of artery formation. *Blood* 105, 3155-3161.

Begemann, G., Meyer, A., 2001. Hindbrain patterning revisited: timing and effects of retinoic acid signalling. *Bioessays* 23, 981-986.

Begemann, G., Schilling, T.F., Rauch, G.-J., Geisler, R., Ingham, P.W., 2001. The zebrafish neckless mutation reveals a requirement for *raldh2* in mesodermal signals that pattern the hindbrain. *Development* 128, 3081-3094.

Belandia, B., Parker, M.G., 2003. Nuclear receptors: a rendezvous for chromatin remodeling factors. *Cell* 114, 277-280.

Bertrand, J.Y., Cisson, J.L., Stachura, D.L., Traver, D., 2010. Notch signaling distinguishes 2 waves of definitive hematopoiesis in the zebrafish embryo. *Blood* 115, 2777-2783.

Boldajipour, B., Doitsidou, M., Tarbashevich, K., Laguri, C., Yu, S.R., Ries, J., Dumstrei, K., Thelen, S., Dörries, J., Messerschmidt, E.-M., 2011. *Cxcl12* evolution–subfunctionalization of a ligand through altered interaction with the chemokine receptor. *Development* 138, 2909-2914.

Burns, C.E., DeBlasio, T., Zhou, Y., Zhang, J., Zon, L., Nimer, S.D., 2002. Isolation and characterization of *runxa* and *runxb*, zebrafish members of the runt family of transcriptional regulators. *Experimental hematology* 30, 1381-1389.

Burns, C.E., Traver, D., Mayhall, E., Shepard, J.L., Zon, L.I., 2005. Hematopoietic stem cell fate is established by the Notch–Runx pathway. *Genes & development* 19, 2331-2342.

Bussmann, J., Wolfe, S.A., Siekmann, A.F., 2011. Arterial-venous network formation during brain vascularization involves hemodynamic regulation of chemokine signaling. *Development* 138, 1717-1726.

Chanda, B., Ditadi, A., Iscove, N.N., Keller, G., 2013. Retinoic acid signaling is essential for embryonic hematopoietic stem cell development. *Cell* 155, 215-227.

- Choi, J., Dong, L., Ahn, J., Dao, D., Hammerschmidt, M., Chen, J.-N., 2007. FoxH1 negatively modulates flk1 gene expression and vascular formation in zebrafish. *Developmental biology* 304, 735-744.
- Clements, W.K., Kim, A.D., Ong, K.G., Moore, J.C., Lawson, N.D., Traver, D., 2011. A somitic Wnt16/Notch pathway specifies haematopoietic stem cells. *Nature* 474, 220.
- Cumano, A., Godin, I., 2007. Ontogeny of the hematopoietic system. *Annu. Rev. Immunol.* 25, 745-785.
- Davidson, A.J., Zon, L.I., 2004. The 'definitive'(and 'primitive') guide to zebrafish hematopoiesis. *Oncogene* 23, 7233.
- Drummond, D.L., Cheng, C.S., Selland, L.G., Hocking, J.C., Prichard, L.B., Waskiewicz, A.J., 2013. The role of Zic transcription factors in regulating hindbrain retinoic acid signaling. *BMC developmental biology* 13, 31.
- Dzierzak, E., 2005. The emergence of definitive hematopoietic stem cells in the mammal. *Current opinion in hematology* 12, 197-202.
- Ellertsdóttir, E., Lenard, A., Blum, Y., Krudewig, A., Herwig, L., Affolter, M., Belting, H.-G., 2010. Vascular morphogenesis in the zebrafish embryo. *Developmental biology* 341, 56-65.
- French, C.R., Erickson, T., French, D.V., Pilgrim, D.B., Waskiewicz, A.J., 2009. Gdf6a is required for the initiation of dorsal-ventral retinal patterning and lens development. *Developmental Biology* 333, 37-47.
- Gates, M.A., Kim, L., Egan, E.S., Cardozo, T., Sirotkin, H.I., Dougan, S.T., Lashkari, D., Abagyan, R., Schier, A.F., Talbot, W.S., 1999. A genetic linkage map for zebrafish: comparative analysis and localization of genes and expressed sequences. *Genome research* 9, 334-347.
- Gerety, S.S., Breau, M.A., Sasai, N., Xu, Q., Briscoe, J., Wilkinson, D.G., 2013. An inducible transgene expression system for zebrafish and chick. *Development* 140, 2235-2243.
- Gering, M., Patient, R., 2010. Notch signalling and haematopoietic stem cell formation during embryogenesis. *Journal of cellular physiology* 222, 11-16.
- Glass, C.K., Rosenfeld, M.G., 2000. The coregulator exchange in transcriptional functions of nuclear receptors. *Genes & development* 14, 121-141.
- Goldie, L.C., Lucitti, J.L., Dickinson, M.E., Hirschi, K.K., 2008. Cell signaling directing the formation and function of hemogenic endothelium during murine embryogenesis. *Blood* 112, 3194-3204.

Gongal, P.A., March, L.D., Holly, V.L., Pillay, L.M., Berry-Wynne, K.M., Kagechika, H., Waskiewicz, A.J., 2011. Hmx4 regulates Sonic hedgehog signaling through control of retinoic acid synthesis during forebrain patterning. *Developmental biology* 355, 55-64.

Gongal, P.A., Waskiewicz, A.J., 2007. Zebrafish model of holoprosencephaly demonstrates a key role for TGIF in regulating retinoic acid metabolism. *Human molecular genetics* 17, 525-538.

Grandel, H., Lun, K., Rauch, G.-J., Rhinn, M., Piotrowski, T., Houart, C., Sordino, P., Küchler, A.M., Schulte-Merker, S., Geisler, R., 2002. Retinoic acid signalling in the zebrafish embryo is necessary during pre-segmentation stages to pattern the anterior-posterior axis of the CNS and to induce a pectoral fin bud. *Development* 129, 2851-2865.

Hadland, B.K., Huppert, S.S., Kanungo, J., Xue, Y., Jiang, R., Gridley, T., Conlon, R.A., Cheng, A.M., Kopan, R., Longmore, G.D., 2004. A requirement for Notch1 distinguishes 2 phases of definitive hematopoiesis during development. *Blood* 104, 3097-3105.

Harrison, C.A., Al-Musawi, S.L., Walton, K.L., 2011. Prodomains regulate the synthesis, extracellular localisation and activity of TGF- β superfamily ligands. *Growth Factors* 29, 174-186.

Iso, T., Kedes, L., Hamamori, Y., 2003. HES and HERP families: multiple effectors of the Notch signaling pathway. *Journal of cellular physiology* 194, 237-255.

Jin, H., Xu, J., Wen, Z., 2007. Migratory path of definitive hematopoietic stem/progenitor cells during zebrafish development. *Blood* 109, 5208-5214.

Jouve, C., Palmeirim, I., Henrique, D., Beckers, J., Gossler, A., Ish-Horowicz, D., Pourquié, O., 2000. Notch signalling is required for cyclic expression of the hairy-like gene HES1 in the presomitic mesoderm. *Development* 127, 1421-1429.

Kalev-Zylinska, M.L., Horsfield, J.A., Flores, M.V.C., Postlethwait, J.H., Vitas, M.R., Baas, A.M., Crosier, P.S., Crosier, K.E., 2002. Runx1 is required for zebrafish blood and vessel development and expression of a human RUNX1-CBF2T1 transgene advances a model for studies of leukemogenesis. *Development* 129, 2015-2030.

Kim, A.D., Melick, C.H., Clements, W.K., Stachura, D.L., Distel, M., Panáková, D., MacRae, C., Mork, L.A., Crump, J.G., Traver, D., 2014. Discrete Notch signaling requirements in the specification of hematopoietic stem cells. *The EMBO journal* 33, 2363-2373.

Kimmel, C.B., Ballard, W.W., Kimmel, S.R., Ullmann, B., Schilling, T.F., 1995. Stages of embryonic development of the zebrafish. *Developmental dynamics* 203, 253-310.

Kobayashi, I., Kobayashi-Sun, J., Kim, A.D., Pouget, C., Fujita, N., Suda, T., Traver, D., 2014. Jam1a–Jam2a interactions regulate haematopoietic stem cell fate through Notch signalling. *Nature* 512, 319.

Kopinke, D., Sasine, J., Swift, J., Stephens, W.Z., Piotrowski, T., 2006. Retinoic acid is required for endodermal pouch morphogenesis and not for pharyngeal endoderm specification. *Developmental Dynamics* 235, 2695-2709.

Kumano, K., Chiba, S., Kunisato, A., Sata, M., Saito, T., Nakagami-Yamaguchi, E., Yamaguchi, T., Masuda, S., Shimizu, K., Takahashi, T., 2003. Notch1 but not Notch2 is essential for generating hematopoietic stem cells from endothelial cells. *Immunity* 18, 699-711.

Lai, L., Bohnsack, B.L., Niederreither, K., Hirschi, K.K., 2003. Retinoic acid regulates endothelial cell proliferation during vasculogenesis. *Development* 130, 6465-6474.

Liu, Y., Pathak, N., Kramer-Zucker, A., Drummond, I.A., 2007. Notch signaling controls the differentiation of transporting epithelia and multiciliated cells in the zebrafish pronephros. *Development* 134, 1111-1122.

Livak, K.J., Schmittgen, T.D., 2001. Analysis of relative gene expression data using real-time quantitative PCR and the 2- $\Delta\Delta$ CT method. *methods* 25, 402-408.

Ma, D., Wei, Y., Liu, F., 2013. Regulatory mechanisms of thymus and T cell development. *Developmental & Comparative Immunology* 39, 91-102.

Ma, M., Jiang, Y.-J., 2007. Jagged2a-notch signaling mediates cell fate choice in the zebrafish pronephric duct. *PLoS Genetics* 3, e18.

Marcelo, K.L., Sills, T.M., Coskun, S., Vasavada, H., Sanglikar, S., Goldie, L.C., Hirschi, K.K., 2013. Hemogenic endothelial cell specification requires c-Kit, Notch signaling, and p27-mediated cell-cycle control. *Developmental cell* 27, 504-515.

Maves, L., Kimmel, C.B., 2005. Dynamic and sequential patterning of the zebrafish posterior hindbrain by retinoic acid. *Developmental biology* 285, 593-605.

Moore, M.A., Metcalf, D., 1970. Ontogeny of the haemopoietic system: yolk sac origin of in vivo and in vitro colony forming cells in the developing mouse embryo. *British journal of haematology* 18, 279-296.

Murayama, E., Kissa, K., Zapata, A., Mordelet, E., Briolat, V., Lin, H.-F., Handin, R.I., Herbomel, P., 2006. Tracing hematopoietic precursor migration to successive hematopoietic organs during zebrafish development. *Immunity* 25, 963-975.

Nguyen, P.D., Hollway, G.E., Sonntag, C., Miles, L.B., Hall, T.E., Berger, S., Fernandez, K.J., Gurevich, D.B., Cole, N.J., Alaei, S., 2014. Haematopoietic stem cell induction by somite-derived endothelial cells controlled by meox1. *Nature* 512, 314.

Niederreither, K., Subbarayan, V., Dollé, P., Chambon, P., 1999. Embryonic retinoic acid synthesis is essential for early mouse post-implantation development. *Nature genetics* 21, 444.

- Niederreither, K., Vermot, J., Schuhbaur, B., Chambon, P., Dollé, P., 2000. Retinoic acid synthesis and hindbrain patterning in the mouse embryo. *Development* 127, 75-85.
- North, T.E., Goessling, W., Peeters, M., Li, P., Ceol, C., Lord, A.M., Weber, G.J., Harris, J., Cutting, C.C., Huang, P., 2009. Hematopoietic stem cell development is dependent on blood flow. *Cell* 137, 736-748.
- Packham, I.M., Gray, C., Heath, P.R., Hellewell, P.G., Ingham, P.W., Crossman, D.C., Milo, M., Chico, T.J., 2009. Microarray profiling reveals CXCR4a is downregulated by blood flow in vivo and mediates collateral formation in zebrafish embryos. *Physiological genomics*.
- Palis, J., Yoder, M.C., 2001. Yolk-sac hematopoiesis: the first blood cells of mouse and man. *Experimental hematology* 29, 927-936.
- Peled, A., Petit, I., Kollet, O., Magid, M., Ponomaryov, T., Byk, T., Nagler, A., Ben-Hur, H., Many, A., Shultz, L., 1999. Dependence of human stem cell engraftment and repopulation of NOD/SCID mice on CXCR4. *Science* 283, 845-848.
- Perz-Edwards, A., Hardison, N.L., Linney, E., 2001. Retinoic acid-mediated gene expression in transgenic reporter zebrafish. *Developmental biology* 229, 89-101.
- Pillay, L.M., A. Michael Forrester, Timothy Erickson, Jason N. Berman, Andrew J. Waskiewicz, 2010. The Hox cofactors Meis1 and Pbx act upstream of *gatal* to regulate primitive hematopoiesis. *Developmental Biology* 340, 306-317.
- Purton, L.E., Bernstein, I.D., Collins, S.J., 1999. All-trans retinoic acid delays the differentiation of primitive hematopoietic precursors (*lin⁻ c-kit⁺ Sca-1⁺*) while enhancing the terminal maturation of committed granulocyte/monocyte progenitors. *Blood* 94, 483-495.
- Purton, L.E., Bernstein, I.D., Collins, S.J., 2000. All-trans retinoic acid enhances the long-term repopulating activity of cultured hematopoietic stem cells. *Blood* 95, 470-477.
- Robert-Moreno, À., Espinosa, L., de la Pompa, J.L., Bigas, A., 2005. RBPjk-dependent Notch function regulates Gata2 and is essential for the formation of intra-embryonic hematopoietic cells. *Development* 132, 1117-1126.
- Robert-Moreno, À., Guiu, J., Ruiz-Herguido, C., López, M.E., Inglés-Esteve, J., Riera, L., Tipping, A., Enver, T., Dzierzak, E., Gridley, T., 2008. Impaired embryonic haematopoiesis yet normal arterial development in the absence of the Notch ligand Jagged1. *The EMBO journal* 27, 1886-1895.
- Siekman, A.F., Standley, C., Fogarty, K.E., Wolfe, S.A., Lawson, N.D., 2009. Chemokine signaling guides regional patterning of the first embryonic artery. *Genes & development* 23, 2272-2277.

Stückemann, T., Wegleiter, T., Stefan, E., Nägele, O., Tarbashevich, K., Böck, G., Raz, E., Aanstad, P., 2012. Zebrafish Cxcr4a determines the proliferative response to Hedgehog signalling. *Development* 139, 2711-2720.

Tachibana, K., Hirota, S., Iizasa, H., Yoshida, H., Kawabata, K., Kataoka, Y., Kitamura, Y., Matsushima, K., Yoshida, N., Nishikawa, S.-i., 1998. The chemokine receptor CXCR4 is essential for vascularization of the gastrointestinal tract. *Nature* 393, 591.

Takabatake, Y., Sugiyama, T., Kohara, H., Matsusaka, T., Kurihara, H., Koni, P.A., Nagasawa, Y., Hamano, T., Matsui, I., Kawada, N., 2009. The CXCL12 (SDF-1)/CXCR4 axis is essential for the development of renal vasculature. *Journal of the American Society of Nephrology* 20, 1714-1723.

Thompson, M.A., Ransom, D.G., Pratt, S.J., MacLennan, H., Kieran, M.W., Detrich III, H.W., Vail, B., Huber, T.L., Paw, B., Brownlie, A.J., 1998. The cloche and spade tail genes differentially affect hematopoiesis and vasculogenesis. *Developmental biology* 197, 248-269.

Traver, D., Paw, B.H., Poss, K.D., Penberthy, W.T., Lin, S., Zon, L.I., 2003. Transplantation and in vivo imaging of multilineage engraftment in zebrafish bloodless mutants. *Nature immunology* 4, 1238.

Walters, K.B., Green, J.M., Surfus, J.C., Yoo, S.K., Huttenlocher, A., 2010. Live imaging of neutrophil motility in a zebrafish model of WHIM syndrome. *Blood* 116, 2803-2811.

Weinstein, B., Lawson, N., 2002. Arteries, veins, Notch, and VEGF, Cold Spring Harbor symposia on quantitative biology. Cold Spring Harbor Laboratory Press, pp. 155-162.

Westerfield, M., 2000. The zebrafish book. A guide for the library use of zebrafish (*Danio rerio*). University of Oregon Press, Eugene.

Xu, L., Glass, C.K., Rosenfeld, M.G., 1999. Coactivator and corepressor complexes in nuclear receptor function. *Current opinion in genetics & development* 9, 140-147.

Xu, Q., Wang, Z., Chen, X., Duan, W., Lei, J., Zong, L., Li, X., Sheng, L., Ma, J., Han, L., 2015. Stromal-derived factor-1 α /CXCL12-CXCR4 chemotactic pathway promotes perineural invasion in pancreatic cancer. *Oncotarget* 6, 4717.

Yu, C., Liu, Y., Miao, Z., Yin, M., Lu, W., Lv, Y., Ding, M., Deng, H., 2010. Retinoic acid enhances the generation of hematopoietic progenitors from human embryonic stem cell-derived hemato-vascular precursors. *Blood* 116, 4786-4794.

Zhang, Y., Jin, H., Li, L., Qin, F.X.-F., Wen, Z., 2011. cMyb regulates hematopoietic stem/progenitor cell mobilization during zebrafish hematopoiesis. *Blood* 118, 4093-4101.

Zou, Y.-R., Kottmann, A.H., Kuroda, M., Taniuchi, I., Littman, D.R., 1998. Function of the chemokine receptor CXCR4 in haematopoiesis and in cerebellar development. *Nature* 393, 595.